UNIVERSIDAD COMPLUTENSE DE MADRID

FACULTAD DE CIENCIAS MATEMATICAS

Departamento de Matemática Aplicada

ANÁLISIS MATEMÁTICO Y TRATAMIENTO NUMÉRICO DE UNA CLASE DE PROBLEMAS DE VALORES DE CONTORNO DE TIPO ELÍPTICO SUPERLINEAL INDEFINIDO.
(MATHEMATICAL ANALYSIS AND NUMERICAL TREATMENT OF A CLASS OF SUPERLINEAR INDEFINITE BOUNDARY VALUE PROBLEMS OF ELLIPTIC TYPE)

MEMORIA PARA OPTAR AL GRADO DE DOCTOR
PRESENTADA POR

Andrea Tellini

Bajo la dirección de los doctores

Julián López Gómez
Marcela Molina Meyer

MADRID, 2013

UNIVERSIDAD COMPLUTENSE DE MADRID

Facultad de Ciencias Matemáticas
Departamento de Matemática Aplicada

Doctorado de Investigación Matemática

Memoria para optar al título de Doctor

Análisis matemático y tratamiento numérico de una clase de problemas de valores de contorno de tipo elíptico superlineal indefinido

(Mathematical analysis and numerical treatment of a class of superlinear indefinite boundary value problems of elliptic type)

Directores:
Julián López Gómez
Marcela Molina Meyer

Presentada por:
Andrea Tellini

Madrid, Abril 2013

Agradecimientos

Si este trabajo ha llegado a ser tal y como está se lo debo a:

- Julián y Marcela, mis directores. A ellos les agradezco todo el tiempo que me han dedicado, los ánimos y lo que me han espoleado para hacerme mejorar en mi trabajo científico, por haberme enseñado a pensar en profundidad en las ideas matemáticas y por el trato amistoso, casi filial, que me han reservado en todo momento.

- Fabio, por haberme dado la posibilidad de venir a Madrid en 2009, ocasión a partir de la cual he tenido la suerte de poder quedarme aquí por todos estos años y crecer mucho, desde múltiples puntos de vista. Además es siempre un gran placer trabajar y discutir con él de matemáticas.

- Carlos, por haber *estado allí* siempre, en las buenas y en las malas, incondicionalmente; Espe, por su empatía y optimismo contagiosos; Alfonso, por la sensibilidad que ha demostrado hacia mí. A todos ellos mil gracias por haber querido incluirme en sus vidas.

- Clemente, Ana, Juan, Paz, Marta y María, por los conciertos, las exposiciones y las innumerables actividades que hemos hecho juntos y por las numerosas cenas y discusiones profundas.

- Alex, Yvan, Albert, Almu, Salva y Aldo, por todos los momentos de diversión que hemos tenido y haberme hecho sentir menos solo desde el primer momento, como en una gran familia internacional.

- Todos los compañeros y las compañeras de la Facultad y las otras personas que me han hecho pasar muchos buenos ratos en estos años.

- A mi familia y mis amigos, que me han estado tan cerca aun estando lejos, les doy las gracias por haberme apoyado en toda decisión.

A todos ellos van mis más sentidos agradecimientos, de todo el corazón.

Por la parte económica tengo que agradecer el Ministerio de Economía y Competitividad (antiguo Ministerio de Ciencia e Innovación) del Gobierno de España, que me ha financiado a través de la beca de Formación de Personal Investigador BES-2010-039030 y del Proyecto MTM2009-08259 "Metasoluciones en ecología espacial".

Madrid, 21 de diciembre de 2012

Contents

List of Figures

Summary

Introduction and goals

This thesis studies different properties of the positive steady states of the evolution problem

$$\begin{cases} u_t - \Delta u = \lambda u + a(x)u^p, & t > 0, \quad x \in \Omega, \\ u(t,x) = M > 0, & t > 0, \quad x \in \partial\Omega, \\ u(0,x) = u_0(x) \geq 0, & x \in \Omega, \end{cases} \tag{S.1}$$

where Ω is a bounded domain (open and connected set) of $\mathbb{R}^N$, $N \geq 1$, with smooth boundary $\partial\Omega$, $\lambda \in \mathbb{R}$, $p > 1$ and $M \in (0, \infty]$ are constants and $u_0 : \Omega \to \mathbb{R}$ is a non-negative function. The steady states of (S.1) are the positive solutions of the associated elliptic boundary value problem

$$\begin{cases} -\Delta u = \lambda u + a(x)u^p & \text{in } \Omega, \\ u(x) = M & \text{on } \partial\Omega. \end{cases} \tag{S.2}$$

In these models, $a(x)$ is a bounded and measurable function which might change of sign in Ω; it is often referred to as the *weight function*. If $a < 0$ in Ω, then

$$\lambda u + a(x)u^p < \lambda u$$

for all $u \geq 0$, and, hence, the problem is of *sublinear* type, while if $a > 0$, then

$$\lambda u + a(x)u^p > \lambda u$$

and, so, the problem is of *superlinear* type. In the case when a changes sign, which is the case treated in this dissertation, the problem is said to be of *superlinear indefinite* type.

In population dynamics, (S.1) models the evolution of a single species in an inhabiting region Ω, which is surrounded by territories where the population density equals M. In these models, $u(t,x)$ stands for the density of the species at the location $x \in \Omega$ after time $t > 0$, while $u_0 > 0$ is the initial population

density. The quantity λ measures the neat intrinsic birth ($\lambda > 0$) or death ($\lambda < 0$) rate of the species in Ω. In nature it is negative when pesticides are used in high concentrations, or a certain patch of the natural environment is polluted by introducing chemicals, waste products, or poisonous substances, while it is positive in the presence of good climatic conditions or abundance of nutrients, for example.

The generalized logistic nonlinearity measures the interspecific relations among the individuals of the species u. They compete for the natural resources in the region Ω_- where $a < 0$, while they cooperate in the patch Ω_+ where $a > 0$. When $a = 0$ in some subdomain Ω_0, the population obeys an exponential growth law, named after Malthus, in that region, where the natural resources are essentially unlimited. Therefore, in our superlinear indefinite problem, the previous three behaviors can occur simultaneously.

Although there are extensive reviews about the experimental evidence of interspecific competition (see, e.g., T. W. Shoener [69] and J. H. Connell [23]) and positive interactions are well documented among organisms from different kingdoms, as they can make significant contributions to each other's needs without sharing the same resources (see, e.g., G. E. Hutchinson [39], J. L. Wulff [70], M. B. Saffo [67]), finding positive interactions between similar organisms in the abundance seems to be a huge task in empirical studies, since they do not arise alone but in combination with competition. However, according to the abiotic stress hypothesis of M. D. Bertness and R. M. Callaway [10], the importance of positive interactions in plant communities increases with abiotic stress or consumer pressure. Several empirical studies support the validity of the abiotic stress hypothesis and, actually, a substantial number of documented positive interactions in plant communities has been isolated in harsh environmental conditions (see, e.g., R. M. Callaway, L. R. Walker [15] and F. I. Pugnaire [65]). Consequently, (S.1) seems to be a rather reasonable mathematical model for studying the effects of combined facilitation and competition in polluted habitat patches, i.e. when $\lambda < 0$.

As far as the boundary condition concerns, in the singular case $M = \infty$, we mean that

$$\lim_{d(x,\partial\Omega)\downarrow 0} u(x) = \infty,$$

where $d(x, \partial\Omega)$ is the distance of the point x from the boundary of Ω. Such solutions are known as *large* or *blow-up* solutions of the problem.

Although an infinite boundary condition could seem meaningless from the point of view of the biological interpretation, this is not the case, as the large solutions play a fundamental role to describe the dynamics of the parabolic problem, as in the sublinear case (see [46]). Therefore, their study is imperative to ascertain the dynamics of any superlinear indefinite problem (see [45, 59]).

Naturally, there is a huge amount of literature regarding the sublinear case, both for homogeneous and inhomogeneous boundary conditions. Precisely, the exact ranges of λ, depending on the weight and on the domain Ω, for which a solution of (S.2) exists have been obtained in this context by means of sub- and supersolutions methods. Again by some comparison principles, which are strongly based on the fact that $a \leq 0$, uniqueness has been proved (see e.g. [30, 46]). Analogous results hold for large solutions, however, besides monotonicity methods, one has to deal with the extremely delicate question of determining the blow-up rate of the solutions along $\partial\Omega$ in order to obtain the uniqueness (see e.g. [19, 20, 21, 22, 44, 46, 47]).

Superlinear indefinite problems have generated a certain literature, but mainly for homogeneous Dirichlet boundary conditions (see [3, 7, 8, 9, 36, 37, 42, 43, 45]). However, the elegant monotonicity methods that provide the key to obtain most of the results in the sublinear problems, are not longer available in the superlinear counterparts, which makes the mathematical analysis much more technically sophisticated. Actually, the uniqueness of solution no longer holds, which is in the roots of this dissertation, and the underlying global bifurcation diagrams change dramatically. Nevertheless, the superlinear indefinite problem (S.2), with inhomogeneous boundary conditions, has not been studied yet. It is the case that we treat in this thesis.

Content

In Chapter 1 we study a paradigmatic example of (S.2) in the one-dimensional case. Precisely, we consider

$$\begin{cases} -u'' = \lambda u + a_b(x)u^p & \text{in } (0,1), \\ u(0) = u(1) = M, \end{cases} \tag{S.3}$$

with the piecewise constant weight

$$a_b(x) := \begin{cases} -c & \text{if } x \in (0,\alpha) \cup (1-\alpha, 1), \\ b & \text{if } x \in (\alpha, 1-\alpha), \end{cases} \tag{S.4}$$

where $c > 0$, $b \geq 0$ and $\alpha \in (0, 0.5)$.

When $b = 0$, (S.3) is a diffusive degenerated logistic equation perturbed from the more classical case when $a(x) < 0$ for all $x \in \Omega = (0,1)$. As $a_0 = 0$ in $\Omega_0 = (\alpha, 1-\alpha)$, the species u grows according to Malthus' law of population dynamics in that patch and, in particular, natural resources are unlimited therein, whereas the evolution of u is governed by the logistic law, with exponent p, in $\Omega_- = (0,\alpha) \cup (1-\alpha, 1)$.

More precisely, as a very special case of J. M. Fraile et al. [30], if $b = M = 0$, then (S.3) possesses a unique solution (necessarily, symmetric around 0.5) if, and only if,

$$\pi^2 < \lambda < \lambda_\alpha := \left(\frac{\pi}{1-2\alpha}\right)^2.$$

Moreover, if we denote it by u_λ, it turns out that u_λ bifurcates from 0 at $\lambda = \pi^2$, and that it bifurcates from infinity at λ_α. Actually,

$$\lim_{\lambda\uparrow\lambda_\alpha} u_\lambda(x) = \begin{cases} \ell_\alpha(x) & x \in [0,\alpha), \\ \infty & x \in [\alpha, 0.5], \end{cases}$$

where ℓ_α stands for the unique solution of the singular problem

$$\begin{cases} -u'' = \lambda_\alpha u - cu^p & \text{in } (0,\alpha) \\ u(0) = 0, \quad u(\alpha) = \infty \end{cases}$$

(see J. García-Melián et al. [32], J. López-Gómez and J. C. Sabina [60] and J. López-Gómez [44, 46], if necessary). The same result holds for all $M > 0$ if $b = 0$, but, in this case, u_λ is defined not only for $\lambda > \pi^2$ but for all $\lambda < \lambda_\alpha$ (see [46]). In all these cases, when the (unique) solution exists, according to J. López-Gómez [46], it is a global attractor for the one-dimensional counterpart of (S.1)

$$\begin{cases} \partial_t u - \partial_{xx} u = \lambda u + a_b(x)u^p & x \in (0,1), \quad t > 0, \\ u(0,t) = u(1,t) = M, & t > 0, \\ u(x,0) = u_0(x), & x \in (0,1). \end{cases}$$

If in (S.3) we consider again the case $b = 0$ and assume, in addition, that $\lambda < 0$, then necessarily $u_\lambda < M$ in the inhabiting region, because $u'' > 0$. In the light of our biological interpretation of the model, this means that there is a continuous flow of individuals through the edges of the polluted area who die in its interior at the rate $\lambda < 0$ by the action of the contaminant. This flow through the boundary of the polluted area can maintain the population at the level u_λ as time grows. Basically, the same situation occurs if $\lambda > 0$ but the length of $(\alpha, 1-\alpha)$ is sufficiently small so that $\lambda < [\pi/(1-2\alpha)]^2$. Surprisingly, when the birth rate of the species, measured by λ, crosses the threshold $[\pi/(1-2\alpha)]^2$, the population remains bounded in $(0,\alpha)\cup(1-\alpha,1)$, much like in the classical logistic model, while it grows approximating infinity in $(\alpha, 1-\alpha)$, which is the region where the evolution of u is governed by Malthus' law.

All these features change drastically when $b > 0$, even in the simplest case when $M = 0$. Indeed, in such a case, it is well known that there exists $b^* > 0$ such that for every $0 < b < b^*$ there is a unique

$$\lambda_t = \lambda_t(b) \in (\pi^2, \lambda_\alpha)$$

such that:

a) (S.3) does not admit any solution if $\lambda > \lambda_t(b)$;

b) (S.3) admits, at least, one solution if $\lambda \leq \lambda_t(b)$;

c) (S.3) admits at least two solutions for each $\lambda \in (\pi^2, \lambda_t(b))$.

Moreover,

$$\lim_{b\downarrow 0} \lambda_t(b) = \lambda_\alpha \quad \text{and} \quad \lim_{b\uparrow b^*} \lambda_t(b) = \pi^2.$$

On the other hand, if $b \geq b^*$, then (S.3) admits a positive solution if, and only if, $\lambda \leq \pi^2$. These results are direct consequences from the general theory developed in J. López-Gómez [42], H. Amann and J. López-Gómez [7], and R. Gómez-Reñasco and J. López-Gómez [36, 37], where some pioneering findings by H. Berestycki et al. [8, 9], and S. Alama and G. Tarantello [3] were substantially sharpened.

Rather strikingly, although (S.3) looks so simple, in the general case when $b > 0$ and $0 < M \leq \infty$ there are very few results concerning the global structure of the solution set of (S.3). Among them, J. Mawhin, D. Papini and F. Zanolin [63] found some multiplicity results of sign-changing solutions, J. López-Gómez [45] established the existence and global attractive character of the minimal solution of (S.3) when $M = \infty$ for sufficiently small $b > 0$, and, more recently, J. García-Melián established the general shape of the bifurcation diagram of a general multidimensional prototype of (S.3) for $M = \infty$ and $\lambda = 0$ using b as the main bifurcation parameter. The device of using b as a parameter in the context of superlinear indefinite problems goes back, at least, to J. López-Gómez [43].

Since we assume (S.4), our problem is autonomous in each of the intervals where a_b is constant and we can apply phase plane techniques in each of these regions.

Analogous techniques, but for a rather different kind of problems, have been used by Harris [38] and Dambrosio [28] in connection with inhomogeneous boundary value problems of the form

$$\begin{cases} -u'' = f(u) + h & \text{in } (0,1) \\ u(0) = A,\ u(1) = B. \end{cases} \tag{S.5}$$

In [38] the author studies the case of jumping nonlinearities $f(u)/u \to C, D$ as $u \to \pm\infty$, while in [28] the superlinear case $f(u)/u \to +\infty$ as $u \to \pm\infty$, is discussed. The main difference of our study with respect to previous ones like [28, 38] concerns the fact that in our situation we deal with a superlinear indefinite problem, due to the change of sign in the weight $a_b(x)$ and, furthermore,

we also show the crucial role played by the parameter λ when $\lambda < 0$. Such facts produce multiplicity results of positive solutions which are completely different and not comparable to the previous ones. Precisely, for problem (S.5) in the superlinear case one obtains a large number of sign changing oscillatory solutions (see [28]) and, as proved in [63], such kind of strong oscillatory behavior persists also for blow-up solutions of $-u'' = a(x)f(u)$, when $a(x)$ (like in our case) is negative in a neighborhood of $t = 0, 1$ and positive elsewhere, but these solutions were not, in general, positive, as it occurs in this thesis, where we find for problem (S.3) a new and broad complementary class of multiple large solutions which are *positive* and oscillate around a positive level (see Section 1.3). Such multiplicity result relies on the fast oscillation of the solutions of (S.3) for sufficiently negative λ. The topological structure of the bifurcation curves associated to such positive oscillatory solutions, in dependence of the parameter b, has been also determined (see Section 1.6) and it is astonishingly rich and somehow surprising. Moreover, differently from [28, 38], we can treat in the same framework both the cases $M \in \mathbb{R}$ and $M = +\infty$. This gives us the advantage to obtain some new multiplicity results for *positive blow-up solutions* as well (Section 1.7).

In Chapter 2 we consider the general $N-$dimensional problem (S.1) with $M \in (0, +\infty)$ and our main result is the uniqueness of the positive linearly stable steady-state (see Section 2.5). The result is absolutely non trivial, in the light of the results of Chapter 1, since the model can admit an arbitrarily large number of steady-states. Our techniques differ substantially from those used in Chapter 1, since the problem is no longer piecewise-autonomous nor one-dimensional. They rely on some local and global continuations and on some global variational estimates.

As in Chapter 1, the uniqueness of the linearly stable steady-state for the case of homogeneous boundary conditions had been already proved by R. Gómez-Reñasco and J. López-Gómez in [36, 37], but here the situation is different because, due to the inhomogeneous boundary conditions, the constant solution $u = 0$ is no longer a solution of the problem, but just a subsolution, and this changes the dynamics of the problem.

Moreover we obtain some optimal existence and multiplicity results through some additional monotonicity and topological techniques (see Sections 2.4 and 2.6). Once again results of the same nature were known for the homogeneous boundary value problem (see [7]) but they are new in our context.

Some similar results have recently been obtained for large solutions by J. García-Melián in [31], but just for $\lambda = 0$, where only two solutions are expected to exist, as discussed in Chapter 1. As in this dissertation, the theory of [31] adapted the ideas and methods of [36, 37].

Finally, in Chapter 3 we present a rather detailed study of some numerical computations of the bifurcation diagrams arisen in the previous chapters (Section 3.4) and the techniques that we have used to obtain them. Quite surprisingly, from the numerical experiments it is apparent that the range of b for which (S.3) admits a positive solution becomes larger and larger as λ decreases to $-\infty$, while, simultaneously, the solutions of the problem approach 0 in the sublinear part, which is quite reasonable in the light of the biological interpretation of the model. Indeed, if large amounts of pesticide are used, even if the species does not disappear, by the continuous flow of individuals through the boundary, its density should be small, at least where competition arise in the polluted patch. Nevertheless this effect could be overcome by the facilitative effects in the superlinear part, as it happens for the linearly unstable solutions. In any case, the fact that the complexity of the dynamics increases as the environmental conditions become harsher, measured by the size of λ, is rather astonishing.

The mathematical analysis of Chapter 1 facilitated tremendously the numerics of Chapter 3, where these bifurcation diagrams were computed by combining some updated path-following solvers with spectral methods and collocation. The knowledge of their qualitative properties found in Chapter 1 has shown to be crucial for carrying out the numerical computations of Chapter 3, since the extreme closeness of the turning points, which is a consequence of the strong squashing phenomenon described above, and the proximity of the two tangents at the bifurcation points caused severe problems in the classical numerical codes which had been adapted to construct the diagrams predicted by the theory of Chapter 1.

Once solved these computational problems, we used the numerical codes to calculate the bifurcation diagrams of (S.3) for a series of different weights from (S.4). The results of these numerical experiments are presented in Section 3.5 and essentially show that the multiplicity result of Chapter 1 seemingly holds for very general classes of a_b, even if the topological structure of the bifurcation diagrams can vary dramatically depending on the symmetry properties of the weights. To the best of our knowledge, there are no available analytical tools to prove such results rigorously. From this perspective, this dissertation shows how fruitful is the interplay between theoretical and numerical analysis in practice. Indeed, it seems hard to figure out how one should have computed all these global bifurcation diagrams, exhibiting a so dramatic squashing effect, without the previous knowledge of their fine topological structure.

We conclude this summary by remarking that the contents of this thesis gave rise to the papers [61] (Chapter 1), [57] (Chapter 2) and [55, 56] (Chapter 3), which have been submitted for publication.

Chapter 1

High multiplicity and complexity of the bifurcation diagrams for a class of one dimensional problems

1.1. Introduction

This chapter analyzes the problem of the existence and the multiplicity of solutions for the one dimensional boundary value problem

$$\begin{cases} -u'' = \lambda u + a(t)u^p & \text{in } (0,1) \\ u(0) = u(1) = M \end{cases} \tag{1.1}$$

where $M \in (0, \infty]$, $p > 1$ and the coefficient λ is regarded as a real parameter. The function $a(t)$ is the symmetric piecewise constant function defined by

$$a(t) = \begin{cases} -c & \text{if } t \in [0, \alpha) \cup (1-\alpha, 1] \\ b & \text{if } t \in [\alpha, 1-\alpha] \end{cases}$$

with $\alpha \in (0, 0.5)$, $b \geq 0$ and $c > 0$. We remark that Problem (1.1) is the same as (S.3), but here we are calling t to the independent variable, instead of x, because this is a more appropriate notation in the context of dynamical systems, which is the approach that we use here.

We are interested in the positive solutions of (1.1), hence, unless differently specified, with the term 'solution'we mean a positive one. Thanks to the maximum principle, any solution $u \geq 0$, $u \neq 0$, of (1.1) must satisfy $u(t) > 0$ for all $t \in [0, 1]$.

When $M = \infty$, the solutions of (1.1) are referred to as *large solutions*, or *blow-up solutions*, of

$$-u'' = \lambda u + a(t)u^p \tag{1.2}$$

in $(0, 1)$. In such case, the boundary condition should be understood as

$$\lim_{t\downarrow 0} u(t) = \infty, \qquad \lim_{t\uparrow 1} u(t) = \infty,$$

or, shortly, as

$$u(0) = u(1) = \infty.$$

Naturally, the limits as $M \uparrow \infty$ of the positive solutions of (1.1) should provide us with large solutions of (1.2) in $(0, 1)$. Consequently, both problems, the classical one with $M < \infty$ and the singular boundary value problem with $M = \infty$, are closely related, as we will see (cf. Sections (1.2) and (1.7)).

When $b = 0$, (1.1) is sublinear boundary value problem, while if $b > 0$, the nonlinearity of (1.1) changes sign in $(0, 1)$ and (1.1) becomes a superlinear indefinite boundary value problem, which is singular, if, in addition, $M = \infty$.

As remarked in the Introduction, the study of the superlinear indefinite case for $0 < M \leq \infty$ is, to the best of our knowledge, new, in spite of its simplicity. The main goal of this chapter is to ascertain the global bifurcation diagrams of (1.1) for $-\lambda > 0$ sufficiently large, using b as the main bifurcation parameter, and obtaining quasi-optimal multiplicity results in the appropriate ranges of values of the secondary parameter $\lambda < 0$.

As a result of the inhomogeneous boundary condition M, it turns out that there exists $m^* > 0$ such that (1.1) exhibits an arbitrarily large number of solutions for $M \in (m^*, \infty]$ and sufficiently large $-\lambda > 0$ provided

$$b = -\lambda/(u(\alpha))^{p-1}, \tag{1.3}$$

where $u(t)$ stands for the unique positive solution of

$$\begin{cases} -u'' = \lambda u - cu^p \quad \text{in} \ \ (0, \alpha) \\ u(0) = M, \ \ u'(\alpha) = 0. \end{cases} \tag{1.4}$$

Up to the best of our knowledge, this is the first example in which such a multiplicity result has been observed. Starting from this local result, we further perform a global continuation in the parameter b to construct all admissible bifurcation diagrams of (1.1), using b as the main parameter, at the values of $\lambda < 0$ where a precise multiplicity result holds.

The main tools which allow us to produce very precise bifurcation diagrams for equation (1.1) are based on a careful and detailed analysis of the time-maps associated to the corresponding phase plane systems. This approach had been

previously used to obtain some multiplicity results for other problems (see the Introduction for detailed references) but this is the first time in which it is used to determine a sharp multiplicity result for positive solutions and the structure of the bifurcation diagrams for superlinear indefinite problems. Moreover the treatment of both the cases $M \in \mathbb{R}$ and $M = \infty$ with the same techniques is new as well.

Except for the last section, where we adapt most of the previous results to the special case when $M = \infty$, this chapter focuses into the case $M < \infty$, and it is distributed as follows.

Section 1.2 analyzes the restriction of (1.1) to the intervals $(0, \alpha)$ and $(1-\alpha, 1)$, where (1.1) is a sublinear problem. Regarding the first interval $(0, \alpha)$, Section 1.2 characterizes the precise structure of the set of solutions of

$$\begin{cases} -u'' = \lambda u - cu^p & \text{in } (0, \alpha), \\ u(0) = M. \end{cases} \tag{1.5}$$

More precisely, if we denote by Σ_0 the set of solutions of (1.5), Section 1.2 shows that

$$\Gamma_{0,M} := \{\, (u(\alpha), u'(\alpha)) \ : \ u \in \Sigma_0 \,\}$$

is a differentiable strictly increasing curve. Similarly, if we denote by Σ_1 the set of solutions of

$$\begin{cases} -u'' = \lambda u - cu^p & \text{in } (1-\alpha, 1), \\ u(1) = M, \end{cases}$$

then,

$$\Gamma_{1,M} := \{\, (u(\alpha), u'(\alpha)) \ : \ u \in \Sigma_1 \,\}$$

is a differentiable decreasing curve. Actually, by the symmetries of (1.1), $\Gamma_{0,M}$ must be the reflection around the u-axis of $\Gamma_{1,M}$. The interest of these curves relies on the fact that the solutions of (1.1) restricted to the central interval $(\alpha, 1-\alpha)$ must be solutions of

$$-u'' = \lambda u + bu^p \tag{1.6}$$

linking $\Gamma_{0,M}$ with $\Gamma_{1,M}$ in a time $1 - 2\alpha$. Conversely, any solution of (1.6) satisfying this property provides us with a solution of (1.1). This technical device goes back to J. Mawhin, D. Papini and F. Zanolin [63].

Section 1.3 gives the main multiplicity result of this chapter through a systematic use of phase portrait techniques. Section 1.4 introduces a series of Poincaré maps which will provide us with the local and global bifurcation diagrams in b of the positive solutions of (1.1). Section 1.5 gives a series of global properties of these time maps which are going to be pivotal in constructing all the global bifurcation diagrams of Section 1.6. Finally, in Section 1.7 we adapt most of the previous results to cover the singular case when $M = \infty$.

1.2. The problem (1.1) in the interval $[0, \alpha]$

In the interval $[0, \alpha]$ the equation (1.2) reduces to

$$-u'' = \lambda u - cu^p, \tag{1.7}$$

which is autonomous, and, hence, phase portrait techniques can be applied to the equivalent first order system

$$\begin{cases} u' = v \\ v' = -\lambda u + cu^p \end{cases} \tag{1.8}$$

which admits the first integral

$$\phi(u, v) = v^2 + \lambda u^2 - \frac{2c}{p+1} u^{p+1}.$$

The main result of this section reveals the structure of the positive solutions of the Cauchy problem

$$\begin{cases} -u'' = \lambda u - cu^p \\ u(0) = M, \quad u'(0) = v \in \mathbb{R}, \end{cases} \tag{1.9}$$

in the interval $[0, \alpha]$, for sufficiently large $M > 0$. Obviously, these solutions include the restrictions to $[0, \alpha]$ of the positive solutions of (1.1). It can be stated as follows.

Theorem 1.1. *There exists a unique value of m, denoted by m^*, for which the unique solution of the Cauchy problem*

$$\begin{cases} -u'' = \lambda u - cu^p, \\ u(0) = m, \quad u'(0) = 0, \end{cases} \tag{1.10}$$

satisfies

$$u(t) > 0 \quad \textit{for all} \quad t \in [0, \alpha) \quad \textit{and} \quad \lim_{t \uparrow \alpha} u(t) = \infty.$$

For any $M \in (m^*, \infty)$, there exist $v_* < v^* < 0$ satisfying the following properties:

i) For every $v \in (v_*, v^*)$ the unique solution of (1.9) satisfies $u(t) > 0$ for all $t \in [0, \alpha]$.

ii) Let u_* denote the unique solution of (1.9) with $v = v_*$. Then, $u_*(t) > 0$ for all $t \in [0, \alpha)$ and $u_*(\alpha) = 0$.

iii) *Let u^* denote the unique solution of (1.9) with $v = v^*$. Then, $u^*(t) > 0$ for all $t \in [0, \alpha)$ and $\lim_{t\uparrow\alpha} u^*(t) = \infty$.*

iv) *For every $v > v^*$, there exists $T < \alpha$ such that the solution of (1.9) satisfies $u(t) > 0$ for all $t \in [0, T)$ and*

$$\lim_{t\uparrow T} u(t) = \infty.$$

v) *For every $v < v_*$, there exists $T_0 < \alpha$ such that the solution of (1.9) satisfies $u(t) > 0$ for all $t \in [0, T_0)$ and $u(T_0) = 0$.*

Consequently, the candidates to provide us with (positive) solutions of (1.1) are those of (1.9) with $v_* < v < v^*$.

Proof. The proof will be divided into several steps.

Step 1: Essentially, this step shows the existence and uniqueness of m^*. First, we focus our attention in case $\lambda > 0$. So, suppose $\lambda > 0$. Then, (1.8) has two non-negative equilibria. Namely, $(0, 0)$ and $(\omega, 0)$, where

$$\omega := \left(\frac{\lambda}{c}\right)^{\frac{1}{p-1}}. \tag{1.11}$$

As the generalized potential energy

$$\varphi(u) := \lambda u^2 - \frac{2c}{p+1} u^{p+1}$$

has a quadratic minimum at 0 and a quadratic maximum at ω, $(0, 0)$ must be a nonlinear center, while $(\omega, 0)$ is a saddle point of (1.8). Consequently, the phase portrait of the non-negative solutions of (1.7) looks like shown in Figure 1.1.

By simply looking at Figure 1.1, it becomes apparent that the solution of the problem (1.10) cannot blow-up at time $t = \alpha$ if $m \leq \omega$. So, suppose $m > \omega$ and denote by

$$t_{max} = t_{max}(m)$$

the global existence time of the solution of (1.10). Integrating the differential equation we find that, for every $t \in [0, t_{max})$,

$$t = \int_1^{u(t)/m} \frac{d\theta}{\sqrt{\frac{2c}{p+1} m^{p-1}(\theta^{p+1} - 1) - \lambda(\theta^2 - 1)}} \tag{1.12}$$

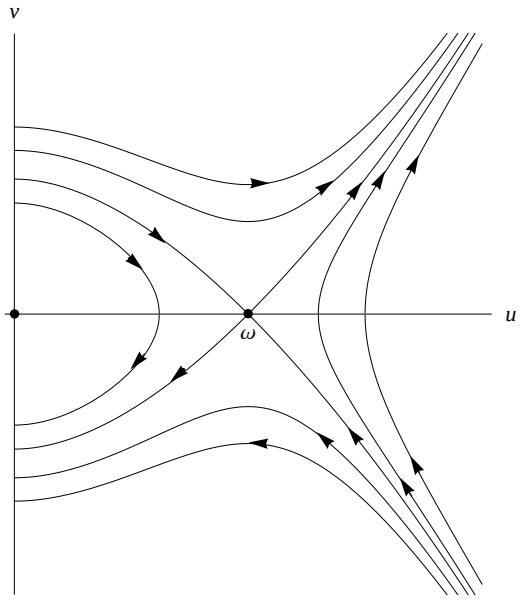

Figure 1.1: Phase diagram of (1.7) for $\lambda > 0$

and, hence,

$$t \leq \int_1^\infty \frac{d\theta}{\sqrt{\frac{2c}{p+1}m^{p-1}(\theta^{p+1}-1)-\lambda(\theta^2-1)}} < \infty.$$

Thus, $t_{max} < \infty$ and, therefore, u blows up at a finite time. Moreover, letting $t \uparrow t_{max}$ in (1.12), it becomes apparent that

$$t_{max}(m) = \int_1^\infty \frac{d\theta}{\sqrt{\frac{2c}{p+1}m^{p-1}(\theta^{p+1}-1)-\lambda(\theta^2-1)}}. \tag{1.13}$$

According to (1.13), $t_{max}(m)$ is decreasing with respect to m. Moreover, by continuous dependence,

$$\lim_{m\downarrow\omega} t_{max}(m) = \infty,$$

because $(\omega, 0)$ is an equilibrium, and letting $m \uparrow \infty$ in (1.13) leads to

$$\lim_{m\uparrow\infty} t_{max}(m) = 0.$$

Therefore, there exists a unique m^* $(> \omega)$ such that

$$t_{max}(m^*) = \alpha.$$

By construction,

$$t_{max}(m) \begin{cases} < t_{max}(m^*) = \alpha & \text{if } m > m^*, \\ > t_{max}(m^*) = \alpha & \text{if } m < m^*. \end{cases} \tag{1.14}$$

This shows the existence and the uniqueness of m^* when $\lambda > 0$. The previous proof can be easily adapted to cover the general case when $\lambda \leq 0$. In such case, the phase diagram looks like shown in Figure 1.2 and the proof of the case $\lambda > 0$ can be adapted *mutatis mutandis* to cover this case. So, the technical details of the proof in this special case are omitted.

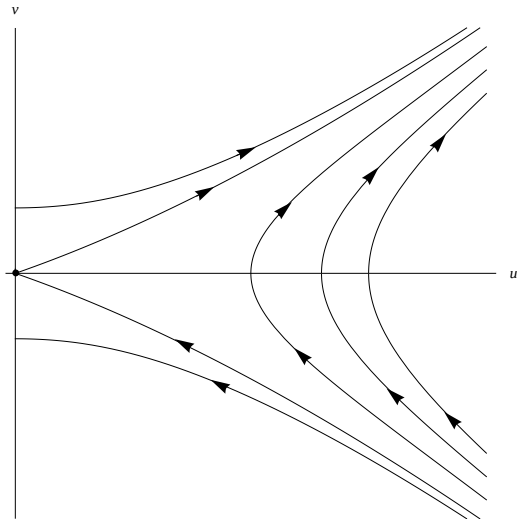

Figure 1.2: Phase diagram of (1.7) in case $\lambda \leq 0$

According to (1.14), the unique solution of (1.10) blows up in a time $t_{max}(m) \leq \alpha$ if $m \geq m^*$, while it is globally defined in the time interval $[0, \alpha]$ if $m < m^*$.

Step 2: Let $M > m^*$ be and denote by $v_u > 0$ the unique value of the derivative $v = u'$ for which (M, v_u) lies on the unstable manifold of $(\omega, 0)$ (resp. $(0, 0)$) if $\lambda > 0$ (resp. $\lambda \leq 0$). By symmetry, $(M, -v_u)$ is the unique point on the stable manifold of that equilibrium with $u = M$. Subsequently, for every $v \in (-v_u, 0)$, we consider the Cauchy problem (1.9). According to the phase portrait, it is apparent that the solution of (1.9) needs a time, say $t_{min} := t_{min}(v)$, to reach its minimum, denoted by $m := m(v)$. So, by symmetry,

$$m = u(t_{min}) \in (0, M), \qquad u'(t_{min}) = 0, \qquad u(2t_{min}) = M.$$

Actually, $m > \omega$ if $\lambda > 0$. Step 2 consists in showing that there exists a unique $v_0 \in (-v_u, 0)$ such that

$$t_{min}(v_0) = \alpha \quad \text{and} \quad t_{min}(v) \begin{cases} > \alpha & \text{if } v < v_0, \\ < \alpha & \text{if } v > v_0. \end{cases} \tag{1.15}$$

As a byproduct, the boundary value problem

$$\begin{cases} -u'' = \lambda u - cu^p, \\ u(0) = M, \quad u'(\alpha) = 0, \end{cases} \tag{1.16}$$

possesses a unique solution. Namely, the solution of (1.9) with $v = v_0$.

Indeed, by simply looking at the phase portrait of (1.7), it becomes apparent that the map $m : (-v_u, 0) \to \mathbb{R}^+$ is increasing, since two different trajectories cannot meet. Moreover,

$$\lim_{v \uparrow 0} m(v) = M \quad \text{and} \quad \lim_{v \downarrow -v_u} m(v) = \begin{cases} \omega & \text{if } \lambda > 0, \\ 0 & \text{if } \lambda \leq 0. \end{cases}$$

On the other hand, by integrating the differential equation, we are easily driven to the identity

$$t_{min}(v) = \int_1^{\frac{M}{m(v)}} \frac{d\theta}{\sqrt{\frac{2c}{p+1} m^{p-1}(v)(\theta^{p+1} - 1) - \lambda(\theta^2 - 1)}}. \tag{1.17}$$

Consequently, $t_{min}(v)$ is decreasing, because $m(v)$ increases with v. Moreover, $t_{min}(0) = 0$, by construction, and

$$\lim_{v \downarrow -v_u} t_{min}(v) = \infty,$$

by continuous dependence. Therefore, (1.15) holds for a unique $v_0 \in (-v_u, 0)$. This ends the proof of Step 2.

Setting

$$m_0 := m(v_0), \tag{1.18}$$

it follows from (1.14) that

$$m_0 < m^*,$$

since $t_{max}(m_0) > \alpha$.

Step 3. This step constructs v_* and v^* and completes the proof. It should be remembered that, according to Step 2, the solutions of (1.9) need a larger time than α to reach the u-axis if $v \in (-v_u, v_0)$, while they do it before time α if $v \in (v_0, 0)$.

Next, we suppose $M > m^*$ and consider the map

$$T : (-v_u, 0) \to \mathbb{R}^+$$

defined by

$$T(v) := t_{min}(v) + t_{max}(m(v)), \qquad v \in (-v_u, 0), \tag{1.19}$$

which measures the blow-up time of the solution of (1.9). According to Steps 1 and 2, T is continuous and decreasing. Moreover, by continuous dependence,

$$\lim_{v \downarrow -v_u} T(v) = \infty,$$

and, due to (1.14),

$$\lim_{v \uparrow 0} T(v) = t_{max}(M) < \alpha,$$

because $M > m^*$. Thus, there exists a unique

$$v^* := v^*(\lambda, c, p, M) \in (-v_u, 0)$$

such that

$$T(v^*) = \alpha \qquad \text{and} \qquad T(v) \begin{cases} > \alpha & \text{if } v \in (-v_u, v^*) \\ < \alpha & \text{if } v \in (v^*, 0). \end{cases} \tag{1.20}$$

Consequently, the solutions of (1.9) blow-up before time α if $v > v^*$, while they are globally defined in $[0,\alpha]$ if $v \in (-v_u, v^*)$. Moreover, $v = v^*$ is the unique shooting speed for which the solution of (1.9) blows-up at time α.

Now, we will study the behavior of the solutions of (1.9) with $v \leq -v_u$. By simply looking at the phase portrait of (1.7) (cf. Figures 1.1 and 1.2), it becomes apparent that such solutions vanish for some positive time if $v < -v_u$, while they stabilize to ω (resp. 0) if $\lambda > 0$ (resp. $\lambda \leq 0$) and $v = -v_u$ (of course in an infinite time). Integrating the differential equation, we find that the necessary time to reach the v-axis when $v < -v_u$, denoted by $T_0(v)$, is given through the formula

$$T_0(v) = \int_0^M \frac{du}{\sqrt{v^2 + \frac{2c}{p+1}(u^{p+1} - M^{p+1}) - \lambda(u^2 - M^2)}}.$$

Clearly, T_0 is a continuous and increasing function of v, since v^2 decreases if $v < 0$ grows. Moreover, by continuous dependence,

$$\lim_{v \uparrow -v_u} T_0(v) = \infty,$$

because $-v_u$ is the critical shooting speed of the stable manifold of the equilibrium. Also, letting $v \downarrow -\infty$, shows that

$$\lim_{v\downarrow-\infty} T_0(v) = 0.$$

Therefore, there exists a unique $v_* < -v_u$ such that

$$T_0(v_*) = \alpha.$$

Necessarily, by the definition of v_0 (cf. (1.15)),

$$v_* < v_0 < v^*,$$

because the solution of (1.9) for $v = v_0$ is positive in $[0, \alpha]$. From these features, the proof of the theorem can be easily completed. □

Figure 1.3 illustrates all the posible behaviors of the solutions of problem (1.9) according to the different ranges of values of the shooting speed v as discussed in Theorem 1.1. The profiles on the first row correspond to two solution plots of (1.9) for $v < v_*$ and $v = v_*$, respectively. By Theorem 1.1, v_* is the unique value of v for which the solution u of (1.9) satisfies $u(t) > 0$ for all $t \in [0, \alpha)$ and $u(\alpha) = 0$. If $v < v_*$, then u vanishes at some $t_0 < \alpha$.

The profiles on the second row are two solution plots for $v \in (v_*, v_0)$ and $v = v_0$, respectively. According to (1.15), v_0 is the unique value of v for which the solution u of (1.9) satisfies $u'(\alpha) = 0$, and, thanks to (1.18),

$$m_0 = u(\alpha).$$

By (1.15), $t_{min}(v) > \alpha$ if $v < v_0$, and, hence, $u'(\alpha) < 0$ if $v < v_0$, as illustrated by the first plot of the second row of Figure 1.3.

The third row of Figure 1.3 shows the plots of two (different) solutions of (1.9) for two values of $v \in (v_0, v^*)$. Finally, in the fourth row we have represented the plots of the solutions of (1.9) for $v = v^*$ and some $v > v^*$, respectively. In the first case, the solution blows-up at time $t = \alpha$, whereas the solution blows-up at some $T < \alpha$ if $v > v^*$.

Throughout the rest of this chapter, for every $\lambda \in \mathbb{R}$ and $M > m^*$ we denote by Σ_0 the set of solutions of (1.9) with $v \in [v_*, v^*)$ and consider the set of points of $\mathbb{R}^2$ reached by the solutions of (1.9) at time α as the shooting speed v ranges in between v_* and v^*,

$$\Gamma_0 := \{\, (u(\alpha), u'(\alpha)), \quad u \in \Sigma_0 \,\}. \tag{1.21}$$

The next result collects the main features of Γ_0.

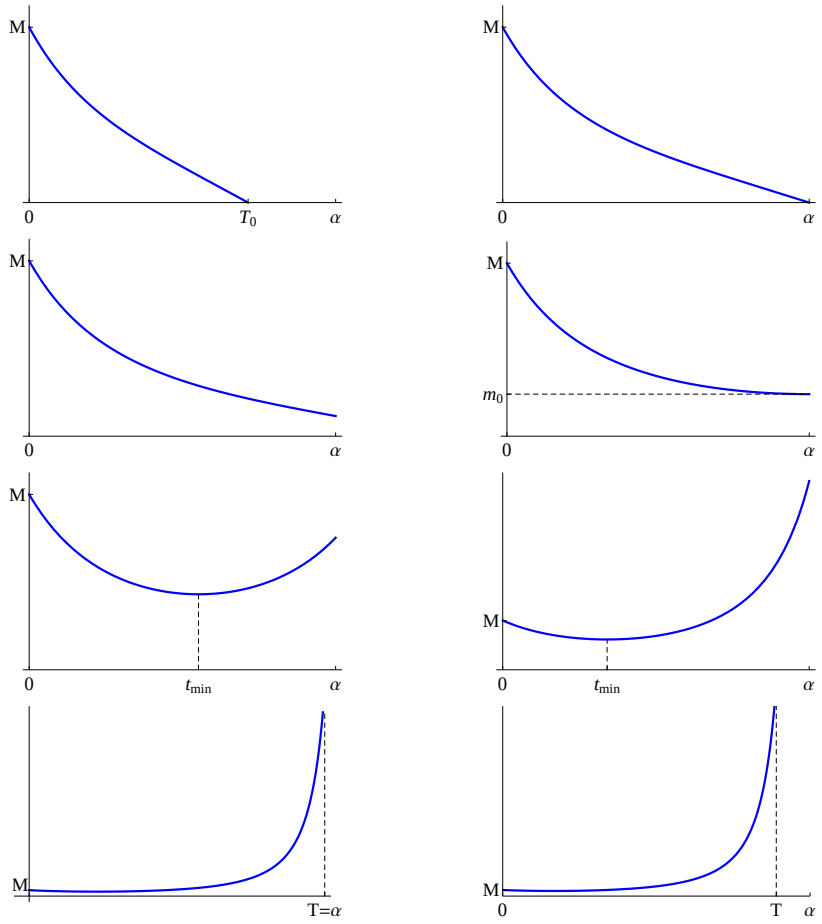

Figure 1.3: Plots of the solutions of (1.9) according to the value of v.

Theorem 1.2. *For every $\lambda \in \mathbb{R}$ and $M > m^*$, Γ_0 is a $\mathcal{C}^1$–curve in $\mathbb{R}^+ \times \mathbb{R}$ such that:*

i) $\pi_u(\Gamma_0) = \mathbb{R}^+$, where π_u stands for the projection of $\mathbb{R}^2$ on the first component.

ii) The value of m_0 defined by (1.18) satisfies the following properties:

$$\begin{aligned} (u, v) \in \Gamma_0, \quad u < m_0 \quad &\Longrightarrow \quad v < 0, \\ (u, v) \in \Gamma_0, \quad u > m_0 \quad &\Longrightarrow \quad v > 0. \end{aligned}$$

Note that, thanks to the proof of Theorem 1.1, $(m_0, 0) \in \Gamma_0$.

Proof. Consider the map

$$S : [v_*, v^*) \to \Sigma_0,$$

where, for every $v \in [v_*, v^*)$, $S(v)$ is the unique solution of (1.9), and the Poincaré map

$$\mathcal{P} : [v_*, v^*) \to \mathbb{R}^+ \times \mathbb{R}$$

defined through

$$\mathcal{P}(v) := (u(\alpha), u'(\alpha)), \qquad \text{where} \quad u := S(v) \in \Sigma_0.$$

Thanks to the proof of Theorem 1.1, $\mathcal{P}$ is well defined and

$$\Gamma_0 = \mathcal{P}\left([v_*, v^*)\right) = \operatorname{Im} \mathcal{P}.$$

According to the theorem of differentiation of G. Peano, $\mathcal{P}$ provides us with a diffeomorphism of $[v_*, v^*)$ onto $\operatorname{Im}\mathcal{P}$. Therefore, $\mathcal{P}$ establishes a diffeomorphism between $[v_*, v^*)$ and Γ_0. Consequently, Γ_0 is a curve of class $\mathcal{C}^1$ in $\mathbb{R}^+ \times \mathbb{R}$.

As π_u is a continuous map, $\pi_u(\Gamma_0)$ must be an interval and, since

$$\lim_{v \downarrow v_*} u(\alpha) = 0, \qquad \lim_{v \uparrow v^*} u(\alpha) = \infty,$$

we can infer that $\pi_u(\Gamma_0) = \mathbb{R}^+$, which ends the proof of Part i). Part ii) is an easy consequence from (1.15) and (1.18). This ends the proof. □

By performing the following inversion of temporal scale

$$s = 1 - t, \qquad t \in [1 - \alpha, 1].$$

one can easily infer the next counterpart of Theorem 1.1.

Corollary 1.3. *Let m^* be the value constructed by Theorem 1.1 and suppose $M > m^*$. Then, the unique solution of*

$$\begin{cases} -u'' = \lambda u - c u^p, \\ u(1) = m^*, \quad u'(1) = 0, \end{cases} \tag{1.22}$$

satisfies

$$u(t) > 0 \quad \textit{for all} \quad t \in (1 - \alpha, 1] \quad \textit{and} \quad \lim_{t \downarrow 1-\alpha} u(t) = \infty.$$

Moreover:

i) For every $v \in (-v^*, -v_*)$ the unique solution of

$$\begin{cases} -u'' = \lambda u - cu^p \\ u(1) = M, \quad u'(1) = v, \end{cases} \tag{1.23}$$

satisfies $u(t) > 0$ for all $t \in [1-\alpha, 1]$.

ii) Let u_* denote the unique solution of (1.23) with $v = -v_*$. Then, $u_*(t) > 0$ for all $t \in (1-\alpha, 1]$ and $u_*(1-\alpha) = 0$.

iii) Let u^* denote the unique solution of (1.23) with $v = -v^*$. Then, $u^*(t) > 0$ for all $t \in (1-\alpha, 1]$ and $\lim_{t\downarrow 1-\alpha} u^*(t) = \infty$.

iv) For every $v < -v^*$, there exists $t_{max} < \alpha$ such that the solution of (1.23) satisfies $u(t) > 0$ for all $t \in (1-t_{max}, 1]$ and

$$\lim_{t\downarrow 1-t_{max}} u(t) = \infty.$$

v) For every $v > -v_*$, there exists $t_0 < \alpha$ such that the solution of (1.23) satisfies $u(t) > 0$ for all $t \in (1-t_0, 1]$ and $u(1-t_0) = 0$.

Consequently, the candidates to provide us with positive solutions of (1.1) are those of (1.23) with $-v^* < v < -v_*$.

Throughout the rest of this chapter, for every $\lambda \in \mathbb{R}$ and $M > m^*$ we denote by Σ_1 the set of solutions of (1.23) with $v \in (-v^*, -v_*]$ and consider the set of points of $\mathbb{R}^2$ reached by the solutions of (1.23) at time $1-\alpha$ as v ranges in between $-v^*$ and $-v_*$,

$$\Gamma_1 := \{\, (u(1-\alpha), u'(1-\alpha)), \quad u \in \Sigma_1 \,\}. \tag{1.24}$$

Obviously, the next counterpart of Theorem 1.2 holds.

Corollary 1.4. *For every $\lambda \in \mathbb{R}$ and $M > m^*$, Γ_1 is a $\mathcal{C}^1$–curve of $\mathbb{R}^+ \times \mathbb{R}$ such that*

$$\Gamma_1 = \{\, (u, -v) \ : \ (u, v) \in \Gamma_0 \,\}.$$

In particular, $\pi_u(\Gamma_1) = \mathbb{R}^+$ and

$$\begin{aligned} (u,v) \in \Gamma_1, \quad u < m_0 \quad &\Longrightarrow \quad v > 0, \\ (u,v) \in \Gamma_1, \quad u > m_0 \quad &\Longrightarrow \quad v < 0. \end{aligned}$$

The next result establishes that Γ_0 is an increasing arc of curve with respect to u.

Proposition 1.5. *For every $\lambda \in \mathbb{R}$, $M > m^*$ and $t \in (0, \alpha]$, the following holds*

$$v_* \leq v_1 < v_2 < v^* \quad \Longrightarrow \quad u_1(t) < u_2(t) \quad \text{and} \quad u_1'(t) < u_2'(t),$$

where u_i stands for the unique solution of

$$\begin{cases} -u'' = \lambda u - cu^p \\ u(0) = M, \;\; u'(0) = v_i \in \mathbb{R}, \end{cases} \qquad i \in \{1, 2\}.$$

Proof. First, we will show the monotonicity of u. Suppose $u_1(\tilde{t}) \geq u_2(\tilde{t})$ for some $0 < \tilde{t} \leq \alpha$. Then, as $u_1(t) < u_2(t)$ for sufficiently small $t > 0$, there exists $\theta \in (0, \tilde{t}]$ such that

$$u_1(\theta) = u_2(\theta)$$

and, hence, setting $N := u_1(\theta)$, u_1 and u_2 are solutions of the boundary value problem

$$\begin{cases} -u'' = \lambda u - cu^p \\ u(0) = M, \;\; u(\theta) = N. \end{cases} \tag{1.25}$$

According to the main theorem of S. Cano-Casanova [16], (1.25) has a unique positive solution in $[0, \theta]$. Therefore, $u_1 = u_2$ in $[0, \theta]$, which implies $v_1 = v_2$. As this is a contradiction, necessarily $u_1(t) < u_2(t)$ for all $t \in (0, \alpha]$.

Next, suppose that $u_1'(\tilde{t}) \geq u_2'(\tilde{t})$ for some $\tilde{t} \in (0, \alpha]$. Then, as

$$u_1'(0) = v_1 < u_2'(0) = v_2,$$

there exists $\theta \in (0, \tilde{t}]$ such that

$$u_1'(\theta) = u_2'(\theta).$$

Setting $N := u_1'(\theta)$, it is apparent that u_1 and u_2 solve

$$\begin{cases} -u'' = \lambda u - cu^p \\ u(0) = M, \;\; u'(\theta) = N, \end{cases}$$

and, owing again to S. Cano-Casanova [16], we find that $u_1 = u_2$ and, therefore, $v_1 = v_2$, which is impossible. This completes the proof. □

In Figure 1.4 we have represented two admissible curves Γ_0 and Γ_1 according to Theorem 1.2, Corollary 1.4 and Proposition 1.5. By Corollary 1.4, Γ_1 is the reflection of Γ_0 around the u-axis.

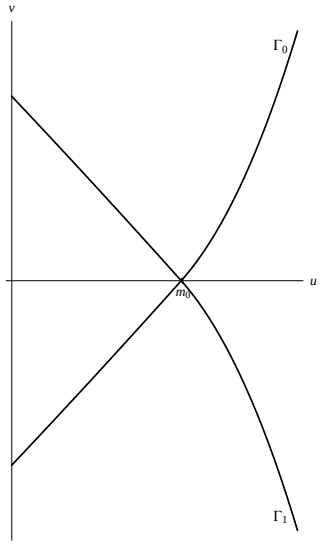

Figure 1.4: The curves Γ_0 and Γ_1

Our interest in the curves Γ_0 and Γ_1 comes from the fact that the solutions of the nonlinear boundary value problem (1.1) are given through the solutions of the autonomous equation

$$-u'' = \lambda u + bu^p \tag{1.26}$$

connecting the curves Γ_0 and Γ_1 in the phase portrait of (u, u') in time $1-2\alpha$. Note that $1-2\alpha$ is the length of the subinterval $(\alpha, 1-\alpha)$ of $(0,1)$ where (1.2) becomes (1.26). More precisely, let $(u_i, v_i) \in \Gamma_i$, $i = 0, 1$, for which there exists a solution of (1.26), say u_c, such that

$$(u_c(\alpha), u_c'(\alpha)) = (u_0, v_0), \qquad (u_c(1-\alpha), u_c'(1-\alpha)) = (u_1, v_1),$$

and let u_ℓ and u_r be the solutions of (1.7) in $[0, \alpha]$ and $[1-\alpha, 1]$ such that

$$u_\ell(0) = M, \quad (u_\ell(\alpha), u_\ell'(\alpha)) = (u_0, v_0),$$

and

$$(u_r(1-\alpha), u_r'(1-\alpha)) = (u_1, v_1), \qquad u_r(1) = M,$$

respectively. Then, the function

$$u(t) := \begin{cases} u_\ell(t), & \text{if } t \in [0, \alpha], \\ u_c(t), & \text{if } t \in (\alpha, 1-\alpha), \\ u_r(t), & \text{if } t \in [1-\alpha, 1], \end{cases}$$

provides us with a solution of the superlinear indefinite problem (1.1).

This section concludes with a further fundamental property of Γ_0 which will be used throughout the rest of this chapter.

Theorem 1.6. *Suppose $\lambda \leq 0$ and $M > m^*$. Then, there exists a unique function of class $\mathcal{C}^1$, $y : [0, \infty) \to \mathbb{R}$, such that*

$$\Gamma_0 := \{\, (x, y(x)) \ : \ x \geq 0 \,\}.$$

Moreover,

$$y'(x) > 0 \qquad \text{for all } \ x \geq 0.$$

Actually, if $(x, y(x)) = \mathcal{P}(v)$, $v \in [v_*, v^*)$, i.e., $x = \pi_u(\mathcal{P}(v))$, then,

$$y'(x) = \frac{\xi'(\alpha)}{\xi(\alpha)},$$

where ξ stands for the unique solution of

$$\begin{cases} -\xi'' = (\lambda - cpu^{p-1})\,\xi \\ \xi(0) = 0, \ \ \xi'(0) = 1, \end{cases}$$

u being the solution of

$$\begin{cases} -u'' = \lambda u - cu^p \\ u(0) = M, \ \ u'(0) = v. \end{cases}$$

Proof. Subsequently, the notations introduced in the proof of Theorem 1.2 will be maintained. By definition,

$$\mathcal{P}(v) = \left(S(v)(\alpha), \frac{d}{dt} S(v)(\alpha) \right)$$

for all $v \in [v_*, v^*)$, where $S(v)$ is the unique solution of

$$\begin{cases} -\frac{d^2}{dt^2} S(v) = \lambda S(v) - c(S(v))^p \\ S(v)(0) = M, \ \ \frac{d}{dt} S(v)(0) = v. \end{cases}$$

Thus, according to the theorem of differentiation of G. Peano, we have that

$$D\mathcal{P}(v) = \left(DS(v)(\alpha), \frac{d}{dt} DS(v)(\alpha) \right)$$

for all $v \in [v_*, v^*)$, where $DS(v)$ is the unique solution of

$$\begin{cases} -\frac{d^2}{dt^2} DS(v) = (\lambda - cp(S(v))^{p-1})\, DS(v) \\ DS(v)(0) = 0, \ \ \frac{d}{dt} DS(v)(0) = 1. \end{cases}$$

As we are imposing $\lambda \leq 0$, and, due to Proposition 1.5,

$$DS(v)(t) \geq 0$$

for all $t \in [0, \alpha]$ and $v \in [v_*, v^*)$, we obtain that

$$-\frac{d^2}{dt^2} DS(v) \leq 0 \qquad \text{in } [0, \alpha]$$

for all $v \in [v_*, v^*)$. Consequently,

$$DS(v)(\alpha) > 0 \qquad \text{and} \qquad \frac{d}{dt} DS(v)(\alpha) > 0.$$

Therefore, the two components of $DP(v)$ are positive real numbers for all $v \in [v_*, v^*)$. As $DP(v)$ is the tangent vector to the curve Γ_0 at $P(v)$ for all $v \in [v_*, v^*)$, the rest of the proof follows easily from well known features on differential geometry of curves. □

1.3. Multiplicity results for the superlinear indefinite problem

Throughout this section we impose that $\lambda < 0$ and $b = b^*$, where

$$b^* := -\lambda / m_0^{p-1},$$

being m_0 the one introduced in (1.18). Under this conditions, the following result holds.

Theorem 1.7. *Suppose*

$$b = -\lambda / m_0^{p-1}. \tag{1.27}$$

Then, the number of solutions of (1.1) grows up to infinity as $\lambda \downarrow -\infty$. More precisely, if

$$\lambda < -\frac{4\lambda_\alpha}{p-1} n^2 \quad \text{for some integer } n \geq 1, \tag{1.28}$$

where we are denoting

$$\lambda_\alpha := \left(\frac{\pi}{1 - 2\alpha} \right)^2,$$

then, (1.1) possesses, at least, $4n$ solutions; among them, $2n$ are symmetric and the remaining $2n$ are asymmetric.

Proof. As $\lambda < 0$, (1.26) has two equilibria. Namely, 0 and the positive steady-state

$$\Omega := \left(\frac{-\lambda}{b}\right)^{\frac{1}{p-1}}. \tag{1.29}$$

According to (1.27), it turns out that

$$\Omega = m_0. \tag{1.30}$$

The first order system associated to (1.26) admits the first integral

$$\psi(u, v) := v^2 + \lambda u^2 + \frac{2b}{p+1}u^{p+1}$$

whose generalized potential energy is

$$\varphi(u) := \lambda u^2 + \frac{2b}{p+1}u^{p+1}.$$

As φ has a quadratic maximum at 0 and a quadratic minimum at Ω, $(0, 0)$ is a saddle point and $(\Omega, 0)$ is a center. Moreover, as $\varphi(u)$ is a potential well, there is an homoclinic connection of $(0, 0)$ surrounding $(\Omega, 0)$ and any periodic orbit around $(\Omega, 0)$. Figure 1.5 sketches the phase portrait of (1.26) in case $\lambda < 0$, as well as the curves Γ_0 and Γ_1.

Naturally, by the definition of m_0 (cf. (1.18)), if $u_\ell(t)$ stands for the unique solution of

$$\begin{cases} -u'' = \lambda u - cu^p, \\ u(0) = M, \quad u(\alpha) = m_0, \end{cases}$$

then, the function

$$u_0(t) := \begin{cases} u_\ell(t), & t \in [0, \alpha], \\ m_0, & t \in (\alpha, 1-\alpha), \\ u_\ell(1-t), & t \in [1-\alpha, 1], \end{cases}$$

provides us with a symmetric solution of problem (1.1). Throughout the rest of the chapter we will call this function the *trivial solution*.

To construct more solutions, one should note that the limiting period of the small amplitude periodic oscillations around $(\Omega, 0)$, as the amplitude goes down to zero, equals the period of the solutions of the linearized equation

$$-u'' = \lambda u + pb\Omega^{p-1}u = \lambda(1-p)u,$$

which is given through

$$\tau_\Omega := \frac{2\pi}{\sqrt{\lambda(1-p)}}. \tag{1.31}$$

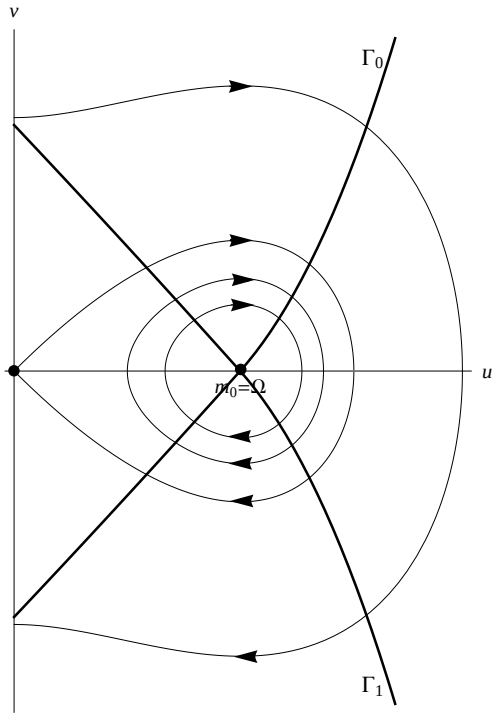

Figure 1.5: Phase portrait of (1.26) under condition (1.27)

Having a glance at Figure 1.5 it becomes apparent from Theorem 1.6 that Γ_0 meets the homoclinic of $(0,0)$ twice. Let (x_0^-, y_0^-) denote the second crossing point, as time passes by, between them. By Theorem 1.6, $y_0^- = y(x_0^-)$. Note that $x_0^- < \Omega$. For every $(x,y) \in \Gamma_0$ with $x \in (x_0^-, \Omega)$ (necessarily $y = y(x)$), consider the initial value problem

$$\begin{cases} -u'' = \lambda u + bu^p, \\ u(0) = x, \quad u'(0) = y(x). \end{cases} \tag{1.32}$$

Let $\tau_1(x)$ denote the time taken by the trajectory of the solution of (1.32) to reach Γ_1 for the first time, and $\tau(x)$ the period of the solution of (1.32). By definition, $\tau_1(x) < \tau(x)$ for all $x \in (x_0^-, \Omega)$. Thus, by continuous dependence and taking into account that

$$\lim_{x \uparrow \Omega} \tau(x) = \tau_\Omega,$$

it is easily seen that

$$\lim_{x \downarrow x_0^-} \tau_1(x) = \infty \quad \text{and} \quad \limsup_{x \uparrow \Omega} \tau_1(x) \leq \tau_\Omega. \tag{1.33}$$

Thus, if we assume that

$$\tau_\Omega = \frac{2\pi}{\sqrt{\lambda(1-p)}} < 1-2\alpha \quad \Longleftrightarrow \quad \lambda < -\frac{4\lambda_\alpha}{p-1}, \tag{1.34}$$

then, $\tau_1(x) < 1-2\alpha$ for some $x < \Omega$, $x \sim \Omega$, and, hence, by the continuity of τ_1 in (x_0^-, x) along Γ_0, there exists $(x_1, y_1) \in \Gamma_0$, $y_1 = y(x_1)$, with $x_1 \in (x_0^-, x)$ such that

$$\tau_1(x_1) = 1-2\alpha;$$

τ_1 is continuous by the transversality of the trajectories with the curves Γ_0 and Γ_1. Consequently, reasoning as at the end of Section 1.2, the unique solution of (1.26) such that

$$(u(\alpha), u'(\alpha)) = (x_1, y_1)$$

provides us with another symmetric solution of (1.1) having a unique critical point (a local minimum) in the interval $(\alpha, 1-\alpha)$.

Now, for every $(x, y) \in \Gamma_0$ with $x \in (x_0^-, \Omega)$, let $\tau_2(x)$ denote the necessary time to reach Γ_1 exactly twice. As for (1.33), (1.34) implies that

$$\lim_{x \downarrow x_0^-} \tau_2(x) = \infty \quad \text{and} \quad \limsup_{x \uparrow \Omega} \tau_2(x) \le \tau_\Omega < 1-2\alpha$$

and, therefore, there exists $(x_2, y_2) \in \Gamma_0$ ($y_2 = y(x_2)$), with $x_2 \in (x_0, \Omega)$, such that

$$\tau_2(x_2) = 1-2\alpha.$$

Consequently, the unique solution of (1.26) such that

$$(u(\alpha), u'(\alpha)) = (x_2, y_2)$$

provides us with an asymmetric solution of (1.1) under condition (1.34). This solution has two critical points in $(\alpha, 1-\alpha)$: a local minimum and a local maximum. Naturally, if we denote it by $u(t)$, then, the reflected function

$$\tilde{u}(t) := u(1-t), \qquad t \in [0,1],$$

provides us with another asymmetric solution of (1.1). The associated orbit $(\tilde{u}, \tilde{u}')$ leaves Γ_0 at $\tilde{u}(\alpha) > m_0$ and meets Γ_1 twice ending on it. This solution also has a local minimum and a local maximum.

The four solutions that we have just constructed have been represented in the first row of Figure 1.6. It should be noted that they do exist provided (1.34) holds, which has been emphasized in the first column of Figure 1.6, where the requested *conditions* for the existence of the solutions of the corresponding row are given. Except for the solutions of the first column, the remaining

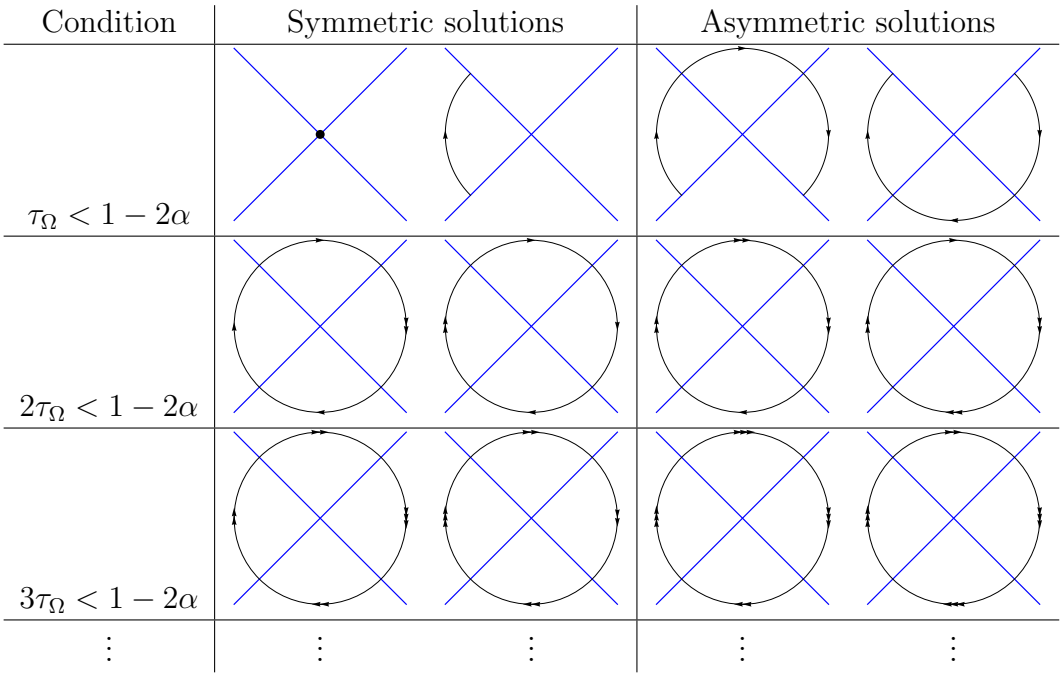

Figure 1.6: The restriction of the solutions of (1.1) to $[\alpha, 1-\alpha]$ when $b = b^*$

solutions of Figure 1.6 are constructed by adding $n \geq 1$ laps around $(\Omega, 0)$ to the solution at the top of the corresponding column.

Figure 1.6 consists of 12 pictures and three conditions. Each of the pictures exhibits two crossing curves. As we move from the left to the right, one of them increases and the other decreases. The one increasing represents Γ_0, whereas the decreasing one stands for Γ_1. The arcs of curve connecting them stand for trajectories of solutions of (1.26). The number of arrows counts how many times the corresponding piece of trajectory between Γ_0 and Γ_1 is run. One always has to start at Γ_0 and end at Γ_1.

Next, we will construct the first solution of the second column. Let (x_0^+, y_0^+) be the first crossing point, as time passes by, between Γ_0 and the homoclinic of $(0,0)$. Obviously, $\Omega < x_0^+$ and, thanks to Theorem 1.6, $y_0^+ = y(x_0^+)$. For every $(x,y) \in \Gamma_0$ with $x \in (\Omega, x_0^+)$, let $\tau_3(x)$ denote the time needed by the solution of (1.32) to reach Γ_1 for the first time after a complete lap. By definition, $\tau_3 < 2\tau_\Omega$ and, arguing as above, it becomes apparent that

$$\lim_{x \uparrow x_0^+} \tau_3(x) = \infty \quad \text{and} \quad \limsup_{x \downarrow \Omega} \tau_3(x) \leq 2\tau_\Omega.$$

Consequently, under condition

$$2\frac{2\pi}{\sqrt{\lambda(1-p)}} < 1-2\alpha \quad \Longleftrightarrow \quad \lambda < -\frac{4\lambda_\alpha}{p-1}2^2, \tag{1.35}$$

there exists $(x_3, y_3) \in \Gamma_0$ with $x_3 > \Omega$ such that $\tau_3(x_3) = 1-2\alpha$. As in all previous cases, the unique solution of (1.26) satisfying

$$(u(\alpha), u'(\alpha)) = (x_3, y_3)$$

provides us with a symmetric solution of (1.1) which has three critical points in $(\alpha, 1-\alpha)$: two local maxima and one local minimum. The remaining solutions of the first column of Figure 1.6 are constructed from this one by adding an additional lap every time we pass from one row to the next one, as it happens with the remaining three columns. Consequently, under condition

$$n\tau_\Omega < 1-2\alpha \quad \Longleftrightarrow \quad \lambda < -\frac{4\lambda_\alpha}{p-1}n^2, \tag{1.36}$$

(1.1) possesses, at least, $4n$ solutions, $2n$ among them being symmetric (those on the first two columns), and the remaining $2n$ solutions (those on the last two columns) asymmetric. The proof is complete. □

By Theorem 1.7, it is natural to introduce the following concept.

Definition 1.8. A solution u of (1.1) is said to be of type $n \geq 0$, which can be shortly expressed by writing $u \in T_n$, if it has $n \geq 0$ strict critical points in the central interval $(\alpha, 1-\alpha)$. According to this terminology, the trivial solution u_0 is of type 0, i.e., $u_0 \in T_0$.

The proof of Theorem 1.7 reveals that, under conditions (1.27) and (1.28), the problem (1.1) has, at least, one solution of type 1 and two solutions of type j, for every $j \in \{1, ..., n\}$, besides the trivial solution (cf. Figure 1.6).

1.3.1. A sharp pivotal property of the time-map τ_1

The time map τ_1 defined in the proof of Theorem 1.7 can be extended for every $x > \Omega$ in a natural way. Indeed, for each $x > \Omega$, $\tau_1(x)$ is the minimal necessary time to reach Γ_1 by the solution of the problem (1.32), where $y(x)$ is the function introduced by Theorem 1.6. The extended function τ_1 is defined in $(x_0^-, \infty) \setminus \{\Omega\}$. The next result shows that the singularity Ω can be overcome.

Theorem 1.9. *Suppose* $\lambda < 0$ *and* (1.27). *Then,*

$$\lim_{x\uparrow\Omega} \tau_1(x) = \frac{2}{\sqrt{\lambda(1-p)}} \arctan \frac{y'(\Omega)}{\sqrt{\lambda(1-p)}} = \lim_{x\downarrow\Omega} \tau_1(x). \tag{1.37}$$

Consequently, $\tau_1 \in \mathcal{C}(u_0, \infty)$ *if we extend* τ_1 *by setting*

$$\tau_1(\Omega) := \frac{2}{\sqrt{\lambda(1-p)}} \arctan \frac{y'(\Omega)}{\sqrt{\lambda(1-p)}} > 0.$$

Moreover,

$$\lim_{x\downarrow x_0^-} \tau_1(x) = \infty, \qquad \lim_{x\uparrow\infty} \tau_1(x) = 0.$$

The value $y'(\Omega)$ has already been calculated in Theorem 1.6.

Proof. Suppose $x < \Omega = m_0$, $x \sim \Omega$, and let $x_L < x < \Omega$ be the unique $x_L = x_L(x)$ for which the trajectory of the solution of (1.32) reaches $(x_L, 0)$ at a (minimal) time $\tau_1(x)/2$. As the nonlinearity of (1.32) is analytic at Ω, the differential equation of (1.32) can be equivalently written as follows

$$-(u-\Omega)'' = \lambda(1-p)(u-\Omega) + \sum_{j\geq 2} h_j (u-\Omega)^j, \qquad u \sim \Omega, \tag{1.38}$$

for some coefficients h_j, $j \geq 2$, whose knowledge is not relevant in this proof; the series being absolutely convergent in some interval around Ω. Multiplying (1.38) by $(u-\Omega)' = u'$ and rearranging terms, we are driven to

$$\frac{d}{dt}\left\{ \frac{[(u-\Omega)']^2}{2} + \frac{\lambda(1-p)}{2}(u-\Omega)^2 + \sum_{j\geq 2} \frac{h_j}{j+1}(u-\Omega)^{j+1} \right\} = 0.$$

Therefore, the orbit of the periodic solution of (1.32) is given through

$$v^2 + \lambda(1-p)(u-\Omega)^2 + \sum_{j\geq 3} c_j (u-\Omega)^j = E,$$

where

$$v := u' = (u-\Omega)', \qquad c_{j+1} := 2h_j/(j+1), \quad j \geq 2,$$

and

$$E = y^2(x) + \lambda(1-p)(x-\Omega)^2 + \sum_{j\geq 3} c_j (x-\Omega)^j.$$

Consequently, shortening the notations by setting

$$\Sigma_\xi(x) := \sum_{j\geq 3} c_j(x-\xi)^j, \qquad x \sim \xi,$$

it is easily seen that

$$\tau_1(x) = 2\int_{x_L}^{x} \frac{du}{\sqrt{y^2(x)+\lambda(1-p)(x-\Omega)^2+\Sigma_\Omega(x)-\lambda(1-p)(u-\Omega)^2-\Sigma_\Omega(u)}}.$$

Equivalently, by performing the change of variable $\theta = u-\Omega$, $u \sim \Omega$,

$$\tau_1(x) = 2\int_{x_L-\Omega}^{x-\Omega} \frac{d\theta}{\sqrt{y^2(x)+\lambda(1-p)(x-\Omega)^2+\Sigma_\Omega(x)-\lambda(1-p)\theta^2-\Sigma_0(\theta)}}. \quad (1.39)$$

On the other hand, since

$$x_L - \Omega < \theta = u - \Omega < x - \Omega < 0$$

implies

$$|\theta| \leq |x_L - \Omega|,$$

we find the estimate

$$|\Sigma_0(\theta)| \leq \sum_{j\geq 3} |c_j||\theta|^j \leq \sum_{j\geq 3} |c_j||x_L-\Omega|^j. \quad (1.40)$$

Consequently, shortening the notations by naming

$$h_\pm(x,x_L) := y^2(x) + \lambda(1-p)(x-\Omega)^2 + \Sigma_\Omega(x) \pm \sum_{j\geq 3} |c_j||x_L-\Omega|^j \quad (1.41)$$

and

$$I_\pm(x,x_L) := 2\int_{x_L-\Omega}^{x-\Omega} \frac{d\theta}{\sqrt{h_\pm(x,x_L)-\lambda(1-p)\theta^2}} \quad (1.42)$$

it follows from (1.39) and (1.40) that

$$I_+(x,x_L) \leq \tau_1(x) \leq I_-(x,x_L)$$

and, therefore, to prove the first identity of (1.37) it suffices to show that

$$\lim_{x\uparrow\Omega} I_\pm(x,x_L(x)) = \frac{2}{\sqrt{\lambda(1-p)}} \arctan \frac{y'(\Omega)}{\sqrt{\lambda(1-p)}}. \quad (1.43)$$

It should be noted that, in order to do this, we must make sure that the functions

$$g(\theta) := h_{\pm}(x, x_L) - \lambda(1-p)\theta^2, \qquad x_L - \Omega \le \theta \le x - \Omega,$$

are non-negative, at least for x in a neighborhood of Ω.

Through some elementary manipulations, it is easily seen that (1.42) implies

$$I_{\pm}(x, x_L(x)) = \frac{2}{\sqrt{\lambda(1-p)}} \int_{\sqrt{\lambda(1-p)}(x_L-\Omega)/\sqrt{h_{\pm}(x,x_L)}}^{\sqrt{\lambda(1-p)}(x-\Omega)/\sqrt{h_{\pm}(x,x_L)}} \frac{d\theta}{\sqrt{1-\theta^2}}$$

$$= \frac{2}{\sqrt{\lambda(1-p)}} \left[\arcsin\left(\frac{\sqrt{\lambda(1-p)}(x-\Omega)}{\sqrt{h_{\pm}(x,x_L)}} \right) - \arcsin\left(\frac{\sqrt{\lambda(1-p)}(x_L-\Omega)}{\sqrt{h_{\pm}(x,x_L)}} \right) \right].$$

Now, we need to ascertain the asymptotic expansion of $x_L(x)$ in terms of $x-\Omega$, as $x \uparrow \Omega$. As the solution of (1.32) satisfies

$$\frac{d}{dt}\left(\frac{v^2}{2} + \frac{\lambda}{2}\, u^2 + \frac{b}{p+1}\, u^{p+1} \right) = 0, \tag{1.44}$$

necessarily

$$y^2(x) + \lambda x^2 + \frac{2b}{p+1}\, x^{p+1} = \lambda\, x_L^2(x) + \frac{2b}{p+1}\, x_L^{p+1}(x) \tag{1.45}$$

for all $x < \Omega$, $x \sim \Omega$. By Theorem 1.6, we already know that

$$y(x) = y'(\Omega)(x-\Omega) + o(x-\Omega) \quad \text{as} \quad x \to \Omega. \tag{1.46}$$

Moreover, a direct calculation shows that

$$\lambda x^2 + \frac{2b}{p+1}\, x^{p+1} = \lambda\Omega^2 + \frac{2b}{p+1}\, \Omega^{p+1} + \lambda(1-p)(x-\Omega)^2 + O((x-\Omega)^3) \quad \text{as} \quad x \to \Omega,$$

because $\Omega^{p-1} = -\lambda/b$. Thus, substituting these expansions into (1.45) and rearranging terms, it follows that

$$\lambda x_L^2(x) + \frac{2b}{p+1}\, x_L^{p+1}(x) =$$
$$= \lambda\Omega^2 + \frac{2b}{p+1}\, \Omega^{p+1} + [(y'(\Omega))^2 + \lambda(1-p)](x-\Omega)^2 + o((x-\Omega)^2)$$

as $x \uparrow \Omega$. By expanding the left hand side of this identity in powers of $x - \Omega$, or, alternatively, differentiating twice with respect to x and particularizing at $x = \Omega$, it becomes apparent that

$$x_L(x) = \Omega + \sqrt{1 + \frac{(y'(\Omega))^2}{\lambda(1-p)}}\,(x - \Omega) + o(x - \Omega) \tag{1.47}$$

as $x \uparrow \Omega$. Actually, x_L is a function of class $\mathcal{C}^\infty$ in a neighborhood of Ω by the theorem of differentiation of G. Peano, because $y(x)$, and so Γ_0, is of class $\mathcal{C}^\infty$ outside the origin. Consequently, substituting (1.46) and (1.47) into (1.41), we are lead to

$$h_\pm(x, x_L(x)) = [(y'(\Omega))^2 + \lambda(1-p)](x - \Omega)^2 + o((x - \Omega)^2).$$

Using these asymptotic expansions, it is straightforward to check that the function $g(\theta)$ defined above is indeed non-negative and that

$$\lim_{x\uparrow\Omega} \frac{\sqrt{\lambda(1-p)}(x-\Omega)}{\sqrt{h_\pm(x, x_L)}} = \frac{-\sqrt{\lambda(1-p)}}{\sqrt{(y'(\Omega))^2 + \lambda(1-p)}} = \frac{-1}{\sqrt{\frac{(y'(\Omega))^2}{\lambda(1-p)} + 1}}.$$

As a byproduct, by (1.47), we also have that

$$\lim_{x\uparrow\Omega} \frac{\sqrt{\lambda(1-p)}(x_L-\Omega)}{\sqrt{h_\pm(x, x_L)}} = -1.$$

Consequently, letting $x \uparrow \Omega$, it becomes apparent that

$$\lim_{x\uparrow\Omega} I_\pm(x, x_L(x)) = \frac{2}{\sqrt{\lambda(1-p)}} \left[\frac{\pi}{2} - \arcsin\left(\frac{1}{\sqrt{\frac{(y'(\Omega))^2}{\lambda(1-p)} + 1}}\right)\right]$$

$$= \frac{2}{\sqrt{\lambda(1-p)}} \arctan \frac{y'(\Omega)}{\sqrt{\lambda(1-p)}}.$$

This proves (1.43) and ends the proof of the first identity of (1.37). The previous argument can be easily adapted, with the appropriate necessary changes, to show the validity of the second identity of (1.37). Therefore, we omit the technical details here. The fact that $\tau_1(x) \to \infty$ as $x \downarrow x_0^-$ was already shown in the proof of Theorem 1.7. To conclude the proof it remains to show that

$$\lim_{x\uparrow\infty} \tau_1(x) = 0. \tag{1.48}$$

Subsequently, for every $x > \Omega$, we denote by $x_M = x_M(x) > x$ the first crossing point of the trajectory of the solution of (1.32) with the u-axis in its phase portrait. Going back to (1.44), it is apparent that the solution of (1.32) satisfies

$$v^2 + \lambda u^2 + \frac{2b}{p+1}\, u^{p+1} = \lambda x_M^2 + \frac{2b}{p+1} x_M^{p+1}$$

and, hence, for every $x > x_0^+$,

$$\begin{aligned}
\tau_1(x) &= 2\int_x^{x_M} \frac{du}{\sqrt{\lambda(x_M^2 - u^2) + \frac{2b}{p+1}(x_M^{p+1} - u^{p+1})}} \\
&= 2\int_{x/x_M}^1 \frac{d\theta}{\sqrt{\lambda(1-\theta^2) + \frac{2b}{p+1} x_M^{p-1}(1-\theta^{p+1})}} \\
&< 2\int_0^1 \frac{d\theta}{\sqrt{\lambda(1-\theta^2) + \frac{2b}{p+1} x_M^{p-1}(1-\theta^{p+1})}}.
\end{aligned}$$

As $\lim_{x\uparrow\infty} x_M(x) = \infty$, letting $x \uparrow \infty$ in the previous estimate shows (1.48) and ends the proof. □

As expected, the value of $\tau_1(\Omega)$ for the nonlinear problem (1.32) given through Theorem 1.9 coincides with the value of $\tau_1(\Omega)$ for its linearized problem at the steady-state Ω

$$\begin{cases} -(u-\Omega)'' = \lambda(1-p)(u-\Omega), \\ u(0) = x, \quad u'(0) = y(x). \end{cases} \tag{1.49}$$

Indeed, the general solution of the differential equation of (1.49) can be expressed as

$$u(t) = \Omega + A\sin(\sqrt{\lambda(1-p)}\, t) + B\cos(\sqrt{\lambda(1-p)}\, t),$$

where $A, B \in \mathbb{R}$ are arbitrary integration constants, and, hence,

$$u'(t) = A\sqrt{\lambda(1-p)}\cos(\sqrt{\lambda(1-p)}\, t) - B\sqrt{\lambda(1-p)}\sin(\sqrt{\lambda(1-p)}\, t).$$

As

$$x = u(0) = \Omega + B, \qquad y(x) = u'(0) = A\sqrt{\lambda(1-p)},$$

necessarily

$$B = x - \Omega, \qquad A = \frac{y(x)}{\sqrt{\lambda(1-p)}},$$

and, therefore, the unique solution of (1.49) is given through

$$u(t) = \Omega + \frac{y(x)}{\sqrt{\lambda(1-p)}} \sin(\sqrt{\lambda(1-p)}\, t) + (x-\Omega)\cos(\sqrt{\lambda(1-p)}\, t). \quad (1.50)$$

As $\tau_1(x)/2$ is the first time where u' vanishes, it becomes apparent that

$$y(x)\cos\left(\sqrt{\lambda(1-p)}\,\frac{\tau_1(x)}{2}\right) = (x-\Omega)\sqrt{\lambda(1-p)}\,\sin\left(\sqrt{\lambda(1-p)}\,\frac{\tau_1(x)}{2}\right)$$

and, consequently,

$$\tau_1(x) = \frac{2}{\sqrt{\lambda(1-p)}}\arctan\frac{y(x)}{(x-\Omega)\sqrt{\lambda(1-p)}}. \quad (1.51)$$

Letting $x \to \Omega$ in (1.51), indeed gives the value of $\tau_1(\Omega)$ calculated through Theorem 1.9.

1.3.2. Existence of solutions of type T_1

The following result establishes an *almost optimal* condition for the existence of solutions of type T_1, in the sense that it would be a characterization theorem if $\tau_1(x)$ would be decreasing. But, we have not been able to prove this monotonicity property yet.

Theorem 1.10. *Suppose $\lambda < 0$ and (1.27). Then, the following assertions are true:*

(a) *The problem (1.1) has a solution of type T_1 with a local minimum in $(\alpha, 1-\alpha)$ if*

$$\tau_1(\Omega) < 1 - 2\alpha. \quad (1.52)$$

(b) *The problem (1.1) has a solution of type T_1 with a local maximum in $(\alpha, 1-\alpha)$ if*

$$\tau_1(\Omega) > 1 - 2\alpha. \quad (1.53)$$

Note that, besides these solutions of type T_1, the problem admits the trivial solution u_0.

Proof. The notations introduced in the proof of Theorem 1.7 will be kept through this proof. Under condition (1.52), there exists $x \in (x_0^-, \Omega)$ such that $\tau_1(x) < 1 - 2\alpha$. Thus, since $\lim_{x \downarrow x_0^-} \tau_1(x) = \infty$, there exists $\tilde{x} \in (x_0^-, x)$ such that $\tau_1(\tilde{x}) = 1 - 2\alpha$, which ends the proof of Part (a).

Now, suppose (1.53), instead of (1.52). Then, there exists $x > \Omega$ such that $\tau_1(x) > 1 - 2\alpha$. Therefore, owing to (1.48), it becomes apparent that there exists $\tilde{x} > x$ such that $\tau_1(\tilde{x}) = 1 - 2\alpha$. This completes the proof. □

Figure 1.7 represents the two symmetric solutions of (1.1) when conditions $b = b^*$ and $\tau_1(\Omega) > 1 - 2\alpha$ are satisfied. The symmetric solutions in case $\tau_1(\Omega) < 1 - 2\alpha$ have already been represented in Figure 1.6.

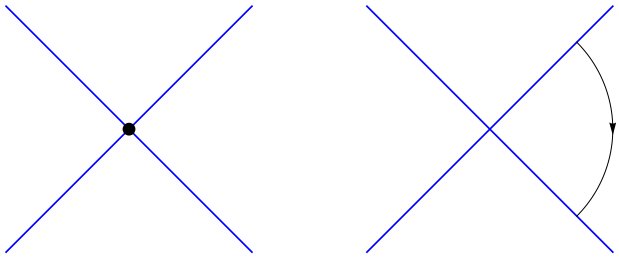

Figure 1.7: The symmetric solutions of (1.1) in case (1.53).

As far as the solutions of type T_1, it should be noted that Theorem 1.10 is substantially sharper than Theorem 1.7. Not only the solutions given by Part (b) were left aside of Theorem 1.7, but the condition $\tau_\Omega < 1 - 2\alpha$ is much stronger than (1.52), since, actually, we do have

$$2\tau_1(\Omega) < \tau_\Omega. \tag{1.54}$$

The next result complements Theorem 1.9 ensuring that there are open ranges of values of the parameters involved in the setting of (1.1) for which any of the conditions (1.52) and (1.53) can be satisfied.

Proposition 1.11. *Suppose* $\lambda < 0$ *and* (1.27). *Then, there exist* $\lambda_1^- \leq \lambda_1^+ < 0$ *such that:*

(a) $\tau_1(\Omega) < 1 - 2\alpha$ *if* $\lambda < \lambda_1^-$.

(b) $\tau_1(\Omega) > 1 - 2\alpha$ *if* $\lambda \in (\lambda_1^+, 0)$.

Proof. According to (1.14),

$$\tau_1(\Omega) < \frac{\tau_\Omega}{2} = \frac{\pi}{\sqrt{\lambda(1-p)}} < 1 - 2\alpha$$

provided

$$\lambda < -\frac{1}{p-1}\left(\frac{\pi}{1-2\alpha}\right)^2,$$

which concludes the proof of Part (a).

By the theorem of differentiation of G. Peano, it follows from Theorem 1.6 that the positive real number $y'(\Omega)$ can be regarded as a continuous function of $\lambda \leq 0$, say $y'(\Omega) = y'(\Omega, \lambda)$. Therefore,

$$\lim_{\lambda \uparrow 0} \arctan \frac{y'(\Omega, \lambda)}{\sqrt{\lambda(1-p)}} = \pi/2$$

and, consequently, Theorem 1.9 implies that

$$\lim_{\lambda \uparrow 0} \tau_1(\Omega) = \lim_{\lambda \uparrow 0} \left(\frac{2}{\sqrt{\lambda(1-p)}} \arctan \frac{y'(\Omega, \lambda)}{\sqrt{\lambda(1-p)}} \right) = \infty,$$

which completes the proof of Part (b). □

1.3.3. The time-maps τ_j, $j \geq 2$. Sharpening Theorem 1.7

Throughout this section, we suppose $\lambda < 0$ and (1.27). As for τ_1, the time map τ_2 constructed in the proof of Theorem 1.7 can be extended, in a rather natural way, to be defined for all

$$x \in J^* := J \setminus \{\Omega\}, \qquad J := (x_0^-, x_0^+),$$

where, according to the notations introduced in the proof of Theorem 1.7, $(x_0^+, y(x_0^+))$ and $(x_0^-, y(x_0^-))$ are the first and the second crossing points, respectively, as time increases, between Γ_0 and the homoclinic orbit through $(0,0)$; $x_0^- < \Omega = m_0 < x_0^+$. Similarly, the map τ_3 can be extended to be defined in J^* too. Also, by construction (see Figure 1.6, if necessary), we have that

$$\tau_3(x) = \tau_1(x) + \tau(x) \qquad \text{for all } \ x \in J^*, \tag{1.55}$$

where $\tau(x)$ stands for the period of the solution of (1.32).

More generally, throughout the rest of this section, for every integer number $n \geq 2$, we consider the time-maps τ_{2n} and τ_{2n+1} defined in J^* through

$$\tau_{2n+1} = \tau_1 + n\tau, \qquad \tau_{2n} = \tau_2 + (n-1)\tau. \tag{1.56}$$

By (1.55), (1.56) does actually make sense for every $n \geq 1$.

According to Theorem 1.9, one can easily infer, by the symmetry of the problem, that

$$\lim_{x \to \Omega} \tau_2(x) = 2\tau_1(\Omega) + \frac{\tau_\Omega - 2\tau_1(\Omega)}{2} = \tau_1(\Omega) + \frac{\tau_\Omega}{2}. \tag{1.57}$$

Consequently,

$$\lim_{x\to\Omega}\tau_{2n+1}(x)=\tau_1(\Omega)+n\tau_\Omega,\qquad \lim_{x\to\Omega}\tau_{2n}(x)=\tau_1(\Omega)+\left(n-\frac{1}{2}\right)\tau_\Omega, \tag{1.58}$$

for all $n\geq 1$, and, therefore, all these time-maps can be extended to J so that $\tau_j\in\mathcal{C}(J)$, $j\geq 1$, by simply setting

$$\tau_{2n+1}(\Omega):=\tau_1(\Omega)+n\tau_\Omega,\qquad \tau_{2n}(\Omega):=\tau_1(\Omega)+\left(n-\frac{1}{2}\right)\tau_\Omega,\qquad n\geq 1. \tag{1.59}$$

By continuous dependence, all these time-maps satisfy

$$\lim_{x\downarrow x_0^-}\tau_n(x)=\infty,\quad \lim_{x\uparrow x_0^+}\tau_{n+1}(x)=\infty,\qquad n\geq 1. \tag{1.60}$$

Moreover, by construction,

$$\tau_n(x)<\tau_{n+1}(x),\qquad n\geq 1,\qquad x\in J. \tag{1.61}$$

Actually, τ_1 is globally defined in (x_0^-,∞) and, due to Theorem 1.9,

$$\lim_{x\uparrow\infty}\tau_1(x)=0.$$

Figure 1.8 represents the plots of τ_n, $1\leq n\leq 7$, that we have computed using *Mathematica* for an appropriate choice of the several parameters involved in the formulation of (1.1). The numerics gave the nice monotonicity properties shown in Figure 1.8, though we were not able to prove them analytically.

By Corollary 1.4 and the symmetry of the equation (1.26), the solutions of type T_{2n}, $n\geq 2$, must appear by pairs $(u,\tilde{u})$ with

$$\tilde{u}(t)=u(1-t),\qquad t\in[0,1],$$

similarly to the case $n=1$ already analyzed in the proof of Theorem 1.7.

It should be noted that, according to (1.59),

$$\tau_{n+1}(\Omega)=\tau_n(\Omega)+\frac{\tau_\Omega}{2},\qquad n\geq 1. \tag{1.62}$$

By simply counting the number of roots of $\tau_n=1-2\alpha$, for every $n\geq 1$, one can get the next substantial improvement of Theorem 1.7 and Proposition 1.11(a).

Theorem 1.12. *Suppose* $\lambda<0$, (1.27) *and*

$$\tau_n(\Omega)<1-2\alpha<\tau_{n+1}(\Omega) \tag{1.63}$$

for some $n\geq 2$. *Then,* (1.1) *admits, at least, one solution of type* T_1 *and two solutions of type* T_j *for all* $2\leq j\leq n$, *besides the trivial solution* $u_0\in T_0$. *When* $n=1$, *the problem possesses at least one solution of type* T_1 *plus the trivial solution, as already established by Proposition 1.11(a).*

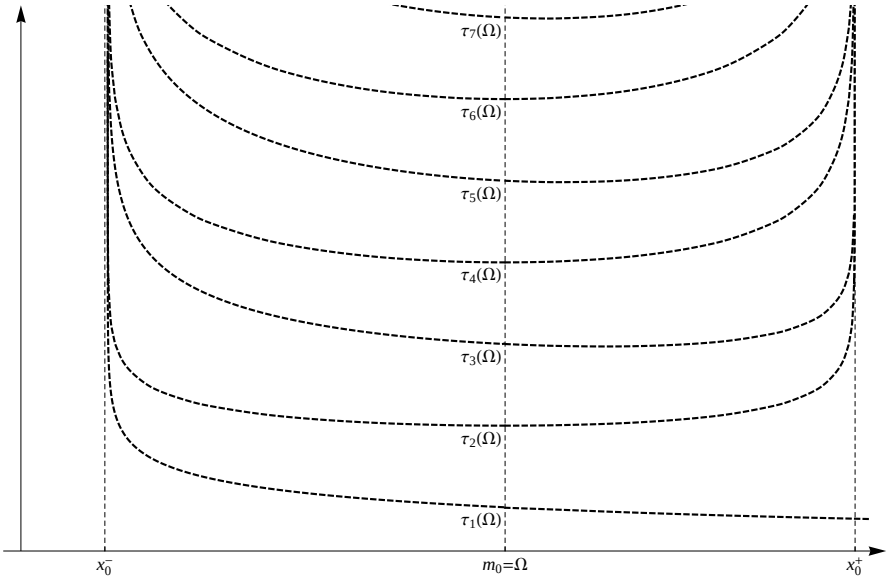

Figure 1.8: The graphs of the curves τ_n, $1 \leq n \leq 7$.

1.4. Local perturbation from $b = b^*$

The main goal of this section is to analyze the behavior of the solutions already constructed in Section 1.3 as the parameter b perturbs from b^*. In Section 1.5 we will ascertain the global behavior of these solution as b separates away from b^*, obtaining in this way the corresponding global bifurcation diagrams. One of the main differences between the cases $b = b^*$ and $b \neq b^*$ is that in case $b = b^*$ all solutions of odd type must be symmetric, whereas in case $b \neq b^*$ the problem (1.1) can admit asymmetric solutions of odd type, which play the same role as solutions of even type.

1.4.1. The case $b > b^*$

Now, $\Omega < m_0$. Clearly, for $b > b^*$, $b \sim b^*$, the phase portrait of (1.26) looks like shown in Figure 1.9, where we also have superimposed Γ_0 and Γ_1. Besides the homoclinic through the origin, we have represented three trajectories. One exterior to the homoclinic and two interior orbits. The interior ones are rather special, as the inner one is the unique orbit which is tangent to Γ_0 at $(x_t, y(x_t))$, and the exterior one is the unique orbit passing through the crossing point between Γ_0 and Γ_1, $(m_0, 0)$. The points x_0^- and x_0^+ are defined as in the proof of Theorem 1.7. We have denoted by x_{m_0} the unique value of $x \neq m_0$ for which $(x, y(x)) \in \Gamma_0$ lies on the orbit through $(m_0, 0)$. All these points are going to

play a very important role in the subsequent analysis. Naturally, except m_0, all of them are regular functions of b,

$$x_0^- = x_0^-(b) < x_{m_0} = x_{m_0}(b) < x_t = x_t(b) < m_0 < x_0^+ = x_0^+(b).$$

Although Figure 1.9 illustrates the special case when

$$\Omega = \left(\frac{-\lambda}{b}\right)^{\frac{1}{p-1}} < x_{m_0}(b) < x_t = x_t(b),$$

in general, this condition does not need to be satisfied.

Besides $(0,0)$, the homoclinic connection meets the u-axis at $(u_M, 0)$, where

$$u_M = u_M(b) := \left(\frac{-\lambda(p+1)}{2b}\right)^{\frac{1}{p-1}}. \tag{1.64}$$

Thus, setting

$$b_{m_0} := \frac{-\lambda(p+1)}{2m_0^{p-1}}, \tag{1.65}$$

we have that

$$u_M(b) \begin{cases} > m_0 & \text{if } b < b_{m_0}, \\ = m_0, & \text{if } b = b_{m_0}, \\ < m_0 & \text{if } b > b_{m_0}. \end{cases} \tag{1.66}$$

Figure 1.9 represents the phase portrait of (1.26) in the range of values $b \in (b^*, b_{m_0})$, where we recall that $b^* = -\lambda/m_0^{p-1}$. This is the range of values of b on which we are going to focus our attention in this section. Figure 1.10 describes the most relevant general features of the phase portrait of (1.26) as b increases from b^*. Precisely, Figure 1.10A shows the phase portrait for $b^* < b < b_{m_0}$. As b reaches the critical value b_{m_0} (Figure 1.10B) and crosses it, m_0 moves outside the homoclinic until b attains a further critical value, say $b_t > b_{m_0}$, where the homoclinic is tangent to Γ_0 and Γ_1 (Figure 1.10C). As $b > b_t$, the homoclinic connection cannot meet $\Gamma_0 \cup \Gamma_1$, and, actually, it shrinks to $(0,0)$ as $b \uparrow \infty$. These features are straightforward consequences of the fact that the family of homoclinic connections shrinks monotonically to $(0,0)$ as b increases.

As in Section 1.3, the solutions of (1.26) connecting Γ_0 with Γ_1 in a time $1 - 2\alpha$ provide us with solutions of (1.1), as it was described in Section 1.2. But, since the phase portrait changes as when b increases from b^*, the time-maps τ_n, $n \geq 1$, also change. Most of our effort to understand what is going on when b perturbs from b^* relies on the appropriate definitions of these time-maps, which will be subsequently denoted by $\tau_n(x, b)$, in order to emphasize their dependence on b.

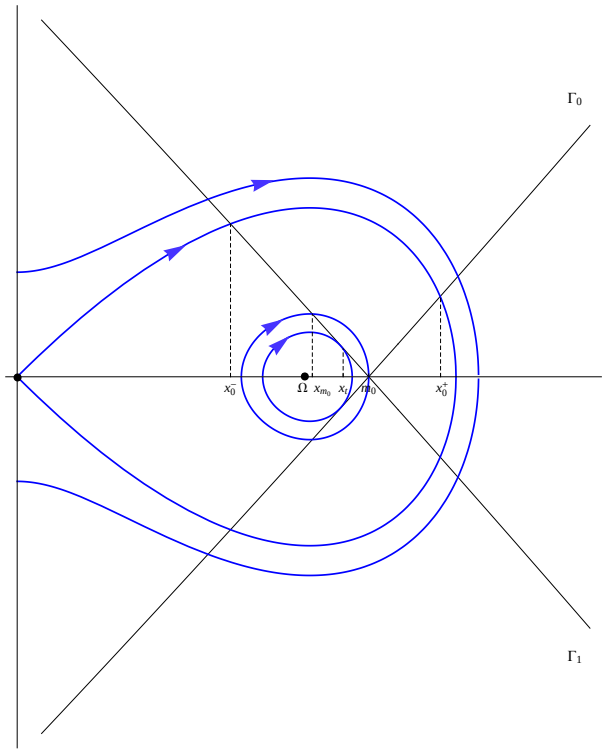

Figure 1.9: The phase portrait of (1.26) for $b > b^*$, $b \sim b^*$.

For every $b \in (b^*, b_{m_0})$, we denote by

$$\tau_1(\cdot, b) \ : \ D_1 = D_1(b) := (x_0^-, x_t] \cup (m_0, \infty) \to [0, \infty) \tag{1.67}$$

the Poincaré map defined, for every $x \in D_1$, as the minimal time needed by the solution of (1.32) to reach Γ_1. Figure 1.11 shows the corresponding orbits of two of these solutions for some $x < x_t$ (A) and $x > m_0$ (B). By continuous dependence,

$$\lim_{x \downarrow x_0^-} \tau_1(x, b) = \infty. \tag{1.68}$$

Moreover,

$$\lim_{x \downarrow m_0} \tau_1(x, b) = 0, \tag{1.69}$$

because m_0 is not an equilibrium of (1.26). Also, the proof of (1.48) (for $b = b^*$) adapts *mutatis mutandis* to show that

$$\lim_{x \uparrow \infty} \tau_1(x, b) = 0 \tag{1.70}$$

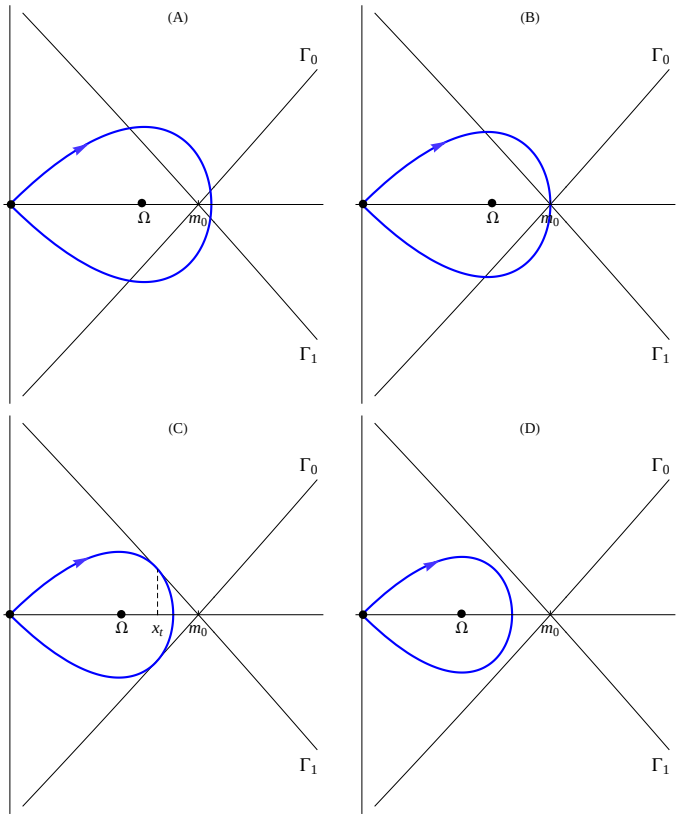

Figure 1.10: Geometry of the phase plane as b increases from b^*.

for all $b > b^*$. Note that $\tau_1(x_t, b)$ is the minimal time needed by the solution of (1.32), with $x = x_t$, to connect $(x_t, y(x_t)) \in \Gamma_0$ with Γ_1.

Subsequently, for every $b \in (b^*, b_{m_0})$, we denote by

$$\tau_{1,s}(\cdot, b) \ : \ D_{1,s} = D_{1,s}(b) := [x_t, m_0] \to [0, \infty) \tag{1.71}$$

the Poincaré-map defined, for every $x \in (x_t, m_0)$, as the minimal time needed by the solution of (1.32) to reach Γ_1 exactly twice, while

$$\begin{aligned} \tau_{1,s}(x_t, b) &:= \lim_{x \downarrow x_t} \tau_{1,s}(x, b) = \tau_1(x_t, b) \\ \tau_{1,s}(m_0, b) &:= \lim_{x \uparrow m_0} \tau_{1,s}(x, b) = \tau(m_0, b), \end{aligned} \tag{1.72}$$

where, for every $x \in (x_0^-, x_0^+)$, $\tau(x, b)$ stands for the period of the orbit through $(x, y(x))$. Figure 1.12 shows the corresponding orbits of two of these solutions for some $x \sim x_t$ (A) and $x \sim m_0$ (B).

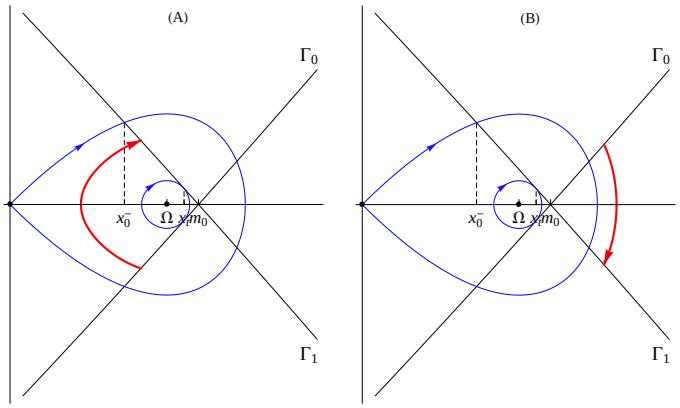

Figure 1.11: The time-map $(x, y(x)) \mapsto \tau_1(x, b)$ for $b^* < b < b_{m_0}$

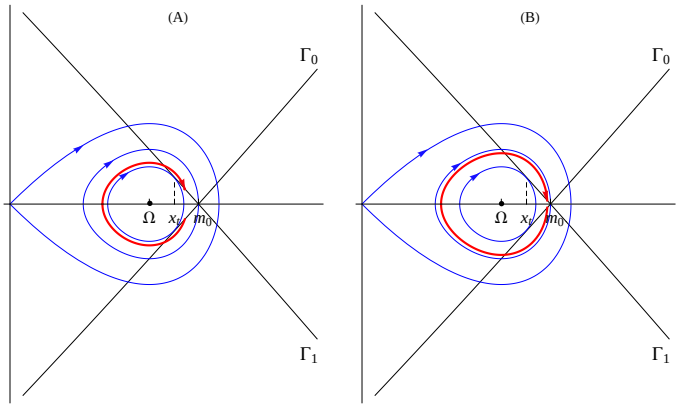

Figure 1.12: The time-map $(x, y(x)) \mapsto \tau_{1,s}(x, b)$ for $b^* < b < b_{m_0}$

Similarly, we introduce the Poincaré map

$$\tau_{1,a}(\cdot, b) \ : \ D_{1,a} := [x_{m_0}, m_0] \to [0, \infty) \tag{1.73}$$

defined, for every $x \in [x_{m_0}, x_t)$, as the minimal time needed by the solution of (1.32) to reach Γ_1 twice (see Figure 1.13A), and, for every $x \in [x_t, m_0]$, as the minimal time needed to reach Γ_1 by the first time (see Figure 1.13B).

Note that

$$\lim_{x \to x_t} \tau_{1,a}(x, b) = \tau_{1,a}(x_t, b) = \tau_1(x_t, b)$$

and, hence, by (1.72), we obtain that

$$\tau_{1,a}(x_t, b) = \tau_{1,s}(x_t, b) = \tau_1(x_t, b), \tag{1.74}$$

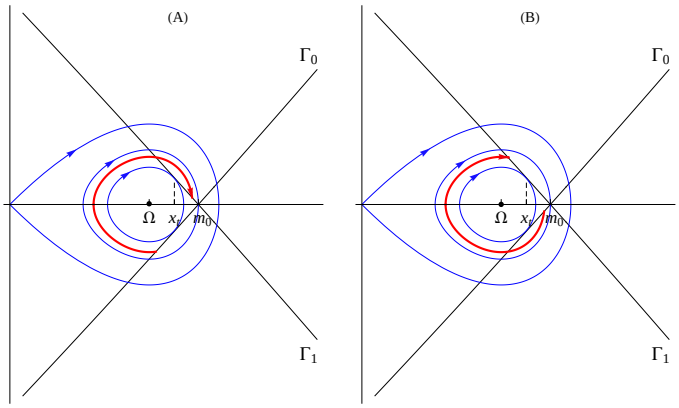

Figure 1.13: The time-map $(x, y(x)) \mapsto \tau_{1,a}(x, b)$ for $b^* < b < b_{m_0}$

though, by definition,

$$\begin{aligned} \tau_1(x,b) < \tau_{1,a}(x,b), \quad & x_{m_0} \le x < x_t, \\ \tau_{1,a}(x,b) < \tau_{1,s}(x,b), \quad & x_t < x \le m_0. \end{aligned} \tag{1.75}$$

Incidentally, the solutions of $\tau_1 = 1 - 2\alpha$ and $\tau_{1,s} = 1 - 2\alpha$ provide us with symmetric solutions of (1.1), whereas the solutions constructed from $\tau_{1,a} = 1 - 2\alpha$ are asymmetric, except at $x = x_t$, and, by definition of the time maps, all these solutions provide us with solutions of (1.1) with a single critical point. Conversely, any solution of problem (1.1) with a single critical point in $(\alpha, 1-\alpha)$ must be of some of these forms. Actually, this is why we have introduced all these time-maps.

Naturally, in order to look for solutions of type T_2 of (1.1), we must introduce the Poincaré map

$$\tau_2(\cdot, b) \ : \ D_2 = D_2(b) := (x_0^-, x_{m_0}] \cup [m_0, x_0^+) \to [0, \infty) \tag{1.76}$$

defined, for every $x \in D_2 \setminus \{x_{m_0}, m_0\}$, as the minimal time needed by the solution of (1.32) to reach Γ_1 exactly twice, and

$$\begin{aligned} \tau_2(x_{m_0}, b) &:= \lim_{x \uparrow x_{m_0}} \tau_2(x,b) = \tau_{1,a}(x_{m_0}, b), \\ \tau_2(m_0, b) &:= \lim_{x \downarrow m_0} \tau_2(x,b) = \tau_{1,a}(m_0, b). \end{aligned} \tag{1.77}$$

By continuous dependence and the symmetry properties of our problem, these identities are consistent. Figure 1.14 shows the corresponding orbits of two of these solutions for some $x \in (x_0^-, x_{m_0})$ (A) and $x \in (m_0, x_0^+)$ (B). It is easy to see that (1.1) cannot admit a solution of type T_2 passing through $(x, y(x))$

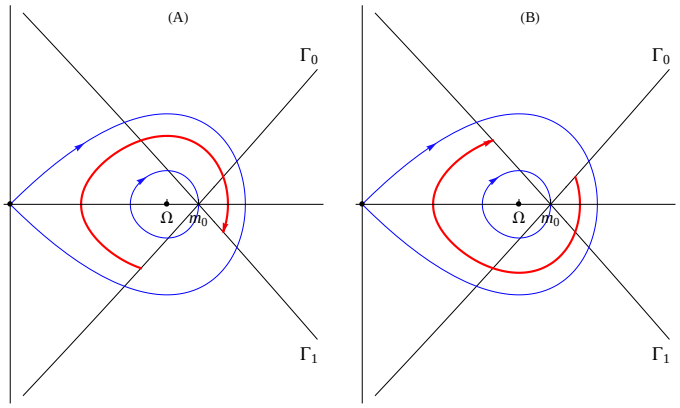

Figure 1.14: The time-map $(x, y(x)) \mapsto \tau_2(x, b)$ for $b^* < b < b_{m_0}$

if $x_{m_0} < x < m_0$. Incidentally, by symmetry, each of the solutions on Figure 1.14(A) must be the reflection around $t = 1/2$ of some solution in Figure 1.14(B).

More generally, we may introduce the time maps

$$\begin{aligned} \tau_{2n+1}(x,b) &:= \tau_1(x,b) + n\tau(x,b), && x \in D_1(b), \\ \tau_{2n+1,s}(x,b) &:= \tau_{1,s}(x,b) + n\tau(x.b), && x \in D_{1,s}(b), \end{aligned} \tag{1.78}$$

$$\begin{aligned} \tau_{2n+1,a}(x,b) &:= \tau_{1,a}(x,b) + n\tau(x,b), && x \in D_{1,a}(b), \\ \tau_{2n}(x,b) &:= \tau_2(x,b) + (n-1)\tau(x,b), && x \in D_2(b), \end{aligned} \tag{1.79}$$

for all $n \geq 1$.

According to (1.69), it follows from (1.72) and (1.78) that

$$\lim_{x \downarrow m_0} \tau_3(x,b) = \tau(m_0,b) = \tau_{1,s}(m_0,b).$$

Thus, the graph of $\tau_{1,s}$ in the interval $[x_t, m_0]$ connects the graph of τ_1 in $(x_0^-, x_t]$ (*left branch* of τ_1) with the graph of τ_3 in $[m_0, x_0^+)$ (*right branch* of τ_3), as illustrated by Figure 1.15, where those graphs have been plotted together. Consequently, by (1.78), the graph of $\tau_{2n+1,s}$ in $[x_t, m_0]$ must connect the graph of τ_{2n+1} in the interval $(x_0^-, x_t]$ with the graph of $\tau_{2(n+1)+1}$ in $[m_0, x_0^+)$, for all $n \geq 1$. Similarly, by (1.77), the graph of $\tau_{1,a}$ in $[x_{m_0}, m_0]$ connects the graph of τ_2 in $(x_0^-, x_{m_0}]$ with the graph of τ_2 in $[m_0, x_0^+)$. As, according to (1.74), the graphs of τ_1, $\tau_{1,s}$ and $\tau_{1,a}$ cross at x_t, owing to (1.75) and (1.78), it becomes apparent that the graphs of all these functions look like shown by Figure 1.15,

where we have collected the plots of the first seven time maps for an appropriate special case with $b > b^*$. Note that

$$\lim_{x \uparrow x_0^+} \tau(x, b) = \infty,$$

and

$$\lim_{x \downarrow x_0^-} \tau_n(x, b) = \infty = \lim_{x \uparrow x_0^+} \tau_{n+1}(x, b), \qquad n \geq 1.$$

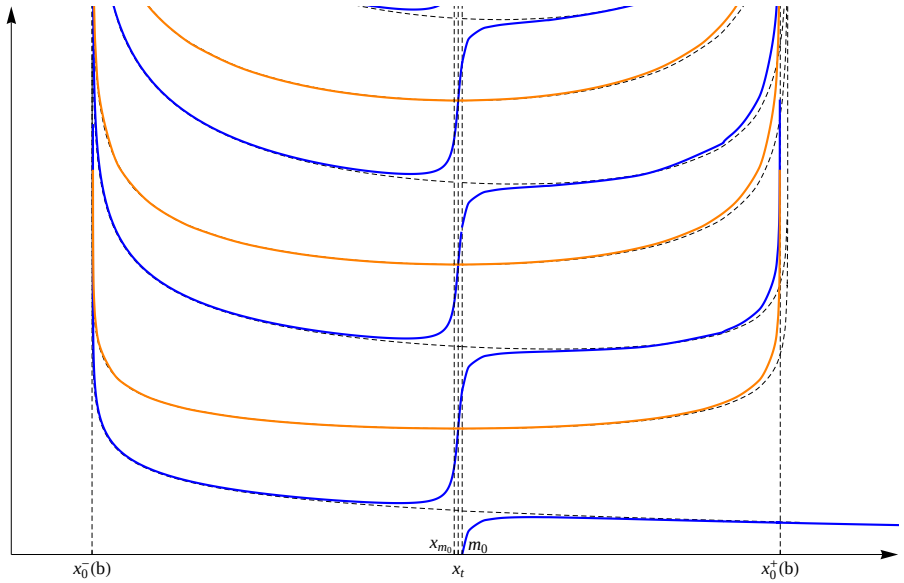

Figure 1.15: The graphs of the curves (1.78) for $b^* < b < b_{m_0}$

More precisely, Figure 1.15 represents the graphs of the functions θ_j, $j \geq 1$, defined by

$$\theta_{2n+1}(x, b) := \begin{cases} \tau_{2n+1}(x, b) & \text{if} \quad x \in (x_0^-, x_t], \\ \tau_{2n+1,s}(x, b) & \text{if} \quad x \in (x_t, m_0], \\ \tau_{2(n+1)+1}(x, b) & \text{if} \quad x \in (m_0, x_0^+), \end{cases} \tag{1.80}$$

for all $n \geq 0$, and

$$\theta_{2n}(x, b) := \begin{cases} \tau_{2n}(x, b) & \text{if} \quad x \in (x_0^-, x_{m_0}], \\ \tau_{2(n-1)+1,a}(x, b) & \text{if} \quad x \in (x_{m_0}, m_0), \\ \tau_{2n}(x, b) & \text{if} \quad x \in [m_0, x_0^+), \end{cases} \tag{1.81}$$

for all $n \geq 1$. According to (1.78) and (1.79), it is apparent that

$$\theta_{2n+1} := \theta_1 + n\tau, \qquad \theta_{2n} := \theta_2 + (n-1)\tau, \qquad n \geq 1.$$

The next result collects some global monotonicity properties of these auxiliary functions, which are reflected in Figure 1.15.

Lemma 1.13. *For every integer $n \geq 0$ and $b \in (b^*, b_{m_0})$, we have that*

$$\theta_{2n+1}(x,b) \begin{cases} < \theta_{2(n+1)}(x,b) & \text{if} \quad x \in (x_0^-, x_t), \\ = \theta_{2(n+1)}(x_t,b) & \text{if} \quad x = x_t, \\ > \theta_{2(n+1)}(x,b) & \text{if} \quad x \in (x_t, x_0^+). \end{cases} \tag{1.82}$$

Moreover, for every $x \in (x_0^-, x_0^+)$,

$$\max\left\{\theta_{2n+1}(x,b), \theta_{2(n+1)}(x,b)\right\} < \min\left\{\theta_{2(n+1)+1}(x,b), \theta_{2(n+2)}(x,b)\right\}. \tag{1.83}$$

Proof. Suppose $x \in (x_0^-, x_{m_0}]$. Then, by (1.80), (1.81), (1.78) and (1.79), taking into account that $\tau_1(x,b) < \tau_2(x,b)$, we find that

$$\begin{aligned} \theta_{2n+1}(x,b) &= \tau_{2n+1}(x,b) = \tau_1(x,b) + n\tau(x,b) < \tau_2(x,b) + n\tau(x,b) \\ &= \tau_{2(n+1)}(x,b) = \theta_{2(n+1)}(x,b). \end{aligned}$$

Suppose $x \in (x_{m_0}, x_t)$. Then, by (1.80), (1.78), (1.79), (1.75) and (1.81),

$$\begin{aligned} \theta_{2n+1}(x,b) &= \tau_{2n+1}(x,b) = \tau_1(x,b) + n\tau(x,b) < \tau_{1,a}(x,b) + n\tau(x,b) \\ &= \tau_{2n+1,a}(x,b) = \theta_{2(n+1)}(x,b). \end{aligned}$$

Moreover, thanks to (1.74),

$$\theta_{2n+1}(x_t,b) = \tau_1(x_t,b) + n\tau(x_t,b) = \tau_{1,a}(x_t,b) + n\tau(x_t,b) = \theta_{2(n+1)}(x_t,b).$$

Now, let $x \in (x_t, x_{m_0}]$. Then, according to (1.80), (1.78), (1.79), (1.81) and (1.75),

$$\theta_{2n+1}(x,b) = \tau_{1,s}(x,b) + n\tau(x,b) > \tau_{1,a}(x,b) + n\tau(x,b) = \theta_{2(n+1)}(x,b).$$

Finally, for every $x \in (m_0, x_0^+)$, we find that

$$\begin{aligned} \theta_{2n+1}(x,b) &= \tau_{2(n+1)+1}(x,b) = \tau_1(x,b) + (n+1)\tau(x,b) > \tau_2(x,b) + n\tau(x,b) \\ &= \tau_{2(n+1)}(x,b) = \theta_{2(n+1)}(x,b), \end{aligned}$$

because $\tau_3 = \tau_1 + \tau > \tau_2$, which completes the proof of (1.82).

Naturally, (1.83) relies on (1.82). For every $x \in (x_0^-, x_{m_0}]$, using (1.82), (1.81), (1.78), (1.79) and (1.80), we find that

$$\begin{aligned} \max\left\{\theta_{2n+1}(x,b), \theta_{2(n+1)}(x,b)\right\} &= \theta_{2(n+1)}(x,b) = \tau_{2(n+1)}(x,b) \\ &= \tau_2(x,b) + n\tau(x,b) \\ &< \tau_1(x,b) + (n+1)\tau(x,b) \\ &= \tau_{2(n+1)+1}(x,b) = \theta_{2(n+1)+1}(x,b) \\ &= \min\left\{\theta_{2(n+1)+1}(x,b), \theta_{2(n+2)}(x,b)\right\}. \end{aligned}$$

Similarly, for every $x \in (x_{m_0}, x_t)$, we obtain that

$$\begin{aligned}\max\left\{\theta_{2n+1}(x,b), \theta_{2(n+1)}(x,b)\right\} &= \theta_{2(n+1)}(x,b) = \tau_{2n+1,a}(x,b)\\ &= \tau_{1,a}(x,b) + n\tau(x,b)\\ &< \tau_1(x,b) + (n+1)\tau(x,b)\\ &= \tau_{2(n+1)+1}(x,b) = \theta_{2(n+1)+1}(x,b)\\ &= \min\left\{\theta_{2(n+1)+1}(x,b), \theta_{2(n+2)}(x,b)\right\},\end{aligned}$$

because $\tau_{1,a} < \tau < \tau_1 + \tau$. Analogously, for every $x \in [x_t, m_0]$, we have that

$$\begin{aligned}\max\left\{\theta_{2n+1}(x,b), \theta_{2(n+1)}(x,b)\right\} &= \theta_{2n+1}(x,b) = \tau_{2n+1,s}(x,b)\\ &= \tau_{1,s}(x,b) + n\tau(x,b)\\ &< \tau_{1,a}(x,b) + (n+1)\tau(x,b)\\ &= \tau_{2(n+1)+1,a}(x,b) = \theta_{2(n+2)}(x,b)\\ &= \min\left\{\theta_{2(n+1)+1}(x,b), \theta_{2(n+2)}(x,b)\right\},\end{aligned}$$

because $\tau_{1,s} < \tau < \tau_{1,a} + \tau$. Finally, for any $x \in (m_0, x_0^+)$, we have that

$$\begin{aligned}\max\left\{\theta_{2n+1}(x,b), \theta_{2(n+1)}(x,b)\right\} &= \theta_{2n+1}(x,b) = \tau_{2(n+1)+1}(x,b)\\ &= \tau_1(x,b) + (n+1)\tau(x,b)\\ &< \tau_2(x,b) + (n+1)\tau(x,b)\\ &= \tau_{2(n+2)}(x,b) = \theta_{2(n+2)}(x,b)\\ &= \min\left\{\theta_{2(n+1)+1}(x,b), \theta_{2(n+2)}(x,b)\right\},\end{aligned}$$

which concludes the proof. □

Since

$$\lim_{b\downarrow b^*} x_{m_0}(b) = \lim_{b\downarrow b^*} x_t(b) = \lim_{b\downarrow b^*} \Omega(b) = m_0,$$

we have that

$$\lim_{b\downarrow b^*} D_{1,a}(b) = \lim_{b\downarrow b^*} D_{1,s}(b) = \{m_0\},$$

and the graphs of all these θ_j's in the intervals $[x_{m_0}(b), m_0]$ shrink either to a single point, or a certain segment, as $b \downarrow b^*$. Moreover, the crossing points between the homoclinic and Γ_0 satisfy

$$\lim_{b\downarrow b^*} x_0^{\pm}(b) = x_0^{\pm},$$

where $x_0^{\pm} = x_0^{\pm}(b^*)$ are those introduced in the proof of Theorem 1.7. Naturally, by well known results on continuous dependence, the next result holds.

Proposition 1.14. *For every $n \geq 1$ and $\varepsilon > 0$ sufficiently small,*

$$\lim_{b \downarrow b^*} \tau_n(x, b) = \tau_n(x)$$

uniformly in

$$x \in [x_0^-(b^*) + \varepsilon, m_0 - \varepsilon] \cup [m_0 + \varepsilon, x_0^+(b^*) - \varepsilon].$$

Proposition 1.14 guarantees that, for any $n \geq 1$, the graphs of the time map $\tau_n(\cdot, b)$ constructed in this section converges, as $b \downarrow b^*$, to the graph of the corresponding time map τ_n constructed in Section 1.2; the convergence being uniform in the complement in $(x_0^-(b^*), x_0^+(b^*))$ of any neighborhood of m_0. This has been illustrated by Figure 1.15, where the graphs of the perturbed Poincaré maps, $\tau_n(\cdot, b)$, for $b > b^*$, plotted with continuous lines, are very close to the graphs of the corresponding unperturbed time maps τ_n, plotted with dashed lines. Not surprisingly, in between x_{m_0} and m_0 (very close if $b \sim b^*$), the nature of these graphs changes drastically. Indeed, in the interval $[x_{m_0}(b), m_0]$ each τ_{2n+1} breaks down and its perturbed *left branch* can be connected with the perturbed *right branch* of $\tau_{2(n+1)+1}$ through the graph of $\tau_{2n+1,s}$, while the graph of τ_{2n} breaks down and its perturbed *left branch* can be connected with its perturbed *right branch* through the graph of $\tau_{2n-1,a}$. In other words, the unperturbed τ_n's of Section 1.3 perturb into the θ_n's constructed through (1.80) and (1.81). The next theorem provides us with the precise behavior of these time-maps as $b \downarrow b^*$.

Theorem 1.15. *The following assertions are true:*

(a) $\lim_{b \downarrow b^*} \tau_{1,a}(x, b) = \tau_2(\Omega)$ *for all* $x \in [x_{m_0}(b), m_0]$, *as well as for the linearized problem.*

(b) $\lim_{b \downarrow b^*} \tau_{1,s}(m_0, b) = \tau(\Omega)$.

(c) $\lim_{b \downarrow b^*} \lim_{x \downarrow m_0} \tau_3(x, b) = \tau(\Omega)$.

Thus, owing to Parts (a), (b) *and* (1.74), *the function $\tau_{1,s}$ must jump from a value very close to $\tau_2(\Omega)$ to a value very close to $\tau(\Omega)$ in the interval $[x_t(b), m_0]$ for sufficiently close $b > b^*$, whereas, due to Parts* (b), (c) *and Proposition 1.14, the graph of $\tau_3(\cdot, b)$ approximates the graph of τ_3 as $b \downarrow b^*$ plus a vertical segment linking $\tau(\Omega)$ with $\tau_3(\Omega) = \tau_1(\Omega) + \tau(\Omega)$ at $x = m_0$.*

Naturally, thanks to (1.78) *and* (1.79), *we also have that*

$$\lim_{b \downarrow b^*} \tau_{2n-1,a}(x, b) = \tau_{2n}(\Omega) \qquad \textit{for all} \quad x \in [x_{m_0}(b), m_0],$$

$$\lim_{b\downarrow b^*} \tau_{2n-1,s}(m_0, b) = n\tau(\Omega),$$

and that

$$\lim_{b\downarrow b^*} \lim_{x\downarrow m_0} \tau_{2n+1}(x, b) = n\tau(\Omega)$$

for all $n \geq 1$.

Proof. Part (b) is an immediate consequence of (1.72), as

$$\lim_{b\downarrow b^*} \tau_{1,s}(m_0, b) = \lim_{b\downarrow b^*} \tau(m_0, b) = \tau(\Omega).$$

Part (c) follows directly from (1.78) and (1.69), as

$$\lim_{b\downarrow b^*} \lim_{x\downarrow m_0} \tau_3(x, b) = \lim_{b\downarrow b^*} \tau(m_0, b) = \tau(\Omega).$$

Therefore, we only have to prove Part (a).

We begin with the study of the linearized problem

$$-u'' = \lambda u + pb\Omega^{p-1}u = \lambda(1-p)u,$$

whose integral curve through a generic point (x, y) in the phase plane (u, v) is the ellipse with equation

$$v^2 + \lambda(1-p)(u-\Omega)^2 = y^2 + \lambda(1-p)(x-\Omega)^2. \tag{1.84}$$

Figure 1.16 represents three of these integral curves. Precisely, Figure 1.16 shows the tangent straight lines

$$v = \pm y'(m_0)(u - m_0) \tag{1.85}$$

to the curves Γ_0 and Γ_1 at $(m_0, 0)$ (subsequently referred to as $\tilde{\Gamma}_0$ and $\tilde{\Gamma}_1$, respectively), the integral curves through $(m_0, 0)$, (x_t, y_t), and a generic point (x, y) with $x_{m_0} < x < x_t$, where (x_{m_0}, y_{m_0}) stands for the other crossing point between the integral curve through $(m_0, 0)$ and the line $\tilde{\Gamma}_0$, and (x_t, y_t) denotes the crossing point with $\tilde{\Gamma}_0$ of the unique integral curve tangent to it.

For every $x \in [x_{m_0}, x_t)$, we define $\tilde{\tau}_{1,a}(x)$ as the time needed to cross $\tilde{\Gamma}_1$ twice, starting at the point $(x, y) \in \tilde{\Gamma}_0$ and moving along the orbit up to reach (x_2, y_2), while $\tilde{\tau}_{1,a}(x_t)$ stands for the necessary time to reach $\tilde{\Gamma}_1$ for the first time starting at (x_t, y_t). By continuous dependence,

$$\tilde{\tau}_{1,a}(x_t) := \lim_{x\uparrow x_t} \tilde{\tau}_{1,a}(x).$$

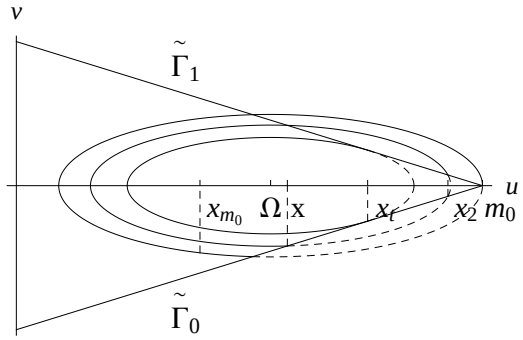

Figure 1.16: Some significant integral curves in the linearized case

We want to prove that

$$\tilde{\tau}_{1,a}(x) = \tau_2(\Omega) \qquad \text{for all } \; x \in [x_{m_0}, x_t].$$

To this end, we will show that $\tilde{\tau}_{1,a}(x)$ is actually constant as a function of x, and that

$$\tilde{\tau}_{1,a}(x_t) = \tau_2(\Omega).$$

Substituting (1.85) in (1.84) and solving yields to

$$x_2 = \frac{(y'(m_0))^2(2m_0 - x) + \lambda(1-p)(2\Omega - x)}{(y'(m_0))^2 + \lambda(1-p)}. \tag{1.86}$$

Similarly, substituting (1.85) in

$$v^2 + \lambda(1-p)(u-\Omega)^2 = y_t^2 + \lambda(1-p)(x_t - \Omega)^2$$

and imposing that x_t is a double solution, shows that

$$x_t = \frac{(y'(m_0))^2 m_0 + \lambda(1-p)\Omega}{(y'(m_0))^2 + \lambda(1-p)}.$$

Consequently,

$$x_t - \Omega = \frac{(y'(m_0))^2}{(y'(m_0))^2 + \lambda(1-p)}(m_0 - \Omega)$$

and, therefore, since $m_0 > \Omega$, $x_t > \Omega$. As it is apparent from Figure (1.16), $x_2 \geq x_t > \Omega$, since $x \in [x_{m_0}, x_t]$.

Subsequently, we denote by $x_L = x_L(x)$ and $x_M = x_M(x)$ the minimum and maximum values of the u-coordinate along the orbit E_x passing through (x, y), and, for every pair of points, (x_a, y_a), $(x_b, y_b) \in E_x$, $\tilde{t}_{x_a,x_b}$ stands for the

necessary time to reach (x_b, y_b) from (x_a, y_a) for the first time along E_x. By definition,

$$\tilde{\tau}_{1,a}(x) = \tilde{t}_{x,x_L} + \tilde{t}_{x_L,x_M} - \tilde{t}_{x_2,x_M} \tag{1.87}$$

(see Figure 1.16).

To calculate $\tilde{t}_{x_L,x_M}$, we consider the general solution of the linearized differential equation, which is given by

$$u(t) = \Omega + A\sin\left(\sqrt{\lambda(1-p)}\,t\right) + B\cos\left(\sqrt{\lambda(1-p)}\,t\right) \tag{1.88}$$

subjected to the initial conditions $(u(0), u'(0)) = (x_L, 0)$. Then, $\tilde{t}_{x_L,x_M}$ is the first (positive) time where u' vanishes. As

$$A = 0, \qquad B = x_L - \Omega,$$

we have that

$$u(t) = \Omega + (x_L - \Omega)\cos\left(\sqrt{\lambda(1-p)}\,t\right)$$

and, hence, the first (positive) time where $u' = 0$ is

$$\tilde{t}_{x_L,x_M} = \frac{\pi}{\sqrt{\lambda(1-p)}}.$$

Similarly, the unique solution of (1.88) such that $(u(0), u'(0)) = (x, y)$ satisfies

$$A = \frac{y}{\sqrt{\lambda(1-p)}} = \frac{y'(m_0)(x-m_0)}{\sqrt{\lambda(1-p)}} < 0, \qquad B = x - \Omega,$$

and, therefore, the first (positive) time where $u' = 0$ is

$$\tilde{t}_{x,x_L} = \begin{cases} \frac{1}{\sqrt{\lambda(1-p)}}\arctan\left(\frac{y'(m_0)}{\sqrt{\lambda(1-p)}}\frac{x-m_0}{x-\Omega}\right) & \text{if} \quad x < \Omega, \\ \frac{\pi}{2\sqrt{\lambda(1-p)}} & \text{if} \quad x = \Omega, \\ \tilde{t}_{x_M,x_L} - \frac{1}{\sqrt{\lambda(1-p)}}\arctan\left(\frac{-y'(m_0)}{\sqrt{\lambda(1-p)}}\frac{x-m_0}{x-\Omega}\right) & \text{if} \quad x > \Omega, \end{cases}$$

where it should be noted that

$$\tilde{t}_{x_M,x_L} = \tilde{t}_{x_L,x_M} = \frac{\pi}{\sqrt{\lambda(1-p)}}.$$

Analogously, the unique solution such that $(u(0), u'(0)) = (x_2, y_2)$ is given by (1.88) with

$$A = \frac{y_2}{\sqrt{\lambda(1-p)}} = -\frac{y'(m_0)(x_2-m_0)}{\sqrt{\lambda(1-p)}} > 0, \qquad B = x_2 - \Omega > 0,$$

where x_2 is given by (1.86). Thus, since $\tilde{t}_{x_2,x_M}$ is the first positive time where $u' = 0$, we obtain that

$$\tilde{t}_{x_2,x_M}=\frac{-1}{\sqrt{\lambda(1-p)}}\arctan\left(\frac{y'(m_0)}{\sqrt{\lambda(1-p)}}\frac{(y'(m_0))^2(m_0-x)+\lambda(1-p)(2\Omega-m_0-x)}{(y'(m_0))^2(2m_0-\Omega-x)+\lambda(1-p)(\Omega-x)}\right).$$

Consequently, setting

$$\begin{aligned}\beta &:= (y'(m_0))^2(m_0-x)+\lambda(1-p)(2\Omega-m_0-x),\\ \gamma &:= (y'(m_0))^2(2m_0-\Omega-x)+\lambda(1-p)(\Omega-x),\end{aligned}$$

differentiating with respect to x, and using (1.86), we find that,

$$\begin{aligned}\tilde{\tau}'_{1,a}(x) &= \tilde{t}'_{x,x_L}-\tilde{t}'_{x_2,x_M}\\ &= \frac{y'(m_0)(m_0-\Omega)}{y^2+\lambda(1-p)(x-\Omega)^2}-\frac{y'(m_0)[(y'(m_0))^2+\lambda(1-p)]^2(m_0-\Omega)}{(y'(m_0))^2\beta^2+\lambda(1-p)\gamma^2}\\ &= \frac{y'(m_0)(m_0-\Omega)}{y^2+\lambda(1-p)(x-\Omega)^2}-\frac{y'(m_0)(m_0-\Omega)}{y_2^2+\lambda(1-p)(x_2-\Omega)^2}=0,\end{aligned}$$

for all $x \neq \Omega$, because (x,y), $(x_2,y_2) \in E_x$ (see (1.84)). As, thanks to the theorem of differentiation of G. Peano, the function $\tilde{\tau}_{1,a}(x)$ is differentiable in x, necessarily it must be constant for all x. Therefore,

$$\tilde{\tau}_{1,a}(x)=\tilde{\tau}_{1,a}(x_t)$$

for all $x \in [x_{m_0}, x_t]$.

Adapting our previous calculations, it is easily seen that

$$\tilde{\tau}_{1,a}(x_t)=\frac{2}{\sqrt{\lambda(1-p)}}\left(\pi-\arctan\frac{\sqrt{\lambda(1-p)}}{y'(m_0)}\right),$$

which equals

$$\tau_2(\Omega)=\tau_1(\Omega)+\frac{\tau(\Omega)}{2}=\frac{1}{\sqrt{\lambda(1-p)}}\left(\pi+2\arctan\frac{y'(m_0)}{\sqrt{\lambda(1-p)}}\right),$$

by Theorem 1.9, since $\tan\theta+\tan 1/\theta=\pi/2$. This completes the proof of Part (a) for the linearization.

Now, we will prove Part (a) for the nonlinear problem. The basic idea will be adapting the technical device introduced in the proof of Theorem 1.9 by expanding $x_{m_0}(b)$ and $x_t(b)$ as power series centered at $b=b^*$ and then letting

$b \to b^*$ in the formulas for the time maps. By construction, $x_t(b)$ is uniquely determined by

$$\begin{cases} v^2 + \lambda u^2 + \frac{2b}{p+1}u^{p+1} = y^2(x_t(b)) + \lambda x_t^2(b) + \frac{2b}{p+1}x_t^{p+1}(b), \\ v'(x_t(b)) = y'(x_t(b)). \end{cases}$$

Thus, since $y(x_t) < 0$,

$$v(u) = -\sqrt{y^2(x_t(b)) + \lambda x_t^2(b) + \frac{2b}{p+1}x_t^{p+1}(b) - \lambda u^2 - \frac{2b}{p+1}u^{p+1}}$$

and, hence, $x_t(b)$ may be characterized as

$$y(x_t(b))y'(x_t(b)) + \lambda x_t(b) + bx_t^p(b) = 0 \tag{1.89}$$

for all $b > b^*$, $b \sim b^*$. Differentiating (1.89) with respect to b yields to

$$\left[(y'(x_t(b)))^2 + y(x_t(b))y''(x_t(b)) + \lambda + bpx_t^{p-1}(b)\right] x_t'(b) + x_t^p(b) = 0$$

and, so, particularizing at b^* yields to

$$x_t'(b^*) = -\frac{m_0^p}{(y'(m_0))^2 + \lambda(1-p)}.$$

Note that, thanks to the implicit function theorem and the theorem of differentiation of G. Peano, as a consequence from

$$(y'(m_0))^2 + \lambda(1-p) > 0$$

it follows the existence and the uniqueness of a real analytic function $x_t(b)$, $b \sim b^*$, such that

$$x_t(b) = m_0 - \frac{m_0^p}{(y'(m_0))^2 + \lambda(1-p)}(b - b^*) + O((b-b^*)^2), \qquad b \sim b^*. \tag{1.90}$$

Similarly, $x_{m_0}(b)$ is given through

$$y^2(x_{m_0}(b)) + \lambda x_{m_0}^2(b) + \frac{2b}{p+1}x_{m_0}^{p+1}(b) = \lambda m_0^2 + \frac{2b}{p+1}m_0^{p+1}. \tag{1.91}$$

To show its analyticity in b one can argue as follows. Setting

$$H(x,b) := y^2(x) + \lambda x^2 + \frac{2b}{p+1}x^{p+1} - \lambda m_0^2 - \frac{2b}{p+1}m_0^{p+1},$$

we consider the map

$$\tilde{H}(x,b) := \begin{cases} (x-m_0)^{-1}H(x,b), & \text{if } x \neq m_0, \quad x \sim m_0, \\ D_x H(m_0,b), & \text{if } x = m_0, \end{cases}$$

which is real analytic around $(x,b) = (m_0,b^*)$. It should be noted that $H(m_0,b) = 0$ for all $b \sim b^*$. Moreover,

$$\tilde{H}(m_0,b^*) = 2(y(m_0)y'(m_0) + \lambda m_0 + b^* m_0^p) = 0$$

and

$$D_x\tilde{H}(m_0,b^*) = 2[(y'(m_0))^2 + \lambda(1-p)] > 0.$$

Consequently, the analyticity of $x_{m_0}(b)$, $b \sim b^*$, with $x_{m_0}(b^*) = m_0$, follows from the implicit function theorem applied to $\tilde{H}$ at (m_0,b^*). Now, differentiating twice in (1.91) with respect to b, or, alternatively, differentiating with respect to b in

$$\tilde{H}(x_{m_0}(b),b) = 0,$$

yields to

$$x_{m_0}(b) = m_0 - \frac{2m_0^p}{(y'(m_0))^2 + \lambda(1-p)}\,(b-b^*) + O((b-b^*)^2), \qquad b \sim b^*. \quad (1.92)$$

Subsequently, we consider a generic point $x \in [x_{m_0}(b), x_t(b)]$, which can be parameterized as

$$x(s,b) := (1-s)x_{m_0}(b) + s x_t(b), \qquad s \in [0,1].$$

According to (1.90) and (1.92),

$$x(s,b) = m_0 + \frac{(s-2)m_0^p}{(y'(m_0))^2 + \lambda(1-p)}(b-b^*) + O((b-b^*)^2) \quad (1.93)$$

for all $b \sim b^*$, uniformly in $s \in [0,1]$.

Let $x_L(s,b)$ denote the minimum u-coordinate of the orbit through the point $(x(s,b), y(x(s,b))$. It satisfies

$$\lambda x_L^2(s,b) + \frac{2b}{p+1}x_L^{p+1}(s,b) = y^2(x(s,b)) + \lambda x^2(s,b) + \frac{2b}{p+1}x^{p+1}(s,b). \quad (1.94)$$

The fact that it is real analytic can be shown by brute force by computing all the Taylor series and checking that the coefficients can be locally estimated by those of a convergent series. Differentiating twice with respect to b in (1.94) we find that

$$x_L(s,b) = m_0 + \frac{\partial x_L}{\partial b}(s,b^*)\,(b-b^*) + O((b-b^*)^2) \quad (1.95)$$

as $b \downarrow b^*$, where

$$\frac{\partial x_L}{\partial b}(s,b^*) = -\frac{m_0^p + \sqrt{(m_0^p+\lambda(1-p)\partial_b x(s,b^*))^2 + \lambda(1-p)(y'(m_0)\partial_b x(s,b^*))^2}}{\lambda(1-p)}.$$

For every $s \in [0,1]$ and $b \sim b^*$, let $(x_2(s,b), y_2(s,b))$ be the second crossing point of the orbit through $(x(s,b), y(x(s,b))$ with the curve Γ_1, starting at $(x(s,b), y(x(s,b))$. It is given by

$$y^2(x_2(s,b)) + \lambda x_2^2(s,b) + \frac{2b}{p+1}x_2^{p+1}(s,b) = y^2(x(s,b)) + \lambda x^2(s,b) + \frac{2b}{p+1}x^{p+1}(s,b). \tag{1.96}$$

Being the existence already known, to prove its analyticity in b, we introduce the mappings

$$J(\xi,s,b) := y^2(\xi) + \lambda\xi^2 + \frac{2b}{p+1}\xi^{p+1} - y^2(x(s,b)) - \lambda x^2(s,b) - \frac{2b}{p+1}x^{p+1}(s,b),$$

and

$$\tilde{J}(\xi,s,b) := \begin{cases} (\xi - x(s,b))^{-1} J(\xi,s,b), & \text{if } \xi \neq x(s,b), \\ D_\xi J(m_0,s,b), & \text{if } \xi = x(s,b), \end{cases}$$

for $\xi \sim m_0$, $s \in [0,1]$, and $b \sim b^*$, which are real analytic at (m_0, s, b^*) for all $s \in [0,1]$. It should be noted that $J(x(s,b),s,b) = 0$ and that $\tilde{J}(x(s,b^*),s,b^*) = 0$ for all $s \in [0,1]$. Moreover,

$$D_\xi \tilde{J}(x(s,b^*),s,b^*) = 2[(y'(m_0))^2 + \lambda(1-p)] > 0.$$

Consequently, the analyticity of $x_2(s,b)$ is an easy consequence from the implicit function theorem. Moreover, by implicit differentiation, we obtain that

$$x_2(s,b) = m_0 - \left(\frac{2m_0^p}{(y'(m_0))^2 + \lambda(1-p)} + \partial_b x(s,b^*)\right)(b-b^*) + O((b-b^*)^2) \tag{1.97}$$

as $b \to b^*$.

The time $\tau_{1,a}(x(s,b),b)$ is given through

$$\tau_{1,a}(x(s,b),b) = I_1(s,b) + I_2(s,b),$$

where

$$I_1(s,b) := \int_{x_L(s,b)}^{x(s,b)} \frac{du}{\sqrt{f(x(s,b),b,u)}}, \qquad I_2(s,b) := \int_{x_L(s,b)}^{x_2(s,b)} \frac{du}{\sqrt{f(x(s,b),b,u)}},$$

with

$$f(x,b,u) := y^2(x) + \lambda(x^2-u^2) + \frac{2b}{p+1}\left(x^{p+1}-u^{p+1}\right).$$

By developing f around $(x,b,u) = (m_0, b^*, m_0)$, we have that

$$\begin{aligned} f(x(s,b),b,u) = &\left[(y'(m_0))^2+\lambda(1-p)\right](x(s,b)-m_0)^2+2m_0^p(x(s,b)-m_0)(b-b^*) \\ &- 2m_0^p(b-b^*)(u-m_0) - \lambda(1-p)(u-m_0)^2 + R(x(s,b),b,u), \end{aligned}$$

where

$$R(x(s,b),b,u) := \sum_{i+j+k\geq 3} c_{ijk}(x(s,b)-m_0)^i(b-b^*)^j(u-m_0)^k$$

for some constants c_{ijk} whose explicit knowledge is not important in this proof. According to (1.93), (1.95) and (1.97), and taking into account that $u \in [x_L(s,b), x(s,b)]$ in the first integral, while $u \in [x_L(s,b), x_2(s,b)]$ in the second one, we find that

$$\begin{aligned} |u-m_0| &\leq |\partial_b x_L(s,b^*)|\cdot|b-b^*| + O(|b-b^*|^2), \\ |x(s,b)-m_0| &\leq |\partial_b x(s,b^*)|\cdot|b-b^*| + O(|b-b^*|^2), \end{aligned}$$

as $b \to b^*$. Thus,

$$|R(x(s,b),b,u)| \leq \sum_{i+j+k\geq 3} |c_{ijk}||x(s,b)-m_0|^i|b-b^*|^j|u-m_0|^k \leq \sum_{h\geq 3} c_h(s)|b-b^*|^h,$$

for some positive $c_h(s)$, $h \geq 3$. Subsequently, we set

$$g(s,\xi) := \sum_{h\geq 3} c_h(s)\xi^h, \qquad s\in[0,1], \quad \xi \geq 0, \quad \xi \sim 0.$$

Note that

$$\lim_{b\downarrow b^*} \frac{g(s,|b-b^*|)}{(b-b^*)^2} = 0 \tag{1.98}$$

for all $s \in [0,1]$. Setting

$$\begin{aligned} h_\pm(s,b) := &\left[(y'(m_0))^2+\lambda(1-p)\right](x(s,b)-m_0)^2 \\ &+ 2m_0^p(x(s,b)-m_0)(b-b^*) \pm g(s,|b-b^*|) \end{aligned} \tag{1.99}$$

$$f_\pm(s,b,u) := h_\pm(s,b) - 2m_0^p(b-b^*)(u-m_0) - \lambda(1-p)(u-m_0)^2,$$

and

$$I_{1,\pm}(s,b) := \int_{x_L(s,b)}^{x(s,b)} \frac{du}{\sqrt{f_\pm(s,b,u)}}, \qquad I_{2,\pm}(s,b) := \int_{x_L(s,b)}^{x_2(s,b)} \frac{du}{\sqrt{f_\pm(s,b,u)}},$$

we find that

$$I_{j,+}(s,b) \le I_j(s,b) \le I_{j,-}(s,b), \qquad j \in \{1,2\}, \tag{1.100}$$

for all $s \in [0,1]$ and $b > b^*$ sufficiently close to b^*.

Now, performing the change of variable $\theta = u - m_0$ and completing squares in the radicand of all the integrals, one can proceed as in the proof of Theorem 1.9 to obtain that

$$\begin{aligned} I_{1,\pm}(s,b) &= \frac{1}{\sqrt{\lambda(1-p)}} \left(\arcsin \theta_{\pm}(s,b) - \arcsin \theta_{L,\pm}(s,b)\right), \\ I_{2,\pm}(s,b) &= \frac{1}{\sqrt{\lambda(1-p)}} \left(\arcsin \theta_{2,\pm}(s,b) - \arcsin \theta_{L,\pm}(s,b)\right), \end{aligned} \tag{1.101}$$

where

$$\theta_{\pm}(s,b) := \frac{\lambda(1-p)(x(s,b)-m_0) + m_0^p(b-b^*)}{\sqrt{m_0^{2p}(b-b^*)^2 + \lambda(1-p)h_{\pm}(s,b)}},$$

$$\theta_{L,\pm}(s,b) := \frac{\lambda(1-p)(x_L(s,b)-m_0) + m_0^p(b-b^*)}{\sqrt{m_0^{2p}(b-b^*)^2 + \lambda(1-p)h_{\pm}(s,b)}},$$

$$\theta_{2,\pm}(s,b) := \frac{\lambda(1-p)(x_2(s,b)-m_0) + m_0^p(b-b^*)}{\sqrt{m_0^{2p}(b-b^*)^2 + \lambda(1-p)h_{\pm}(s,b)}}.$$

Now, setting

$$\theta(s) := \lim_{b \downarrow b^*} \theta_{\pm}(s,b), \quad \theta_L(s) := \lim_{b \downarrow b^*} \theta_{L,\pm}(s,b), \quad \theta_2(s) := \lim_{b \downarrow b^*} \theta_{2,\pm}(s,b),$$

we find from (1.93), (1.95), (1.97), (1.99), and (1.98), letting $b \downarrow b^*$, that

$$\theta(s) = \frac{\lambda(1-p)\partial_b x(s,b^*) + m_0^p}{\sqrt{m_0^{2p} + \lambda(1-p)\left\{[(y'(m_0))^2 + \lambda(1-p)]\left(\frac{\partial x}{\partial b}(s,b^*)\right)^2 + 2m_0^p \frac{\partial x}{\partial b}(s,b^*)\right\}}},$$

$$\theta_L(s) = \frac{\lambda(1-p)\partial_b x_L(s,b^*) + m_0^p}{\sqrt{m_0^{2p} + \lambda(1-p)\left\{[(y'(m_0))^2 + \lambda(1-p)]\left(\frac{\partial x}{\partial b}(s,b^*)\right)^2 + 2m_0^p \frac{\partial x}{\partial b}(s,b^*)\right\}}},$$

$$\theta_2(s) = \frac{\lambda(1-p)\partial_b x_2(s,b^*) + m_0^p}{\sqrt{m_0^{2p} + \lambda(1-p)\left\{[(y'(m_0))^2 + \lambda(1-p)]\left(\frac{\partial x}{\partial b}(s,b^*)\right)^2 + 2m_0^p \frac{\partial x}{\partial b}(s,b^*)\right\}}}.$$

Thus,

$$\lim_{b\downarrow b^*} I_{1,\pm}(s,b) = \frac{1}{\sqrt{\lambda(1-p)}}\left(\arcsin\theta(s) - \arcsin\theta_L(s)\right),$$
$$\lim_{b\downarrow b^*} I_{2,\pm}(s,b) = \frac{1}{\sqrt{\lambda(1-p)}}\left(\arcsin\theta_2(s) - \arcsin\theta_L(s)\right),$$

and, consequently, thanks to (1.100), we find that

$$I_1(s) := \lim_{b\downarrow b^*} I_1(s,b) = \frac{1}{\sqrt{\lambda(1-p)}}\left(\arcsin\theta(s) - \arcsin\theta_L(s)\right),$$
$$I_2(s) := \lim_{b\downarrow b^*} I_2(s,b) = \frac{1}{\sqrt{\lambda(1-p)}}\left(\arcsin\theta_2(s) - \arcsin\theta_L(s)\right),$$

for all $s \in [0,1]$. Finally, invoking again (1.93), (1.95), and (1.97), and differentiating with respect to s, it is easily seen, after some tedious, but straightforward, manipulations, that

$$\frac{dI_1}{ds}(s) = -\frac{dI_2}{ds}(s) = \frac{y'(m_0)}{(y'(m_0))^2 + \lambda(1-p)(1-s)^2} \qquad \text{for all } \ s \in [0,1],$$

and, therefore,

$$I_1(s) + I_2(s) = I_1(1) + I_2(1) = \tau_{1,a}(x_t(b^*), b^*)$$

for all $s \in [0,1]$. As

$$\begin{aligned}\tau_{1,a}(x_t(b^*), b^*) &= \frac{1}{\sqrt{\lambda(1-p)}}\left(\arcsin\theta(1) + \arcsin\theta_2(1) - 2\arcsin\theta_L(1)\right)\\ &= \frac{1}{\sqrt{\lambda(1-p)}}\left(2\arcsin\sqrt{\frac{(y'(m_0))^2}{(y'(m_0))^2 + \lambda(1-p)}} + \pi\right)\\ &= \frac{1}{\sqrt{\lambda(1-p)}}\left(2\arctan\frac{y'(m_0)}{\sqrt{\lambda(1-p)}} + \pi\right) = \tau_2(\Omega),\end{aligned}$$

and, by symmetry, all these times equal the corresponding times when x runs over the interval $[x_t(b), m_0]$, instead of $[x_{m_0}(b), x_t(b)]$, the proof is complete. □

The results established by Theorem 1.15 are extremely sharp. Indeed, since $x_t(b) \in (x_{m_0}(b), m_0)$, Part (a), in particular, entails that

$$\lim_{b\downarrow b^*} \tau_1(x_t(b), b) = \tau_2(\Omega),$$

which is far from being obvious, as using directly some (not valid) continuous dependence argument, one might have been tempted to argue that $\tau_1(x_t(b), b)$ approximates $\tau_1(\Omega)$ as $b \downarrow b^*$, which is not true. Moreover, by Proposition 1.14,

$$\lim_{x\downarrow m_0}\lim_{b\downarrow b^*}\tau_3(x,b) = \lim_{x\downarrow m_0}\tau_3(x,b^*) = \lim_{x\downarrow m_0}\tau_3(x) = \tau_3(\Omega) > \tau(\Omega),$$

which, according to Theorem 1.15(c), shows that one cannot commute the double limit. This is utterly attributable to the lack of uniformity in the limit as $b \downarrow b^*$.

It should be noted that if the equation

$$\tau_{2n+1,s}(x,b) = 1 - 2\alpha$$

has some solution $x \in (x_{m_0}(b), m_0)$ for a b sufficiently close to b^*, then the graph of the orbit through $(x, y(x)) \in \Gamma_0$ must approach $(m_0, 0)$ as $b \downarrow b^*$. Therefore, these solutions must perturb from the trivial solution u_0. Similarly, if for some of these b's

$$\tau_{2n-1,a}(x,b) = 1 - 2\alpha,$$

then the graph of the orbit through $(x, y(x))$ must approximate $(m_0, 0)$ as $b \downarrow b^*$, and, therefore, these asymmetric solutions must perturb from u_0 too.

Throughout the rest of this chapter, we will use the following terminology, extending Definition 1.8.

Definition 1.16. Let u be a solution of (1.1) and an integer $n \geq 1$. Then:

- u is said to be of type T_n if $\tau_n(u(\alpha), b) = 1 - 2\alpha$.
- u is said to be of type $T_{2n-1,a}$ if $\tau_{2n-1,a}(u(\alpha), b) = 1 - 2\alpha$.
- u is said to be of type $T_{2n-1,s}$ if $\tau_{2n-1,s}(u(\alpha), b) = 1 - 2\alpha$.

It should be noted that the solutions of type T_n possess n local extrema in $(\alpha, 1-\alpha)$ and that, similarly, the solutions of type $T_{2n-1,j}$, $j \in \{s, a\}$, exhibit $2n-1$ local extrema there in. Also, note that the solutions of type T_{2n} and $T_{2n-1,a}$ are asymmetric, whereas the solutions of type T_{2n-1} and $T_{2n-1,s}$ are symmetric.

As an immediate consequence from the previous analysis, the following multiplicity result, sharpening Theorems 1.10 and 1.12, holds. Subsequently, given two arbitrary functions $u, v \in \mathcal{C}[0,1]$, we will denote

$$\|u - v\|_\infty := \max_{t\in[0,1]} |u(t) - v(t)|.$$

Theorem 1.17. *The following assertions are true:*

(a) *Suppose*

$$\tau_1(\Omega) > 1 - 2\alpha.$$

Then, there exists $\varepsilon > 0$ such that (1.1) has, at least, two solutions of type T_1 for every $b \in (b^*, b^* + \varepsilon)$. Moreover, the trivial solution u_0 perturbs into a solution of type T_1 as b separates away from b^*, in the sense that there exists a family of solutions of type T_1 of (1.1), say u_ε^1, $\varepsilon > 0$, $\varepsilon \sim 0$, with $b = b^* + \varepsilon$, such that

$$\lim_{\varepsilon \downarrow 0} \|u_\varepsilon^1 - u_0\|_\infty = 0.$$

(b) *Suppose*

$$\tau_1(\Omega) < 1 - 2\alpha < \tau_2(\Omega).$$

Then, there exists $\varepsilon > 0$ such that (1.1) has, at least, two solutions of type T_1 for every $b \in (b^*, b^* + \varepsilon)$. Moreover, the trivial solution u_0 perturbs into one of these solutions as b separates away from b^*. Precisely, there exist a family of solutions of type T_1, say u_ε^1, $\varepsilon > 0$, $\varepsilon \sim 0$, such that

$$\lim_{\varepsilon \downarrow 0} \|u_\varepsilon^1 - u_0\|_\infty = 0.$$

(c) *Suppose*

$$\tau_{2n+1}(\Omega) < 1 - 2\alpha < \tau_{2n+2}(\Omega) \tag{1.102}$$

for some integer $n \geq 1$. Then, there exists $\varepsilon > 0$ such that (1.1) possesses, at least, $2(2n+1)$ solutions for each $b \in (b^*, b^*+\varepsilon)$. More precisely, (1.1) possesses, at least, two solutions of type T_j, for each $2 \leq j \leq 2n+1$, one solution of type T_1 and an additional solution of type T_{2n+1}. Moreover, the trivial solution u_0 perturbs, at least, into one solution of type T_{2n+1}.

(d) *Suppose*

$$\tau_{2n}(\Omega) < 1 - 2\alpha < n\tau(\Omega) \tag{1.103}$$

for some integer $n \geq 1$. Then, there exists $\varepsilon > 0$ such that (1.1) possesses, at least, $4n$ solutions for every $b \in (b^*, b^* + \varepsilon)$. More precisely, (1.1) possesses, at least, two solutions of type T_j for every $j \in \{2, \ldots, 2n\}$, one solution of type T_1, and a solution of type $T_{2n-1,s}$. Moreover, the trivial solution u_0 perturbs, at least, into one solution of type $T_{2n-1,s}$.

(e) *Suppose*

$$n\tau(\Omega) < 1 - 2\alpha < \tau_{2n+1}(\Omega) \tag{1.104}$$

for some integer $n \geq 1$. Then, there exists $\varepsilon > 0$ such that (1.1) possesses, at least, $4n$ solutions for every $b \in (b^*, b^* + \varepsilon)$. More precisely, (1.1) possesses, at least, two solutions of type T_j for every $j \in \{2, \dots, 2n\}$, one solution of type T_1, and a solution of type T_{2n+1}. Moreover, the trivial solution u_0 perturbs, at least, into one solution of type T_{2n+1}.

Proof. For Part (b), one should take into account that, thanks to Theorem 1.15,

$$\tau(\Omega) \geq \lim_{b \downarrow b^*} \tau(x, b) \geq \lim_{b \downarrow b^*} \tau_{1,s}(x, b) \geq \lim_{b \downarrow b^*} \tau_{1,a}(x, b) = \tau_2(\Omega)$$

for all $x \in [x_t(b), m_0]$, and, consequently, u_0 must have a perturbed solution of type T_1. Actually, the proof of Theorem 1.15 can be adapted to show that $\lim_{b \downarrow b^*} \tau_{1,s}(x, b)$ is well defined for all $x \in [x_t(b), m_0]$ and

$$\left\{ \lim_{b \downarrow b^*} \tau_{1,s}(x, b) \ : \ x \in [x_t(b), m_0] \right\} = [\tau_2(\Omega), \tau(\Omega)];$$

the end-points reached at $x_t(b)$ and m_0, respectively. This information is needed in the proof of Part (d). □

1.4.2. The case $b < b^*$

Now, $\Omega > m_0$ and the phase portrait of (1.26) looks like shown in Figure 1.17 for all $0 < b < b^*$. Naturally, Figure 1.17 is reminiscent of Figure 1.9 and, consequently, we will not paraphrase its construction again. The main difference we can observe between the cases $b > b^*$ and $b < b^*$ is that the relative positions of the points x_{m_0}, x_t and Ω have been interchanged, so that, in case $b < b^*$,

$$x_0^-(b) < m_0 < x_t(b) < x_{m_0}(b) < x_0^+(b).$$

Note that $\Omega(b) \uparrow \infty$ if $b \downarrow 0$.

We already know that the solutions of (1.26) connecting Γ_0 with Γ_1 in a time $1 - 2\alpha$ provide us with the solutions of (1.1), as described in Section 1.2. But, as the phase portrait changes when b separates away from b^*, the time-maps $\tau_n = \tau_n(\cdot, b)$, $n \geq 1$, also change with b. In order to understand what happens when $0 < b < b^*$ we should first introduce an exhaustive list of Poincaré maps, much like in the previous section, which will provide us with all the solutions of (1.1).

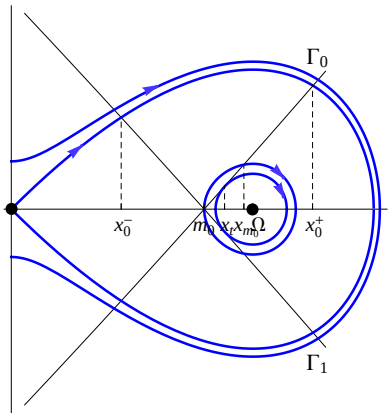

Figure 1.17: The phase portrait of (1.26) for $0 < b < b^*$

For every $b \in (0, b^*)$, we denote by

$$\tau_1(\cdot, b) \ : \ D_1(b) := (x_0^-, m_0) \cup [x_t, \infty) \to [0, \infty)$$

the Poincaré map defined, for every $x \in D_1$, as the minimal time needed by the solution of (1.32) to reach Γ_1. Figure 1.18 shows the corresponding orbits of two of these solutions for some $x < m_0$ (A) and $x > x_t$ (B). Note that $\tau_1(x_t, b)$ is the minimal time needed by the orbit through $(x_t, y(x_t))$ to reach Γ_1.

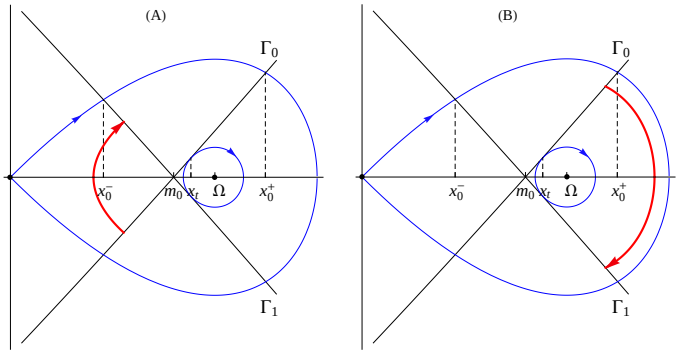

Figure 1.18: The time-map $(x, y(x)) \mapsto \tau_1(x, b)$ for $0 < b < b^*$

By continuous dependence, it is apparent that, for every $b \in (0, b^*)$,

$$\lim_{x \downarrow x_0^-} \tau_1(x, b) = \infty, \qquad \tau_1(m_0, b) := \lim_{x \uparrow m_0} \tau_1(x, b) = 0,$$

being m_0 not an equilibrium. In particular, $\tau_1(\cdot, b)$ admits a continuous extension to m_0 by setting $\tau_1(m_0, b) = 0$.

Next, we denote by

$$\tau_{1,s}(\cdot, b) \ : \ D_{1,s}(b) := [m_0, x_t] \to [0, \infty) \tag{1.105}$$

the Poincaré-map defined, for every $x \in (x_{m_0}, x_t)$, as the minimal time needed by the solution of (1.32) to reach Γ_1 exactly twice, whereas

$$\begin{aligned} \tau_{1,s}(x_t, b) &:= \lim_{x \uparrow x_t} \tau_{1,s}(x, b) = \tau_1(x_t, b) \\ \tau_{1,s}(m_0, b) &:= \lim_{x \downarrow m_0} \tau_{1,s}(x, b) = \tau(m_0, b). \end{aligned} \tag{1.106}$$

Figure 1.19 shows the orbit of one of these solutions with $x \in (m_0, x_t)$.

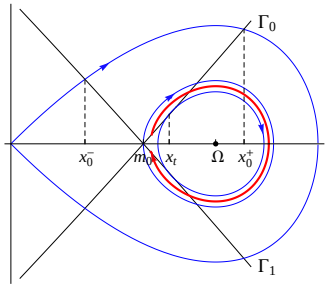

Figure 1.19: The time-map $(x, y(x)) \mapsto \tau_{1,s}(x, b)$ for $0 < b < b^*$

Now, for every $0 < b < b^*$, we consider the map

$$\tau_{1,a}(\cdot, b) \ : \ D_{1,a}(b) := [m_0, x_{m_0}] \to [0, \infty) \tag{1.107}$$

defined, for every $x \in [m_0, x_t)$, as the minimal time needed by the solution of (1.32) to reach Γ_1 by the first time (see Figure 1.20A), and, for every $x \in [x_t, x_{m_0}]$, as the minimal time needed by the solution of (1.32) to cross Γ_1 twice (see Figure 1.20B).

Since

$$\lim_{x \uparrow x_t} \tau_{1,a}(x, b) = \tau_{1,a}(x_t, b) = \tau_1(x_t, b)$$

it follows from (1.106) that

$$\tau_{1,a}(x_t, b) = \tau_{1,s}(x_t, b) = \tau_1(x_t, b).$$

Moreover,

$$\begin{aligned} \tau_{1,a}(x, b) &< \tau_{1,s}(x, b), \quad m_0 \le x < x_t, \\ \tau_1(x, b) &< \tau_{1,a}(x, b), \quad x_t \le x \le x_{m_0}. \end{aligned}$$

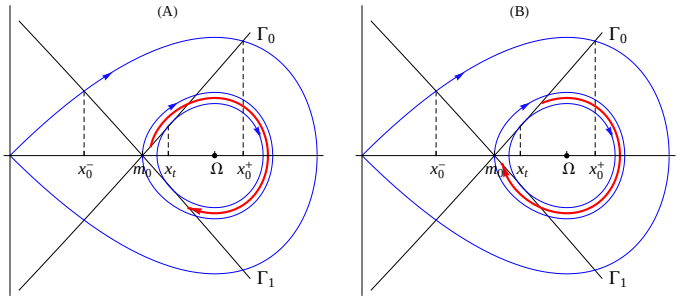

Figure 1.20: The time-map $(x, y(x)) \mapsto \tau_{1,a}(x, b)$ for $0 < b < b^*$

By construction, the solutions of $\tau_{1,s} = 1-2\alpha$ and $\tau_1 = 1-2\alpha$ provide us with symmetric solutions of (1.1), whereas the solutions given by $\tau_{1,a} = 1-2\alpha$ are asymmetric, except at $x = x_t$. All these solutions provide us with solutions of (1.1) with a single critical point in $(\alpha, 1-\alpha)$. Conversely, any solution of (1.1) with a single critical point in $(\alpha, 1-\alpha)$ must be of one of these forms.

As in the previous sections, we also introduce the Poincaré map

$$\tau_2(\cdot, b) \ : \ D_2(b) := (x_0^-, m_0] \cup [x_{m_0}, x_0^+) \to [0, \infty) \tag{1.108}$$

defined, for every $x \in D_2(b) \setminus \{m_0\}$, as the minimal time needed by the solution of (1.32) to reach Γ_1 exactly twice, while $\tau_2(m_0, b)$ is the minimal time needed by the solution of (1.32) to reach Γ_1. Figure 1.21 shows the corresponding orbits of two of these solutions for some $x \in (x_0^-, m_0)$ (A) and $x \in (x_{m_0}, x_0^+)$ (B). It should be observed that (1.1) cannot admit a solution of type T_2 passing

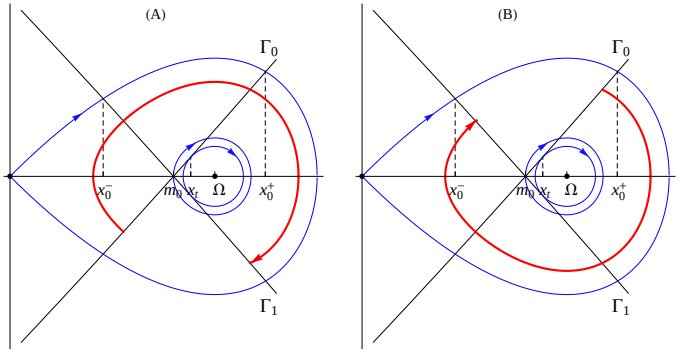

Figure 1.21: The time-map $(x, y(x)) \mapsto \tau_2(x, b)$ for $0 < b < b^*$

through $(x, y(x))$ if $m_0 \le x \le x_{m_0}$.

By continuous dependence and symmetry, it is easily seen that

$$\tau_{1,a}(x_{m_0}, b) = \tau_2(x_{m_0}, b) = \tau_2(m_0, b) = \tau_{1,a}(m_0, b),$$

and, by symmetry, each of the solutions on Figure 1.21(A) is the reflection of some solution in Figure 1.21(B).

Once defined the time maps $\tau_1(\cdot, b)$, $\tau_{1,a}(\cdot, b)$, $\tau_{1,s}(\cdot, b)$ and $\tau_2(\cdot, b)$ in the whole interval $0 < b < b_{m_0}$, one can introduce *mutatis mutandis*, as in Subsection 1.4.1, the Poincaré maps (1.78) and (1.79). Similarly, one can extend the θ_n's introduced in (1.80) and (1.81) to the case $0 < b < b^*$ by setting

$$\theta_{2n+1}(x, b) := \begin{cases} \tau_{2(n+1)+1}(x, b) & \text{if} \quad x \in (x_0^-, m_0], \\ \tau_{2n+1,s}(x, b) & \text{if} \quad x \in (m_0, x_t], \\ \tau_{2n+1}(x, b) & \text{if} \quad x \in (x_t, x_0^+), \end{cases} \tag{1.109}$$

for all $n \geq 0$, and

$$\theta_{2n}(x, b) := \begin{cases} \tau_{2n}(x, b) & \text{if} \quad x \in (x_0^-, m_0], \\ \tau_{2(n-1)+1,a}(x, b) & \text{if} \quad x \in (m_0, x_{m_0}), \\ \tau_{2n}(x, b) & \text{if} \quad x \in [x_{m_0}, x_0^+), \end{cases} \tag{1.110}$$

for all $n \geq 1$. These functions satisfy the following counterpart of Lemma 1.13, whose repetitive proof will be omitted here.

Lemma 1.18. *For every integer $n \geq 0$ and $b \in (0, b^*)$, we have that*

$$\theta_{2n+1}(x, b) \begin{cases} > \theta_{2(n+1)}(x, b) & \text{if} \quad x \in (x_0^-, x_t), \\ = \theta_{2(n+1)}(x_t, b) & \text{if} \quad x = x_t, \\ < \theta_{2(n+1)}(x, b) & \text{if} \quad x \in (x_t, x_0^+). \end{cases}$$

Moreover,

$$\max\left\{\theta_{2n+1}(x, b), \theta_{2(n+1)}(x, b)\right\} < \min\left\{\theta_{2(n+1)+1}(x, b), \theta_{2(n+2)}(x, b)\right\}$$

for all $x \in (x_0^-, x_0^+)$.

Naturally, since $x_{m_0}(b) \downarrow m_0$ if $b \uparrow b^*$, the following counterpart of Proposition 1.14 holds.

Proposition 1.19. *For every $n \geq 1$ and $\varepsilon > 0$ sufficiently small,*

$$\lim_{b \uparrow b^*} \tau_n(x, b) = \tau_n(x)$$

uniformly in

$$x \in [x_0^-(b^*) + \varepsilon, m_0 - \varepsilon] \cup [m_0 + \varepsilon, x_0^+(b^*) - \varepsilon].$$

Similarly, the following counterpart of Theorem 1.15 holds.

Theorem 1.20. *The following assertions are true:*

(a) $\lim_{b\uparrow b^*} \tau_{1,a}(x,b) = \tau_2(\Omega)$ *for all* $x \in [m_0, x_{m_0}(b)]$.

(b) $\lim_{b\uparrow b^*} \tau_{1,s}(m_0,b) = \tau(\Omega)$.

(c) $\lim_{b\uparrow b^*} \lim_{x\uparrow m_0} \tau_3(x,b) = \tau(\Omega)$.

Naturally, thanks to (1.78) *and* (1.79)*, we also have that*

$$\lim_{b\uparrow b^*} \tau_{2n-1,a}(x,b) = \tau_{2n}(\Omega) \qquad \text{for all } x \in [m_0, x_{m_0}(b)],$$

$$\lim_{b\uparrow b^*} \tau_{2n-1,s}(m_0,b) = n\tau(\Omega),$$

and that

$$\lim_{b\uparrow b^*} \lim_{x\uparrow m_0} \tau_{2n+1}(x,b) = n\tau(\Omega)$$

for all $n \geq 1$.

According to these properties, the graphs of these functions, for $0 < b < b^*$ should be of the type illustrated in Figure 1.22. Through the remaining of this chapter we will use the concepts introduced in Definition 1.16 extended to $0 < b < b^*$. By simply looking at Figure 1.22 one can easily infer the next counterpart of Theorem 1.17 for $b \in (0, b^*)$. Figure 1.22 collects the plots of the first seven Poincaré maps for an appropriate choice of the parameters with $b < b^*$.

Theorem 1.21. *The following assertions are true:*

(a) *Suppose* $\tau_1(\Omega) > 1 - 2\alpha$. *Then, there exists* $\varepsilon > 0$ *such that* (1.1) *has, at least, two solutions of type* T_1 *for each* $b \in (b^* - \varepsilon, b^*)$. *Moreover, the trivial solution* u_0 *perturbs into a solution of type* T_1 *as* b *separates away from* b^*.

(b) *Suppose* $\tau_1(\Omega) < 1-2\alpha < \tau_2(\Omega)$. *Then, there exists* $\varepsilon > 0$ *such that* (1.1) *has, at least, two solutions of type* T_1 *for every* $b \in (b^* - \varepsilon, b^*)$. *Moreover, the trivial solution* u_0 *perturbs, at least, into one solution of type* T_1 *as* b *separates away from* b^*.

(c) *Suppose* (1.102) *for some integer* $n \geq 1$. *Then, there exists* $\varepsilon > 0$ *such that* (1.1) *possesses, at least,* $2(2n+1)$ *solutions for each* $b \in (b^* - \varepsilon, b^*)$. *More precisely,* (1.1) *possesses, at least, two solutions of type* T_j*, for each* $2 \leq j \leq 2n+1$*, one solution of type* T_1 *and an additional solution of type* T_{2n+1}. *Moreover, the trivial solution* u_0 *perturbs, at least, into a solution of type* T_{2n+1}.

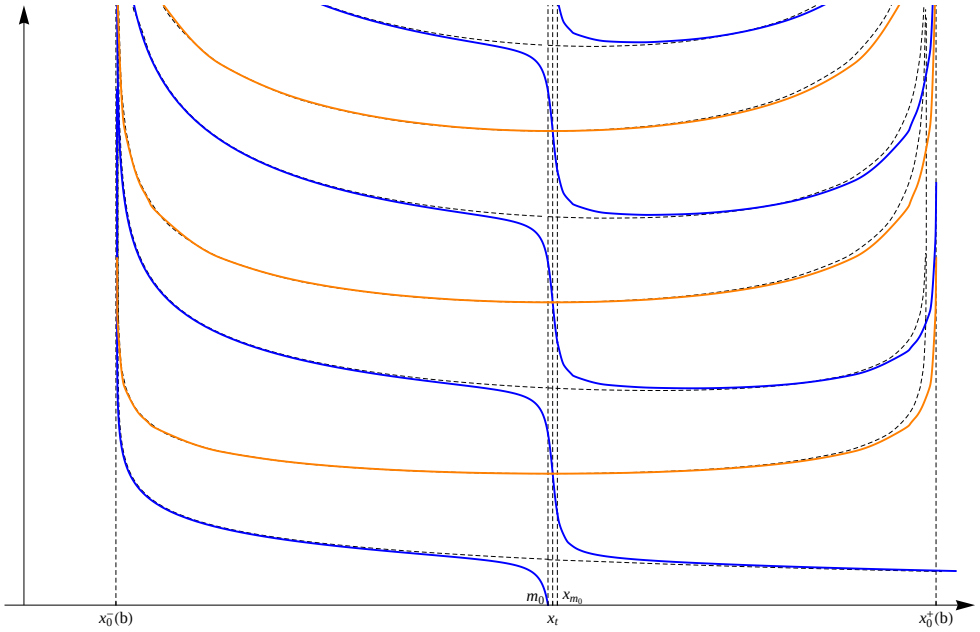

Figure 1.22: The graphs of the curves (1.78) and (1.79) for $0 < b < b^*$

(d) *Suppose* (1.103) *for some integer* $n \geq 1$. *Then, there exists* $\varepsilon > 0$ *such that* (1.1) *possesses, at least,* $4n$ *solutions for every* $b \in (b^* - \varepsilon, b^*)$. *More precisely,* (1.1) *possesses, at least, two solutions of type* T_j *for every* $j \in \{2, \ldots, 2n\}$, *one solution of type* T_1, *and a solution of type* $T_{2n-1,s}$. *Moreover, the trivial solution* u_0 *perturbs into one solution of type* $T_{2n-1,s}$.

(e) *Suppose* (1.104) *for some integer* $n \geq 1$. *Then, there exists* $\varepsilon > 0$ *such that* (1.1) *possesses, at least,* $4n$ *solutions for every* $b \in (b^* - \varepsilon, b^*)$. *More precisely,* (1.1) *possesses, at least, two solutions of type* T_j *for every* $j \in \{2, \ldots, 2n\}$, *one solution of type* T_1, *and a solution of type* T_{2n+1}. *Moreover, the trivial solution* u_0 *perturbs into one solution of type* T_{2n+1}.

1.5. Some general existence and non-existence results

Lemma 1.22. *Suppose that* $b \in (0, b_{m_0})$ *and* (1.1) *possesses a solution of type* T_n *for some* $n \geq 2$. *Then,*

(a) (1.1) *has, at least, two solutions of type* T_j *for all* $2 \leq j \leq n$, *if* n *is even.*

(b) (1.1) *has, at least, two solutions of type* T_j *for all* $2 \leq j \leq n-1$*, if* n *is odd.*

In both cases, (1.1) *exhibits, at least, a solution of type* T_1*.*

Proof. Under the assumptions of the lemma, there exists $x \in (x_0^-(b), x_0^+(b))$ such that

$$\tau_n(x, b) = 1 - 2\alpha. \tag{1.111}$$

Consequently, thanks to Lemmas 1.13 and 1.18, the equation

$$\tau_j(x, b) = 1 - 2\alpha$$

has, at least, two solutions for all $2 \leq j \leq n-1$ (see Figures 1.8, 1.15 and 1.22) and one solution for $j = 1$. If, in addition, n is even, then, by reflection and symmetry, the solutions of (1.111) must appear by pairs. This ends the proof. □

Lemma 1.23. *The following assertions are true:*

(a) *Suppose* $b_{m_0} \leq b < b_t$*. Then, the problem* (1.1) *cannot admit any solution of type* T_{2n} *with* $n \geq 1$*.*

(b) *Suppose* $b \geq b_t$*. Then,* (1.1) *admits, at most, solutions of type* T_1*. Moreover, any of these solutions* u *has a unique local maximum in* $(\alpha, 1-\alpha)$ *and satisfies*

$$u_L := \min_{[\alpha, 1-\alpha]} u = u(\alpha) > m_0.$$

Proof. Remember that b_{m_0} is the unique value of $b > b^*$ for which $(m_0, 0)$ belongs to the homoclinic trajectory through $(0, 0)$ (cf. Figure 1.10B if necessary), and that $b_t > b_{m_0}$ is the unique value of b for which this homoclinic is tangent to Γ_0, and, hence, to Γ_1 (see Figure 1.10C). Suppose

$$b_{m_0} < b < b_t.$$

By simply looking at the phase portraits of (1.26) it is easily seen that (1.1) cannot admit any solution of type T_2.

Indeed, the exterior trajectories of the solutions of (1.32) look like shown in Figure 1.23A and, consequently, they might provide us, at most, with solutions of type T_1 with a single local maximum in $(\alpha, 1-\alpha)$. The interior trajectories are orbits of periodic solutions around Ω. Let u be denote the solution of (1.32) with $P = (x, y(x)) \in \Gamma_0$. Its first critical point occurs at some time, say t_1 such that $u(t_1) = x_L$. The second one at some further time $t_2 > t_1$ such that

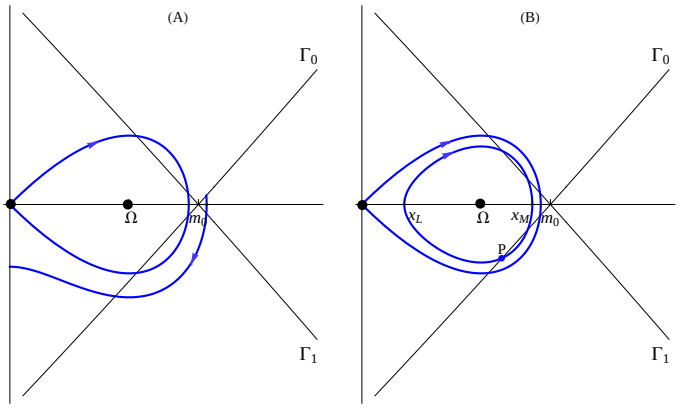

Figure 1.23: The phase portrait in case $b_{m_0} < b < b_t$

$u(t_2) = x_M$. But $(u(t), u'(t))$ cannot reach the curve Γ_1 without crossing again $(x_L, 0)$. Therefore, (1.1) cannot admit a solution of type T_2. Consequently, it cannot admit any solution of even order, however it might admit solutions of type T_{2n+1}, $T_{2n+1,s}$, and $T_{2n+1,a}$, for some integer $n \geq 0$. The proof of the lemma in this case can be adapted *mutatis mutandis* to cover the case $b = b_{m_0}$.

Now, suppose $b \geq b_t$. Then, the proof of the lemma is straightforward, as a glance to the phase portrait reveals that (1.1) might only admit solutions of type T_1, corresponding to solutions of (1.32) with $x > m_0$ (see Figure 1.24). The proof is complete. □

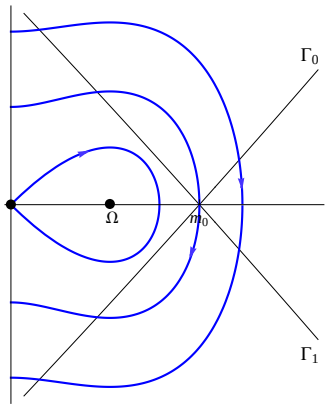

Figure 1.24: The phase portrait in case $b > b_t$

Weighting Lemma 1.22 against Lemma 1.23 might cause a little bit of confusion, as their results seem paradoxical. On one hand, Lemma 1.22 establishes

that if (1.1) admits a solution of type T_n, $n \geq 1$, then the problem must have solutions of type T_j for all $1 \leq j \leq n$ provided $0 < b < b_{m_0}$. On the other, Lemma 1.23 establishes that, in case $b_{m_0} \leq b < b_t$, (1.1) might have a solution of type T_{2n+1} but not solutions of type T_{2n}. As a byproduct, the structure of the diagram of Poincaré maps given by Figure 1.22, if $b^* < b < b_{m_0}$, should change as b crosses b_{m_0}. Actually, the graphs of the τ_{2n}'s in Figure 1.22 should disappear when b crosses b_{m_0}. In order to realize what happens, we will study all the possible solutions of (1.1) in case

$$b_{m_0} \leq b < b_t. \tag{1.112}$$

As in Section 1.4, we introduce the points $x_0^{\pm} = x_0^{\pm}(b)$ and $x_t = x_t(b)$ similarly, and define the time map

$$\tau_1 \ : \ D_1(b) := (x_0^-, x_t] \cup (m_0, \infty) \to [0, \infty), \tag{1.113}$$

for every $x \in D_1(b)$, as the minimal time needed by the solution of (1.32) to reach Γ_1. Figure 1.25 shows two trajectories corresponding to $x \in (x_0^-, x_t)$ and $x > m_0$.

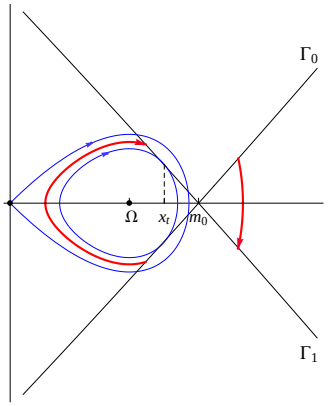

Figure 1.25: The Poincaré map τ_1 in case $b_{m_0} < b < b_t$

By continuous dependence,

$$\lim_{x \downarrow x_0^-} \tau_1(x, b) = \infty, \qquad \lim_{x \downarrow m_0} \tau_1(x, b) = 0. \tag{1.114}$$

Similarly, we introduce the map

$$\tau_{1,s} \ : \ D_{1,s}(b) := (x_t, x_0^+) \to [0, \infty), \tag{1.115}$$

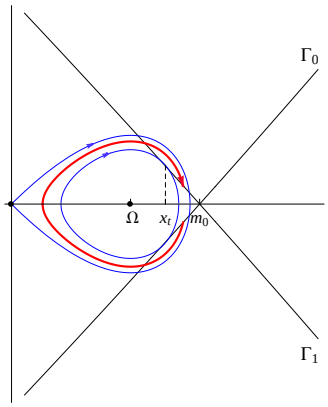

Figure 1.26: The Poincaré map $\tau_{1,s}$ in case $b_{m_0} < b < b_t$

defined, for every $x \in D_{1,s}(b)$, as the time needed by the solution of (1.32) to reach Γ_1 exactly twice (see Figure 1.26).
By continuous dependence, we have that

$$\lim_{x \downarrow x_t} \tau_{1,s}(x,b) = \tau_1(x_t,b), \qquad \lim_{x \uparrow x_0^+} \tau_{1,s}(x,b) = \infty. \tag{1.116}$$

Thus, $\tau_{1,s}$ may be regarded as a sort of continuous prolongation of τ_1 from $(x_0^-, x_t]$ to the wider interval (x_0^-, x_0^+).

In addition, we introduce the map

$$\tau_{1,a} \ : \ D_{1,a}(b) := (x_0^-, x_0^+) \to [0, \infty)$$

as follows. For every $x \in (x_0^-, x_t)$, $\tau_{1,a}(x,b)$ is the time needed by the solution of (1.32) to reach Γ_1 twice. For every $x \in (x_t, x_0^+)$, $\tau_{1,a}(x,b)$ is the minimal time needed by the solution of (1.32) to reach Γ_1. Finally,

$$\tau_{1,a}(x_t,b) := \lim_{x \to x_t} \tau_{1,a}(x,b) = \tau_1(x_t,b) = \tau_{1,s}(x_t,b). \tag{1.117}$$

Figure 1.27 shows the trajectories of these solutions in each of these situations. Note that, by construction,

$$\begin{aligned} \tau_1(x,b) &< \tau_{1,a}(x,b), \qquad x \in (x_0^-, x_t), \\ \tau_{1,a}(x,b) &< \tau_{1,s}(x,b), \qquad x \in (x_t, x_0^+). \end{aligned} \tag{1.118}$$

Consequently, the relative positions of the graphs of these curves are in complete agreement with Figure 1.28.

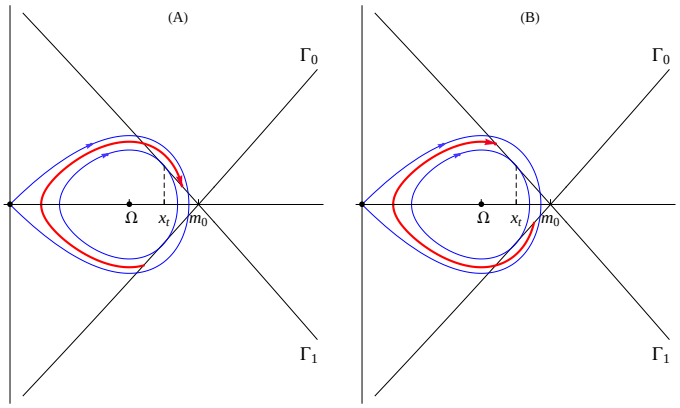

Figure 1.27: The Poincaré map $\tau_{1,a}$ in case $b_{m_0} < b < b_t$

Finally, for every integer $n \geq 1$, we introduce the maps

$$\begin{aligned} \tau_{2n+1}(x,b) &:= \tau_1(x,b) + n\tau(x,b), && x \in D_1(b), \\ \tau_{2n+1,s}(x,b) &:= \tau_{1,s}(x,b) + n\tau(x,b), && x \in D_{1,s}(b), \\ \tau_{2n+1,a}(x,b) &:= \tau_{1,a}(x,b) + n\tau(x,b), && x \in D_{1,a}(b), \end{aligned} \tag{1.119}$$

for all $b \in [b_{m_0}, b_t)$, where $\tau(x,b)$ is the period of the solution of (1.32).

According to Lemma 1.23, if the solution of (1.32) provides us with a solution of (1.1), necessarily

$$x \in \Sigma := \bigcup_{n\geq 0} \tau_{2n+1}^{-1}(1-2\alpha) \cup \tau_{2n+1,s}^{-1}(1-2\alpha) \cup \tau_{2n+1,a}^{-1}(1-2\alpha).$$

Conversely, if $x \in \Sigma$, then, the solution of (1.32) provides us with a solution of (1.1).

It should be noted that, by construction, we have that

$$\begin{aligned} \tau_{2n+1,a}(x,b) &< \tau_{2(n+1)+1}(x,b), && x \in (x_0^-, x_t), \\ \tau_{2n+1,s}(x,b) &< \tau_{2(n+1)+1,a}(x,b), && x \in (x_t, x_0^+), \end{aligned} \tag{1.120}$$

for all $n \geq 0$. Consequently, the set of graphs of all these Poincaré maps looks like shown in Figure 1.28, which shows the plots of some of these time maps.

To explain the transition from the set of τ_n's described in Figure 1.15 to the scheme shown in Figure 1.28, as b crosses the critical value b_{m_0}, one should be aware that

$$\lim_{b\uparrow b_{m_0}} x_{m_0}(b) = x_0^-(b_{m_0}), \qquad \lim_{b\uparrow b_{m_0}} x_0^+(b) = m_0 = x_0^+(b_{m_0}).$$

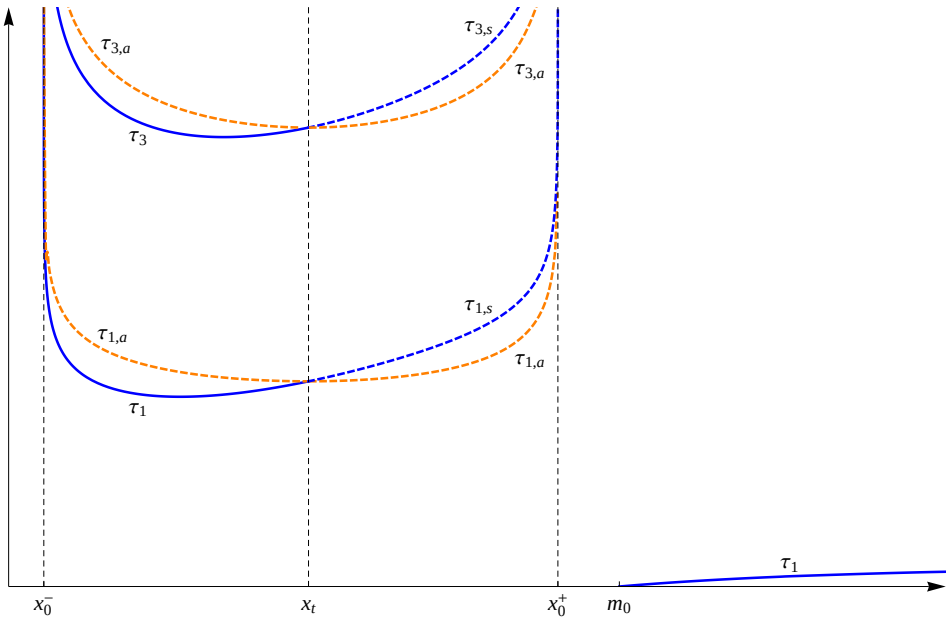

Figure 1.28: The Poincaré maps in case $b_{m_0} < b < b_t$

Actually, $x_0^+(b)$ crosses m_0 as b crosses b_{m_0}. Consequently,

$$\bigcap_{b<b_{m_0}} D_2(b) \subset \{x_0^{\pm}(b_{m_0})\},$$

i.e., the domains of definition of the τ_{2n}'s shrink towards the end points of the intervals as $b \uparrow b_{m_0}$, which explains why such time maps cannot be defined for $b \geq b_{m_0}$. Actually, by continuous dependence, it is easily seen that for any sequences $\varepsilon_n > 0$, $n \geq 1$, such that $\lim_{n\to\infty} \varepsilon_n = 0$, and $x_n \in D_2(b_{m_0} - \varepsilon_n)$, $n \geq 1$, one has that

$$\lim_{n\to\infty} \tau_2(x_n, b_{m_0} - \varepsilon_n) = \infty.$$

Therefore, the graphs of the τ_{2n}'s in Figure 1.15 grow up to infinity as $b \uparrow b_{m_0}$ while their domains of definition shrink to the limiting points, $x_0^{\pm}(b_{m_0})$. Consequently, letting $b \uparrow b_{m_0}$ in Figure 1.15, we exclusively keep the local structures bifurcated when b separated away from $b = b^*$, i.e., the left branch of τ_{2n+1}, and the whole branches of $\tau_{2n+1,s}$ and $\tau_{2n+1,a}$, for all $n \geq 0$. As in Figure 1.15, $\tau_{2n+1,s}$ linked the left branch of τ_{2n+1} with the right branch of $\tau_{2(n+1)+1}$, and $\tau_{2n+1,a}$ linked the left and the right branches of the τ_{2n}'s, it becomes apparent that indeed there is a continuous transition between all these time maps as b crosses b_{m_0}, though, at first glance, the natures of Figures 1.15 and 1.28 might look so different. It should be remarked that such a transition

still respects Lemma 1.13 as b crosses b_{m_0}, because the τ_{2n}'s gradually shorten their supports around their edges. This allows us to overcome the apparent paradox between the results established by Lemmas 1.22 and 1.23.

In the light of this discussion, it becomes apparent how emphasizing the superlinear character of (1.1), by increasing the value of b, has the effect of magnifying dramatically the local effects emerged from $\Omega = m_0$ as b separated away from b^*.

Later, as b increases and crosses b_{m_0}, the point $x_0^-(b)$ increases, while $x_0^+(b)$ decreases, until they meet at $b = b_t$. Therefore, all the graphs shown in Figure 1.28 collapse as b crosses b_t, except the right branch of τ_1 emerging from zero at m_0. A careful analysis of the phase portrait of (1.26) as b crosses b_t reveals that the graphs of the Poincaré maps τ_{2n+1}, $\tau_{2n+1,s}$ and $\tau_{2n+1,a}$, $n \geq 0$, do actually blow up as $b \uparrow b_t$.

The next result sharpens Lemma 1.23(b), establishing that (1.1) cannot admit any solution for sufficiently large b.

Lemma 1.24. *There exists $b_c \geq b_t$ such that (1.1) cannot admit any solution if $b \geq b_c$.*

Proof. Let $x > m_0$, $b \geq b_t$, and denote by u the unique solution of (1.32). Then, arguing as in the last part of the proof of Theorem 1.9 and setting

$$x_M = \max_{[\alpha,1-\alpha]} u > m_0,$$

it becomes apparent that

$$\begin{aligned}
\tau_1(x,b) &= 2\int_x^{x_M} \frac{d\xi}{\sqrt{\lambda(x_M^2-\xi^2)+\frac{2b}{p+1}(x_M^{p+1}-\xi^{p+1})}} \\
&= 2\int_{x/x_M}^1 \frac{d\theta}{\sqrt{\lambda(1-\theta^2)+\frac{2b}{p+1}x_M^{p-1}(1-\theta^{p+1})}} \\
&< 2\int_0^1 \frac{d\theta}{\sqrt{\lambda(1-\theta^2)+\frac{2b}{p+1}x_M^{p-1}(1-\theta^{p+1})}} \\
&< 2\int_0^1 \frac{d\theta}{\sqrt{\lambda(1-\theta^2)+\frac{2b}{p+1}m_0^{p-1}(1-\theta^{p+1})}}.
\end{aligned}$$

Thus, letting $b \uparrow \infty$ in this estimate, we are lead to

$$\lim_{b\uparrow\infty} \tau_1(x,b) = 0 \qquad \text{uniformly in } \ x \in (m_0,\infty).$$

Consequently, there exists $b_c \geq b_t$ such that $\tau_1(x,b) < 1-2\alpha$ for all $x > m_0$ and $b \geq b_c$. Therefore, (1.1) cannot admit any solution of type T_1. Lemma 1.23(b) completes the proof. □

Similarly, the following result holds.

Lemma 1.25. *For sufficiently small $b > 0$, the problem (1.1) cannot admit a solution of type T_n, nor of type $T_{2n-1,s}$, or $T_{2n-1,a}$, with $n \geq 2$.*

Proof. On the contrary, suppose that (1.1) admits one of such solutions, say u. Then, there are $t_1, t_2 \in [\alpha, 1-\alpha]$, with $t_1 < t_2$, such that

$$u'(t_1) = u'(t_2) = 0,$$

with $u'(t) > 0$ for all $t \in (t_1, t_2)$. Thus, setting $v = u'$, we have that

$$\begin{aligned} v^2(t) + \lambda u^2(t) + \frac{2b}{p+1}u^{p+1}(t) &= \lambda u^2(t_1) + \frac{2b}{p+1}u^{p+1}(t_1) \\ &= \lambda u^2(t_2) + \frac{2b}{p+1}u^{p+1}(t_2). \end{aligned}$$

By looking at the phase portrait for $0 < b < b^*$, it should be noted that $(u(t), u'(t))$ must lie on a closed orbit inside the homoclinic connection through $(0,0)$ in the phase portrait and that

$$u_1 := u(t_1) < m_0 < \Omega(b) < u_2 := u(t_2).$$

Thus,

$$\begin{aligned} 1 - 2\alpha \geq t_2 - t_1 &= \int_{u_1}^{u_2} \frac{d\xi}{\sqrt{-\lambda(\xi^2 - u_1^2) - \frac{2b}{p+1}(\xi^{p+1} - u_1^{p+1})}} \\ &= \int_1^{u_2/u_1} \frac{d\theta}{\sqrt{-\lambda(\theta^2 - 1) - \frac{2b}{p+1}u_1^{p-1}(\theta^{p+1} - 1)}}, \end{aligned}$$

and, hence,

$$1 - 2\alpha > \int_1^{u_2/u_1} \frac{d\theta}{\sqrt{-\lambda(\theta^2 - 1)}}.$$

Moreover,

$$\frac{u_2}{u_1} > \frac{\Omega(b)}{m_0}$$

and, consequently, we find that

$$1-2\alpha > \int_1^{\Omega(b)/m_0} \frac{d\theta}{\sqrt{-\lambda(\theta^2-1)}}. \tag{1.121}$$

As

$$\lim_{b\downarrow 0} \int_1^{\Omega(b)/m_0} \frac{d\theta}{\sqrt{-\lambda(\theta^2-1)}} = \int_1^{\infty} \frac{d\theta}{\sqrt{-\lambda(\theta^2-1)}} = \infty,$$

the estimate (1.121) cannot be satisfied for small $b > 0$. This concludes the proof. □

The proof of Lemma 1.25 does actually entail that

$$\lim_{b\downarrow 0} \tau_2(x,b) = \infty \qquad \text{for all } \ x \le m_0 \ \text{ and } \ x \ge x_{m_0}(b), \tag{1.122}$$

and that the period of any periodic solution around Ω blows up to ∞ as $b \downarrow 0$. On the other hand, we already know that

$$\tau_{1,a}(x_{m_0},b) = \tau_2(x_{m_0},b) = \tau_2(m_0,b) = \tau_{1,a}(m_0,b).$$

Thus,

$$\lim_{b\downarrow 0} \tau_{1,a}(m_0,b) = \infty = \lim_{b\downarrow 0} \tau_{1,a}(x_{m_0},b).$$

Consequently, it seems a reasonable conjecture that

$$\lim_{b\downarrow 0} \tau_{1,a}(x,b) = \infty \qquad \forall \ x > m_0. \tag{1.123}$$

It should be noted that, since

$$\tau_{1,a}(x,b) < \tau_{1,s}(x,b), \quad m_0 \le x < x_t,$$

if condition (1.123) holds, then

$$\tau_{1,a}^{-1}(1-2\alpha) = \varnothing = \tau_{1,s}^{-1}(1-2\alpha)$$

for sufficiently small $b > 0$ and, therefore, in such case, (1.1) cannot admit any solution

$$u \in T_{1,a} \cup T_{1,s}$$

for this range of b's. The next result characterizes the structure of the solution set of (1.1) with $M < \infty$ for sufficiently small $b > 0$ under conjecture (1.123).

Lemma 1.26. *There exist $\varepsilon > 0$ and a differentiable curve $u : [0, \varepsilon) \to \mathcal{C}^{2-}[0,1]$ such that, for every $b \in (0, \varepsilon)$, $u[b]$ provides us with a solution of type T_1 of (1.1), and $u[0]$ is the unique solution of (1.1) with $b = 0$. In particular, the solutions $u[b]$ bifurcate from $u[0]$ at $b = 0$. Moreover, the map $b \to u[b]$ is pointwise increasing.*

Furthermore, there exists $\delta > 0$ such that for every $b \in (0, \delta)$ the problem (1.1) admits a solution $U[b]$ such that

$$\max_{[\alpha,1-\alpha]} u[b] < m_0 < \Omega(b) = \left(\frac{-\lambda}{b}\right)^{\frac{1}{p-1}} < \max_{[\alpha,1-\alpha]} U[b]. \tag{1.124}$$

Consequently, the solutions $U[b]$ bifurcate from infinity at $b = 0$.

Proof. Throughout this proof it is appropriate to denote

$$a(t, b) = a(t),$$

to emphasize the dependence of the weight function a on the parameter $b \geq 0$.

According to Theorem 4.4 of [46], Problem (1.1) with the choice $b = 0$ possesses a unique positive solution. Let us denote it by $u[0]$. As in the interval $[0, 1]$ we have that

$$\left(-\frac{d^2}{dt^2} - \lambda - a(t, 0)(u[0])^{p-1}\right) u[0] = 0,$$

almost everywhere, and

$$u[0](0) = u[0](1) = M > 0,$$

it is apparent that $u[0]$ provides us with a positive strict supersolution of the second order operator

$$\mathfrak{L} := -\frac{d^2}{dt^2} - \lambda - a(t, 0)(u[0])^{p-1}$$

under Dirichlet boundary conditions in $[0, 1]$. Thus, owing to Theorem 2.1 of [50], the principal eigenvalue of $\mathfrak{L}$, denoted by $\sigma[\mathfrak{L}]$, is positive, i.e. $\sigma[\mathfrak{L}] > 0$.

Subsequently, we consider the nonlinear differential operator

$$\mathfrak{F} : D(\mathfrak{F}) := \mathcal{C}_0^1[0,1] \times [0, \infty) \to \mathcal{C}_0^1[0,1]$$

defined through

$$\mathfrak{F}(v, b) := v + M - \left(-\frac{d^2}{dt^2} + \omega\right)^{-1} \left[(\lambda + \omega)(v + M) + a(\cdot, b)(v + M)^p\right], \quad (v, b) \in D(\mathfrak{F}),$$

where $\omega > -\pi^2$ is fixed. Naturally, the change of variable

$$u = v + M$$

establishes a bijection between the solutions of (1.1) and the zeros of $\mathfrak{F}$. By construction, we have that

$$\mathfrak{F}(u[0] - M, 0) = 0.$$

Moreover, differentiating with respect to v leads to

$$\begin{aligned} D_v\mathfrak{F}(u[0] - M, 0) &= \mathrm{Id} - \left(-\frac{d^2}{dt^2} + \omega\right)^{-1} \left[\lambda + \omega + pa(\cdot, 0)(u[0])^{p-1}\right] \\ &= \mathrm{Id} - \left(-\frac{d^2}{dt^2} + \omega\right)^{-1} \left[\lambda + \omega - pc\chi_{[0,\alpha)\cup(1-\alpha,1]}(u[0])^{p-1}\right], \end{aligned}$$

where, as usual, for any given measurable subset $L \subset \mathbb{R}$, we have denoted by $\chi_{_L}$ the characteristic function of L. Note that $D_v\mathfrak{F}(u[0] - M, 0)$ is a Fredholm operator of index zero and suppose

$$D_v\mathfrak{F}(u[0] - M, 0)\psi = 0$$

for some $\psi \in \mathcal{C}_0^1[0, 1]$, $\psi \neq 0$. Then, by elliptic regularity theory,

$$\psi \in \mathcal{C}_0^{2-}[0, 1] \cap \mathcal{C}_0^2([0, 1] \setminus \{\alpha, 1 - \alpha\})$$

and

$$-\psi'' = \lambda\psi - pc\chi_{[0,\alpha)\cup(1-\alpha,1]}(u[0])^{p-1}\psi,$$

almost everywhere. Thus, zero is an eigenvalue of

$$\begin{aligned} \mathfrak{M} &:= -\frac{d^2}{dt^2} - \lambda + pc\chi_{[0,\alpha)\cup(1-\alpha,1]}(u[0])^{p-1} \\ &= \mathfrak{L} + (p-1)c\chi_{[0,\alpha)\cup(1-\alpha,1]}(u[0])^{p-1} \end{aligned}$$

and, therefore, as the principal eigenvalue is dominant, $\sigma[\mathfrak{M}] \leq 0$. But this is impossible, because, by the monotonicity of the principal eigenvalue with respect to the potential, we should have that

$$\sigma[\mathfrak{M}] > \sigma[\mathfrak{L}] > 0.$$

Consequently, $D_v\mathfrak{F}(u[0] - M, 0)$ is a topological isomorphism. Therefore, the existence of the solution curve $u[b]$, $b > 0$, $b \sim 0$, is a direct consequence of the

implicit function theorem. Actually, as $\mathfrak{M}$ satisfies the strong maximum principle, by differentiating with respect to b in (1.1) it is apparent that $D_b u[b] > 0$ for sufficiently small $b > 0$. Consequently, the map $b \to u[b]$ is increasing for such b's. Furthermore, as in the interval $[\alpha, 1-\alpha]$ we have that

$$-u''[0] = \lambda u[0] < 0,$$

the solution $u[b]$ must be strictly convex for sufficiently small $b > 0$. Thus, $u'[b](\alpha) < 0$ for sufficiently small $b > 0$, and, hence, owing to Theorem 1.1, $u[b] < m_0$ in $(\alpha, 1-\alpha)$ and it possesses a unique critical point (a local minimum) for small $b > 0$.

As a byproduct of these properties, thanks to the fact that $\tau_1(m_0, b) = \tau(m_0, b) \uparrow \infty$ as $b \downarrow 0$, it follows that, for every $b \in [0, \delta)$, (1.1) possesses a further solution, denoted by $U[b]$, such that $U[b](\alpha) > m_0$. Actually, according to Lemma 1.25, we have that

$$U[b](\alpha) \in \tau_1^{-1}(1-2\alpha) \cup \tau_{1,s}^{-1}(1-2\alpha)$$

for sufficiently small $b > 0$, and, consequently,

$$\max_{[\alpha, 1-\alpha]} U[b] > \Omega(b),$$

because $U[b](\alpha) > m_0$. This ends the proof. □

1.6. Global bifurcation diagrams

The main goal of this section is to ascertain all the possible global bifurcation diagrams of the set of solutions of (1.1) regarding $b \geq 0$ as the main bifurcation parameter. The reader should be aware that the one presented here are just "theoretical" bifurcation diagrams whose construction is based on the qualitative analysis of the time maps carried out in Sections 1.4 and 1.5. As far as the "real" diagrams, i.e. the one computed numerically, we send the reader to Chapter 3 where they are introduced and their quantitative properties are discussed.

It turns out that the more negative the secondary parameter λ is, the more complex is the structure of these global diagrams, in complete agreement with the multiplicity results found in Section 1.3.

In the light of the analysis already done in the previous sections, it becomes apparent that, as a general tendency, the $\tau_n(\cdot, b)$'s decrease with b for $b < b^*$, whereas they are increasing functions of b when $b > b^*$; independently on

whether the conjecture (1.123) holds or not. Indeed, by construction, (1.122) implies that $\tau_n(\cdot, b)$, $n \geq 3$, must grow up as $b \downarrow 0$ while they adjust to the profiles of the τ_n's constructed in Section 1.3 at the critical value of the parameter $b = b^*$, which plays the role of a sort of *organizing center* in our mathematical analysis. Similarly, thanks to Lemmas 1.24 and 1.25, the τ_n's must grow up as $b > b^*$ separates away from b^*, except for the right branch of τ_1 which approximates zero uniformly as $b \uparrow \infty$. Incidentally, this does not mean that all these functions will be pointwise monotonic in b. As a matter of fact, our numerical computations show that they are not (see the discussion at page 137).

At a first instance, in order to construct the global bifurcation diagrams of (1.1), it might be of great help to assume that all the graphs of the Poincaré maps τ_n, $\tau_{2n-1,a}$, $\tau_{2n-1,s}$, $n \geq 1$, are well-shaped, as those already represented in Figures 1.15 and 1.22. Since those shown in these figures, and some others that we have computed but not included here, adjust to this property, there is no serious reason to doubt that, in general, they will have a similar shape. Anyway, even if in the general case this is not true, the lack of such assumption would not change substantially the topological nature of the global bifurcation diagrams, and the readers should be able to implement very easily by themselves all the necessary changes in the forthcoming discussion.

Throughout this section we assume conjecture (1.123). Consequently, according to Lemmas 1.25 and 1.26, for small $b > 0$ all the global bifurcation diagrams consist of two curves consisting of solutions of type T_1: one emanating from the unique solution of (1.1) for $b = 0$, and the other one bifurcating from infinity at $b = 0$.

1.6.1. The case $\tau_1(\Omega) < 1 - 2\alpha < \tau_2(\Omega)$

Throughout this section we assume that

$$\tau_1(\Omega) = \tau_1(\Omega, b^*) < 1 - 2\alpha < \tau_2(\Omega, b^*) = \tau_2(\Omega). \tag{1.125}$$

According to Theorems 1.10, 1.17(b) and 1.21(b), the local bifurcation diagram around b^* looks like shown in Figure 1.29. The trivial solution, u_0, exhibits a bilateral bifurcation to one solution of type T_1.

In Figure 1.29, as in the remaining global bifurcation diagrams of this section, we are representing the value of $u(\alpha)$ versus the parameter b. It should be remember that

$$(u(\alpha), y(u(\alpha))) \in \Gamma_0.$$

Although in Figure 1.29, and in all subsequent bifurcation diagrams, we are representing a bifurcation from infinity at $b = 0$, it should be noted that (1.124)

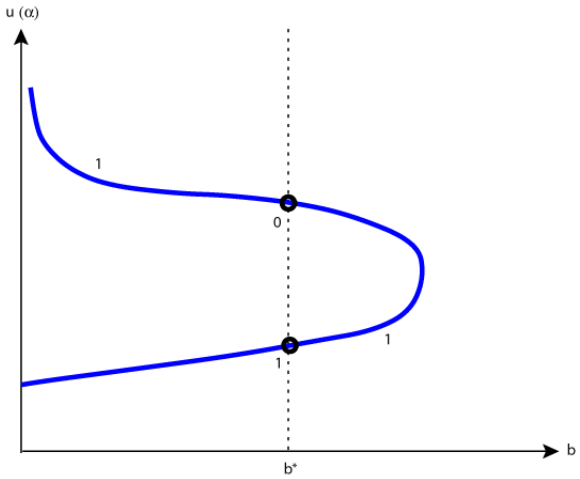

Figure 1.29: An admissible bifurcation diagram under condition (1.125)

does not necessarily entail

$$\lim_{b\downarrow 0} u(\alpha, b) = \infty,$$

but, simply,

$$\lim_{b\downarrow 0} u(1/2, b) = \infty.$$

Anyway, although we were not able to prove it, in the light of our numerical computations (see Section 3.4) we conjecture that this is what actually happens. For this reason we still represent a bifurcation from infinity in our qualitative bifurcation diagrams.

Figure 1.29 provides us with the same bifurcation diagram found by J. García-Melián [31] for a general multidimensional prototype of (1.1) with $\lambda = 0$ and $M = \infty$, which was already suggested by the mathematical analysis of J. López-Gómez [45].

1.6.2. The case $\tau_2(\Omega) < 1 - 2\alpha < \tau(\Omega)$

Throughout this section we assume that

$$\tau_2(\Omega) = \tau_2(\Omega, b^*) < 1 - 2\alpha < \tau(\Omega) = \tau(\Omega, b^*). \tag{1.126}$$

A significant difference with respect to the previous case is that now the trivial solution, u_0, exhibits a bilateral bifurcation to a solution of type $T_{1,s}$. By simply

having a look at Figures 1.15 and 1.22 it is easily realized that these solutions will be defined until we reach the first values of b where

$$\min \tau_{1,s}(\cdot, b) = 1 - 2\alpha, \tag{1.127}$$

which has been marked with a thick dot on the bifurcation diagram. In the case represented, there are two of such values of b. Beyond, the solutions become of type one.

Another noteworthy difference is that, under condition (1.126), Problem (1.1) with $b = b^*$ possesses two additional solutions of type T_2, which can be globally path-followed in the parameter b until

$$\tau_2(m_0, b) = \tau_2(x_{m_0}, b) = 1 - 2\alpha,$$

At these two values of b, the solutions of type T_2 become solutions of type $T_{1,a}$ until they further meet the branch of solutions of type $T_{1,s}$.

Figure 1.30 shows an admissible global bifurcation diagram under condition (1.126).

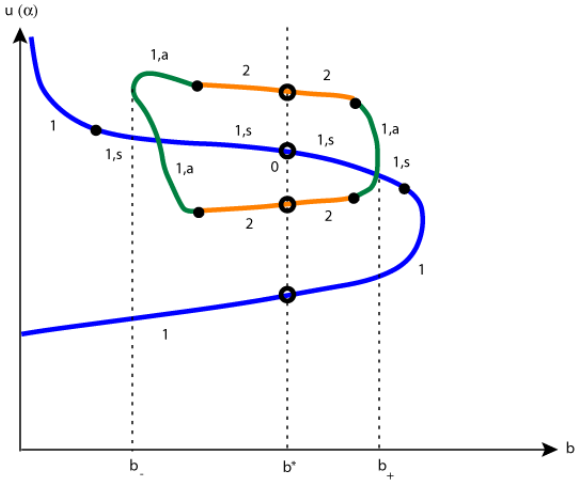

Figure 1.30: An admissible bifurcation diagram under condition (1.126)

In this case, there are two values of b, denoted by $b_- < b^* < b_+$, such that

$$\min \tau_{1,a}(\cdot, b) = 1 - 2\alpha.$$

In each of these values two different situations might occur. Either,

$$\min \tau_{1,a}(\cdot, b_\pm) \in \tau_{1,s}^{-1}(1 - 2\alpha), \tag{1.128}$$

or not. When condition (1.128) holds, the three solution curves meet at the solution u determined by the unique x such that

$$\min \tau_{1,a}(\cdot, b_\pm) = \tau_{1,s}(x, b_\pm),$$

which has been the situation illustrated by Figure 1.30 at b_+. If not, the branch of solutions of type $T_{1,a}$ must exhibit a turning point besides its crossing point with the branch of solutions of type $T_{1,s}$, which has been the situation illustrated by Figure 1.30 at $b = b_-$. The remaining features of the diagram can be easily inferred in the light of the results of Section 1.5.

1.6.3. The case $\tau(\Omega) < 1 - 2\alpha < \tau_3(\Omega)$

Figure 1.31 shows an admissible global bifurcation diagram in case

$$\tau(\Omega) < 1 - 2\alpha < \tau_3(\Omega). \tag{1.129}$$

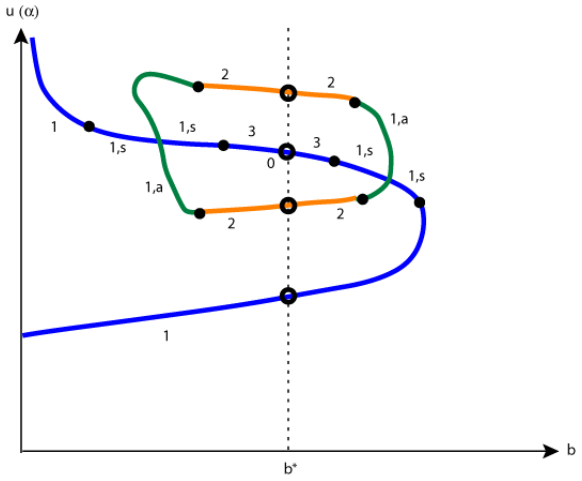

Figure 1.31: An admissible bifurcation diagram under condition (1.129)

The unique significant difference with respect to the diagram of Figure 1.30 is that, in the considered situation, according to Theorems 1.17(e) and 1.21(e), the trivial solution u_0 perturbs, as b separates away from b^*, into a solution of type T_3, instead of type $T_{1,s}$ as it happened under condition (1.126). Further, these solutions of type T_3 become solutions of type $T_{1,s}$ as $|b - b^*|$ increases, and beyond the situation evolves as in the previous case.

1.6.4. The case $\tau_3(\Omega) < 1 - 2\alpha < \tau_4(\Omega)$

Now, we assume that

$$\tau_3(\Omega) < 1 - 2\alpha < \tau_4(\Omega). \tag{1.130}$$

As in the previous cases, a careful analysis based on Figures 1.15 and 1.22 and the general properties of Section 1.5 reveals that an admissible global bifurcation diagram is the one sketched in Figure 1.32.

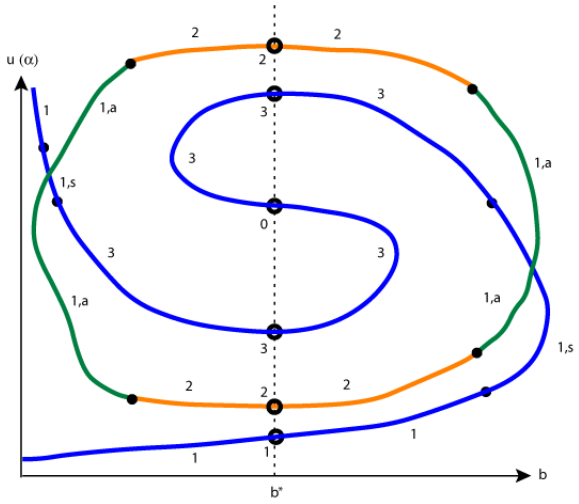

Figure 1.32: An admissible bifurcation diagram under condition (1.130)

As already predicted by Theorem 1.12, Problem (1.1) has, at least, six solutions for $b = b^*$. Among them, two of type T_3, two of type T_2, and one of type T_1, besides the trivial solution u_0. According to Theorems 1.17 and 1.21, the solutions of type T_j, $j = 1, 2, 3$, perturb, as b separates away from b^*, into solutions of the same type, while the trivial solution u_0 perturbs into an additional solution of type T_3. The b-evolution of the perturbed solutions as b moves far away from b^* has been ascertained by analyzing how the Poincaré maps illustrated in the Figures 1.15 and 1.22 vary as discussed at the beginning of Section 1.6.

Basically, much like in Figure 1.31, the diagram consists of two main curves. One filled in by solutions of odd type, which for this reason will be referred to as *odd* or *principal curve* and joins to infinity the solution of the sublinear problem associated to (1.1) by switching to zero the parameter b, plus a sort of close loop filled it by asymmetric solutions, which bifurcates from the odd curve at some points on the arcs of solutions of type $T_{1,s}$, and behaves globally

like the loop shown in Figure 1.31. Along the odd curve, the trivial solution perturbs into solutions of type T_3, which further switch to solutions of type $T_{1,s}$ before reaching, eventually, the solution arcs consisting of solutions of type T_1. Note that, in any circumstances, $m_0 = u_0(\alpha)$ is the value of $u(\alpha)$ where solutions of type T_3 become of type $T_{1,s}$. So, these transition points are at the same level in Figure 1.32.

A careful comparison between the structure of the global bifurcation diagrams of Figures 1.31 and 1.32 reveals that they are really very similar, in the sense that we are going to explain now. Indeed, under condition (1.129), as $\tau_3(\Omega)$ decreases crossing the value $1-2\alpha$ (for example because λ becomes sufficiently negative), there is some critical value of the parameters where the trivial solution u_0 must perturb into three solutions of type T_3. This entails that the structure of the bifurcation diagram in a neighborhood of u_0 is S-shaped for slightly perturbed values of the parameters. Initially, the S is small, as it perturbs from u_0, but, as $\tau_3(\Omega)$ separates away from $1-2\alpha$, the size of the S gradually grows up until it reaches a significant size, which has been the situation illustrated in Figure 1.32.

The structure of the solutions on the diagram fits the theoretical analytical results of Section 1.5, of course. In particular, for every $b \in (0, b^*)$ the problem has a solution of type T_2 whenever it has a solution of type T_3, however in Figure 1.32 there are some values of $b > b^*$ where the model has some solution of type T_3 and no solution of type T_2. According to Lemma 1.23, necessarily $b \geq b_{m_0}$.

1.6.5. The case $\tau_4(\Omega) < 1-2\alpha < 2\tau(\Omega)$

When

$$\tau_4(\Omega) < 1-2\alpha < 2\tau(\Omega), \tag{1.131}$$

a further loop of higher order asymmetric solutions emerges from the solutions of type T_4 of (1.1) at $b = b^*$. These solutions must bifurcate on the odd curve from the solutions of type $T_{3,s}$ perturbed from the trivial solution. An admissible bifurcation diagram following these patterns has been represented in Figure 1.33.

1.6.6. The case $2\tau(\Omega) < 1-2\alpha < \tau_5(\Omega)$

When

$$2\tau(\Omega) < 1-2\alpha < 2\tau_5(\Omega), \tag{1.132}$$

the only difference with respect to the previous case is the fact that the trivial solution perturbs into solutions of type T_5, instead of solutions of type $T_{3,s}$, as

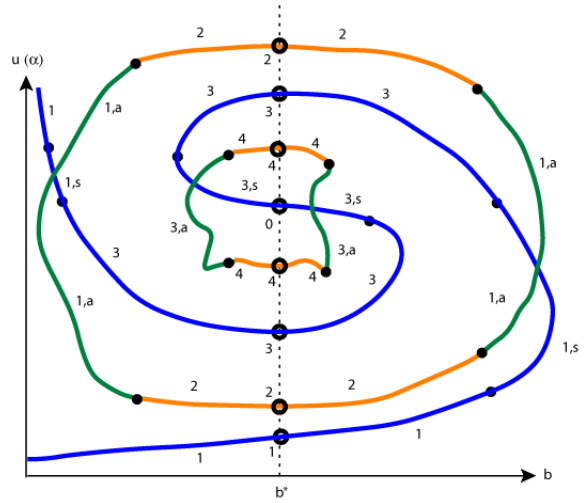

Figure 1.33: An admissible bifurcation diagram under condition (1.131)

b moves away from b^*. These solutions of type T_5 further become of type $T_{3,s}$ as b reaches some critical values. Figure 1.34 shows an admissible bifurcation diagram.

1.6.7. The case $\tau_5(\Omega) < 1 - 2\alpha < \tau_6(\Omega)$

When

$$\tau_5(\Omega) < 1 - 2\alpha < \tau_6(\Omega), \tag{1.133}$$

the main difference with respect to the previous case is that the odd curve exhibits an additional wind emerged from the trivial solution as $\tau_5(\Omega)$ crossed $1 - 2\alpha$. The other features of the bifurcation diagram can be explained reasoning as in the previous cases.

At this step, it should be rather apparent how to get all the admissible global bifurcation diagrams using b as the main parameter as the value of the secondary parameter λ becomes more and more negative.

1.7. Large solutions

This section is devoted to the construction of large solutions of equation (1.2), i.e., the solutions of (1.1) with $M = \infty$. As the basic idea for constructing them is letting $M \uparrow \infty$ in the analysis already done in Section 1.2, in this section we emphasize the dependence on $M > m^*$ of the differentiable

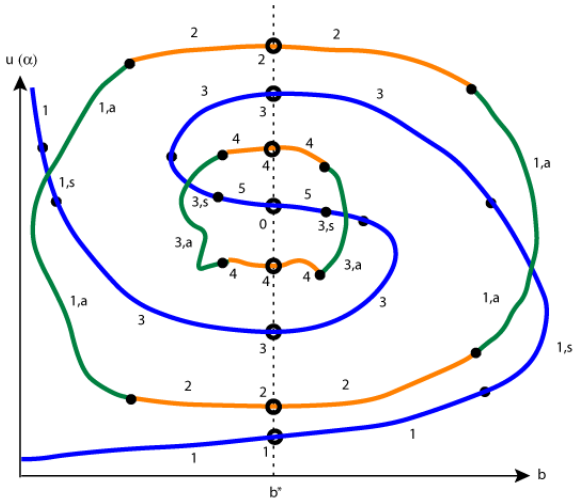

Figure 1.34: An admissible bifurcation diagram under condition (1.132)

curves Γ_0 and Γ_1 constructed in Theorem 1.2 and Corollary 1.9 by renaming them $\Gamma_{0,M}$ and $\Gamma_{1,M}$, respectively. Essentially, the methodology adopted in this section consists in showing that, the limiting curves

$$\Gamma_{0,\infty} := \lim_{M\uparrow\infty} \Gamma_{0,M}, \qquad \Gamma_{1,\infty} := \lim_{M\uparrow\infty} \Gamma_{1,M}, \tag{1.134}$$

do actually possess similar properties to those of $\Gamma_{0,M}$ and $\Gamma_{1,M}$, and play an analogous role in the construction of the solutions of (1.1) carried out in Sections 1.3, 1.4, 1.5 and 1.6. According to Theorem 1.6, $\Gamma_{0,M}$ is the graph of an smooth function denoted by $y(x)$. In this section, it is appropriate to rename this function by y_M so that

$$\Gamma_{0,M} = \{\, (x, y_M(x)) \quad : \quad x \geq 0 \,\}. \tag{1.135}$$

Although most of the proofs in this section follow the general patterns of the proofs of Section 1.2, by the sake of completeness, we will detail their main parts.

We begin our analysis with the following pivotal proposition which will provide us with $\Gamma_{0,\infty}$ in a compact way, without passing to the limit as $M \uparrow \infty$.

Proposition 1.27. *Suppose $\lambda \leq 0$. Then, the following properties hold:*

(a) *For every $x \geq 0$, the singular boundary value problem*

$$\begin{cases} -u'' = \lambda u - cu^p, \\ u(0) = \infty, \quad u(\alpha) = x, \end{cases} \tag{1.136}$$

has a unique positive solution.

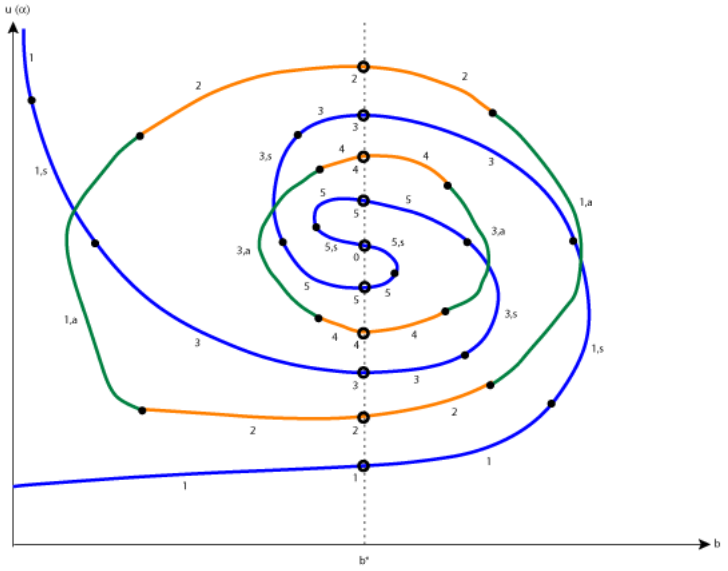

Figure 1.35: An admissible bifurcation diagram under condition (1.133)

(b) *There exists a unique value of x, denoted by $m_{0,\infty}$, for which the solution of (1.136) satisfies $u'(\alpha) = 0$. In other words, $m_{0,\infty} = u(\alpha)$, where $u(t)$ is the (unique) solution of the singular problem*

$$\begin{cases} -u'' = \lambda u - cu^p, \\ u(0) = \infty, \quad u'(\alpha) = 0. \end{cases} \tag{1.137}$$

(c) *For every $x \geq 0$, let denote by $y_\infty(x)$ the value of $u'(\alpha)$, where $u(t)$ is the unique solution of (1.136). Then,*

$$y_\infty(x) \begin{cases} < 0 & \text{if} \quad 0 \leq x < m_{0,\infty} \\ = 0 & \text{if} \quad x = m_{0,\infty} \\ > 0 & \text{if} \quad x > m_{0,\infty} \end{cases}$$

Throughout the rest of this section, we will consider the curve

$$\Gamma_{0,\infty} := \{\, (x, y_\infty(x)) \quad : \quad x \geq 0 \,\}.$$

Although (1.134) holds, the proof is postponed.

Proof. First, we will prove the existence and the uniqueness of $m_{0,\infty}$. Let $t^\infty_{min}(x)$ denote the time needed by a solution of (1.7) with $u(0) = \infty$ to reach

the u-axis in the phase plane (see Figure 1.2) at the point x, i.e., the necessary time to attain its minimum value x. Then,

$$t^{\infty}_{min}(x) = \int_x^{\infty} \frac{d\xi}{\sqrt{-\lambda(\xi^2 - x^2) + \frac{2c}{p+1}(\xi^{p+1} - x^{p+1})}} = \int_1^{\infty} \frac{d\theta}{\sqrt{-\lambda(\theta^2 - 1) + \frac{2c}{p+1}x^{p-1}(\theta^{p+1} - 1)}}$$

and, hence, t^{∞}_{min} is decreasing and it satisfies

$$\lim_{x\downarrow 0} t^{\infty}_{min}(x) = \infty, \qquad \lim_{x\uparrow\infty} t^{\infty}_{min}(x) = 0.$$

Therefore, there exists a unique value of $x > 0$ for which

$$t^{\infty}_{min}(x) = \alpha.$$

Let us denote it by $m_{0,\infty}$. Due to the monotonicity of t^{∞}_{min}, we have that

$$t^{\infty}_{min}(x) \begin{cases} > \alpha & \text{if} \quad 0 \le x < m_{0,\infty}, \\ = \alpha & \text{if} \quad x = m_{0,\infty}, \\ < \alpha & \text{if} \quad x > m_{0,\infty}. \end{cases} \tag{1.138}$$

Note that $t^{\infty}_{min}(0) = \infty$. This proves the first sentence of Part (b). To show that (1.137) admits a unique solution, we proceed by contradiction. Suppose it admits two solutions, $u_1 \neq u_2$. Then, by the uniqueness of the Cauchy problem at $t = \alpha$, we infer that $u_1(\alpha) \neq u_2(\alpha)$, but this contradicts the uniqueness of $m_{0,\infty}$ and completes the proof of Part (b).

Thanks to (1.138), we have that the solution of (1.136), if it exists, satisfies $u'(\alpha) < 0$ when $0 \le x < m_{0,\infty}$, whereas $u'(\alpha) > 0$ if $x > m_{0,\infty}$.

Now, we will prove Part (a). By Part (b), we already know that (1.136) does indeed admit a positive solution if $x = m_{0,\infty}$. Suppose $0 \le x < m_{0,\infty}$ and denote by $T_{\infty}(v)$ the backward blow-up time of the solution of

$$\begin{cases} -u'' = \lambda u - cu^p, \\ u(\alpha) = x, \quad u'(\alpha) = v < 0, \end{cases} \tag{1.139}$$

which is given by

$$T_{\infty}(v) = \int_x^{\infty} \frac{d\xi}{\sqrt{v^2 - \lambda(\xi^2 - x^2) + \frac{2c}{p+1}(\xi^{p+1} - x^{p+1})}}.$$

Obviously, $T_\infty(v)$ is increasing in $(-\infty, 0)$ and, due to (1.138), it satisfies

$$\lim_{v\downarrow-\infty} T_\infty(v) = 0 \quad \text{and} \quad \lim_{v\uparrow 0} T_\infty(v) = t^\infty_{min}(x) > \alpha.$$

Therefore, there exists a unique $v < 0$ such that $T_\infty(v) = \alpha$, which completes the proof of Part (a) in this case.

Suppose $x > m_{0,\infty}$ and let $v_u(x) > 0$ denote the intersection between the unstable manifold passing through $(0, 0)$ in the phase plane of (1.7) and the straight line $u = x$. For every $v \in (0, v_u(x))$, let $(m(v), 0)$ be the crossing point between the orbit through (x, v) and the u-axis. With these notations, it is easy to realize that the backward blow-up time of the solution of (1.139) is given by

$$T_\infty(v) = t^\infty_{min}(m(v)) + t_x(m(v)),$$

where

$$t_x(m(v)) := \int_{m(v)}^{x} \frac{d\xi}{\sqrt{v^2 - \lambda(\xi^2 - x^2) + \frac{2c}{p+1}(\xi^{p+1} - x^{p+1})}}$$

is the necessary time to reach $x = u(\alpha)$ from the minimum $m(v)$. According to (1.138), we find that

$$\lim_{v\downarrow 0} T_\infty(v) = t^\infty_{min}(x) < \alpha.$$

Moreover, by continuous dependence,

$$\lim_{v\uparrow v_u(x)} T_\infty(v) = \infty,$$

which implies the existence of a $v(x) \in (0, v_u(x))$ such that $T_\infty(v(x)) = \alpha$. To show the uniqueness and, hence, complete the proof of Part (a), we will prove the monotonicity of $T_\infty(v)$. As $m(v)$ is decreasing in $(0, v_u(x))$, $t^\infty_{min}(m(v))$ is increasing. Moreover,

$$t_x(m(v)) = \int_1^{x/m(v)} \frac{d\theta}{\sqrt{-\lambda(\theta^2 - 1) + \frac{2c}{p+1} m^{p-1}(v)(\theta^{p+1} - 1)}},$$

and, consequently, $t_x(m(v))$ is increasing. Therefore, we conclude that $T_\infty(v)$ is also increasing when $x > m_{0,\infty}$. This completes the proof of Part (a).

Part (c) is a straightforward consequence from the construction that we have just carried out in this proof. □

The next two results are corollaries from Proposition 1.27 and its proof.

Corollary 1.28. *Suppose $\lambda \leq 0$, $M > 0$, and $u(t)$ solves*

$$\begin{cases} -u'' = \lambda u - cu^p \\ u(0) = M, \quad u(\alpha) = x. \end{cases}$$

Then, $u'(\alpha) > y_\infty(x)$.

Proof. Suppose $u'(\alpha) = y_\infty(x)$. Then, by the uniqueness of the solution for the associated Cauchy problem, $M = \infty$, which is impossible. Suppose $u'(\alpha) < y_\infty(x)$. Then, since T_∞ is increasing, we find that

$$T_\infty(u'(\alpha)) < T_\infty(y_\infty(x)) = \alpha,$$

which is also impossible, because u is defined in $[0, \alpha]$. Therefore, $u'(\alpha) > y_\infty(x)$. □

Corollary 1.29. *Any solution of (1.136) achieves its minimum in $(\alpha/2, \alpha]$. In particular, it is decreasing in $(0, \alpha/2)$.*

Proof. Going back to the construction of the solutions of (1.136) in the proof of Proposition 1.27, the result is obvious. Indeed, for every $x \in [0, m_{0,\infty}]$, the solution u of (1.136) is decreasing and, hence,

$$\inf_{(0,\alpha]} u = u(\alpha) = x,$$

whereas, for every $x > m_{0,\infty}$,

$$\inf_{(0,\alpha]} u = m(u'(\alpha)) = u(t^\infty_{min}(x)),$$

where $t^\infty_{min}(x) \in (0, \alpha)$, because $u'(\alpha) = y_\infty(x) > 0$. It remains to prove that $t^\infty_{min}(x) > \alpha/2$. This follows very easily by contradiction. Suppose $t^\infty_{min}(x) \leq \alpha/2$. Then, by reflection around t^∞_{min} and uniqueness, it is apparent that $u(t)$ solves the problem

$$\begin{cases} -u'' = \lambda u - cu^p \\ u(0) = \infty, \quad u(2t^\infty_{min}) = \infty, \end{cases}$$

and, hence, u cannot be a solution of (1.136), because $2t^\infty_{min}(x) \leq \alpha$. This ends the proof. □

The next result establishes the monotonicity in M of the functions $y_M(x)$ constructed in Theorem 1.6 to parameterize the curves $\Gamma_{0,M}$.

Lemma 1.30. *For each $x \geq 0$, the map $M \mapsto y_M(x)$, $M > m^*$, is decreasing; m^* is the value constructed in Theorem 1.1.*

Proof. Let $m^* < M_1 < M_2$ and denote by u_i, $i = 1, 2$, the unique solution of

$$\begin{cases} -u'' = \lambda u - cu^p \\ u(0) = M_i, \quad u(\alpha) = x. \end{cases}$$

We want to prove that, under these conditions,

$$y_{M_1}(x) = u_1'(\alpha) > u_2'(\alpha) = y_{M_2}(x).$$

On the contrary, assume that $u_1'(\alpha) \leq u_2'(\alpha)$. Suppose $u_1'(\alpha) = u_2'(\alpha)$. Then, by the uniqueness of the Cauchy problem associated to (1.7) at $t = \alpha$, we find that $u_1 = u_2$ and, in particular, $M_1 = M_2$, which is a contradiction. Thus, $u_1'(\alpha) < u_2'(\alpha)$. As $u_1(\alpha) = u_2(\alpha) = x$, this implies that there exists $\varepsilon > 0$ such that $u_2(t) < u_1(t)$ for all $t \in (\alpha - \varepsilon, \alpha)$. Therefore, since

$$M_1 = u_1(0) < u_2(0) = M_2,$$

there exists $\theta \in (0, \alpha)$ such that $u_1(\theta) = u_2(\theta) = \tilde{u}$. Consequently, the boundary value problem

$$\begin{cases} -u'' = \lambda u - cu^p \\ u(\theta) = \tilde{u}, \quad u(\alpha) = x, \end{cases}$$

possesses two solutions in (θ, α), which contradicts the main result of [16]. The proof is complete. □

As an immediate consequence of these results, we find the next one.

Theorem 1.31. *For every $x \in [0, m_{0,\infty})$,*

$$y_\infty(x) = \lim_{M \uparrow \infty} y_M(x).$$

In particular, the first relation of (1.134) holds. Moreover, $y_\infty \in \mathcal{C}^1[0, m_{0,\infty})$ and it satisfies the implicit relation

$$G_\infty(x, y_\infty(x)) = \alpha, \qquad 0 \leq x < m_{0,\infty},$$

where

$$G_\infty(x, y) := \int_x^\infty \frac{d\xi}{\sqrt{y^2 - \lambda(\xi^2 - x^2) + \frac{2c}{p+1}(\xi^{p+1} - x^{p+1})}}.$$

Furthermore,

$$y_\infty'(x) = -\frac{\frac{\partial G_\infty}{\partial x}(x, y_\infty(x))}{\frac{\partial G_\infty}{\partial y}(x, y_\infty(x))}.$$

for all $x \in [0, m_{0,\infty})$.

Proof. Fix $x \geq 0$. According to Corollary 1.28, the family $\{y_M(x)\}_{M>m^*}$ is bounded from below by $y_\infty(x)$ and, owing to Lemma 1.30, it is decreasing in M. Therefore, the limit

$$\tilde{y}_\infty(x) := \lim_{M\uparrow\infty} y_M(x) \geq y_\infty(x)$$

is well defined.

Subsequently, for all $(x,y) \in ([0,\infty)\times\mathbb{R}) \setminus \{(0,0)\}$ and $M \in (m^*,\infty]$, we set

$$G_M(x,y) = \int_x^M \frac{d\xi}{\sqrt{y^2 - \lambda(\xi^2 - x^2) + \frac{2c}{p+1}(\xi^{p+1} - x^{p+1})}} \tag{1.140}$$

and denote

$$m_{0,M} := y_M^{-1}(0).$$

By Corollary 1.28 and Lemma 1.30,

$$m_{0,M_1} < m_{0,M_2} < m_{0,\infty}$$

if $m^* < M_1 < M_2 < \infty$. Thus, the limit

$$\tilde{m}_{0,\infty} := \lim_{M\uparrow\infty} m_{0,M} \leq m_{0,\infty}$$

is well defined. Moreover, by definition,

$$\alpha = t_{min,M}(m_{0,M}) = \int_1^{\frac{M}{m_{0,M}}} \frac{d\xi}{\sqrt{-\lambda(\xi^2-1) + \frac{2c}{p+1} m_{0,M}^{p-1}(\xi^{p+1}-1)}}$$

for all $M > m^*$. Thus, letting $M \uparrow \infty$, shows that $t^\infty_{min}(\tilde{m}_{0,\infty}) = \alpha$. As t^∞_{min} is monotone, necessarily $\tilde{m}_{0,\infty} = m_{0,\infty}$.

Let $x \in [0, m_{0,\infty})$. Then, for sufficiently large $M > m^*$, we have that $0 \leq x < m_{0,M}$ and, hence,

$$G_M(x, y_M(x)) = \alpha, \tag{1.141}$$

by construction. Thus, letting $M \uparrow \infty$ in (1.141), yields to

$$G_\infty(x, \tilde{y}_\infty(x)) = \alpha.$$

As $G_\infty(x,\cdot)$ is (strictly) increasing for $y \leq 0$, necessarily

$$\tilde{y}_\infty(x) = y_\infty(x) \qquad \forall\ x \in [0, m_{0,\infty}).$$

This ends the proof of the first assertion.

The regularity of y_∞ in $[0, m_{0,\infty})$ is a straightforward consequence from the implicit function theorem applied to the equation

$$G_\infty(x, y_\infty(x)) = \alpha, \qquad 0 \le x < m_{0,\infty},$$

based on the fact that

$$\frac{\partial G_\infty}{\partial y}(x, y_\infty(x)) = -\int_x^\infty \frac{y_\infty(x)}{\sqrt{\left[(y_\infty(x))^2 - \lambda(\xi^2 - x^2) + \frac{2c}{p+1}(\xi^{p+1} - x^{p+1})\right]^3}}\, d\xi > 0$$

because $y_\infty(x) < 0$ for all $x \in [0, m_{0,\infty})$. The proof is complete. □

We need a last preliminary result about the positive blow-up solutions of (1.7).

Lemma 1.32. *Suppose $\lambda \le 0$, $v < 0$, and let denote by $u(t) = u(t; x)$ the unique solution of the initial value problem*

$$\begin{cases} -u'' = \lambda u - cu^p & \text{in } (-\infty, 0] \\ u(0) = x \ge 0, \quad u'(0) = v. \end{cases}$$

Then, u is positive and blows up in finite time

$$T(x) := -G_\infty(x, v) < 0.$$

Moreover, T is a non-decreasing function such that

$$\lim_{x \uparrow \infty} T(x) = 0.$$

Proof. The unique delicate point is the monotonicity of T. To show it we will proceed by contradiction. Suppose that there are $0 \le x_1 < x_2$ such that $T(x_1) > T(x_2)$ and let u_i, $i = 1, 2$, denote the unique solution of

$$\begin{cases} -u'' = \lambda u - cu^p \\ u(0) = x_i, \quad u'(0) = v. \end{cases}$$

Then, there exists $\theta \in (T(x_1), 0)$ such that $u_1(\theta) = u_2(\theta)$ and, hence, the problem

$$\begin{cases} -u'' = \lambda u - cu^p \\ u(\theta) = u_1(\theta), \quad u'(0) = v. \end{cases}$$

admits two solutions in $(\theta, 0)$, which is impossible. □

The last result we need in order to cover the general case when $M \leq \infty$ is the next counterpart of Theorem 1.6 for $M = \infty$.

Theorem 1.33. *Suppose $\lambda \leq 0$. Then, $y_\infty \in \mathcal{C}^1[0,\infty)$ and it satisfies $y'_\infty(x) > 0$ for all $x \geq 0$.*

Proof. Fix $\varepsilon \in (0, \alpha/2)$. According to Proposition 1.27 (with $\alpha = \varepsilon$), for every $x \geq 0$, the problem

$$\begin{cases} -u'' = \lambda u - cu^p, \\ u(0) = \infty, \quad u(\varepsilon) = x, \end{cases} \tag{1.142}$$

has a unique positive solution. Let $y^\varepsilon_\infty : [0,\infty) \to \mathbb{R}$ denote the map defined by $y^\varepsilon_\infty(x) := u'(\varepsilon)$, where u is the unique solution of (1.142). By Proposition 1.27, y^ε_∞ satisfies

$$y^\varepsilon_\infty(x) \begin{cases} < 0 & \text{if} \quad 0 \leq x < m^\varepsilon_{0,\infty} \\ = 0 & \text{if} \quad x = m^\varepsilon_{0,\infty} \\ > 0 & \text{if} \quad x > m^\varepsilon_{0,\infty} \end{cases}$$

where $m^\varepsilon_{0,\infty}$ is the unique value of x for which $u'(\varepsilon) = 0$.

Thanks to Theorem 1.31 (applied with $\alpha = \varepsilon$), we obtain that $y^\varepsilon_\infty \in \mathcal{C}^1[0, m^\varepsilon_{0,\infty})$ and that it satisfies the implicit relation

$$G_\infty(x, y^\varepsilon_\infty(x)) = \varepsilon \qquad \forall x \in [0, m^\varepsilon_{0,\infty}).$$

As

$$\frac{\partial G_\infty}{\partial y}(x, y^\varepsilon_\infty(x)) > 0,$$

because $y^\varepsilon_\infty(x) < 0$ for all $x \in [0, m^\varepsilon_{0,\infty})$, and, thanks to Lemma 1.32,

$$\frac{\partial G_\infty}{\partial x}(x, y^\varepsilon_\infty(x)) \leq 0,$$

by implicit differentiation, it becomes apparent that

$$\frac{d}{dx} y^\varepsilon_\infty(x) = -\frac{\frac{\partial G_\infty}{\partial x}(x, y^\varepsilon_\infty(x))}{\frac{\partial G_\infty}{\partial y}(x, y^\varepsilon_\infty(x))} \geq 0$$

for every $x \in [0, m^\varepsilon_{0,\infty})$.

Let $\bar{u}$ be the unique solution of

$$\begin{cases} -u'' = \lambda u - cu^p, \\ u(0) = \infty, \quad u'(\alpha/2) = 0, \end{cases}$$

and set

$$\bar{x}(\varepsilon) := \bar{u}(\varepsilon);$$

it is defined by Proposition 1.27 (b) applied at $\alpha/2$. Similarly, we denote

$$\underline{x}(\varepsilon) := \underline{u}(\varepsilon),$$

where $\underline{u}$ is the unique solution of (1.136) with $x = 0$. Then,

$$\Gamma_{0,\infty} = \mathcal{P}_{\alpha-\varepsilon}\left(\{\,(x, y^{\varepsilon}_{\infty}(x)) \;\; : \;\; x \in [\underline{x}(\varepsilon), \bar{x}(\varepsilon))\,\}\right),$$

where $\mathcal{P}_{\alpha-\varepsilon}$ is the Poincaré map

$$x \in [\underline{x}(\varepsilon), \bar{x}(\varepsilon)) \longrightarrow \mathcal{P}_{\alpha-\varepsilon}(x) := (u(\alpha), u'(\alpha));$$

$u(t)$ being the unique solution of the Cauchy problem

$$\left\{\begin{array}{l} -u'' = \lambda u - cu^p \\ u(\varepsilon) = x, \;\; u'(\varepsilon) = y^{\varepsilon}_{\infty}(x). \end{array}\right. \tag{1.143}$$

As $\mathcal{P}_{\alpha-\varepsilon}$ is a diffeomorphism and

$$\{\,(x, y^{\varepsilon}_{\infty}(x)) \;\; : \;\; x \in [\underline{x}(\varepsilon), \bar{x}(\varepsilon))\,\}$$

is a curve of class $\mathcal{C}^1$, $\Gamma_{0,\infty}$ must be a curve of class $\mathcal{C}^1$.

The differential of the Poincaré map $\mathcal{P}_{\alpha-\varepsilon}$ is given by $(D\mathcal{S}(\alpha), \frac{d}{dt}D\mathcal{S}(\alpha))$, where $D\mathcal{S}(t)$ is the solution of

$$\left\{\begin{array}{l} -\frac{d^2}{dt^2}D\mathcal{S} = (\lambda - cpu^{p-1})\, D\mathcal{S} \\ D\mathcal{S}(\varepsilon) = 1, \;\; \frac{d}{dt}D\mathcal{S}(\varepsilon) = \frac{d}{dx}y^{\varepsilon}_{\infty}(x) \geq 0, \end{array}\right.$$

and u is the solution of (1.143). Obviously, the same device used in the proof of Theorem 1.6 shows that both components of $D\mathcal{P}_{\alpha-\varepsilon}$ are strictly positive. Consequently, $\Gamma_{0,\infty}$ is the graph of an increasing $\mathcal{C}^1$-function. Therefore, y_{∞} must be increasing and of class $\mathcal{C}^1$. The proof is complete. □

Naturally, the change of variables $\tilde{t} = 1-t$ provides us with the counterparts of the previous results in the interval $[1-\alpha, 1]$. As in Section 1.2, $\Gamma_{1,\infty}$ must be the reflection around the $u-$axis of $\Gamma_{0,\infty}$.

Remark 1.34. (a) Combining the results of this section with the techniques of Sections 1.3–1.6, it is easily realized that all the results for $M < \infty$ found in this chapter hold for $M = \infty$ too, except for the local perturbation result established by Lemma 1.26, which can be proven anyway by following the general patterns of M. Bertsch and R. Rostamian [11]. J. López-Gómez [45] and J. García-Melián [31].

(b) Throughout all this section we have used that some integrals, like the one defining $t^{\infty}_{min}(x)$ in the proof of Proposition 1.27, are finite and tend to 0 as $x \uparrow \infty$. This is a very special case of the so-called *Keller-Osserman condition*, which allows us to generalize, substantially, our results by dealing with more general classes of nonlinearities, but this is far from being our goal in this work.

Chapter 2

The multidimensional problem: existence, multiplicity and study of the linear stability

2.1. Introduction

This chapter studies the asymptotic behavior of the positive solutions of the parabolic problem

$$\begin{cases} u_t - \Delta u = \lambda u + a_b(x)u^p, & t > 0, \ \ x \in \Omega, \\ u(t,x) = M > 0, & t > 0, \ \ x \in \partial\Omega, \\ u(0,x) = u_0(x) \geq 0, & x \in \Omega, \end{cases} \tag{2.1}$$

where Ω is a bounded domain (open and connected set) of $\mathbb{R}^N$, $N \geq 1$, with sufficiently smooth boundary $\partial\Omega$ ($\mathcal{C}^3$ suffices for all our purposes here), $\lambda \in \mathbb{R}$, $p > 1$ and $M > 0$ are constants and $u_0 : \Omega \to \mathbb{R}$ is a non-negative function. To describe a_b we need to introduce some notation. Given a function $a \in L^\infty(\Omega)$, a_+ and a_- stand for its positive and negative part, respectively, i.e.

$$a_+ := \max\{a, 0\}, \qquad a_- := -\min\{a, 0\}.$$

Then, $a = a_+ - a_-$ and we set

$$\Omega_+ := \operatorname{int}\operatorname{supp} a_+, \quad \Omega_- := \operatorname{int}\operatorname{supp} a_-.$$

In this chapter we require these open sets to be nonempty subdomains of Ω with smooth boundary such that

$$\bar{\Omega}_+ \subset \Omega, \qquad \Omega = \bar{\Omega}_+ \cup \Omega_-.$$

Under these assumptions, we are taking

$$a_b := ba_+ - a_- \in L^\infty(\Omega),$$

where $b \in \mathbb{R}$ is regarded as the main bifurcation parameter of (2.1).

As a previous step to ascertain the dynamics of (2.1), it is imperative to study the existence and stability of its non-negative steady-states, which are the non-negative solutions of the associated elliptic semilinear boundary value problem

$$\begin{cases} -\Delta u = \lambda u + a_b(x)u^p & \text{in } \Omega, \\ u(x) = M & \text{on } \partial\Omega, \end{cases} \tag{2.2}$$

which is of superlinear indefinite type, as a_b changes sign in Ω if $b > 0$.

Observe that (1.1) is a particular case of this problem, with $N = 1$ and

$$\Omega = (0,1) \quad \text{and} \quad a = \chi_{(\alpha,1-\alpha)} - c\chi_{(0,\alpha)\cup(1-\alpha,1)}, \tag{2.3}$$

so that $\Omega_- = (0,\alpha) \cup (1-\alpha,1)$ and $\Omega_+ = (\alpha, 1, \alpha)$. However, the techniques used in Chapter 1 are purely one-dimensional and therefore cannot be used here. They are replaced by some genuine continuation methods of bifurcation theory and topological techniques.

As explained in the Introduction, most of the literature available for these type of problems concerns the simplest homogeneous case $M = 0$. However the inhomogeneous boundary conditions make the problem completely different, especially with regard to the linear asymptotic properties of the steady-states.

Among the main results of this chapter we emphasize the characterization of the range of λ's for which (2.2) admits a positive solution for some $b > 0$, and the proof of the existence of a minimal positive solution, which must be the unique linearly stable positive steady-state of (2.1). According to Theorem 2.9, (2.2) admits a positive solution for some $b > 0$ if, and only if, $\lambda < \sigma[-\Delta; \Omega_+]$, where $\sigma[-\Delta; \Omega_+]$ stands for the principal eigenvalue of $-\Delta$ in Ω_+ under homogeneous Dirichlet boundary conditions on $\partial\Omega_+$. Besides these results, we get some multiplicity results which seem to be optimal in the light of the discussion of Chapter 1 for $\lambda < 0$, $\lambda \sim 0$ (see in particular Proposition 1.11(b)) and the numerics presented here after and in Chapter 3. The multiplicity results have been obtained through the topological degree and the blowing-up techniques of [7], obtaining uniform a priori bounds for the solutions of (2.2) and using the crucial feature that (2.2) cannot admit a positive solution for sufficiently large $b > 0$.

The fact that the minimal positive steady-state of (2.1) is the unique linearly stable positive steady-state of (2.1) is an extremely astonishing and interesting result, because, the results of Chapter 1 show that (2.2), with the

particular choice (2.3), can exhibit an arbitrarily large number of positive solutions for some wide open ranges of the parameter b for sufficiently large $\lambda < 0$. More precisely we recall that a consequence of Theorem 1.12 and expressions (1.31) and (1.37) is that there exists a decreasing discrete sequence $\{\lambda_n\}_{n\geq 1} \subset (-\infty, 0)$ such that, for every $\lambda \in (\lambda_{n+1}, \lambda_n)$, there is $b^* = b^*(\lambda) > 0$ for which Problem (2.2) with $b = b^*$ admits at least $2n$ solutions. Moreover the local perturbation arguments of Section 1.4 show that the same number of solutions exists for the same range of λ and b varying in a neighborhood of b^*.

Figure 2.1 shows some of the bifurcation diagrams in b of Problem (2.2). They have been computed by using a spectral method with collocation, for the special choice (2.3) with $p = 2$, $c = 1$, $\alpha = 0.3$. Therefore, $\Omega^+ = (0.3, 0.7)$ in this case. In all those diagrams, we are representing the values of the bifurcation parameter b on the horizontal axis versus the values of $u(\alpha)$ on the vertical one.

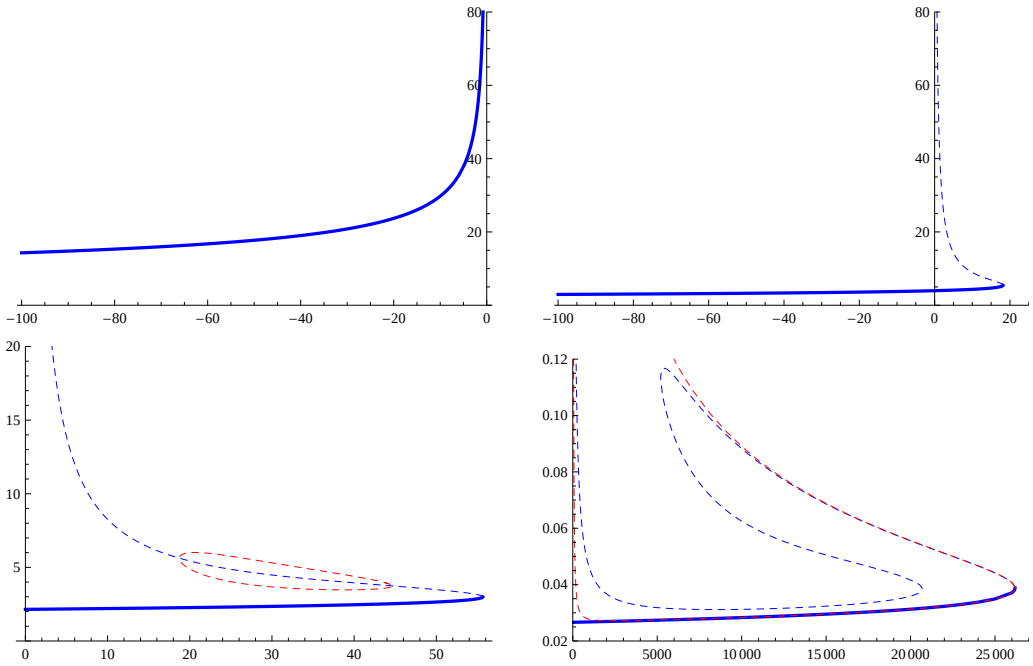

Figure 2.1: Bifurcation diagrams for $\lambda = 70$, $\lambda = -100$, $\lambda = -150$ and $\lambda = -750$, respectively.

In all these plots the thick continuous line represents the curve of minimal solutions, which, owing to Theorem 2.11, are linearly asymptotically stable, except at the biggest admissible value of b, where the minimal solution becomes linearly stable. All the remaining solutions, plotted with dashed lines, are

linearly unstable even if their number can be arbitrarily large for sufficiently large $\lambda < 0$.

The first plot of the first row of Figure 2.1 is the global bifurcation diagram of the positive solutions of (2.2) for $\lambda = 70 > \sigma[-\Delta; \Omega_+] \sim 61.62$. Consequently, according to Theorem 2.9, (2.2) cannot admit any positive solution for $b > 0$. The remaining three global bifurcation diagrams were computed for $\lambda < \sigma[-\Delta; \Omega_+]$ and, hence, owing to Theorem 2.9 and Theorem 2.10, there exists $b_\omega > 0$ such that (2.2) admits a positive solution if, and only if, $b < b_\omega$. As these plots were computed for a one-dimensional prototype model, thanks to Remark 2.18(c), the positive solutions of (2.2) have uniform a priori bounds and, consequently, according to Theorem 2.19, (2.2) must admit at least two positive solutions for every $b \in (0, b_\omega)$. Naturally, for $\lambda < \sigma[-\Delta; \Omega_+]$ sufficiently close to $\sigma[-\Delta; \Omega_+]$, the model should have exactly two solutions, as expected from our numerical computations, and, therefore, our multiplicity result seems again optimal.

We leave the exhaustive description of the numerical methods involved in these computations, and a complete description of all relevant features concerning the generation of these rather intricate bifurcation diagrams in Chapter 3.

The distribution of the chapter is the following. Section 2.2 collects some fundamental results which are going to be used throughout the rest of this chapter. Section 2.3 characterizes the local structure of the b-bifurcation diagrams around any linearly stable positive solution. Section 2.4 characterizes the existence of positive solutions for $b > 0$, and establishes the existence and stability of the minimal positive solutions. Section 2.5 shows that the minimal positive solution of (2.2) is the unique stable steady-state of (2.1), and, finally, Section 2.6 provides our main multiplicity result for (2.2).

2.2. Some notations and preliminary results

In this section we recall some fundamentals and useful preliminary results.

Throughout this chapter, a function $u : \Omega \to \mathbb{R}$ is said to be *positive* if $u(x) \geq 0$ for all $x \in \Omega$ but $u \neq 0$. In such a case, it is simply said that $u > 0$. Similarly, a function $u \in \mathcal{C}^1(\bar{\Omega})$ is said to be *strongly positive*, and will be denoted by $u \gg 0$, if $u(x) > 0$ for all $x \in \Omega$ and $\partial u(x)/\partial n_x < 0$ for all $x \in \partial\Omega \cap u^{-1}(0)$, where n_x stands for the outward unit normal vector at $x \in \partial\Omega$. Naturally, (b_0, u_0) is said to be a solution (resp. supersolution, or subsolution) of (2.2) if u_0 solves (2.2) (resp. is a supersolution or a subsolution) for $b = b_0$.

As $a_b \in L^\infty(\Omega)$, by elliptic regularity, any weak solution u of (2.2) satisfies

$$u \in \bigcap_{p>1} W^{2,p}(\Omega)$$

and, hence, $u \in \mathcal{C}^{1+\nu}(\bar{\Omega})$ for all $\nu \in [0,1)$ and u is twice classically differentiable almost everywhere (e.g., D. Gilbarg and N. S. Trudinger [35]). Moreover, the change of variable $v := u - M$, transforms the problem of the search for positive solutions of (2.2) into the problem of the search for solutions of

$$\begin{cases} -\Delta v = \lambda(v+M) + a_b(x)(v+M)^p & \text{in } \Omega, \\ v = 0 & \text{in } \partial\Omega, \\ v > -M & \text{in } \Omega, \end{cases} \tag{2.4}$$

Subsequently, for any regular subdomain $D \subset \Omega$ and $V \in L^\infty(D)$ we denote by $\sigma[-\Delta + V, D]$ the principal eigenvalue of $-\Delta + V$ in D under homogeneous Dirichlet boundary conditions, and given any positive solution (b_0, u_0) of (2.2), we denote by

$$\mathfrak{L}_{(b_0,u_0)} := -\Delta - \lambda - a_{b_0} p u_0^{p-1}$$

the linearization with respect to u of (2.2) at (b_0, u_0). Then, according to the *principle of linearized stability* (see e.g., A. Lunardi [62]), the following concepts are consistent

Definition 2.1. A solution (b_0, u_0) of (2.2) is said to be:

- linearly asymptotically stable (l.a.s.) if $\sigma[\mathfrak{L}_{(b_0,u_0)}, \Omega] > 0$,
- linearly unstable (l.u.) if $\sigma[\mathfrak{L}_{(b_0,u_0)}, \Omega] < 0$,
- linearly neutrally stable (l.n.s.) if $\sigma[\mathfrak{L}_{(b_0,u_0)}, \Omega] = 0$,
- linearly stable (l.s.) if $\sigma[\mathfrak{L}_{(b_0,u_0)}, \Omega] \geq 0$.

The following result is pivotal in our analysis. It goes back to [50] and [7]. A complete proof can be found in the monograph [48].

Theorem 2.2 (Characterization of the strong maximum principle)**.** *Let D be a domain in $\mathbb{R}^N$, $N \geq 1$, with boundary of class $\mathcal{C}^2$ and $V \in L^\infty(\Omega)$. Then, the following assertions are equivalent:*

(a) $\sigma[-\Delta + V, D] > 0$;

(b) There exist $p > N$ and $h \in W^{2,p}(D)$, $h > 0$, such that $(-\Delta + V)h \geq 0$ in D, $h|_{\partial D} \geq 0$, with some of these inequalities strict; i.e., h is a positive strict supersolution of $(-\Delta + V, D)$.

(c) $-\Delta + V$ *satisfies the strong maximum principle in* D*, in the sense that* $u \in W^{2,p}(D)$ *for some* $p > N$ *and*

$$(-\Delta + V)u \geq 0 \qquad \text{in } D, \qquad u|_{\partial D} \geq 0,$$

with some of these inequalities strict, imply that $u \gg 0$ *in* D*.*

In particular, from Theorem 2.2 one can easily obtain all the properties of the principal eigenvalue used in our results (see Chapters 8 and 9 of [48]).

The existence and the uniqueness of positive solutions of (2.2) in the special case $b \leq 0$, is an immediate consequence from the abstract theory developed in [46, Section 3], where the reader is sent for all necessary technical details of the proof of the next theorem.

Theorem 2.3. *In case* $b < 0$*,* (2.2) *possesses a positive solution for each* $\lambda \in \mathbb{R}$*, whereas in case* $b = 0$*,* (2.2) *admits a positive solution if, and only if,* $\lambda < \sigma[-\Delta, \Omega_+]$*. Moreover, in both cases, the solution is unique if it exists. It will be throughout denoted by* $\theta_{[\lambda,b]}$*. Furthermore,* $\theta_{[\lambda,b]}$ *is a global attractor for all the positive solutions of* (2.1)*, i.e.,*

$$\lim_{t\uparrow\infty} \left\| u_{[\lambda,b]}(t,\cdot;u_0) - \theta_{[\lambda,b]} \right\|_{\mathcal{C}(\bar{\Omega})} = 0$$

for all $u_0 > 0$*,* $u_0 \in L^\infty(\Omega)$*.*

According to the general theory developed in [46], when $b = 0$ and $\lambda \geq \sigma[-\Delta, \Omega_+]$, though the solution $u_{[\lambda,b]}(t,x;u_0)$ is globally defined in time, because in such case the problem remains sublinear, it might grow to infinity in Ω_+ as $t \uparrow \infty$, while it remains bounded in Ω_-, therefore converging to a metasolution of (2.2) supported in Ω_-.

Naturally, in the circumstances of Theorem 2.3, $\theta_{[\lambda,b]}$ must be linearly asymptotically stable. Indeed, the following result holds

Proposition 2.4. *Suppose* $b_0 \leq 0$ *and* (2.2) *admits a positive solution; necessarily* $\theta_{[\lambda,b_0]}$ *by Theorem 2.3. Then,* $\theta_{[\lambda,b_0]}$ *is linearly asymptotically stable.*

Proof. As $b_0 \leq 0$, we have that $a_{b_0} < 0$ and, since $p > 1$, we find, from the monotonicity of the principal eigenvalue with respect to the potential that

$$\sigma[\mathfrak{L}_{(b_0,\theta_{[\lambda,b_0]})}, \Omega] = \sigma[-\Delta - \lambda - a_{b_0} p \theta_{[\lambda,b_0]}^{p-1}, \Omega] > \sigma[-\Delta - \lambda - a_{b_0} \theta_{[\lambda,b_0]}^{p-1}, \Omega] = 0.$$

The last identity follows easily from the fact that $(b_0, \theta_{[\lambda,b_0]})$ solves (2.2) and the uniqueness of the principal eigenvalue. □

2.3. Bifurcation diagrams of (2.2) near l.a.s. and l.n.s. solutions

2.3.1. Structure of the bifurcation diagram of (2.2) near a l.a.s. solution

The next result, which is the counterpart in this new general setting of the first part of Lemma 1.26, provides us with the local structure of the bifurcation diagram of (2.2) in a neighborhood of a linearly asymptotically stable solution (b_0, u_0).

Proposition 2.5. *Let (b_0, u_0) be a linearly asymptotically stable solution of (2.2). Then, there exist $\varepsilon > 0$ and a differentiable function $u : (b_0-\varepsilon, b_0+\varepsilon) \to \mathcal{C}^1(\bar{\Omega})$ such that $u(b_0) = u_0$ and $(b, u(b))$ is a linearly asymptotically stable positive solution of (2.2) for all $b \in (b_0 - \varepsilon, b_0 + \varepsilon)$. Moreover, the map*

$$\begin{aligned} u : (b_0 - \varepsilon, b_0 + \varepsilon) &\to \mathcal{C}(\bar{\Omega}) \\ b &\mapsto u(b) \end{aligned}$$

is increasing and there exists a neighborhood $\mathcal{U}$ of (b_0, u_0) in $\mathbb{R} \times \mathcal{C}^1(\bar{\Omega})$ such that $\mathcal{P}_b(\mathcal{U}) \subset (b_0 - \varepsilon, b_0 + \varepsilon)$ and $(b, u) = (b, u(b))$ if $(b, u) \in \mathcal{U}$ is a solution of (2.2), where $\mathcal{P}_b$ stands for the projection operator on the b-component.

Proof. As problems (2.2) and (2.4) are equivalent, the solutions of (2.2) are given by the zeroes of the operator $\mathfrak{F} : \mathbb{R} \times \mathcal{C}^1_0(\bar{\Omega}) \to \mathcal{C}^1_0(\bar{\Omega})$ defined by

$$\mathfrak{F}(b, v) := v - (-\Delta)^{-1} \left[\lambda(v + M) + a_b(v + M)^p\right]. \tag{2.5}$$

Since (b_0, u_0) solves (2.2), setting $v_0 := u_0 - M$ we have that $\mathfrak{F}(b_0, v_0) = 0$ and that $D_v\mathfrak{F}(b_0, v_0)$ is an isomorphism, because we are assuming $\sigma[\mathfrak{L}_{(b_0,u_0)}, \Omega] > 0$. Consequently, the implicit function theorem guarantees the existence, the uniqueness and the regularity of a function v, defined in an ε-neighborhood of b_0, for which $u := v + M$ has the desired properties. The points of this curve are solutions of (2.4) since $v_0 > -M$ and, by continuity, $v(b) > -M$ for all b in a neighborhood of b_0. The fact that the solutions $(b, u(b))$ are linearly asymptotically stable follows easily from the fact that $\sigma[\mathfrak{L}_{(b_0,u_0)}, \Omega] > 0$ and the continuity of the principal eigenvalue with respect to the potential, reducing $\mathcal{U}$ if necessary.

Finally, as $(b, u(b))$ is a solution of (2.2), we have that

$$\begin{cases} -\Delta u(b) = \lambda u(b) + (ba_+ - a_-)u^p(b) & \text{in } \Omega, \\ u(b) = M & \text{on } \partial\Omega, \end{cases}$$

and, hence, according to the theorem of differentiation of G. Peano, it becomes apparent that $u'(b)$ satisfies

$$\begin{cases} \mathfrak{L}_{(b,u(b))}u'(b) = a_+u^p(b) > 0 & \text{in } \Omega, \\ u'(b) = 0 & \text{on } \partial\Omega. \end{cases}$$

Therefore, by Theorem 2.2, we find that $u'(b) \gg 0$, which shows the monotonicity of $u(b)$ in b and ends the proof. □

As an immediate consequence from Propositions 2.4 and 2.5, the following result holds.

Corollary 2.6. *Assume $\lambda < \sigma[-\Delta, \Omega_+]$. Then, there exists $\varepsilon > 0$ such that Problem (2.2) admits, at least, a linearly asymptotically stable solution for every $b \in [0, \varepsilon)$.*

2.3.2. Structure of the bifurcation diagram of (2.2) near a l.n.s. solution

In order to study the behavior of the bifurcation diagram of (2.2) in a neighborhood of a neutrally stable solution we will use the following Picone type identity, whose proof, even for general self-adjoint elliptic differential operators can be found in [42, Lemma 4.1].

Lemma 2.7. *Let $u, v \in \mathcal{C}^1(\bar{\Omega}) \cap \mathcal{C}^2(\Omega)$ a.e. be such that $\frac{v}{u} \in \mathcal{C}^1(\bar{\Omega})$. Then, for every $f : \mathbb{R} \to \mathbb{R}$ of class $\mathcal{C}^1$, the following identity holds:*

$$\int_\Omega f\left(\frac{v}{u}\right)[u\Delta v - v\Delta u] = \int_{\partial\Omega} f\left(\frac{v}{u}\right)\left[u\frac{\partial v}{\partial n} - v\frac{\partial u}{\partial n}\right] - \int_\Omega f'\left(\frac{v}{u}\right)u^2\left|\nabla\frac{v}{u}\right|^2. \tag{2.6}$$

The main result of this section establishes that, in a neighborhood of a linearly neutrally stable solution, the bifurcation diagram of (2.2) consists of a subcritical quadratic turning point, with linearly asymptotically stable solutions on its lower half-branch and linearly unstable solutions on the upper one.

Proposition 2.8. *Let (b_0, u_0) be a linearly neutrally stable positive solution of (2.2) and let $\psi_0 > 0$ be a positive eigenfunction associated with $\sigma[\mathfrak{L}_{(b_0,u_0)}, \Omega] = 0$. Then, there exist $\varepsilon > 0$ and a differentiable function*

$$(b, u) : (-\varepsilon, \varepsilon) \to \mathbb{R} \times \mathcal{C}^1(\bar{\Omega})$$

such that $(b(0),u(0))=(b_0,u_0)$ *and* $(b(s),u(s))$ *is a positive solution of* (2.2) *for each* $s\in(-\varepsilon,\varepsilon)$. *Moreover,*

$$u(s)=u_0+s\psi_0+w(s),\qquad b(s)=b_0+b_2s^2+O(s^3),\tag{2.7}$$

where $w(s)=O(s^2)$ *as* $s\downarrow 0$, $\int_\Omega w(s)\psi_0=0$ *for all* $s\in(-\varepsilon,\varepsilon)$, *and*

$$b_2=-\frac{p(p-1)}{2}\frac{\int_\Omega a_{b_0}u_0^{p-2}\psi_0^3}{\int_\Omega a_+u_0^p\psi_0}<0.$$

Moreover, there exists a neighborhood $\mathcal{U}$ *of* (b_0,u_0) *in* $\mathbb{R}\times\mathcal{C}^1(\bar\Omega)$ *such that* $(b,u)=(b(s),u(s))$ *for some* $s\in(-\varepsilon,\varepsilon)$ *if* $(b,u)\in\mathcal{U}$ *solves* (2.2).

With regard to the stability of those solutions, we have that, for every $s\in(-\varepsilon,\varepsilon)$,

$$\operatorname{sign}b'(s)=\operatorname{sign}\sigma[\mathfrak{L}_{(b(s),u(s))},\Omega].\tag{2.8}$$

Proof. After the usual change of variables $u=v+M$, the existence of ε and of the functions $b(s)$ and $u(s)$, as well as the local uniqueness and the expansions (2.7), follow from H. Amann [5, Th. 2.1] applied to the operator $\mathfrak{F}$ introduced in (2.5). Indeed, in this case, $D_v\mathfrak{F}(b_0,v_0)=\mathfrak{L}_{(b_0,u_0)}$, where $u_0=v_0+M$, is a Fredholm operator of index zero and

$$\ker[D_v\mathfrak{F}(b_0,v_0)]=\operatorname{span}[\psi_0],\qquad\int_\Omega a_+u_0^p\psi_0>0.\tag{2.9}$$

To derive (2.8), which describes the stability of the solutions, we can adapt H. Amann [6, Pr. 20.8]. Substituting (2.7) in (2.2) and differentiating with respect to s, yields

$$\mathfrak{L}_{(b(s),u(s))}u'(s)=b'(s)a_+u^p(s)\quad\text{ in }\quad\Omega.$$

Thus, by multiplying this equation by $\psi(s)$, a strictly positive eigenfunction associated to $\sigma[\mathfrak{L}_{(b(s),u(s))},\Omega]$, integrating in Ω, and applying the formula of integration by parts, we obtain that

$$\sigma[\mathfrak{L}_{(b(s),u(s))},\Omega]\int_\Omega u'(s)\psi(s)=b'(s)\int_\Omega a_+u^p(s)\psi(s)$$

which implies (2.8), because, since $u'(0)=\psi_0\gg 0$, we have that $u'(s)\gg 0$ if $s\sim 0$, by continuity.

The formula for b_2 can be easily obtained by substituting (2.7) in (2.2), differentiating twice with respect to s, particularizing the result at $s=0$,

multiplying by ψ_0 and integrating in Ω. To get its sign, we should prove in view of (2.9) that

$$\int_\Omega a_{b_0} u_0^{p-2} \psi_0^3 > 0. \tag{2.10}$$

To show (2.10) we apply Lemma 2.7 with $v = \psi_0$, $u = u_0$ and $f(t) = t^2$. For this choice, all the boundary terms in (2.6) vanish, as $\psi_0 = 0$ on $\partial\Omega$. Moreover, according to the definitions of ψ_0 and u_0, we have that

$$u_0 \Delta\psi_0 - \psi_0 \Delta u_0 = -(p-1) a_{b_0} u_0^p \psi_0$$

and, hence, the left-hand side of (2.6) becomes

$$-(p-1) \int_\Omega a_{b_0} u_0^{p-2} \psi_0^3.$$

Combining this with the fact that the right-hand side of (2.6) equals

$$-2 \int_\Omega \psi_0 u_0 \left| \nabla \frac{\psi_0}{u_0} \right|^2 < 0,$$

because ψ_0 cannot be a multiple of u_0, it is easily seen that (2.10) holds. □

2.4. Necessary and sufficient conditions for the existence when $b > 0$

The next result characterizes the existence of positive solutions of (2.2) in the superlinear indefinite case $b > 0$.

Theorem 2.9. *Problem (2.2) admits a positive solution for some $b > 0$ if, and only if,*

$$\lambda < \sigma[-\Delta, \Omega_+]. \tag{2.11}$$

Moreover, if (2.2) possesses a positive solution (b, u) with $b > 0$, then, it has a minimal positive solution, which is linearly stable.

Proof. The sufficiency of (2.11) has been already established by Corollary 2.6. To show its necessity suppose $\lambda \geq \sigma[-\Delta, \Omega_+]$ and (2.2) admits a positive solution (b_0, u_{b_0}) with $b_0 > 0$. Then,

$$-\Delta u_0 = \lambda u_0 + a_{b_0}(x) u_0^p = \lambda u_0 + (b_0 a_+ - a_-) u_0^p > \lambda u_0 - a_- u_0^p$$

and, hence, $u_0 > 0$ provides us with a supersolution of

$$\begin{cases} -\Delta u = \lambda u - a_-(x) u^p & \text{in } \Omega, \\ u(x) = M & \text{on } \partial\Omega. \end{cases} \tag{2.12}$$

As zero is a subsolution of this problem, (2.12) admits a positive solution, which contradicts the thesis of Theorem 2.3 for $b = 0$. This ends the proof of the first assertion of the theorem.

Now, for the second part of the theorem, suppose that (b, u) is a solution of (2.2) with $b > 0$. As $(0, u)$ is an ordered sub-supersolution pair, the existence of a (unique) minimal solution $u_{\min}$ in the ordered interval $[0, u]$ follows from H. Amann [6, Theorem 6.1]. The linear stability of $u_{\min}$ can be obtained by contradiction, as in H. Amann [6, Theorem 7.3]. Indeed, suppose that

$$\sigma := \sigma[\mathfrak{L}_{(b,u_{\min})}, \Omega] < 0$$

and let $\phi > 0$ be an eigenfunction associated to σ. In these circumstances, we claim that

$$\bar{u} := u_{\min} - \varepsilon\phi > 0$$

is a strict supersolution to (2.2) for sufficiently small $\varepsilon > 0$. Indeed, according to the definition of $u_{\min}$ and ϕ, we find that

$$-\Delta\bar{u} = \lambda\bar{u} + a_b\left(u_{\min}^p - \varepsilon p\phi u_{\min}^{p-1}\right) - \varepsilon\sigma\phi \quad \text{in } \Omega. \tag{2.13}$$

Now, setting $f(\varepsilon) := (u_{\min} - \varepsilon\phi)^p$, the Taylor formula for $\varepsilon \sim 0$ yields

$$\bar{u}^p = f(\varepsilon) = f(0) + \varepsilon f'(0) + o(\varepsilon) = u_{\min}^p - \varepsilon p\phi u_{\min}^{p-1} + o(\varepsilon)$$

and, hence, it becomes apparent from (2.13) that

$$-\Delta\bar{u} = \lambda\bar{u} + a_b\bar{u}^p - \varepsilon\sigma\phi + o(\varepsilon) > \lambda\bar{u} + a_b\bar{u}^p \quad \text{in } \Omega$$

for sufficiently small $\varepsilon > 0$, because $\sigma < 0$. Moreover, $\bar{u} = M$ on $\partial\Omega$, by construction. As $\bar{u} > 0$ for sufficiently small $\varepsilon > 0$ and zero is a subsolution of (2.2), once again from H. Amann [6, Theorem 6.1], we find that (2.2) possesses a minimal positive solution in $[0, u_{\min} - \varepsilon\phi]$. Naturally, this contradicts the minimality of $u_{\min}$ and, hence, it shows that $\sigma \geq 0$, which concludes the proof. □

As this work focuses the attention on the positive solutions of (2.2) for $b > 0$, condition (2.11) will be assumed throughout the rest of the chapter.

The next result establishes that Problem (2.2) cannot admit any positive solution for sufficiently large $b > 0$.

Theorem 2.10. *Suppose $\lambda < \sigma[-\Delta, \Omega_+]$ and let $\theta_{[\lambda,0]}$ be the unique solution of (2.2) for $b = 0$ (given by Theorem 2.3). Then, for any given smooth subdomain*

$D \subset \Omega_+$ with $\bar{D} \subset \Omega_+$, we denote by $\phi \gg 0$ the unique eigenfunction of $\sigma[-\Delta, D]$ satisfying $\int_D \phi = 1$ and set

$$\omega := \sigma[-\Delta, D] - \lambda > 0, \qquad \alpha := -\int_{\partial D} \theta_{[\lambda,0]} \partial_n \phi \, dS > 0, \qquad a_L := \min_{\overline{D}} a_+ > 0,$$

where n stands for the outward unit normal to D, and

$$b^* := \frac{\omega}{a_L p} \left[\frac{(p-1)\omega}{p\alpha} \right]^{p-1}.$$

Then, for every strict subsolution u_0 of (2.2), the unique (maximal) solution of (2.1), denoted by $u_{[\lambda,b]}(t, x; u_0)$, blows up in a finite time for all $b > b^*$. As a by-product, (2.2) cannot admit a positive solution if $b > b^*$.

Proof. The proof follows [45, Theorem 4.1(b)] and it proceeds by contradiction. Suppose $u := u_{[\lambda,b]}(t, \cdot; u_0)$ is globally defined in time. Then, since u_0 is a subsolution of (2.2), we find from D. Sattinger [68] that $\partial_t u > 0$ for all $t > 0$ and, hence,

$$I(t) := \int_D u(t, x)\phi(x) \, dx$$

is increasing, because $I'(t) = \int_D \partial_t u \phi > 0$. Thus, the next limit is well defined

$$L := \lim_{t \uparrow \infty} I(t) \in (0, \infty].$$

Note that, according to the definitions of u and ϕ and taking into account that $\bar{D} \subset \Omega_+$, we find that

$$\begin{aligned} I'(t) &= \int_D \phi \Delta u + \lambda \int_D \phi u + \int_D a_b u^p \phi \\ &= -\omega I(t) - \int_{\partial D} u \partial_n \phi + b \int_D a_+ u^p \phi \\ &\geq -\omega I(t) - \int_{\partial D} u \partial_n \phi + b a_L \int_D u^p \phi. \end{aligned}$$

On the other hand, setting $\frac{1}{q} = 1 - \frac{1}{p}$, we find from Hölder inequality that

$$\int_D \phi u = \int_D \phi^{\frac{1}{q}} \phi^{\frac{1}{p}} u \leq \left(\int_D \phi \right)^{\frac{1}{q}} \left(\int_D \phi u^p \right)^{\frac{1}{p}} = \left(\int_D \phi u^p \right)^{\frac{1}{p}}$$

and, therefore, we infer from the previous estimate that

$$I'(t) \geq -\omega I(t) - \int_{\partial D} u \partial_n \phi + b a_L I^p(t). \tag{2.14}$$

Suppose $L < \infty$. Then, $\lim_{t\uparrow\infty} I'(t) = 0$. Moreover, since $b > 0$, we find from the parabolic maximum principle that

$$u_{[\lambda,b]}(t,\cdot;u_0) > u_{[\lambda,0]}(t,\cdot;u_0)$$

because $b > 0$. Thus, letting $t \uparrow \infty$, Theorem 2.3 implies that

$$\lim_{t\uparrow\infty} u_{[\lambda,b]}(t,\cdot;u_0) \geq \theta_{[\lambda,0]}.$$

Therefore, letting $t \uparrow \infty$ in (2.14) yields

$$0 \geq -\omega L + \alpha + b a_L L^p.$$

Subsequently, we consider the scalar function $f : \mathbb{R} \to \mathbb{R}$ defined by

$$f(x) = \alpha - \omega x + b a_L x^p, \qquad x \in \mathbb{R}.$$

We have that

$$f(0) = \alpha > 0, \quad \lim_{x\uparrow\infty} f(x) = +\infty \quad \text{and} \quad f(L) \leq 0.$$

Thus, f attains a non-positive minimum. But the unique point where f' vanishes is

$$x_0 := \left(\frac{\omega}{b a_L p}\right)^{\frac{1}{p-1}}.$$

Consequently, $f(x_0) \leq 0$, which can be equivalently expressed in the form $b \leq b^*$. Therefore, $L = \infty$ if $b > b^*$. Suppose this is the case. Then, there exists $t_0 > 0$ such that

$$I(t) > \left(\frac{\omega}{b a_L}\right)^{\frac{1}{p-1}} \quad \text{for all} \quad t \geq t_0. \tag{2.15}$$

As, due to the Hopf lemma, $\partial_n \phi < 0$ on ∂D and $u \gg 0$ in Ω, we find from (2.14) that

$$I'(t) > -\omega I(t) + b a_L I^p(t)$$

for all $t > 0$. Hence, by performing the change of variable

$$J(t) = e^{\omega(t-t_0)} I(t), \qquad t \geq t_0,$$

it becomes apparent that

$$J'(t) > b a_L e^{-\omega(p-1)(t-t_0)} J^p(t)$$

for all $t \geq t_0$. By dividing this relation by $J^p(t)$ and integrating in (t_0, t) we are lead to

$$J^{1-p}(t) - J^{1-p}(t_0) < \frac{ba_L}{\omega}\left[e^{-\omega(p-1)(t-t_0)} - 1\right].$$

Therefore, letting $t \uparrow \infty$, we conclude that

$$I(t_0) = J(t_0) \leq \left(\frac{\omega}{ba_L}\right)^{\frac{1}{p-1}},$$

which contradicts (2.15). This contradiction ends the proof.

Note that, for any positive solution u_0 of (2.2), one has that $u_{[\lambda,b]}(t,\cdot;u_0) = u_0$ for all $t > 0$ and, hence, $u_{[\lambda,b]}(t,\cdot;u_0)$ cannot blow up in a finite time. Therefore, $b \leq b^*$ if (2.2) admits a positive solution. □

2.5. Uniqueness of the linearly stable steady-state

This section shows that (2.1) possesses a unique linearly stable positive steady-state for all $b \in \mathbb{R}$ for which (2.2) admits a positive solution. A counterpart of this result for homogeneous Dirichlet boundary conditions was given in [36, 37]. According to Theorem 2.3 and Proposition 2.4, we already know the validity of this result for $b \leq 0$. Consequently, throughout this section we will focus our attention on the more interesting case $b > 0$. Our main result establishes that the minimal positive solution of (2.2) provides us with the unique linearly stable steady-state of (2.1). As already emphasized in Section 2.1, in case $b > 0$ Problem (2.2) can admit an arbitrarily large number of positive solutions by taking a sufficiently negative $\lambda < 0$ and therefore this uniqueness result is extremely striking. The main result of this section reads as follows.

Theorem 2.11. *Suppose* (2.2) *admits a positive solution for* $b = b_0 > 0$ *and let* (b_0, u_0) *denote the minimal positive solution of* (2.2)*, whose existence and stability are established by Theorem 2.9. Then,* (b_0, u_0) *is the unique linearly stable positive solution of Problem* (2.2)*.*

Proof. According to Propositions 2.5 and 2.8, there exists an increasing arc of differentiable curve filled in by linearly asymptotically stable positive solutions of (2.2) in a left neighborhood, in b, of (b_0, u_0). Let $\mathfrak{C}_0$ denote the lower left-component in b of the set of positive solutions of (2.2) containing the solutions on this left-side arc. By a component, it is meant a closed and connected set which is maximal for the inclusion. As $\mathfrak{C}_0$ consists of solutions of (2.2), it

cannot bifurcate from $u = 0$, because $(b, u) \in \mathfrak{C}_0$ implies $u|_{\partial\Omega} = M > 0$. Thus, by construction, and due to Propositions 2.5 and 2.8, we have that $(b, u) \in \mathfrak{C}_0$ implies $b \leq b_0$ and $u \in (0, u_0]$. Actually, $\mathfrak{C}_0$ is a closed arc of differentiable curve. Moreover, one of the following two alternatives occurs:

(A1) Every $(b, u) \in \mathfrak{C}_0$ is linearly asymptotically stable for all $b < b_0$.

(A2) There exists a neutrally stable positive solution $(b_1, u_1) \in \mathfrak{C}_0$ with $b_1 < b_0$.

Alternative (A2) is excluded, because, due to Proposition 2.8, there should not exist any positive solution in a right-side neighborhood of (b_1, u_1), which contradicts the construction of $\mathfrak{C}_0$ by left-path-following from (b_0, u_0). Therefore, (A1) occurs and, consequently, $\mathfrak{C}_0$ consists of linearly asymptotically stable solutions, except, possibly, (b_0, u_0). Using the implicit function theorem as in the proof of Proposition 2.5 this entails that $(0, \theta_{[\lambda,0]}) \in \mathfrak{C}_0$. Moreover, by the local uniqueness given by Propositions 2.5 and 2.8, and compactness, the solutions along $\mathfrak{C}_0$ are the unique ones in a neighborhood of $\mathfrak{C}_0$.

Suppose that $(b_0, \tilde{u}_0)$ is a linearly stable solution with $\tilde{u}_0 \neq u_0$. Reasoning as above, there exists another component of the set of positive solutions of (2.2), denoted by $\tilde{\mathfrak{C}}_0$, such that $(0, \theta_{[\lambda,0]}) \in \tilde{\mathfrak{C}}_0$. Consequently, $\mathfrak{C}_0 = \tilde{\mathfrak{C}}_0$ and, therefore, since $\mathfrak{C}_0$ is a differentiable curve, $\tilde{u}_0 = u_0$, which is a contradiction. □

As an immediate consequence from Theorem 2.11, the following result holds.

Corollary 2.12. *Suppose (b_0, u_0) is a linearly neutrally stable solution of (2.2). Then, Problem (2.2) cannot admit a positive solution for $b > b_0$.*

Proof. By Theorem 2.3, $b_0 > 0$. Moreover, according to Proposition 2.8, the set of positive solutions of (2.2) in a neighborhood of (b_0, u_0) is a subcritical quadratic turning point.

Suppose (2.2) admits a solution (b_1, u_1) with $b_1 > b_0$. Then, due to Theorem 2.9, there exists a positive solution $(b_1, u_{\min})$ which is linearly stable. Adapting the proof of Theorem 2.11, there exists a differentiable curve $\mathfrak{C}_0$ such that $(b_1, u_{\min}) \in \mathfrak{C}_0$, which is filled in by linearly asymptotically stable solutions of (2.2), except, at most, $(b_1, u_{\min})$. Owing to Theorem 2.11 we must have $(b_0, u_0) \in \mathfrak{C}_0$, which is impossible. □

In the rest of this section we will ascertain the global structure of the curve of minimal solutions of problem (2.2). First, we will study the structure of the set

$$B := \{\, b \in \mathbb{R} \text{ for which (2.2) admits a positive solution} \,\}.$$

By Theorem 2.3, we already know that $(-\infty, 0] \subset B$. Owing to Corollary 2.6, there exists $\varepsilon > 0$ such that $(-\infty, \varepsilon] \subset B$. Moreover, if $b \in B$ for some $b > 0$, then $(-\infty, b] \subset B$. Indeed, if (b, u) is a positive solution of (2.2) and $\tilde{b} < b$, then $(\tilde{b}, u)$ provides us with a supersolution of (2.2). As $(\tilde{b}, 0)$ is a subsolution, (2.2) must have a positive solution for $\tilde{b}$. Therefore, B is an interval. As, due to Theorem 2.10, $B \subset (-\infty, b^*]$, there exists $b_\omega \in (0, b^*]$ such that either $B = (-\infty, b_\omega]$, or $B = (-\infty, b_\omega)$.

Subsequently, for every $b \in B$ we denote by $u_s(b)$ the minimal positive solution of (2.2). According to Theorem 2.11, we already know that $u_s(b)$ is the unique linearly stable positive solution of (2.2). Actually, it is linearly asymptotically stable for all $b \in B \setminus \{b_\omega\}$ and linearly neutrally stable if B is closed and $b = b_\omega$. Therefore, as a consequence from the proofs of all the previous results, the set of minimal positive solutions

$$\mathfrak{M} := \{\, (b, u_s(b)) : \quad b \in B \,\} \subset \mathbb{R} \times \mathcal{C}(\bar{\Omega})$$

provides us with the set of all linearly stable positive steady-states of (2.1) and it has the structure of a strictly increasing differentiable curve filled in by linearly asymptotically stable solutions, except at most for $b = b_\omega$. The next result shows that $\mathfrak{M}$ bifurcates from infinity at b_ω if B is open.

Theorem 2.13. *The following assertions are true:*

(a) *If B is open, then $\lim_{b \uparrow b_\omega} \|u_s(b)\|_\infty = \infty$.*

(b) *If B is closed, then $(b_\omega, u_s(b_\omega))$ is a quadratic subcritical turning point of the set of positive solutions of (2.2). Moreover, the solutions on the upper half-branch of the turning point are unstable with one-dimensional unstable manifold in a neighborhood of the turning point.*

Proof. Suppose $B = (-\infty, b_\omega)$ and let $\{b_n\}_{n \geq 1}$ a sequence of b's such that $b_n < b_\omega$ for all $n \geq 1$ and $\lim_{n \to \infty} b_n = b_\omega$. Set $u_n := u_s(b_n)$, $n \geq 1$. If $\{u_n\}_{n \geq 1}$ is bounded in $\mathcal{C}(\bar{\Omega})$, by a rather standard compactness argument, we can extract a subsequence $\{u_{n_m}\}_{m \geq 1}$ such that

$$\lim_{m \to \infty} u_{n_m} = u_\omega \in \mathcal{C}(\bar{\Omega}).$$

By elliptic regularity, (b_ω, u_ω) provides us with a positive solution of (2.2), which is impossible. Therefore, $\{u_n\}_{n \geq 1}$ is unbounded in $\mathcal{C}(\bar{\Omega})$. As $b \mapsto u_s(b)$ is increasing, necessarily (a) holds.

Suppose $B = (-\infty, b_\omega]$ and $u_s(b_\omega)$ is linearly asymptotically stable. Then, according to Proposition 2.5, (2.2) should admit positive solutions for $b > b_\omega$, which is impossible. Therefore, $u_s(b_\omega)$ is linearly neutrally stable and, consequently, the thesis of the theorem is a direct consequence from Proposition 2.8. □

Remark 2.14. In case $\lambda \geq \sigma[-\Delta, \Omega_+]$, we always have that $B = (-\infty, 0)$.

The next section shows that B is closed in the presence of a priori bounds for the positive solutions of (2.2).

2.6. An optimal multiplicity result in the presence of a priori bounds

In this section we derive some a priori bounds for the solutions of (2.2) which will provide a deeper insight into the structure of the bifurcation diagram of (2.2). Naturally, the case of interest is $b > 0$, as in the case $b \leq 0$ the structure of the bifurcation diagram is completely understood and, actually, according to Proposition 2.5 and Theorem 2.3, every solution is bounded above by $u_s(0)$. In the presence of a priori bounds, we will prove that (2.2) possesses at least two positive solutions for every $b \in (0, b_\omega)$.

2.6.1. Some sufficient conditions for the existence of a priori bounds

In this section we will adapt the blowing-up techniques of [7] to derive some uniform a priori bounds for the solutions of (2.2) as b varies in compact subintervals contained in $(0, b_\omega]$. We are giving the complete details of the proofs because the original ones of [7] contain a number of unpleasant misprints which make its reading uncomfortable. For the validity of the results of this section we need to assume that a_+ is continuous.

Proposition 2.15. *Let $J = [\theta_1, \theta_2] \subset (0, b_\omega]$ for which there exist a constant $C_1 > 0$ such that*

$$\sup_{\bar{\Omega}_+} u < C_1 \tag{2.16}$$

for all positive solution (b, u) of (2.2) with $b \in J$. Then, there exists a constant $C_2 > 0$ such that

$$\sup_{\bar{\Omega}} u < C_2$$

for all $b \in J$ and any positive solution (b, u) of (2.2).

Proof. Suppose (2.16) holds for any solution (b, u) of (2.2) with $b \in J$. Then, by (2.16), $u < C_1$ on $\partial\Omega_+$ and, hence, u provides us with a subsolution of the sublinear problem

$$\begin{cases} -\Delta u = \lambda u + a_b u^p & \text{in } \Omega_- \\ u = C_1 & \text{on } \partial\Omega_+ \\ u = M & \text{on } \partial\Omega \end{cases}$$

which admits a unique positive solution u_0, as a by-product of [46, Theorem 3.5]. Moreover, according to that result, $u < u_0$. Therefore, the choice

$$C_2 := \max\left\{C_1, \max_{\bar{\Omega}_-} u_0\right\}$$

provides us with the desired result. □

Thanks to Proposition 2.15, the problem of finding a priori bounds in Ω for the positive solutions of (2.2) can be reduced to the search for a priori bounds in Ω_+. In the case of constant coefficients, it was shown by B. Gidas and J. Spruck [34] that these a priori bounds are available if $N = 1, 2$, or

$$p < \frac{N+2}{N-2} \quad \text{if } N \geq 3. \tag{2.17}$$

Actually these conditions are optimal, as, according to Pohozaev's identity [64] , it is well known that these a priori bounds can be lost if $N \geq 3$ and (2.17) fails. Therefore, we will throughout assume that either $N = 1, 2$ or (2.17) holds. The next result will be useful later. Subsequently, we will denote by $d(x, \partial\Omega_+)$ the distance between x and $\partial\Omega_+$.

Proposition 2.16. *Suppose $N = 1, 2$, or (2.17), and that there is a sequence (b_n, u_n), $n \geq 1$, of positive solutions of (2.2) with $\inf_{n\geq 1} b_n > 0$, and a sequence of points $x_n \in \Omega_+$, $n \geq 1$, such that*

$$u_n(x_n) := \|u_n\|_{L^\infty(\Omega_+)} \to \infty \qquad (n \to \infty). \tag{2.18}$$

Then, $\lim_{n\to\infty} d(x_n, \partial\Omega_+) = 0$.

Proof. Taking a subsequence, if necessary, we may assume that

$$\lim_{n\to\infty} b_n = b_\infty \in (0, \beta_\omega].$$

The proof of the proposition will proceed by contradiction. Suppose there exists a subsequence of x_n, $n \geq 1$, relabeled by n, and a point $x_\infty \in \Omega_+$ such that

$$\lim_{n\to\infty} x_n = x_\infty \in \Omega_+. \tag{2.19}$$

Subsequently, we will denote $m_n := u_n(x_n)$ and consider the change of variable

$$v_n(y) := \frac{u_n(x)}{m_n} \quad \text{where} \quad y := \frac{x - x_n}{m_n^\alpha}, \quad \alpha := \frac{1-p}{2} < 0.$$

As, according to (2.18), $m_n^\alpha \to 0$ as $n \uparrow \infty$, we find from (2.19) that, for every $R > 0$, there exists $n_R \in \mathbb{N}$ such that

$$x_n + m_n^\alpha y \in \Omega_+ \quad \text{for all } n \geq n_R \quad \text{and} \quad y \in B_R = \{y \in \mathbb{R}^N : \ |y| < R\}.$$

Consequently, for any fixed $R > 0$, the functions v_n, $n \geq n_R$, satisfy the differential equation

$$-\Delta v_n(y) = \lambda m_n^{2\alpha} v_n(y) + b_n a_+(x_n + m_n^\alpha y) v_n^p(y), \quad y \in B_R, \tag{2.20}$$

for all $n \geq n_R$. Moreover, by construction, we have that

$$0 < v_n(y) = \frac{u_n(x)}{m_n} \leq \frac{u_n(x_n)}{m_n} = 1 = v_n(0)$$

for all $n \geq n_R$ and $y \in B_R$. Therefore, the sequence v_n, $n \geq n_R$, is bounded in $L^\infty(B_R)$ and, hence, by a rather standard compactness argument, there exists $v \in \mathcal{C}^1(B_R)$ such that, along some subsequence, labeled again by n,

$$\lim_{n\to\infty} v_n = v \quad \text{in } \mathcal{C}^1(B_R).$$

Consequently, multiplying (2.20) by a test function, integrating by parts and letting $n \to \infty$, it becomes apparent that v is a weak solution of

$$-\Delta v = b_\infty a_+(x_\infty) v^p \quad \text{in } B_R. \tag{2.21}$$

Actually, by a standard diagonal process in R and elliptic regularity, we have that $v \in W^{2,q}_{\rm loc}(\mathbb{R}^N)$ for all $q > 1$ and that it satisfies (2.21) in $\mathbb{R}^N$ in the strong sense. Actually, by Morrey's inequality, v is Hölder continuous and, therefore, by elliptic regularity, $v \in \mathcal{C}^2(\mathbb{R}^N)$. As a by-product, after a linear change of coordinates in (2.21), there exists a positive non trivial classical solution of $-\Delta w = w^p$, which contradicts Theorem 1.1 of B. Gidas and J. Spruck [33]. □

The following result gives some sufficient conditions for the existence of a priori bounds in terms of the weight function $a(x)$ and the size of p if $N \geq 3$.

Theorem 2.17. *Assume that there exist a positive continuous function α_+, defined in a neighborhood of $\partial\Omega_+$ and bounded away from zero, and a constant $\gamma > 0$ such that*

$$a_+(x) = \alpha_+(x) d(x, \partial\Omega_+)^\gamma \qquad \text{for all } x \in (\partial\Omega_+ + B_\delta) \cap \Omega_+, \qquad \delta \sim 0. \tag{2.22}$$

Suppose, in addition, that $N = 1, 2$, or

$$N \geq 3 \quad \text{and} \quad p < \min\left\{\frac{N+2}{N-2}, \frac{N+1+\gamma}{N-1}\right\}. \tag{2.23}$$

Then, for every $\varepsilon > 0$ there exists a constant $C = C(\varepsilon)$ such that

$$\|u\|_{L^\infty(\Omega)} < C$$

for all positive solution (b, u) of (2.2) with $b \in [\varepsilon, b_\omega]$.

Proof. By Proposition 2.15, it suffices to prove that there exists a constant C such that, for every solution (b, u) of (2.2) with $b \in [\varepsilon, b_\omega]$,

$$\|u\|_{L^\infty(\Omega_+)} < C.$$

The proof will proceed by contradiction. Suppose there exist $\varepsilon > 0$ and a sequence (b_n, u_n), $n \geq 1$, of positive solutions of (2.2) such that

$$b_n \in [\varepsilon, b_\omega] \quad \text{and} \quad \|u_n\|_{L^\infty(\Omega_+)} > n, \qquad n \geq 1.$$

Then, there exist $x_n \in \bar{\Omega}_+$, $n \geq 1$, such that

$$m_n := u_n(x_n) = \|u_n\|_{L^\infty(\Omega_+)} \to \infty \quad \text{as } n \uparrow \infty.$$

As the sequences b_n and x_n, $n \geq 1$, are bounded, we may assume without loss of generality that

$$\lim_{n\to\infty} b_n = b_\infty \in [\varepsilon, b^*] \quad \text{and} \quad \lim_{n\to\infty} x_n = x_\infty \in \bar{\Omega}_+.$$

According to Proposition 2.16, it becomes apparent that $x_\infty \in \partial\Omega_+$.

By straightening $\partial\Omega_+$ around x_∞ with a change of coordinates, which is independent of n, we can assume that $x_\infty = 0$ and that $U := \Omega_+ \cap B_{R_0}(x_\infty)$, for some fixed $R_0 > 0$, $R_0 \sim 0$, is a neighborhood of zero in the half space $\mathbb{H}^N := \{x \in \mathbb{R}^N : x^{(N)} > 0\}$ (we are denoting by $x^{(N)}$ the N-th component of $x \in \mathbb{R}^N$).

Subsequently, we introduce the sequence ρ_n, $n \geq 1$, defined through

$$\rho_n^\beta m_n = 1 \quad \text{with} \quad \beta := \frac{\gamma + 2}{p - 1} > 0$$

and consider the change of variable

$$v_n(y) := \frac{u_n(x)}{m_n} = \rho_n^\beta u_n(x) \quad \text{where} \quad y := \frac{x - x_n}{\rho_n}. \tag{2.24}$$

Since $\rho \to 0$ as $n \uparrow \infty$, we have that, for every $R > 0$, there exists $n_R \in \mathbb{N}$ such that

$$x_n + \rho_n y \in U \quad \text{for all } n \geq n_R \quad \text{and} \quad y \in H_{R,n} := B_R \cap \left(- \left(0, ..., 0, \frac{x_n^{(N)}}{\rho_n} \right) + \mathbb{H}^N \right).$$

Therefore, a straightforward computation shows that, for any fixed $R > 0$, the functions v_n satisfies, for every $n \geq n_R$,

$$-\Delta v_n(y) = \lambda \rho_n^2 v_n(y) + a_{b_n}(x_n + \rho_n y)\rho_n^{-\gamma} v_n^p(y) \quad \text{in} \quad H_{R,n}.$$

Thus, thanks to (2.22), we find that v_n satisfies

$$-\Delta v_n(y) = \lambda \rho_n^2 v_n(y) + b_n \alpha_+(x_n + \rho_n y)\left(\frac{x_n^{(N)}}{\rho_n} + y^{(N)}\right)^{\gamma} v_n^p(y) \quad \text{in} \quad H_{R,n}. \tag{2.25}$$

Now, we shall distinguish two different situations according to the behavior of $x_n^{(N)}/\rho_n$ as $n \uparrow \infty$:

1. along some subsequence, relabeled by n, we have that

$$\ell := \lim_{n\to\infty} \frac{x_n^{(N)}}{\rho_n} < \infty,$$

2. along some subsequence, labeled again by n,

$$\lim_{n\to\infty} \frac{x_n^{(N)}}{\rho_n} = \infty.$$

In Case 1, $H_{R,n}$ approximates

$$H_R := B_R \cap (-(0, \ldots, 0, \ell) + \mathbb{H}^N)$$

as $n \to \infty$ and, hence, using the L^p boundary estimates estimates of S. Agmon, A. Douglis and L. Niremberg [1, 2], and letting $n \to \infty$ in (2.25), we find that, along some subsequence, v_n converges to a bounded $v \in \mathcal{C}^2(-(0, ..., 0, \ell) + \bar{\mathbb{H}}^N)$ satisfying $v(0) = 1$ and

$$-\Delta v = b_\infty \alpha_+(0)\left(\ell + y^{(N)}\right)^{\gamma} v^p \quad \text{in} \quad -(0, ..., 0, \ell) + \mathbb{H}^N.$$

Thus, through a translation and a dilation, we get a bounded non-trivial solution $w \in \mathcal{C}^2(\bar{\mathbb{H}}^N)$ of

$$-\Delta w = \left(y^{(N)}\right)^{\gamma} w^p \quad \text{in} \quad \mathbb{H}^N,$$

which contradicts Corollary 2.1 of H. Berestycki, I. Capuzzo-Dolcetta and L. Niremberg [8]. Thus Case 2 holds and $H_{R,n}$ approximates B_R as $n \uparrow \infty$. Setting

$$\mu_n := \left(\frac{x_n^{(N)}}{\rho_n}\right)^{-\frac{\gamma}{2}}, \qquad n \geq 1,$$

we have that $\mu_n \to 0$ as $n \to \infty$ and, performing the change of coordinates $w_n(z) = v_n(y)$, where $z = y/\mu_n$, it becomes apparent from (2.25) that w_n satisfies

$$-\Delta w_n = \lambda\rho_n^2\mu_n^2 w_n + b_n\alpha_+(x_n + \rho_n\mu_n z)\left(1 + \mu_n^{\frac{2}{\gamma}+1} z^{(N)}\right)^{\gamma} w_n^p \quad \text{in} \quad \frac{1}{\mu_n}H_{R,n}.$$

Consequently, along some subsequence, w_n converges to a non-trivial bounded function $w \in \mathcal{C}^2(\mathbb{R}^N)$ satisfying

$$-\Delta w = b_\infty\alpha_+(0)w^p$$

which contradicts Theorem 1.1 of B. Gidas and J. Spruck [33]. This ends the proof. □

Remark 2.18. (a) Case 1 of the previous proof occurs when some subsequence of x_n lies in $\partial\Omega_+$. Actually, in such case, $\ell = 0$.

(b) Condition (2.23) is equivalent to (2.17) provided that $\gamma \geq 2N/(N-2)$, though it is stronger if $\gamma < 2N/(N-2)$.

(c) The proof of Theorem 2.17 can be easily adapted to get the existence of a priori bounds for the one-dimensional prototype (2.3), where the weight function a is discontinuous, and does not vanish, on $\partial\Omega_+$. Indeed, one can perform the change of variable (2.24) with $\beta = 2/(p-1)$ and letting $n \to \infty$ in (2.25) with $\gamma = 0$, one obtains the existence of a positive solution of $-w'' = w^p$ in $(0,\infty)$, which is impossible because every solution must vanish in some finite time (the phase portrait in this case is similar to the one of Figure 1.5 except for the fact that it does not exhibit the homoclinic orbit through $(0,0)$) .

A different version of Theorem 2.17 was given by Y. Du and S. Li [27] for $p < (N+2)/(N-2)$ if $N \geq 3$, but, in order to reach the optimal critical exponent, Y. Du and S. Li needed to impose the counterpart of (2.22) from the side of Ω_-. Precisely, they required the existence of a positive continuous function α_-, defined in a neighborhood of $\partial\Omega_+$ and bounded away from zero, and a constant γ_- such that

$$\lim_{\substack{x\to x_0\\ x\in\Omega_-}} \frac{a_-(x)}{d(x,\partial\Omega_+)^{\gamma_-}} = \alpha_-(x_0) \qquad \text{for every} \quad x_0 \in \partial\Omega_+.$$

2.6.2. An optimal multiplicity result

The existence of uniform a priori bounds on any compact interval contained in $(0, b_\omega]$ guarantees the existence of, at least, two positive solutions of (2.2) for every $b \in (0, b_\omega)$. Some sufficient conditions to get these a priori bounds were given in Theorem 2.17. Our main multiplicity result reads as follows.

Theorem 2.19. *Suppose that, for some $\varepsilon \in (0, b_\omega)$, there exists a constant $C = C(\varepsilon)$ such that*

$$\|u\|_{L^\infty(\Omega)} < C \quad \text{for every positive solution } (b,u) \text{ of (2.2) with } b \in [\varepsilon, b_\omega]. \tag{2.26}$$

Then, for every $b \in (\varepsilon, b_\omega)$, besides the l.a.s. positive solution $u_s(b)$, Problem (2.2) admits, at least, a linearly unstable solution $(b, u_i(b))$.

If, in addition, $C(\varepsilon)$ does exist for all $\varepsilon > 0$, then

$$\limsup_{b \downarrow 0} \|u_i(b)\|_{L^\infty(\Omega)} = \infty \tag{2.27}$$

for all family of linearly unstable solutions $(b, u_i(b))$, $b \in (0, b_\omega)$.

Proof. It should be remembered that the positive solutions of (2.2) are given by the zeros of the compact perturbation of the identity $\mathfrak{F}(b, \cdot)$ defined in (2.5), by means of the change of variable $u := v + M$. According to (2.26), for any $b \in [\varepsilon, b_\omega]$, the zeros of $\mathfrak{F}(b, \cdot)$ are contained in

$$\mathcal{U} := \{\, v \in \mathcal{C}^1_0(\bar\Omega) : -M < v < C - M \,\}.$$

By setting $v_s(b) := u_s(b) - M$, for any fixed $b \in (0, b_\omega)$, we observe that, according to Proposition 2.5, $v_s(b)$ is an isolated fixed point of the compact operator $F(b, \cdot)$, where

$$F(b, v) := v - \mathfrak{F}(b, v), \qquad (b, v) \in \mathbb{R} \times \mathcal{C}^1_0(\bar\Omega).$$

Thus, the local index of F at $v_s(b)$ is well defined. Moreover, as all the eigenvalues of $D_v F(b, v_s(b))$ are smaller than 1, because $u_s(b)$ is linearly asymptotically stable, the Leray-Schauder formula for the local index yields

$$\mathrm{i}(F(b, \cdot), v_s(b)) = 1 \quad \text{for all } \ b \in (0, b_\omega) \tag{2.28}$$

(see, e.g., H. Amann [6, Theorem 11.4]).

Suppose $b \in [\varepsilon, b_\omega)$ and pick a sufficiently small $\delta > 0$ so that $v_s(b)$ is the unique solution of (2.4) in the closed ball $\bar B_\delta(v_s(b))$ of $C^1_0(\bar\Omega)$. Then, using the

properties of the Leray-Shauder degree within the cone of positive functions, from (2.27) and (2.28) we can derive the following chain of identities

$$\begin{aligned}
0 &= \deg(\mathrm{Id} - F(b_\omega + 1, \cdot), \mathcal{U}, 0) = \deg(\mathrm{Id} - F(b, \cdot), \mathcal{U}, 0) \\
&= \deg(\mathrm{Id} - F(b, \cdot), B_\delta(v_s(b)), 0) + \deg(\mathrm{Id} - F(b, \cdot), \mathcal{U} \setminus \bar{B}_\delta(v_s(b)), 0) \\
&= \mathrm{i}(F(b, \cdot), v_s(b)) + \deg(\mathrm{Id} - F(b, \cdot), \mathcal{U} \setminus \bar{B}_\delta(v_s(b)), 0) \\
&= 1 + \deg(\mathrm{Id} - F(b, \cdot), \mathcal{U} \setminus \bar{B}_\delta(v_s(b)), 0)
\end{aligned}$$

and, therefore

$$\deg(\mathrm{Id} - F(b, \cdot), \mathcal{U} \setminus \bar{B}_\delta(v_s(b)), 0) = -1.$$

Consequently, $\mathfrak{F}(b, \cdot)$ must possess another positive zero in $\mathcal{U} \setminus \bar{B}_\delta(v_s(b))$. According to Theorem 2.11, this solution must be linearly unstable. This ends the proof of the first assertion of the theorem.

To complete the rest of the proof, suppose that (2.2) possesses a sequence of positive linearly unstable solutions $(b_n, u_i(b_n))$, $n \geq 1$, such that

$$\lim_{n\to\infty} b_n = 0 \quad \text{and} \quad \|u_i(b_n)\|_{L^\infty(\Omega)} < C \quad \text{for all} \quad n \geq 1.$$

Then, by a compactness argument, reminiscent of that of the proof of Theorem 2.13, we can infer that, along some subsequence, relabeled by n, $u_i(b_n)$ converge to a positive solution $(0, u_i(0))$ of (2.2). By the uniqueness of positive solution of (2.2) for $b \leq 0$, $u_s(0) = u_i(0)$, which is impossible by Proposition 2.5, as, in that case, the linearly unstable solutions $(b_n, u_i(b_n))$ should be on the unique differentiable curve passing through $(0, u_s(0))$, which is filled in by l.a.s. solutions. □

Chapter 3

Continuation methods for obtaining the bifurcation diagrams

3.1. Introduction

This chapter presents the numerical methods that we have used to obtain a paradigmatic series of global bifurcation diagrams for a one-dimensional prototype of Problem (2.2). Precisely we are going to consider the following problem

$$\begin{cases} -u'' = \lambda u + a_b(x)u^p & \text{in } (0,1), \\ u(0) = u(1) = M, \end{cases} \tag{3.1}$$

with different choices of the weight a_b. As in the previous chapters $\lambda \in \mathbb{R}$, $p > 1$ and $M > 0$.

From the theoretical analysis of Chapter 1, we already know the high multiplicity of positive solutions that (3.1) can exhibit for the choice

$$a_b(x) = \begin{cases} -c & \text{if } x \in [0,\alpha) \cup (1-\alpha, 1] \\ b & \text{if } x \in [\alpha, 1-\alpha], \end{cases} \tag{3.2}$$

where $\alpha \in (0, 0.5)$, $c > 0$ and $b \geq 0$, as well as the qualitative structure of the bifurcation diagrams in b, and, as a consequence, we could perform very sharp computations up to reach ranges of the parameters where the path-following solvers that we used were extremely stressed. Specifically this caused some computational problems regarding the singular points in the bifurcation diagrams, i.e. the turning points and the bifurcation points. The main technical difficulties relied indeed in the closeness of the former and in the fact that all turning and bifurcation points approximate each other arbitrarily as λ, the

secondary parameter of the problem, becomes very negative. Another problem was the proximity of the two tangents at the bifurcation points. This chapter presents the recipes that we have implemented to overcome all these troubles, the results of our numerical computations and finally discusses some of the ecological implications of the theoretical and numerical results.

We will start with the numerical computations for the weight (3.2). In this case, as proved in Chapter 1, for any given integer $n \geq 0$, Problem (3.1) possesses solutions with n strict critical points in the interval $(\alpha, 1-\alpha)$ if $-\lambda > 0$ is sufficiently large. Moreover, these solutions must be asymmetric if $n \geq 2$ is even, in spite of the symmetry of the problem. As we already know, the solution with 0 strict critical points, referred to as the *trivial solution* of (3.1), defined at page 18, plays a similar role to that of an *organizing center* in singularity theory (see, e.g., M. Golubitsky and D. G. Shaeffer [33]), in the sense that, starting from the local information in a neighborhood of it, we can reconstruct the global nature of the diagram.

Consistently with Definition 1.8, we introduce the following concept, which will be used throughout the rest of the chapter

Definition 3.1. Given a solution u of Problem (3.1) with $n \geq 0$ strict critical points in $(\alpha, 1-\alpha)$, it is said that u is of *type* (n, a) if u is asymmetric around $x = 0.5$, while it is said that it is of type (n, s) if it is symmetric.

As it can be seen in Figure 3.4, the global structure of the positive solutions of (3.1) consists of a *primary curve* establishing an homotopy between the unique solution of

$$\begin{cases} -u'' = \lambda u + a_0(x)u^p & \text{in } (0,1), \\ u(0) = u(1) = M, \end{cases} \tag{3.3}$$

and the *metasolution* (large solution prolonged by infinity to the rest of the interval $(0,1)$)

$$m(x) := \begin{cases} u_s(x), & x \in [0, \alpha), \\ \infty, & x \in [\alpha, 1-\alpha], \\ u_s(1-x), & x \in (1-\alpha, 1], \end{cases} \tag{3.4}$$

where u_s stands for the unique solution of the singular problem

$$\begin{cases} -u'' = \lambda u - cu^p & \text{in } [0, \alpha), \\ u(0) = M, \;\; u(\alpha) = \infty. \end{cases} \tag{3.5}$$

Then, as $-\lambda > 0$ increases, a piece of the primary curve rotates counterclockwise around the trivial solution u_0 and, almost after every half rotation, an

additional closed loop emanates from it. The loop consists of solutions of asymmetric type and it persists for all further values of $-\lambda$ (see the series of Figures 3.4, 3.5, 3.9, 3.10 and 3.12). Indeed, thanks to the analytical studies of Chapter 1, the number of turning points of the primary curve, as well as the number of bifurcation points along it, is unbounded as $\lambda \downarrow -\infty$.

An astonishing phenomenon, observed here by the first time, is that the larger $-\lambda$ is, the larger becomes the range of values of the main parameter b for which (3.1) possesses some positive solution and, simultaneously, the smaller are the positive solutions of (3.1) in the central interval $[\alpha, 1-\alpha]$, where the problem is superlinear. It is this feature which entails that the turning points of the primary curve are extremely closed and makes a very hard task the adaptation of the available continuation codes to perform the numerical computations of this work. By simply having a glance at Figure 3.12, which is the global bifurcation diagram of (3.1) for $\lambda = -2000$, the reader will easily realize what we want to express. Though the maximum value of b for which (3.1) admits a positive solution is $b = 1.2463985 \times 10^7$, where the primary curve exhibits a subcritical turning point, most of the positive solutions in the diagram, independently of their types, satisfy $u(\alpha) \sim 10^{-4}$, and, in addition, the first closed loop bifurcates from the primary branch at $b = 1.2463984 \times 10^7$, which is extremely close to the turning point. Consequently, in spite of looking so simple, the prototype model (3.1) can generate highly involved global bifurcation diagrams whose numerical computation is extremely challenging, not only by the complexity of the structure of the diagrams themselves, but also by the scales of the parameters at which the phenomenologies of practical interest arise.

Moreover, in the final part of this chapter, we will present some further numerical experiments, using again our updated algorithms, to compute a number of bifurcation diagrams of (3.1) for a wider class of weight functions $a_b(x)$ which are no longer piecewise-constant. The numerics suggest that the multiplicity result of Chapter 1 still holds for this larger class of weights, however the structure of the global bifurcation diagrams is based on the symmetry properties of the weight. Surprisingly, breaking the symmetry of $a_b(x)$ around 0.5, provokes the loss of all symmetry breaking bifurcations found in Chapter 1. This result seems very difficult to be proven rigorously.

The structure of the chapter is the following: in Section 3.2 a brief description of the continuation methods used in this work for non-expert readers is given; in Section 3.3 we discuss the computational troubles we have encountered and explain how we have solved them; Section 3.4 fully describes the main features of the bifurcation diagrams of (3.1) that we have computed for the piecewise-constant weight (3.2), while in Section 3.5 we adapt the discus-

sion to the case of some non-piecewise-constant weights. Finally, in Section 3.6 we infer some general conclusions, both mathematical and biological, within the spirit of the discussion carried out in the Introduction.

3.2. Introduction to continuation methods

3.2.1. Spectral methods with collocation

As seen in the proof of Lemma 1.26 at page 71, the resolution of Problem (3.1) is equivalent to the search for the zeros of a differentiable operator

$$\mathfrak{F} : \mathcal{C}_0^1[0,1] \times \mathbb{R} \to \mathcal{C}_0^1(0,1).$$

This problem is infinite-dimensional and, therefore, it cannot be implemented in a computer. For this reason, the first step to solve it numerically consists in approximating its solutions through a truncated Fourier series, and then applying a collocation method in order to obtain a reduced finite dimensional problem.

Precisely, the approximation has been done by considering a truncated Fourier sine-series of a solution $u(x)$ of (3.1) to order N:

$$u_N(x) = M + \sum_{j=1}^{N} v_j \sin(j\pi x).$$

Then, we have chosen $N+2$ collocation points in $[0,1]$, in our case equidistant and with two of them coinciding with the endpoints of the interval, i.e.

$$x_0 = 0, \quad x_{N+1} = 1, \quad x_{i+1} = x_i + \delta, \quad 0 \leq i \leq N,$$

where we have set $\delta = 1/(N+1)$. The collocation process consists in imposing the truncate solutions to satisfy the original boundary value problem at the collocation points, which gives rise to

$$\left(Lv^T\right)_i = \lambda \left[\left(Jv^T\right)_i + M\right] + a_b(x_i) \left[\left(Jv^T\right)_i + M\right]^p, \qquad 1 \leq i \leq N, \tag{3.6}$$

where $v = (v_1, ..., v_N)$, and we have denoted

$$J = \left(\sin(j\pi x_i)\right)_{1\leq i,j\leq N}, \qquad L = \left((j\pi)^2 \sin(j\pi x_i)\right)_{1\leq i,j\leq N}.$$

In this way we have obtained a finite-dimensional problem which consists in determining the zeros of a nonlinear systems of N equations in $N+1$ variables (the v_i's and b). Generically, the solution set is a curve in $\mathbb{R}^{N+1}$.

Although the weight function considered in our numerical experiments possesses a discontinuity at some points $\{\alpha, 1-\alpha\} \subset (0,1)$, the number of modes has always been chosen in such a way that $x_i \notin \{\alpha, 1-\alpha\}$ for all $0 \leq i \leq N$, so that, changing the weight function of (3.1) in the intervals containing α and $1-\alpha$, we can assume, without loss of generality, that the nonlinearity of the differential equation is $\mathcal{C}^2$. This allows us to apply the results of F. Brezzi, J. Rappaz and P. A. Raviart [12, 13, 14] which guarantee (for general Galerkin approximations) the local convergence as $N \uparrow \infty$ of the paths at regular, turning and simple bifurcation points. Incidentally, the convergence for regular codimension two singularities was proven by J. López-Gómez, M. Molina-Meyer and M. Villareal [58] and by J. López-Gómez et al. [49]. In all these situations, the local topological structures of the solution curves and/or surfaces for the continuous and the discrete models are equivalent. Therefore the bifurcation diagrams that we have obtained approximate the original ones.

As far as the error of the approximation concerns, since $u \in \mathcal{C}^1[0,1]$, its j-th Fourier coefficient v_j decays as $O(j^{-1})$ as $j \uparrow \infty$ (cf. C. Canuto et al. [17]) and, hence,

$$\max_{0\leq x\leq 1} |u_{N+1}(x) - u_N(x)| = O(N^{-1})$$

as $N \uparrow \infty$. Due to these features we have used the following criterion to choose the number of modes in all our numerical computations

$$\max_{0\leq j\leq 10} |v_{N-j}| \leq \frac{1}{2}10^{-5}.$$

To respect it we needed to take $N = 300$. This shows that, as it happens in general for the spectral methods, we can achieve a high accuracy at a very low computational cost.

3.2.2. Path-following continuation

Once the discretization procedure described in the previous section has been implemented, we have reduced our problem to the search for the zeros of a certain differentiable (nonlinear) function

$$\begin{aligned} \mathfrak{F} : \mathbb{R}^N \times \mathbb{R} &\to \mathbb{R}^N \\ (v, b) &\mapsto \mathfrak{F}(v, b). \end{aligned}$$

To solve this finite-dimensional problem, we can apply standard global continuation solvers in order to compute the solution curves and the dimensions of the unstable manifolds of all the solutions along them (see e.g. J. C. Eilbeck [29], H. Keller [40], M. Crouzeix and J. Rappaz [26], J. López-Gómez et al. [49],

J. López-Gómez [41], and E. L. Allgower and K. Georg [4]). These solvers are based on a prediction-corrector method, which consists, once a solution (v_0, b_0) is known, in predicting a new solution (v_1, b_1), for example by shooting in the tangential direction to the curve at (v_0, b_0). In general this prediction will not be a solution to our problem, therefore we have to correct it, for example by using a Newton iterative method, up to reach a desired approximation of the new solution (v_2, u_2). In order to determine a first solution where to start from, we adopt a similar procedure: we guess a possible solution (v_{-1}, b_{-1}) and correct it up to reach (v_0, b_0) (see Figure 3.1 for a graphical description of the method).

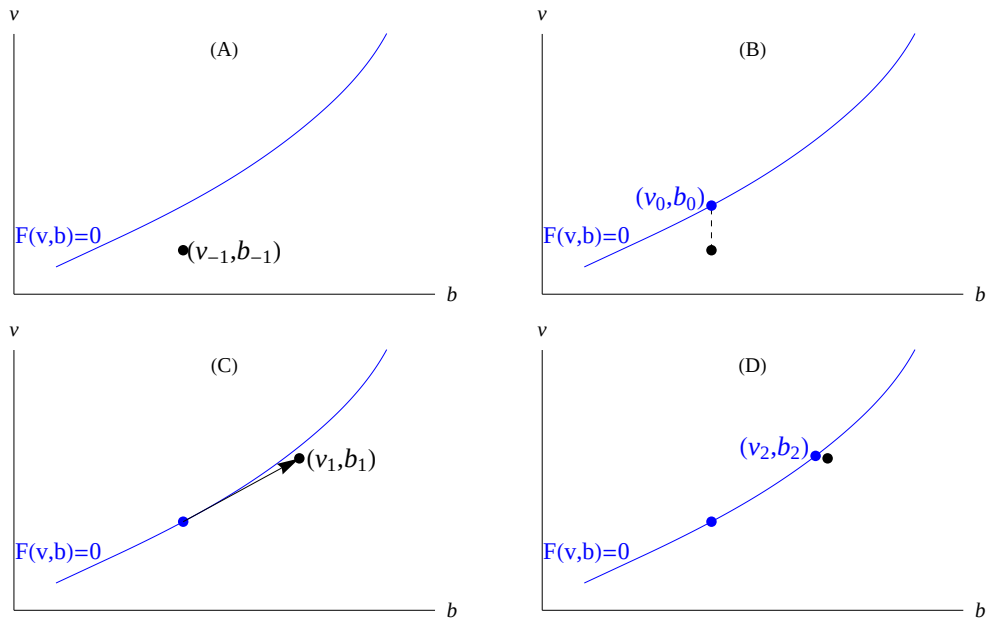

Figure 3.1: Graphical description of the path-following continuation: initial guess (A), first correction (B), first prediction (C) and second correction (D)

Essentially, the key point in the success of the path-following continuation is a correct parametrization of the solution curve in a neighborhood of each regular point (v_0, b_0). To achieve this, the easiest methodology is using the implicit function theorem to express v as a function of b, i.e. to find a function $v : \mathbb{R} \to \mathbb{R}^N$ such that $\mathfrak{F}(v(b), b) = 0$ for all b. However this is not possible at the values (v_0, b_0) where $\mathfrak{F}_v$ is not invertible; $\mathfrak{F}_v$ stands for the differential of $\mathfrak{F}$ with respect to v. Anyway at such points the solution curve might still be regular.

To overcome this difficulty, the standard global continuation solvers con-

sider, at each regular point (v_0, b_0) of $\mathfrak{F}$, an extended problem $\mathfrak{G} : \mathbb{R}\times\mathbb{R}^N\times\mathbb{R} \to \mathbb{R}^{N+1}$ defined like follows

$$\mathfrak{G}(s, v, b) = (\mathfrak{F}(v, b), \langle \psi_0, (v - v_0, b - b_0)\rangle - s), \tag{3.7}$$

where $\psi_0 \in \mathbb{R}^{N+1}$ satisfies

$$\langle \psi_0, \omega\rangle \neq 0, \tag{3.8}$$

being ω a unit vector that generates the kernel of $D_{(v,b)}\mathfrak{F}(v_0, b_0)$ (that is one-dimensional since (v_0, b_0) is a regular point, which means, by definition, that $D_{(v,b)}\mathfrak{F}(v_0, b_0)$ has maximum rank, i.e. equal to N).

The geometric idea behind the definition of $\mathfrak{G}$ like in (3.7) is that

$$\langle \psi_0, (v - v_0, b - b_0)\rangle - s = 0$$

is the equation of the hyperplane perpendicular to ψ_0 and at distance s to the point (v_0, b_0). Therefore, the solutions of $\mathfrak{G} = 0$ are the intersections between such an hyperplane and the curve $\mathfrak{F} = 0$. Since (v_0, b_0) is a regular point of $\mathfrak{F}$ and thanks to condition (3.8), for sufficiently small s there is an unique intersection between the hyperplane and the solution curve (see Figure 3.2) and, therefore, a parametrization of (v, b) as a function of s is possible.

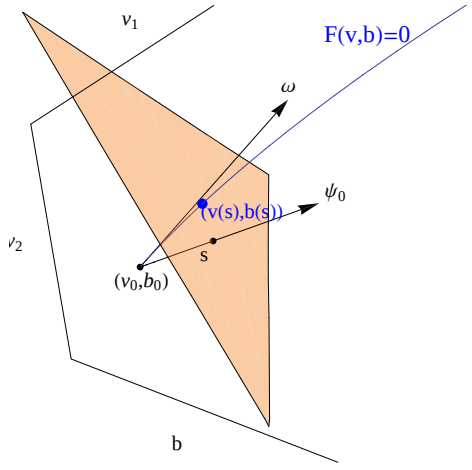

Figure 3.2: Pseudo arc length parametrization

To formalize this idea, observe that $\mathfrak{G}(0, v_0, b_0) = 0$ and that

$$D_{(v,b)}\mathfrak{G}(0, v_0, b_0) = \begin{pmatrix} D_v\mathfrak{F}(v_0, b_0) & D_b\mathfrak{F}(v_0, b_0) \\ \psi_0 & \end{pmatrix}.$$

Therefore, if $(v,b) \in \ker D_{(v,b)}\mathfrak{G}(0,v_0,b_0)$, we have that

$$(v,b) \in \ker D_{(v,b)}\mathfrak{F}(v_0,b_0) = \operatorname{span}[\omega],$$

i.e. $(v,b) = \gamma\omega$ for a certain $\gamma \in \mathbb{R}$. But we have that $\langle \psi_0, (v,b)\rangle = 0$ as well, and this implies, thanks to (3.8), that $\gamma = 0$, i.e. $(v,b) = 0$. This means that $D_{(v,b)}\mathfrak{G}(0,v_0,b_0)$ is an isomorphism and, as a consequence of the implicit function theorem, there exists $\varepsilon > 0$ and a differentiable function

$$(v,b) : (-\varepsilon,\varepsilon) \to \mathbb{R}^{N+1}$$

such that $(v(0),b(0)) = (v_0,b_0)$ and $\mathfrak{G}(s,v(s),b(s)) = 0$ for every $s \in (-\varepsilon,\varepsilon)$, which is equivalent to

$$\mathfrak{F}(v(s),b(s)) = 0,$$
$$\langle \psi_0, (v(s)-v_0, b(s)-b_0)\rangle = s,$$

as we desired. Such a parametrization is called a *pseudo arc length parametrization* because for sufficiently small s, this parameter gives the approximate length of the curve.

Operatively, one has to calculate ψ_0 in order to apply this prediction-correction algorithm. Assuming that the first point of the solution curve is not a turning point, we can proceed as described in Section 3.3.2 to determine the first tangent vector to the curve and then, at the following step of the algorithm, use this vector as ψ_0 to correct the solution. Condition (3.8) holds, provided that the shooting step in the prediction is sufficiently small.

To complete the description of the path-following method, we treat the case of *simple bifurcation points*. First of all, we recall that a simple bifurcation point $(v_0,b_0) = (v(0),b(0))$ on the solution curve $(v(s),b(s))$ satisfies

$$\operatorname{rank} D_{(v,b)}\mathfrak{F}(v_0,b_0) = N-1,$$

or, equivalently,

$$\dim\ker D_{(v,b)}\mathfrak{F}(v_0,b_0) = 2,$$

while

$$\operatorname{rank} D_{(v,b)}\mathfrak{F}(v(s),b(s)) = N \qquad \text{for every } s \sim 0, \quad s \neq 0.$$

As proven in Keller [40], a sufficient condition for this to hold is that the operator $D_{(v,b)}\mathfrak{G}(v(s),b(s))$ is an isomorphism for every $s \sim 0$, $s \neq 0$ and the determinant of this matrix changes sign as s crosses 0. In practice, once a simple bifurcation point has been detected with this criterion, one essentially has to solve

$$\det D_{(v,b)}\mathfrak{G}(v(s),b(s)) = 0$$

and, therefore, the bifurcation point can be approximated by means of a bisection method. The bifurcation directions have been determined as described in Subsection 3.3.1, where we detail the procedures that we have adopted.

3.3. Solving computational troubles

When implementing the available continuation methods in the literature to our problem, we found, essentially, two main difficulties. Namely, one must be extremely careful in choosing the shot direction to compute the bifurcated closed loops from the primary curve, and, in addition, one should adopt an appropriate re-scaling procedure to compute automatically all the turning points along the primary curve, as they are extremely closed and, hence, the available algorithms in the specialized literature do not work when $-\lambda > 0$ is sufficiently large. The resolution of these two difficulties will be the topic of Sections 3.3.1 and 3.3.2 respectively.

3.3.1. Determining the bifurcation directions

Regarding the first difficulty, it turns out that at the bifurcation points one cannot shot in an arbitrary non-tangential direction to get the first predicted point on the bifurcated loop. In particular, shooting in the orthogonal direction to the primary curve does not work in our model, because the tangents to the primary curve and to the bifurcated loop are very close to each other in $\mathbb{R}^{N+1}$ at the bifurcation point for large $-\lambda > 0$; doing so, the iterates in the correction step go back to the primary branch again. Consequently, the Method II of H. B. Keller [40, Chapter V] does not work in our present situation (see Figure 3.3); this was the method used in most of the global continuations in J. López-Gómez et al. [49], J. López-Gómez and M. Molina-Meyer [51]-[54], and R. Gómez-Reñasco and J. López-Gómez [36].

Consequently, to compute the bifurcated loops from the primary curve we had to determine very accurately the tangent vectors to the emanated curves at their bifurcation points from the primary curve, as suggested by H. B. Keller [40, Method I]. Subsequently, we will detail the way we proceeded. Equation (3.6) can be expressed as a nonlinear equation

$$\mathfrak{F}(b, v) = 0, \qquad b \geq 0, \quad v \in \mathbb{R}^N,$$

for a certain

$$\mathfrak{F} : [0, \infty) \times \mathbb{R}^N \subset \mathbb{R}^{N+1} \longrightarrow \mathbb{R}^N.$$

Suppose we have already computed the primary curve, say $(b(s), v(s))$, parameterized by the pseudo-arc length s, around some bifurcation point $(b_0, v_0) := (b(0), v(0))$. Then, there exists $\varepsilon > 0$ such that

$$\mathfrak{F}(b(s), v(s)) = 0, \qquad |s| < \varepsilon, \tag{3.9}$$

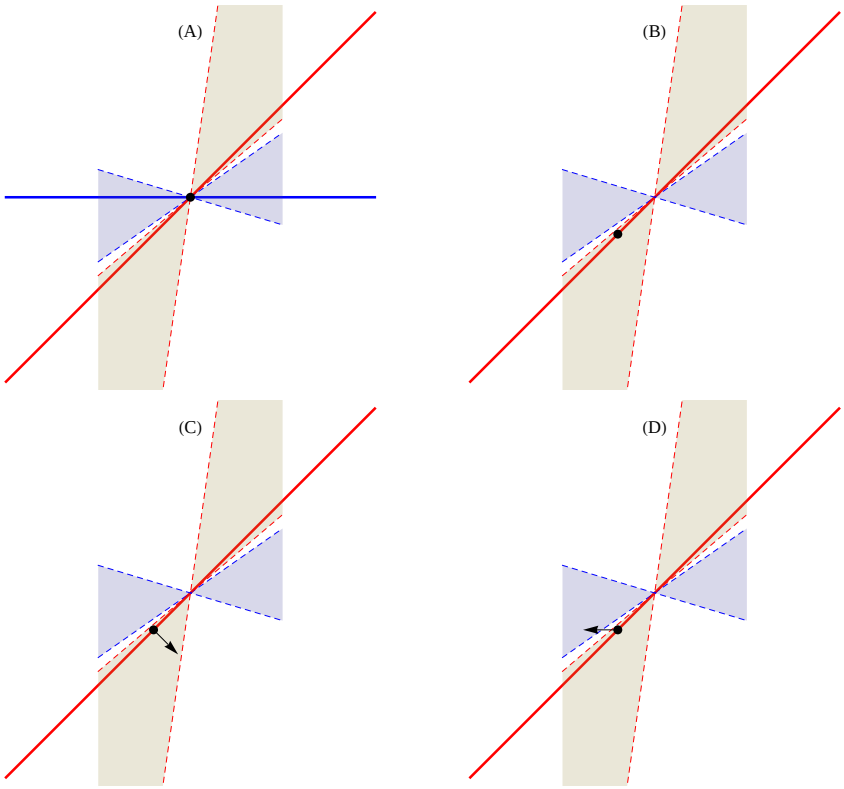

Figure 3.3: Graphical description of the shooting problem: real situation with the two curves and their attraction cones (A), practical situation where only one curve is known and the bifurcation point is approximated (B), shooting in an orthogonal direction that fails (C), shooting along the tangent to the bifurcated curve that succeeds (D)

and differentiating (3.9) with respect to s, we are driven to

$$D_{(b,v)}\mathfrak{F}(b(s),v(s))(\dot{b}(s),\dot{v}(s)) = 0,$$

where " $\cdot$ " stands for d/ds. Consequently,

$$\psi := (\dot{b}(0),\dot{v}(0)) \in \ker D_{(b,v)}\mathfrak{F}(b_0,v_0).$$

Actually, this is the tangent vector to the primary curve at the bifurcation point. It can be easily determined during the computation of $(b(s),v(s))$. As (b_0,v_0) is a simple bifurcation point,

$$\dim \ker D_{(b,v)}\mathfrak{F}(b_0,v_0) = 2.$$

In order to compute the tangent vector to the bifurcated curve, we first need to find out a basis of this kernel. Precisely, we want to determine a vector, denoted by Φ, orthogonal to ψ and normalized so that $\|\Phi\| = 1$. Thus, setting

$$B := \begin{pmatrix} D_{(b,v)}\mathfrak{F}(b_0, v_0) \\ \psi \end{pmatrix},$$

we should solve $B\Phi = 0$. Unlikely, in practice, the matrix B is unknown, as an effect of approximation errors. Actually, B is approximated by some matrix A which might be invertible. But, in general $A\Phi \neq 0$, though, by continuous dependence, $\|A\Phi\| \sim 0$ and A exhibits an eigenvalue perturbed from zero.

Therefore, in our numerical experiments, we have taken as Φ the unique ϕ minimizing $\|A\|$ on the unit sphere, i.e.,

$$\|A\phi\| = \min_{\|v\|=1} \|Av\|.$$

Note that $\Phi = \phi$ if $A = B$. This scheme has shown to be extremely efficient to do all our numerical computations. Up to the best of our knowledge, it goes back to E. L. Allgower and K. Georg [4]. It is well known that ϕ must be an eigenvector of the symmetric matrix A^TA associated to its lowest eigenvalue. Consequently, the inverse power method applied to A^TA provides us with an extremely good approximation of ϕ.

Similarly, one can determine $\hat{\psi} \in \mathbb{R}^N$ such that

$$\ker D_{(b,v)}\mathfrak{F}(b_0, v_0)^T = \text{span}\,[\hat{\psi}].$$

With these ingredients, the tangent vector to the bifurcated curve, say $Y(s)$, $s \sim 0$, is given by

$$\dot{Y}(0) = -\frac{1}{2}\frac{\langle\hat{\psi}, D^2_{(b,v)}\mathfrak{F}(b_0, v_0)[\phi, \phi]\rangle}{\langle\hat{\psi}, D^2_{(b,v)}\mathfrak{F}(b_0, v_0)[\psi, \phi]\rangle}\psi + \phi \tag{3.10}$$

(cf. J. López-Gómez [41, pp. 225] and H. B. Keller [40, Section 5.26] for the details of the derivation of this formula). As

$$\frac{1}{\varepsilon}\langle\hat{\psi}, \left[D_{(b,v)}\mathfrak{F}\left((b_0, v_0)+\varepsilon\phi\right) - D_{(b,v)}\mathfrak{F}(b_0, v_0)\right]\phi\rangle = \langle\hat{\psi}, D^2_{(b,v)}\mathfrak{F}(b_0, v_0)[\phi, \phi]\rangle + o(\varepsilon),$$
$$\frac{1}{\varepsilon}\langle\hat{\psi}, \left[D_{(b,v)}\mathfrak{F}\left((b_0, v_0)+\varepsilon\phi\right) - D_{(b,v)}\mathfrak{F}(b_0, v_0)\right]\psi\rangle = \langle\hat{\psi}, D^2_{(b,v)}\mathfrak{F}(b_0, v_0)[\psi, \phi]\rangle + o(\varepsilon),$$

we have that

$$\dot{Y}(0) = -\frac{1}{2}\frac{\langle\hat{\psi}, \left[D_{(b,v)}\mathfrak{F}\left((b_0, v_0) + \varepsilon\phi\right) - D_{(b,v)}\mathfrak{F}(b_0, v_0)\right]\phi\rangle}{\langle\hat{\psi}, \left[D_{(b,v)}\mathfrak{F}\left((b_0, v_0) + \varepsilon\phi\right) - D_{(b,v)}\mathfrak{F}(b_0, v_0)\right]\psi\rangle}\psi + \phi + o(\varepsilon) \tag{3.11}$$

as $\varepsilon \downarrow 0$. Naturally, (3.11) requires much lower computational cost than (3.10), as it involves only first order derivatives. So, for the numerics of this work, we have taken the approximation

$$\dot{Y}(0) \sim -\frac{1}{2}\frac{\langle \hat{\psi}, \left[D_{(b,v)}\mathfrak{F}\left((b_0,v_0)+\varepsilon\phi\right) - D_{(b,v)}\mathfrak{F}(b_0,v_0)\right]\phi\rangle}{\langle \hat{\psi}, \left[D_{(b,v)}\mathfrak{F}\left((b_0,v_0)+\varepsilon\phi\right) - D_{(b,v)}\mathfrak{F}(b_0,v_0)\right]\psi\rangle}\psi + \phi$$

for an appropriate choice of the auxiliary parameter ε. Our choice was $\varepsilon = 10^{-9}$ for all the computations.

3.3.2. Treatment of the closed turning points

Regarding the turning points along the primary branch, the main difficulty is the exiguous difference between the solutions in each of the half-curves generating the turning point. This causes all the turning points in the bifurcation diagrams to be very closed.

Let $(b(s), v(s))$, $s \in \mathbb{R}$, denote the parametrization by pseudo-arc length s of the primary curve and pick $s_1 < s_2$ such that $P_1 := (b(s_1), v(s_1))$ and $P_2 := (b(s_2), v(s_2))$ are close to some turning point. Then, the tangent vectors to the primary curve at these points are given by

$$\psi_j := (\dot{b}(s_j), \dot{v}(s_j)), \qquad j \in \{1, 2\},$$

and, in our solvers, the sign of the Euclidean scalar product

$$\langle \psi_1, \psi_2 \rangle = \langle \dot{v}(s_1), \dot{v}(s_2) \rangle + \dot{b}(s_1)\dot{b}(s_2) \tag{3.12}$$

decides whether P_1 and P_2 are on the same half-curve of the turning point, or not. More precisely, P_1 and P_2 are on the same half-branch if $\langle \psi_1, \psi_2 \rangle > 0$, while they leave the turning point in between if $\langle \psi_1, \psi_2 \rangle < 0$.

To compute the tangent vector at s, $\psi := (\dot{b}(s), \dot{v}(s))$, we should solve the equation

$$D_b\mathfrak{F}(b,v)\dot{b} + D_v\mathfrak{F}(b,v)\dot{v} = D_{(b,v)}\mathfrak{F}(b,v)\psi = 0, \tag{3.13}$$

subject to the normalization condition

$$\|\psi\|^2 = \dot{b}^2 + \|\dot{v}\|^2 = 1. \tag{3.14}$$

Solving (3.13) for $\dot{v}$ and substituting the result in (3.14) gives

$$\dot{b} = \pm\frac{1}{\sqrt{1 + \| \left(D_v\mathfrak{F}(b,v)\right)^{-1} D_b\mathfrak{F}(b,v)\|^2}}. \tag{3.15}$$

Operatively, one starts by computing $\dot{b}$ from (3.15), then substitutes the resulting value in (3.13) and, finally, solves (3.13) for $\dot{v}$. However, we have to choose one of the signs in identity (3.15). This is the first step in running our path-following solver, depending on whether we want to compute solutions of (3.1) for increasing values of the bifurcation parameter b, or for decreasing ones. Once fixed the sign of $\dot{b}$, it will be kept invariant by the code until a turning point is detected through the negativity of (3.12). When this occurs, the code changes automatically the sign of $\dot{b}$ to compute, going backwards, the other half-curve of the turning point.

When the solutions are approaching a turning point, the term $\dot{b}(s_1)\dot{b}(s_2) > 0$ must converge to zero and, hence, the change of sign of (3.12) can be detected through the change of sign of the scalar product $\langle \dot{v}(s_1), \dot{v}(s_2) \rangle$. But the converse result is far from true, because $\langle \dot{v}(s_1), \dot{v}(s_2) \rangle$ could also change sign at the critical points of the curve, where $\dot{b}(s_1)\dot{b}(s_2) > 0$ is bounded away from zero. Consequently, at the turning points $\langle \dot{v}(s_1), \dot{v}(s_2) \rangle$ changes of sign and $\dot{b}(s_1)\dot{b}(s_2) \sim 0$. However one can distinguish a turning point from a critical point either by the significant reduction of the magnitude of the continuation step as the solutions are approximating a singular point of $\mathfrak{F}$, or through the changes in the dimensions of the unstable manifolds. The most versatile criterion from the practical point of view is the latter, which is the one that we have adopted in our computations.

With the choice (3.2), it turns out that, for $\lambda \leq -800$, the turning points are extremely closed. Actually, the solutions along each of the two half-branches differ from each other in less than 10^{-4}. As a consequence, the correction step of the path-following solver might switch from one half-branch to the other one when $\langle \dot{v}(s_1), \dot{v}(s_2) \rangle < 0$ but $\langle \psi_1, \psi_2 \rangle > 0$. Although $\dot{b}(s_1)\dot{b}(s_2)$ is small, because the continuation step shortened automatically up to order 10^{-7}, $\dot{b}(s_1)\dot{b}(s_2)$ is not sufficiently small to provoke the change of sign of (3.12). In these cases, we know that the solution switched to the other half-branch by comparing the dimensions of the unstable manifolds of the last two solutions. Such dimensions can change either by one or two unities, according to the relative positions of the last correction with respect to the turning point and the bifurcation points of the secondary loops from the primary curve. Nevertheless, even if at a turning point the quantity $\dot{b}(s_1)\dot{b}(s_2)$ goes to zero, the fact that it remained large with respect to $\langle \dot{v}(s_1), \dot{v}(s_2) \rangle$ when the correction jumped to the other half-branch does not necessarily entail that we are far away from the turning point, because, as a result of the numerics, $\dot{b}(s_1)\dot{b}(s_2)$ varies drastically in a neighborhood of the turning point when $\lambda \leq -800$.

Once detected a jump along the primary curve, one must change the sign of $\dot{b}$. Otherwise, again by the closeness of the turning point, the algorithm is

Table 3.1: Approaching the largest subcritical turning point of the primary curve

λ	Value of b at the jump	Value of b at the turning point	Relative difference
-800	36496.29636012	36496.29636015	8×10^{-13}
-1300	604105.50775006	604105.50777582	4×10^{-11}
-2000	12463985.15701294	12463985.21662086	5×10^{-9}

pushed forward to find new solutions in a small neighborhood of the turning point, where, as a result of the number of solutions available, up to four for sufficiently large $-\lambda$, the corrections either might jump to another curve again, or there might be slow convergence of the solver in the correction, causing a severe reduction of the continuation step until reaching the minimal value permitted, which leads to the stop of the algorithm. As it is apparent by having a glance at Figure 3.12 for example, the turning points and the bifurcation points of the secondary loops from the primary curve do approximate each other as $\lambda \downarrow -\infty$. Consequently, in a neighborhood of a turning point the solver might need to discriminate among four extremely close solutions. As a matter of fact, the path-following solver can provide even with a solution on the bifurcated loop. In these degenerate situations, one should ascertain the symmetry of the solution, besides the dimensions of the unstable manifolds, to determine its precise location. It should be remembered that, according to the results of Chapter 1, all the solutions along the primary curve are symmetric, while the solutions on the bifurcated loops are asymmetric.

Table 3.3.2 measures, again for the choice (3.2), the distance between the value of b where the solution jumps to the other half-curve near the first turning point of the primary branch and the value of b where the solver stops if the sign of $\dot{b}$ is not changed in (3.15). We took the latter one as the value of b for the first turning point of the primary curve in all the numerical examples of Section 3.4.

By analyzing Table 3.3.2, it is apparent that we are quite close to the turning point when the algorithm jumps to a new branch, confirming that $\dot{b}(s_1)\dot{b}(s_2)$ varies dramatically in a neighborhood of a closed turning point.

In many circumstances, when the solution jumps from one branch to another it might cross not only the turning point of the primary branch but also the first bifurcation point of the closed loop emanating from it, which are extremely close for sufficiently large $-\lambda > 0$. We know that this occurs because the unstable manifold of the computed solution varied its dimension by 2. In

such cases, at a later stage, we refined the computation of the primary curve, going backwards, to approximate the bifurcation point of the closed loop as much as possible. Two possibilities can occur: either we can cross it, or the algorithm jumps to the bifurcated loop. In the second case, we take as the value of b for the bifurcation point the first one on the loop. The larger $-\lambda > 0$ is, the more emphasized is the previous trouble, since, according to the numerics, the bifurcation points of the loops approximate the turning points of the primary curve as $\lambda \downarrow -\infty$.

To control automatically the change of sign of $\dot{b}$ in (3.15) when a jump along the primary curve occurs, we have used, instead of (3.12), the weighted scalar product

$$\langle \psi_1, \psi_2 \rangle_\varepsilon = \langle \dot{v}(s_1), \dot{v}(s_2) \rangle + \varepsilon \dot{b}(s_1)\dot{b}(s_2) \tag{3.16}$$

for some appropriate $\varepsilon > 0$, which was chosen according to the size of λ, in order to reduce the weight of the term $\dot{b}(s_1)\dot{b}(s_2)$. In the numerical computations of Section 3.4 we used the values of ε given in Table 3.2.

Table 3.2: Size of the rescaling in the scalar product (3.16)

λ	ε
-800	10^{-1}
-1300	10^{-8}
-2000	10^{-15}

For $\lambda < -2000$ we were not able to automatize the continuation codes, since we were outside the machine precision range as it is apparent from Table 3.2.

3.4. Description of the bifurcation diagrams for the choice (3.2)

Throughout this section we will consider problem (3.1) with a_b given by (3.2) and we will fix $p = 2$, $M = 100$, $c = 1$ and $\alpha = 0.3$, whereas as usual b and λ will be regarded as the primary and secondary parameters of the problem, respectively. Since the value of c is substantially smaller than M, the associated solutions of (3.1) can be thought of as approximations to the *large solutions* of the associated equation

$$-u'' = \lambda u + a_b(x)u^p. \tag{3.17}$$

Precisely, we will give to the parameter λ a series of significant values ranging in the interval $(-\infty, 0]$ and, for each of these values, b will be regarded as the main bifurcation parameter to compute the corresponding global bifurcation diagrams of (3.1). Our main goal is to analyze their complexity as $-\lambda > 0$ increases.

Figure 3.4 shows the plot of the global bifurcation diagram of (3.1) for $\lambda = -5$, on the left, as well as the profiles of a series of solutions along it, on the right.

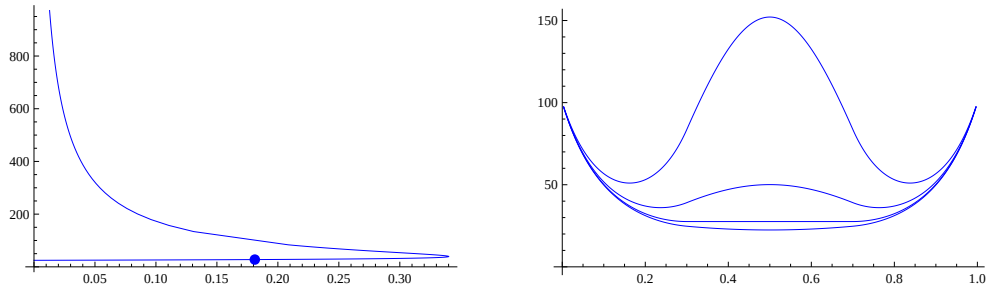

Figure 3.4: Global bifurcation diagram for $\lambda = -5$ and plots of some solutions along it

As in all subsequent global bifurcation diagrams, in the left picture we are representing the value of b, in the horizontal axis, versus the value of $u(\alpha)$, in the vertical one. The bifurcation diagram consists of a single *primary curve* emanating from the unique positive solution of (3.3) at $b = 0$, whose existence and uniqueness was established in J. López-Gómez [46], and it continues towards the right up to reach the critical value $b = 0.3401$, where it goes backwards exhibiting a subcritical turning point. Once passed the turning point, the solutions on the upper half-branch can be continued for every $0 < b < 0.3401$.

All our numerical experiments have revealed that along the upper half-branch the solutions of (3.1) blow up in $[\alpha, 1-\alpha]$ as $b \downarrow 0$, while in $[0, \alpha)$ they approximate the unique solution u_s of the singular problem (3.5). Actually, as $b \downarrow 0$, these solutions approximate the *metasolution* $m(x)$ defined by (3.4), as conjectured in Chapter 1 (see page 75). Therefore, the global bifurcation diagram establishes an homotopy between the unique classical solution of the sublinear problem (3.3) and the unique *metasolution* of (3.17) supported in $(0, \alpha) \cup (1-\alpha, 1)$ (cf. J. López-Gómez [46, 47]). Consequently, for every $b \in (0, 0.3401)$, (3.1) admits, at least, two solutions. Moreover, in accordance with the results of Chapter 2, the solutions along the lower half-branch are linearly asymptotically stable, while the solutions along the upper half-branch

are unstable with one-dimensional unstable manifold. With respect to this point, we remark that in the bifurcation diagrams of this chapter, the stroke of the lines does not have to do with the stability of the solutions, as we did in Chapter 2. Here we have just used different strokes for different solution curves.

The bottom plot of the right picture in Figure 3.4 shows the unique solution of (3.3), the next one shows the trivial solution u_0, whose exact position in the global bifurcation diagram has been marked with a thick point, the third one shows the solution of (3.1) at the turning point and the fourth one shows the solution on the upper half-branch for $b = 0.2097$. The trivial solution arose at $b = b^* = 0.1811$ on the lower half-branch. All the solutions on the lower half-branch to the left of b^* are convex in the central interval $(0.3, 0.7)$, and stay below m_0, while the remaining solutions of the diagram are concave and stay above m_0. A remarkable feature is that the solutions along the global bifurcation diagram are pointwise increasing as we run over it starting at the unique solution of (3.3). Therefore, they decrease with b along the upper half-branch, while they increase with b along the lower one; a genuine superlinear behavior. The solutions along the upper half-branch have been computed up to $b = 2.5 \times 10^{-7}$, where $u(\alpha) \sim 8 \times 10^5$ and $u(0.5) \sim 3 \times 10^8$.

Similarly, the left picture of Figure 3.5 shows the global bifurcation diagram for $\lambda = -70$ and the right one a series of solution plots along it. The unique significant qualitative difference with respect to the previous case is that for $\lambda = -70$ the trivial solution u_0 arises on the upper half-branch of the diagram, instead of on the lower one. Actually, as λ decreased from -5 up to reach -70 the trivial solution u_0 moved along the lower half-branch and crossed the turning point at some intermediate value of λ up to reach the position marked by the thick point in the global bifurcation diagram of Figure 3.5.

The plots of the right picture of Figure 3.5 show the solutions of (3.1) on the lower half-branch for $b = 0$, $b = 7.6585$ (the turning point), and on the upper half-branch for $b^* = 6.4367$ and $b = 3.4651$, 1.2513 and 0.8720, from the bottom to the top. As in the previous and in all subsequent cases, the solutions on the upper half-branch do approximate the metasolution $m(x)$ as $b \downarrow 0$. As before, all the solutions filling in the lower half-branch are linearly asymptotically stable, while the solutions along the upper half-branch are unstable with one-dimensional unstable manifold.

Figure 3.6 shows a magnification of the (subcritical) turning points exhibited by the two previous global bifurcation diagrams. Having a careful look at the scales at which they have been represented, it becomes apparent that the turning point for $\lambda = -5$ is *more open* than the corresponding one for $\lambda = -70$, which goes backwards at a much faster rate. Such behavior has been

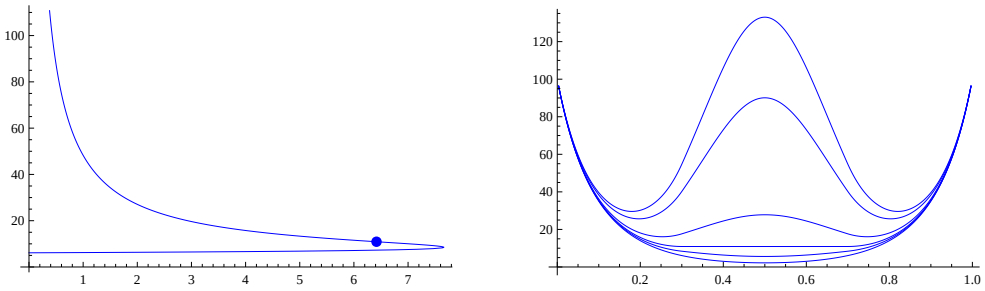

Figure 3.5: Global bifurcation diagram for $\lambda = -70$ and plots of some solutions along it

observed for all values of λ for which we have computed the global bifurcation diagrams of (3.1). The more negative the parameter λ is, the faster is the rate at which the turning point is crossed. Here relays one of the main technical difficulties we had to overcome in order to compute all the turning points for $\lambda \leq -800$, where such a phenomenon is extremely emphasized, as discussed in Section 3.3.2.

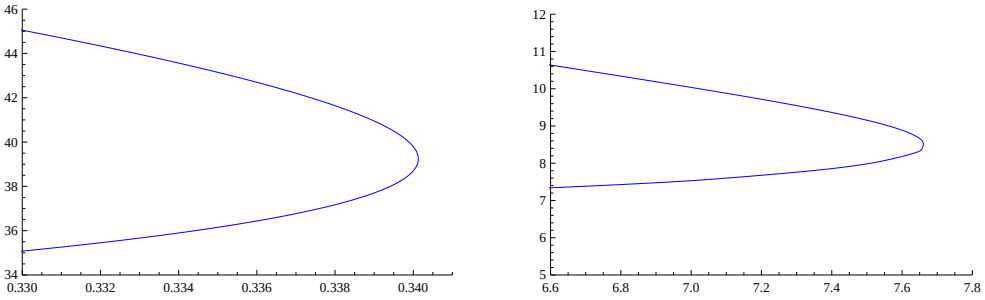

Figure 3.6: Magnification of the turning points of Figures 3.4 and 3.5

In the previous cases, all computed solutions along the global bifurcation diagrams are of type $(1, s)$, except u_0, which is of type $(0, s)$. Actually, the solutions along the curve of the bifurcation diagrams exhibit a minimum before reaching u_0 and a maximum after passing it. A similar phenomenon, consisting in interchanging minima with maxima, occurs every time we cross u_0 on the *primary curve* for all $\lambda < 0$.

Further, as λ decreased from $\lambda = -70$ up to reach the value $\lambda = -140.868$ a solution loop emanated from the upper half-branch of the primary curve. When the loop bifurcated from the primary curve, all solutions on it were of type $(1, a)$. Figure 3.7 shows a series of emerging loops for four decreasing

values of λ. They have been plotted with a red dashed line. The first plot of Figure 3.7 shows a significant piece of the upper half-branch of the primary curve containing one of these loops, where we have also marked the trivial solution u_0 through a thick point. Naturally, since the remaining solutions along the global bifurcation diagram are of type $(1, s)$, the loop emanated as a consequence of a *symmetry breaking* bifurcation phenomenon as λ decreases. The bifurcation points of these loops are of pitchfork type. As λ further decreased from $\lambda = -140.868$ the closed loop of asymmetric solutions gradually enlarged up to reach the trivial solution u_0 at some critical value of the parameter λ. For any smaller value of λ the trivial solution always remained enclosed by the loop. The upper right plot of Figure 3.7 shows a significant piece of the global bifurcation diagram for $\lambda = -140.9$, where the loop did not reach u_0 yet. All solutions on the bifurcated loop were of type $(1, a)$ whenever u_0 remained outside the loop. The bottom left plot of Figure 3.7 shows a piece of the global bifurcation diagram for $\lambda = -142$, where u_0 is extremely close to the bifurcated loop. Indeed, in this case $b^* = 31.5668$ and the subcritical bifurcation point arises at $b = 31.4378$. For smaller values of λ the loop encircled u_0 and some of the solutions along the closed solution loop became of type $(2, a)$, as it happens in the last plot of Figure 3.7 for $\lambda = -145$. This pattern is maintained for all smaller values of λ.

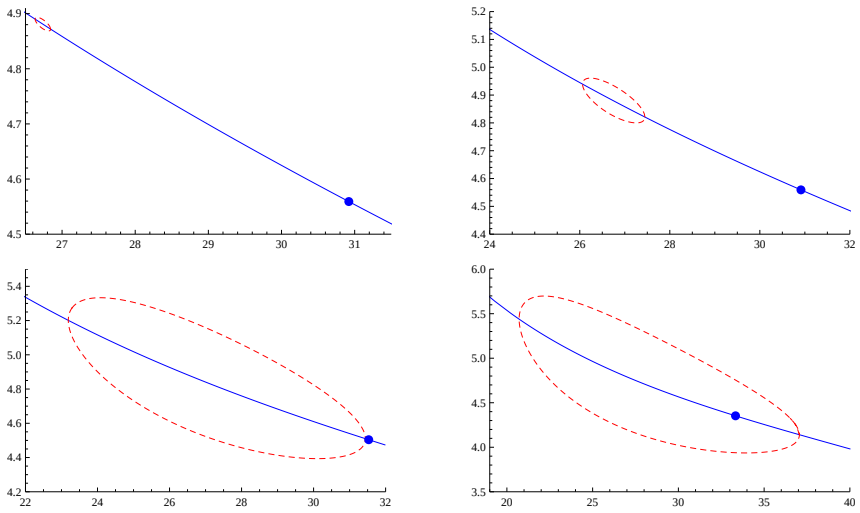

Figure 3.7: Symmetry breaking of the first solution loop

The left picture in Figure 3.8 marks with small squares the points where the type of the solutions along the closed loop changed for $\lambda = -150$. Namely, the two solutions of the closed loop are of type $(2, a)$ if $24.0664 < b < 42.4045$,

while they are of type $(1, a)$ if $18.7512 < b < 24.0664$ or $42.4045 < b < 44.5564$. As usual, the thick point marks the trivial solution u_0. These notations will be maintained throughout the rest of this chapter. In the other two pictures of Figure 3.8 one can see a series of significant solution plots along the closed loop. As in the sequel, we are representing the solutions in the central interval $[0.3, 0.7]$, because of the significant difference of size between $u|_{[0,0.3]}$ and $u|_{[0.7,1]}$ with respect to $u|_{[0.3,0.7]}$; note that $u(0) = u(1) = 100$. The continuous lines are the graphs of the solutions at the bifurcation points and the dashed lines are the plots of three solutions along each of the half-branches of the loop. The central one is of type $(2, a)$ and the remaining two are of type $(1, a)$; naturally, they are closer to the bifurcation points.

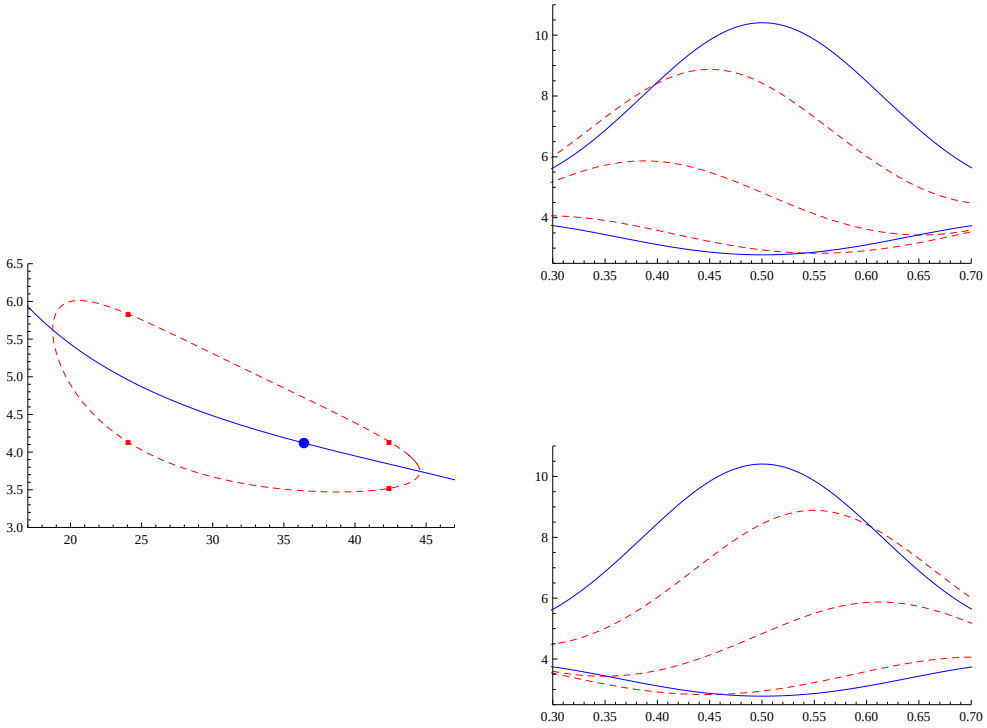

Figure 3.8: The points where the type changes along the bifurcated loop for $\lambda = -150$ (left picture) and plots of some significant solutions along it (right pictures)

The solutions on the central upper right plot were computed on the upper half-loop for $b = 44.5564$ (subcritical bifurcation), $b = 43.0439$ (solution of type $(1, a)$), $b = 31.5391$ (solution of type $(2, a)$), $b = 21.7268$ (solution of type $(1, a)$) and $b = 18.7512$ (supercritical bifurcation point). The solutions on the last plot are the reflections around $x = 0.5$ of the corresponding solutions on

the previous one, as already proven in Chapter 1. All the solutions along these closed loops are unstable, with one-dimensional unstable manifold, while all the solutions on the portion of the primary upper half-branch encircled by the loop have two-dimensional unstable manifolds. This fact is in complete agreement with the local bifurcation theorem and the exchange stability principle of M. G. Crandall and P. H. Rabinowitz [24, 25]. These numerical results reveal moreover that the minimum of the Poincaré map θ_2 introduced in Section 1.4 does not vary monotonically with b , because the emerging loop in Figure 3.7 left outside the trivial solution u_0 when it bifurcated from the primary curve.

As λ decreased from $\lambda = -150$, there was a critical value of λ where a bifurcation to solutions of type $(3, s)$ from u_0 occurred, in such a way that the solutions on the primary curve around u_0 were of type $(3, s)$ before changing type to $(1, s)$. The first picture of Figure 3.9 shows the global bifurcation diagram of (3.1) for $\lambda = -300$, while the last one shows the plots of the trivial solution and two solutions of type $(3, s)$ along the primary branch. They were computed for the values $b = 227.6725$ and $b = 353.6714$. The global bifurcation diagram of Figure 3.9 consists of two curves: the continuous blue line, which is the primary branch connecting the unique solution of (3.3) with the metasolution $m(x)$, and the dashed red line, which is the closed solution loop emanating from the primary curve at the values of the parameter $b = 12.8294$ and $b = 526.4099$, which are the turning points of the bifurcated closed loop. The subcritical turning point of the primary curve occurs at $b = 527.4319$. All solutions on the primary curve between the two squares are of type $(3, s)$, while the remaining ones are of type $(1, s)$. The changes between these two types occur at the values $b = 149.8536$ and $b = 409.4183$. All the changes of type on the primary branch occur at the level of u_0. The type of the solutions along the closed loop follows the general patterns already described; the changes of type along it occur at $b = 36.8971$ and $b = 444.4337$. Consequently, for every $b \in (0, 12.8294)$, (3.1) has two solutions of type $(1, s)$, for every $b \in (12.8294, 36.8971)$, (3.1) has two solutions of type $(1, s)$ and another two of type $(1, a)$, for every $b \in (36.8971, 149.8536)$, (3.1) has two solutions of type $(1, s)$ and two solutions of type $(2, a)$, for every $b \in (149.8536, 409.4183) \setminus \{b^* = 303.8681\}$, (3.1) has two solutions of type $(2, a)$, one solution of type $(1, s)$ and another solution of type $(3, s)$, and so on. The solutions of type $(3, s)$ exhibit two minima and one maximum if $b < b^*$, while they have two maxima and one minimum if $b > b^*$. The stability of the solutions follows the same patterns as in the previous cases. The lower half-branch of the primary curve consists of linearly stable solutions, while the upper one is filled in by unstable solutions. These solutions have one-dimensional unstable manifold if they are outside the loop, whereas they

have two-dimensional unstable manifold if they are encircled by the loop. The solutions along the loop have a one-dimensional unstable manifold.

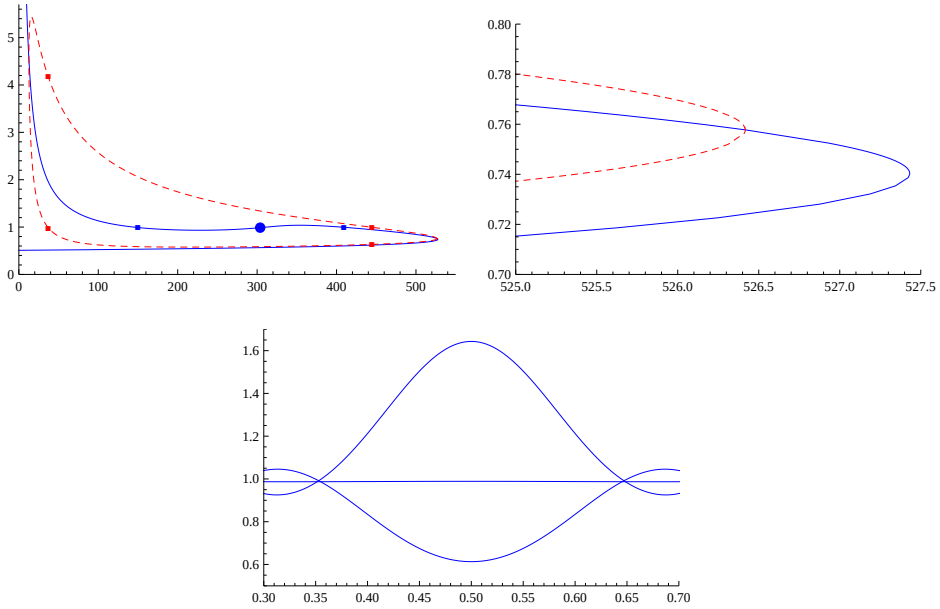

Figure 3.9: Global bifurcation diagram for $\lambda = -300$ (first picture), magnification of the turning point along the primary curve exhibiting the subcritical bifurcation of the first closed loop (second picture) and plots of u_0 and two solutions of type $(3, s)$ (third picture)

A non-expected and rather striking feature is that the subcritical bifurcation point of the loop from the primary branch is very close to the turning point of the primary branch, as shown in the second plot of Figure 3.9. Although in this case the proximity of the two curves does not give any special numerical difficulty, provided that the step of the path following solver is sufficiently small, we have seen in Section 3.3.2 that the proximity of the bifurcation point and the subcritical turning point is a very subtle question that causes some computational troubles for more negative values of λ.

As λ decreased from $\lambda = -300$ up to reach the value $\lambda = -750$, whose associated global bifurcation diagram has been plotted in the first picture of Figure 3.10, the arc of curve of the solutions of type $(3, s)$ along the primary branch rotated counterclockwise around u_0 originating two additional turning points along it. Naturally, one of them supercritical and the other one subcritical. In this case the trivial solution arose at $b^* = 1.4732 \times 10^4$ and the points where the solutions of type $(1, s)$ become solutions of type $(3, s)$ along the primary branch are $b = 0.0768 \times 10^4$ and $b = 2.1758 \times 10^4$; as usual, these points have

been marked with small squares. The turning points of the branch of type $(3, s)$ occur at $b = 0.5206 \times 10^4$ (the supercritical one) and $b = 2.0680 \times 10^4$ (the subcritical one). As in the previous cases, in the first picture of Figure 3.10 we have plotted with a dashed red line the loop bifurcating from the solutions of type $(1, s)$ along the primary curve, and the small squares along it mark the values of b where the solutions changed type from $(1, a)$ to $(2, a)$, or vice versa. These values are $b = 0.0121 \times 10^4$ and $b = 2.1778 \times 10^4$. The last one is sufficiently close to $b = 2.1758 \times 10^4$ so that the two squares are almost superimposed. The maximal subcritical turning point on the primary branch arises at $b = 2.6184588 \times 10^4$ and the bifurcation points of the loop occur at $b = 0.0011 \times 10^4$ and $b = 2.6184574 \times 10^4$. Incidentally, the first subcritical turning point along the primary branch and the subcritical bifurcation point of the closed loop occur almost at the same value of the parameter b, as it has been already commented above.

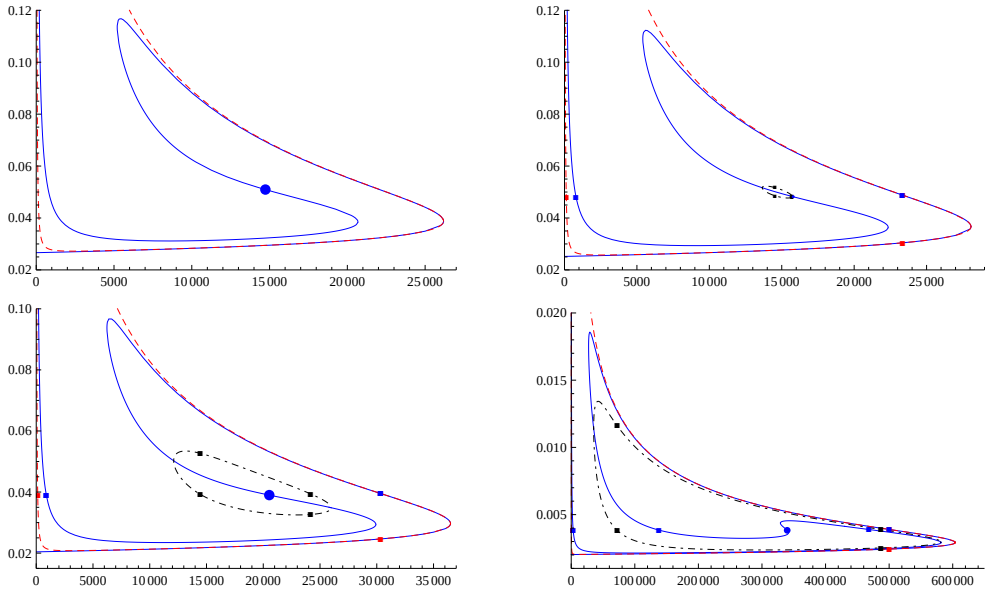

Figure 3.10: Global bifurcation diagram for $\lambda = -750$ (upper left), $\lambda = -760.3$ (upper right), $\lambda = -800$ (bottom left) and $\lambda = -1300$ (bottom right)

At the scale chosen to plot the global bifurcation diagrams of Figure 3.10 we had not enough room to plot the entire loop of asymmetric solutions of type $(1, a)$ and $(2, a)$, since, for example, in the first picture the values of the corresponding $u(\alpha)$'s along the loop reach 2.15, which is substantially larger than 0.12. If we had changed the scale on the vertical axis to plot the entire loop we could not have distinguished properly the counterclockwise rotation

of the branch of solutions of type $(3, s)$ on the primary curve, because it would have been condensed in a $1/18$ fraction of the vertical axis.

The dimensions of the unstable manifolds of the solutions plotted in the first bifurcation diagram of Figure 3.10 adjust to the next patterns. All the solutions along the lower half-branch of the primary curve are linearly asymptotically stable until we reach the subcritical turning point at $b = 2.6184588 \times 10^4$, where they become unstable, with one-dimensional unstable manifold, until we reach the subcritical bifurcation point of the loop, at $b = 2.6184574 \times 10^4$, where the solutions along the primary curve become unstable with two-dimensional unstable manifold until we reach the supercritical turning point on the primary branch, at $b = 0.5206 \times 10^4$, where the unstable manifolds become three-dimensional until the next subcritical turning point at $b = 2.0680 \times 10^4$, where they become two-dimensional again and remain two-dimensional until we meet the supercritical pitchfork bifurcation point of the loop from the primary branch, at $b = 0.0011 \times 10^4$, where they become one-dimensional for all smaller values of b. All solutions along the bifurcated loop are unstable with one-dimensional unstable manifold.

Naturally, as an easy consequence of the previous results, for every b in between the turning points of the $(3, s)$-arc of curve of the primary branch, $b = 0.5206 \times 10^4$ and $b = 2.0680 \times 10^4$, Problem (3.1) possesses at least 6 solutions, and, except for the value where u_0 arises, $b^* = 1.4732 \times 10^4$, three among them are of type $(3, s)$, two of type $(2, a)$ and the remaining one is of type $(1, s)$. At the value $b^* = 1.4732 \times 10^4$, one of the solutions of type $(3, s)$ becomes the trivial solution u_0. Similarly, by simply looking at the bifurcation diagram plotted in the first picture of Figure 3.10, one can easily give some other multiplicity results according to the range where the parameter b varies.

As λ decreased from $\lambda = -750$ and reached the value $\lambda = -760.3$ a new closed loop, the second one, emanated from the $(3, s)$-arc of curve of the primary curve. Initially, soon after it perturbed from the primary curve, this loop consisted of solutions of type $(3, a)$. As λ decreased, the loop grew approaching the trivial solution. The upper right picture of Figure 3.10 shows the global bifurcation diagram of (3.1) for $\lambda = -760.3$, where, being the trivial solution outside the second loop, the type of the solutions along the loop changed from type $(3, a)$ to type $(4, a)$ along two arcs of curve separated away from the two bifurcation points from the primary branch. In Figure 3.10, the second closed loops bifurcated from the primary curves have been represented with a dot-dashed black curve, where we have marked with squares the points where the type of the solutions along them changed.

The second loop of the upper right diagram of Figure 3.10 bifurcates from the primary branch at $b = 1.3656 \times 10^4$ and $b = 1.5716 \times 10^4$. The trivial

solution arises at $b^* = 1.5791 \times 10^4$. The type of the solutions along the second loop changes at $b = 1.4522 \times 10^4$ and $b = 1.5695 \times 10^4$. As the range of b's for which (3.1) admits some solution is very large, the last value looks very close to b^* in the diagram and, hence, two of the small squares marking the change of type along the second loop are almost superimposed with the dot marking the trivial solution u_0. Regarding the stability, it adjusts to the general patterns of the first diagram of Figure 3.10, except for the second loop bifurcated from the primary curve. Precisely, the solutions along the arc of curve of the primary curve enclosed by the second loop have four-dimensional unstable manifolds, while the solutions on the loop have three-dimensional unstable manifolds, again in complete agreement with the exchange stability principle of M. G. Crandall and P. H. Rabinowitz [24, 25].

As λ decreases from $\lambda = -760.3$ the loop grows until reaching the trivial solution u_0 and then encircles it for any smaller value of λ. The bottom left plot of Figure 3.10 shows the global bifurcation diagram of (3.1) for $\lambda = -800$. For this value, the second loop emanates from the primary branch at $b = 1.2110 \times 10^4$ and $b = 2.5941 \times 10^4$, the trivial solution arises at $b^* = 2.0530 \times 10^4$ and the values where the solutions change type from $(3, a)$ to $(4, a)$ along the second closed loop are $b = 1.4455 \times 10^4$ and $b = 2.4152 \times 10^4$. As it happened with the solutions of the first loop, for any fixed b, the solutions of the lower piece of the second loop are the reflections of the solutions along the upper half-loop with respect to $x = 0.5$.

The first plot of Figure 3.11 shows some significant solutions along the second loop emanated from the primary curve for $\lambda = -800$. One solution is of type $(4, a)$, two solutions are of type $(3, a)$, and the remaining two of type $(3, s)$. The solutions plotted with a continuous line are the solutions of the bifurcation points, whereas the solutions plotted with dot-dashed lines are the solutions on the upper part of the second closed loop corresponding to the values of the parameter $b = 1.2951 \times 10^4$, $b = 1.8821 \times 10^4$ and $b = 2.5121 \times 10^4$. The solutions of the second plot are the reflections of the previous ones. Hence, for each of these values of the parameter b we are plotting the two solutions on the second loop.

For a certain value of $\lambda < -800$ a bifurcation to solutions of type $(5, s)$ from u_0 occurred. Then, the arc of curve of the primary branch encircled by the second loop rotated counterclockwise around u_0 originating two additional turning points on the $(5, s)$-arc of curve surrounding u_0. Once these turning points had arisen, they separated gradually as λ decreased. The last plot of Figure 3.10 shows the global bifurcation diagram computed for $\lambda = -1300$. Topologically, this bifurcation diagram is equivalent to the previous one, but it shows another two turning points on the primary curve, consisting of solutions

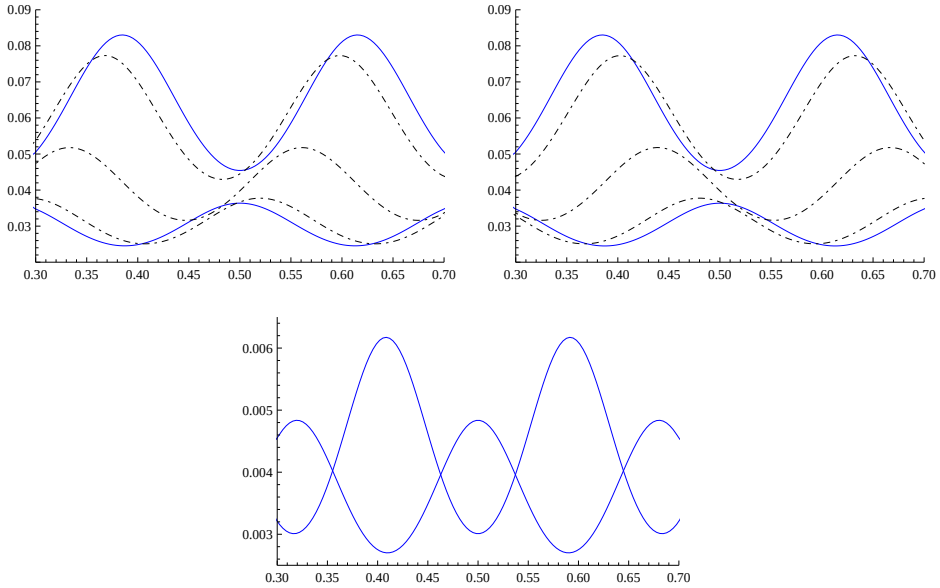

Figure 3.11: Plots of some significant solutions of type $(3, s)$, $(3, a)$, $(4, a)$ and $(5, s)$ along the bottom diagrams of Figure 3.10

of type $(5, s)$, which became of type $(3, s)$ before abandoning the interior of the second loop.

The last plot of Figure 3.11 shows the graphs of two solutions of type $(5, s)$ for $\lambda = -1300$ with $b = 2.7238 \times 10^5$, the one with three minima, and $b = 3.3598 \times 10^5$, the one with three maxima. Naturally, to switch from each of them to the other, one must cross the trivial solution u_0 along the primary curve.

Figure 3.12 shows the global bifurcation diagram of (3.1) for $\lambda = -2000$. Now, the counterclockwise rotation around u_0 exhibited by the last diagram of Figure 3.10 has been tremendously magnified, and a new closed loop, the third one, emanated from the solutions of type $(5, s)$ along the primary curve. In Figure 3.12 such loop has been represented through a dotted purple line. As usual, the small squares on it are marking the points where the solutions of type $(5, a)$ changed their type to $(6, a)$.

To explain the global bifurcation diagram of Figure 3.12, we will run over the entire primary curve to describe its main features. We started by computing the unique solution of (3.3). Then, we continued the curve for increasing values of b and computed the branch of minimal solutions, all of them linearly stable, until we met the first (subcritical) turning point, arisen at $b = 1.2463985 \times 10^7$, where the solutions became unstable with one-dimensional

unstable manifold until we reached the bifurcation point of the first loop, at $b = 1.2463984 \times 10^7$. Then, the solutions along the primary curve became unstable with two-dimensional unstable manifold.

Up to here, all computed solutions were of type $(1, s)$. Next, we continued the primary curve until $b = 1.0292 \times 10^7$, where the type of the solutions changed to $(3, s)$. We continued these solutions until reaching the first supercritical turning point along the primary curve at $b = 0.0135 \times 10^7$. At this turning point the dimension of the unstable manifold changed from 2 to 3 and it remained equal to 3 until we reached the bifurcation point of the second loop at $b = 0.0162 \times 10^7$, where the solutions became unstable with four-dimensional unstable manifold. Then, a new change of type occurred at $b = 0.1045 \times 10^7$, where the solutions became of type $(5, s)$ with three minima and two maxima. The next feature along the primary curve is a subcritical turning point at $b = 1.0035 \times 10^7$, where the unstable manifold of the solutions of (3.1) became five-dimensional, until we crossed the first bifurcation point of the third loop from the primary curve, where it became six-dimensional. This point occurred at $b = 0.9255 \times 10^7$. Once passed it, we continued the curve until reaching the trivial solution at $b^* = 0.7007 \times 10^7$, where the solutions began to exhibit three maxima and two minima; hence, still being of type $(5, s)$. Then, we meet the second bifurcation point of the third loop at $b = 0.4045 \times 10^7$, where the solutions became unstable with five-dimensional unstable manifold, until the next (supercritical) turning point arose, at $b = 0.2771 \times 10^7$, where the unstable manifolds became four-dimensional.

The next remarkable feature along the primary curve is a change of type from $(5, s)$ to $(3, s)$ at $b = 1.0198 \times 10^7$, before reaching the second bifurcation point of the second loop, occurred at $b = 1.23858 \times 10^7$, where the dimensions of the unstable manifolds again decreased to three. Then, we reached the fifth and last (subcritical) turning point at $b = 1.23861 \times 10^7$, where the dimensions of the unstable manifolds reached the value two again. Note that the second bifurcation point of the secondary loop and the fifth turning point are extremely close with respect to their magnitudes. After crossing the last turning point there was a change of type from $(3, s)$ to $(1, s)$ at $b = 0.0011 \times 10^7$. Finally, we crossed the second bifurcation point of the first loop at $b = 5.3703 \sim 0.0000005 \times 10^7$, where the solutions became unstable with one-dimensional unstable manifold. The remaining solutions approximated the metasolution $m(x)$ as $b \downarrow 0$.

An extremely remarkable feature is that the dimension of the unstable manifolds of all solutions along the primary curve increased by one at each bifurcation or turning point we crossed, until we reached the interior of the last emanated loop, where these dimensions began to decrease, according to

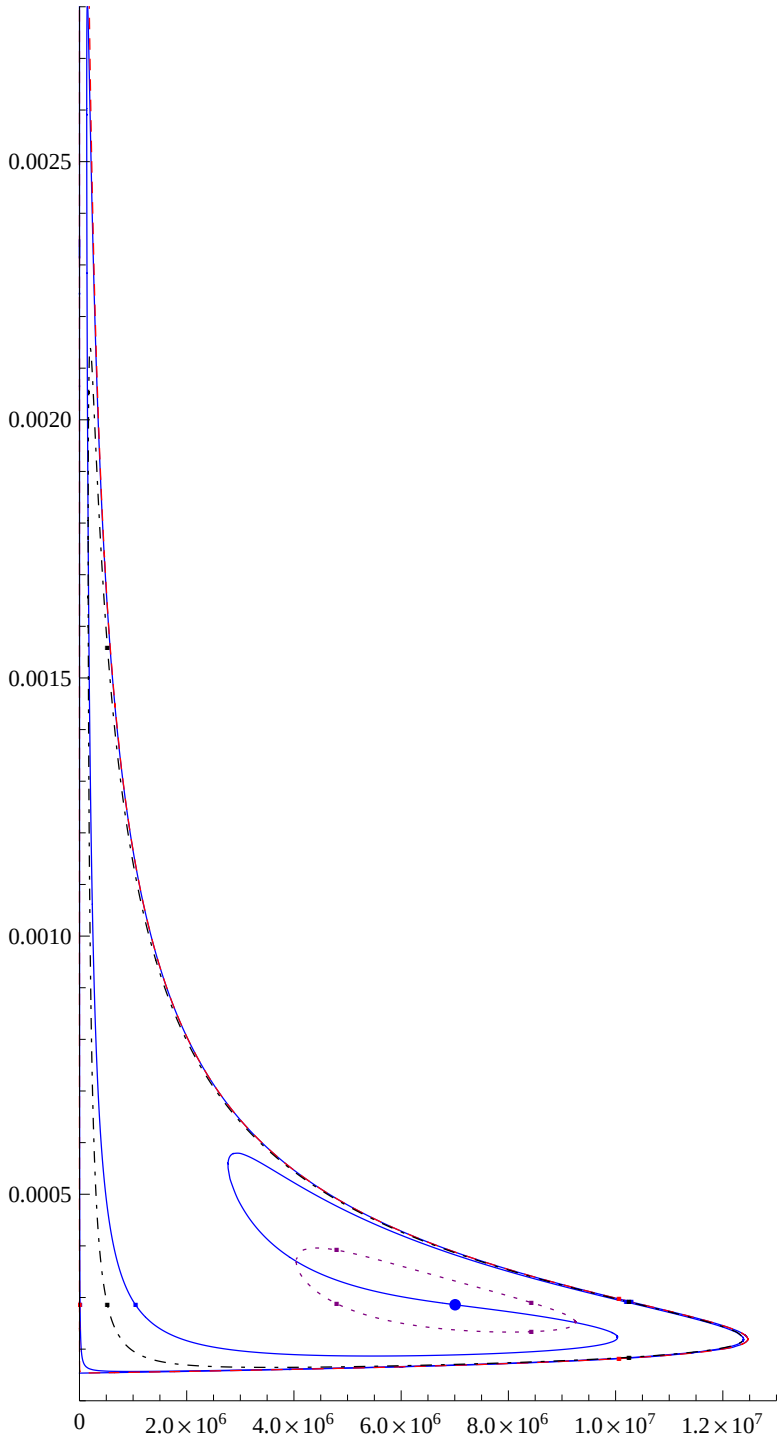

Figure 3.12: Global bifurcation diagram for $\lambda = -2000$

the same rule, until they became one-dimensional again.

Regarding the behavior of the n-th loop, either it fully consists of solutions of type $(2n-1,a)$, as it occurs soon after its bifurcation from the primary branch, or it consists of solutions of type $(2n-1,a)$ near the bifurcation points from the primary curve together with two central arcs of solutions of type $(2n,a)$, for each $n=1,2,3,\dots$.

Note that $b = 1.2463985 \times 10^7$, the value where the first turning point along the primary curve occurs, is extraordinarily high, not only with respect to the value $c=1$, but also with respect to $u(\alpha) = 2.1950 \times 10^{-4}$, whereas $u(0)=u(1)=100$. As the quotient $b/u(\alpha)$ is of order 10^{11}, we are definitely close to the limits of the machine precision. Consequently, our numerical code seems extremely efficient.

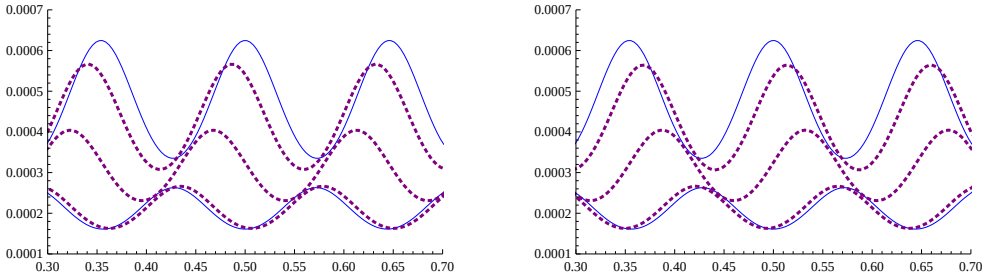

Figure 3.13: Plots of some significant solutions of Figure 3.12

Figure 3.13 shows the plots of some significant solutions along the third closed loop of the global bifurcation diagram of Figure 3.12. More precisely, the left picture shows the plots of a solution of type $(6,a)$, for $b = 0.4446 \times 10^7$, and two solutions of type $(5,a)$, for $b = 0.6146 \times 10^7$ and $b = 0.9143 \times 10^7$, along the upper half-arc of the loop, which have been represented with a purple dotted line. The other two solutions, plotted with continuous lines, are the solutions associated to the bifurcation points of the third loop from the primary curve. The solutions on the right plot were obtained for the same values of the parameters but on the lower half-arc of the third loop. According to the results of Chapter 1, they are reflections around $x=0.5$ of the previous ones.

It should be noted that, for every b in between the two bifurcation points of the third loop from the primary curve, Problem (3.1) possesses at least 12 solutions: 6 among them symmetric and the remaining 6 asymmetric.

For smaller values of λ, we were not able to automatize the continuation codes, since we were outside the machine precision range, as we have shown in Section 3.3.2. So, we stop our discussion here. Refining our numerical codes in order to compute these bifurcation diagrams for a larger range of values of

λ would be an extremely challenging problem.

3.5. Bifurcation diagrams for non-piecewise-constant weights

This section provides some of the most striking results of our very last numerical experiments for a series of weight which perturb from (3.2).

Anyway we start by presenting (see Figure 3.14) four plots of the global bifurcation diagrams for the special choice (3.2) again, with the same values of the parameters as in the previous section, i.e. $M = 100$, $c = 1$, $p = 2$ and $\alpha = 0.3$. Some of these diagrams have been already presented there, but we have decided to represent them again in order to compare them easier with the new ones of this section.

We briefly describe the main quantitative characteristics of the upper right bifurcation diagram, the one for $\lambda = -200$, which was not presented in Section 3.4. It consists of the primary curve, which perturbs from the unique solution of (3.1) at $a_0(x)$, and a loop of asymmetric solutions bifurcating from it at $b = 130.0719$ (subcritical bifurcation) and at $b = 14.0609$ (supercritical bifurcation). The principal curve exhibits a subcritical turning point at $b = 134.2401$, which divides it into and upper and a lower part. The solutions on its lower part are linearly asymptotically stable, while those along its upper part are unstable. More precisely, their unstable manifolds are one-dimensional outside the secondary loop and two-dimensional inside it.

As in the previous section, in each of these diagrams we have marked with a thick point the solution of type 0, which arose at $b^* = 81.1505$ (the value defined in (1.27)) for the special case we are discussing here, and with small squares the points where the types of the solutions along the curves change. These changes occurred, for $\lambda = -200$, at $b = 25.6150$ and $b = 113.4476$ on the secondary loop. The solutions along the portion of the loop between these two values are of type two, while those in between the squares and the bifurcation points are of type one.

To study the effect of non-piecewise-constant weight functions on the results established up to this point, we have considered two types of functions, whose plots have been represented in Figure 3.15. Firstly, we have considered the functions

$$a_b^n(x) := \begin{cases} -c & \text{if } x \in [0,\alpha) \cup (1-\alpha, 1] \\ b & \text{if } x \in [\alpha,\alpha_1) \cup (1-\alpha_1, 1-\alpha] \\ b\left(1+\mu \sin\left(n\pi \frac{x-\alpha_1}{1-2\alpha_1}\right)\right) & \text{if } x \in [\alpha_1, 1-\alpha_1] \end{cases}$$

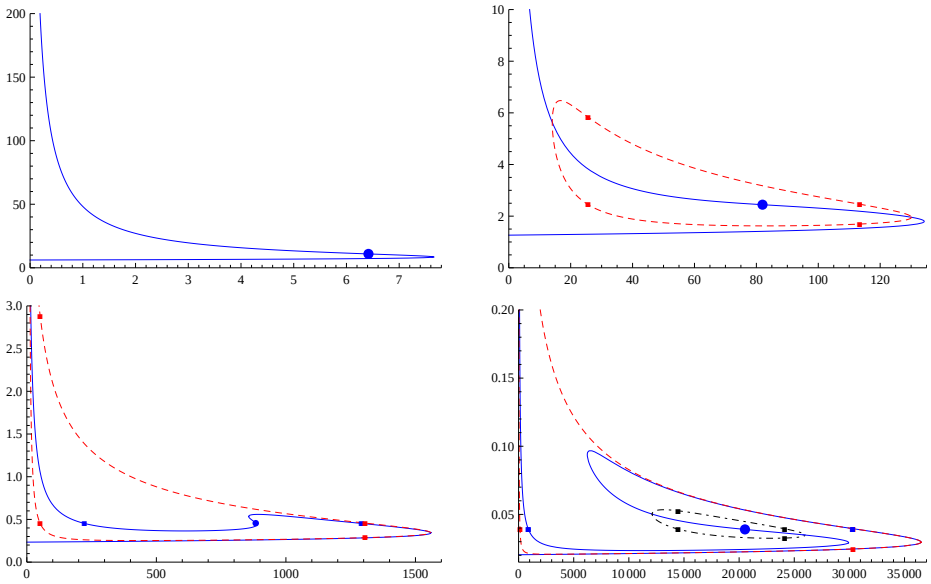

Figure 3.14: Bifurcation diagrams for the special choice (3.2), with $\lambda = -70$ (upper left), $\lambda = -200$ (upper right), $\lambda = -400$ (lower left) and $\lambda = -800$ (lower right).

with $0 < \alpha < \alpha_1 < 0.5$, $0 < \mu < 1$, $n \in \mathbb{N}$, $b \geq 0$ and $c > 0$. This choice has been made in order to let $a_b^n > 0$ in $(\alpha, 1-\alpha)$ even for $b \sim 0$, so that (3.1) becomes purely superlinear in this interval. Observe that n denotes the number of oscillations of the weight around b in the interval $[\alpha_1, 1-\alpha_1]$ (see Figure 3.15 (A)) and that $a_b^0 = a_b$.

Figure 3.16 shows the plots of the four global bifurcation diagrams computed for the special choice $\alpha_1 = 0.45$, $\mu = 0.1$ and $n = 3$, so that the weight is still symmetric around 0.5, with the remaining parameters unchanged with respect to those taken for generating the plots of Figure 3.14.

In this case, as it can be realized by having a glance at the plots of Figure 3.16, there is no significant qualitative difference with respect to the global bifurcation diagrams plotted in Figure 3.14, which have been obtained for the same values of λ, except for the number of turning points of the secondary loops emanating from the principal curve of the diagram. In particular, all the features described in Section 3.4 are preserved; among them, the coiling effect of the principal curve from which the secondary loops emanate as λ decreases.

Naturally, in this case the solution of type 0 on the principal curve cannot exist, as a_b^3 is not constant in $(\alpha, 1-\alpha)$, however a new clustering phenomenon of points where the solutions change type, represented with small squares on

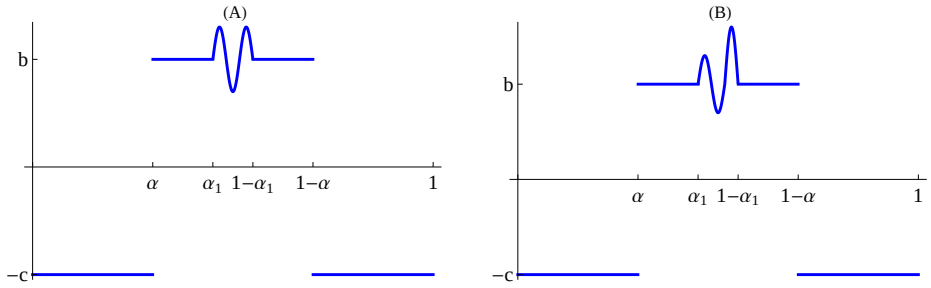

Figure 3.15: Plot of $a_b^3(x)$ (left) and $a_b^{3,2}(x)$ (right).

the diagrams, occurs. For example, in the first plot of Figure 3.16, the simplest one, following the curve starting at $b = 0$, we first have solutions of type 1, then, on the upper half-branch of curve, the type of the solutions becomes 5 at $b = 6.4753$, 3 at $b = 6.3486$ and, finally, it gets the original value 1 after $b = 5.5997$. The plots of Figure 3.17 (A) represent, from the bottom to the top, solutions on the portion of the diagram with a high number of type-changes, precisely on the upper half-branch for $b = 6.4836$ (of type 1), for $b = 6.4120$ (type 5) and for 6.3416 (type 3), respectively.

Another newly observed phenomenon is that the number of turning points on the secondary loops increases as λ decreases, which is illustrated in the third and fourth plots of Figure 3.16. Indeed, first an inflexion point on the upper branch of the loop is formed and then two additional turning points arise from it. As a consequence, two additional turning points also arise on the lower part of the loop, because the asymmetric solutions must occur in pairs of the form $(u(x), u(1-x))$. As a consequence, in the last plot of Figure 3.16, the problem admits at least 8 solutions if $1798.9437 < b < 5303.5426$. Five of them, for the special value $b = 4300$, have been represented in Figure 3.17 (B). Among them, the two plotted with continuous lines are the ones on the principal curve, and the remaining three lie on the lower part of the loop; for increasing values of $u(\alpha)$ they have been represented with dashed, dotted and dot-dashed lines, respectively. The three solutions that have not been represented are the reflections with respect to $x = 0.5$ of the ones on the lower half of the loop and lie on its upper half.

The last qualitative difference observed between the cases a_b and a_b^3 is the fact that there are more changes of type of the solutions along the loops when the weight is not constant in $(\alpha, 1-\alpha)$. Contrarily to what happened in the case of piecewise constant weight, where one could count the exact number of critical points of the solutions in $(\alpha, 1-\alpha)$, some critical points that remained in $(0, \alpha) \cup (1-\alpha, 1)$ with a_b have entered into $(\alpha, 1-\alpha)$ with a_b^3.

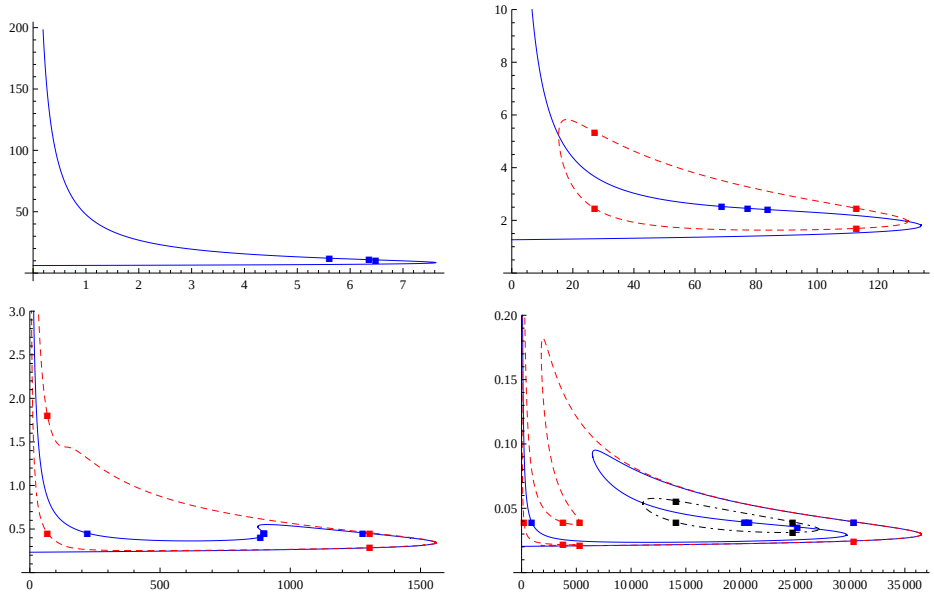

Figure 3.16: Bifurcation diagrams for weight a_b^3, with $\lambda = -70$ (upper left), $\lambda = -200$ (upper right), $\lambda = -400$ (lower left) and $\lambda = -800$ (lower right).

Now, we will consider the next asymmetrization of a_b^n

$$a_b^{n,\varepsilon}(x) := \begin{cases} -c & \text{if } x \in [0,\alpha) \cup (1-\alpha, 1] \\ b & \text{if } x \in [\alpha, \alpha_1) \cup (1-\alpha_1, 1-\alpha] \\ b\left(1+\mu \sin\left(n\pi \frac{x-\alpha_1}{1-2\alpha_1}\right)\right) & \text{if } x \in \left[\alpha_1, \frac{n-1+(2-n)\alpha_1}{n}\right) \\ b\left(1+\varepsilon\mu \sin\left(n\pi \frac{x-\alpha_1}{1-2\alpha_1}\right)\right) & \text{if } x \in \left[\frac{n-1+(2-n)\alpha_1}{n}, 1-\alpha_1\right] \end{cases}$$

with $\varepsilon > 0$. Observe that the main effect of ε is modulating the amplitude of the last hump of a_b^n and that $a_b^{n,1} = a_b^n$. Obviously, we should consider an odd value of n in order to preserve the superlinear character of (3.1) in $(\alpha, 1-\alpha)$. A paradigmatic plot of these asymmetric weights has been represented in Figure 3.15 (B). In the subsequent numerical experiments we took $n = 3$ and $\varepsilon \neq 1$ in order to compare the corresponding diagrams with the ones already presented.

In Figure 3.18 we have plotted the bifurcation diagrams, with $\lambda = -200$, for the choices $a_b^{3,0.999}$ (left) and $a_b^{3,1.001}$ (right). In both cases one can observe a dramatic change in the global bifurcation diagrams, with respect to the case of weight $a_b^{3,1} = a_b^3$, as each of them consists of two components. Namely, the primary curve, plotted with a continuous (blue) line, and an isola, plotted with a dashed (red) line. Hence, breaking the symmetry of the weight function provokes the emergence of isolas, instead of loops connected to the primary

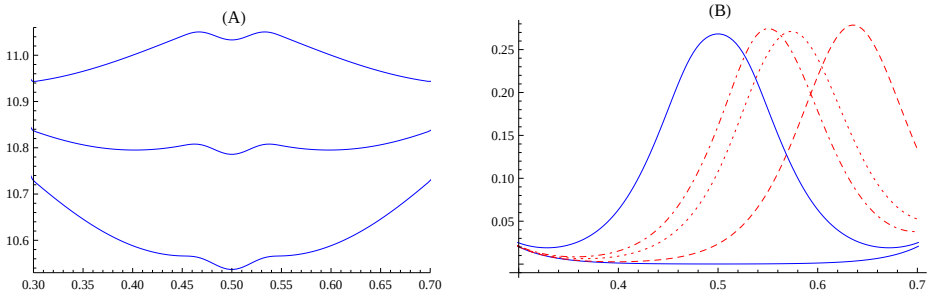

Figure 3.17: Some solutions related to the diagrams of Figure 3.16: change of type of the solutions for $\lambda = -70$ (left) and new solutions arising from the new turning points generated on the first loop for $\lambda = -800$ (right).

branch of the global bifurcation diagram, as it has been the case in all previous (symmetric) situations.

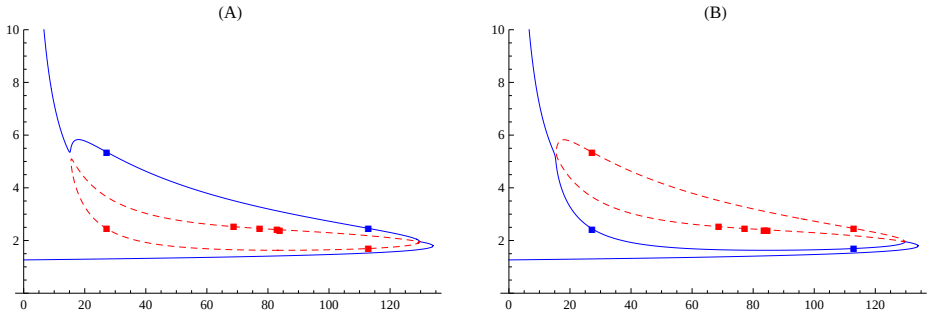

Figure 3.18: Bifurcation diagrams with weight $a_b^{3,\varepsilon}$ for $\lambda = -200$ and $\varepsilon = 0.999$ (left) and $\varepsilon = 1.0001$ (right).

It should be observed that the isola perturbs from the arc of the principal curve in between the bifurcation points of the loop in case $a = a_b^3$ and the lower half-arc of the bifurcated loop if $\varepsilon < 1$ (see Figure 3.18 (A)), or the upper half-arc of the bifurcated loop if $\varepsilon > 1$ (see Figure 3.18 (B)). According to these patterns, the unstable manifolds of the solutions along the upper arc of the isola are two-dimensional, while they are one-dimensional on the lower arc, if $\varepsilon < 1$. Similarly, they are two-dimensional on the lower arc and one-dimensional on the upper one if $\varepsilon > 1$. Moreover, there is a continuous transition among the several points where the solutions change of type along these arcs of curve when ε perturbs from 1.

As a consequence of the continuous dependence, though the topological

structure of the bifurcation diagrams plotted in the second picture of Figure 3.16 and in Figure 3.18 are different, as in the first case the diagram is connected while in each of the last two cases it possesses two components, from a quantitative point of view these diagrams do not differ substantially when ε perturbs from 1. Naturally, the differences should be magnified when ε separates away from 1. As a matter of fact, when ε grows the previous isolas shrink to a single point up to disappear. This striking phenomenon has been depicted in Figure 3.19. Table 3.3 provides us with some relevant information related to it.

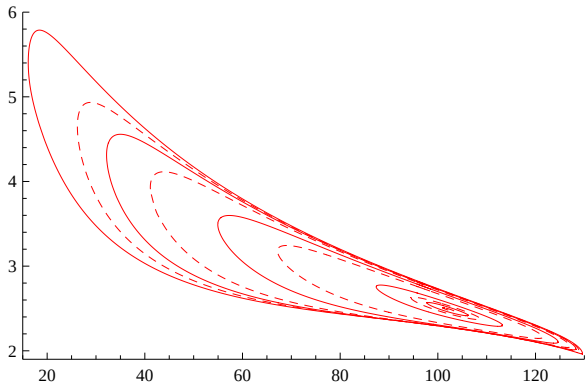

Figure 3.19: A series of isolas for the weight $a_b^{3,\varepsilon}$ with $\varepsilon = 1.01, 2, 3, 5, 7, 10, 11$. As ε grows, the isolas shrink to a single point.

Table 3.3: The size of the isolas for a series of values of ε.

ε	Supercritical turning point	Subcritical turning point
1.001	15.5207	129.6564
1.01	16.1301	129.6203
2	32.1680	128.2709
3	41.1264	127.1216
5	54.9458	124.6365
7	67.1596	121.5130
10	87.3711	113.2365
10.7	94.5425	108.6993
11	101.0036	103.3568
11.0084	102.0154	102.3763

Regarding the primary curves, the quantitative differences as ε separates

away from 1 are not that accentuated, as it becomes apparent by comparing the left plot of Figure 3.20, which represents the bifurcation diagram for $\lambda = -200$ and $\varepsilon = 11.0084$, and the right plot of Figure 3.18, which gives the corresponding bifurcation diagram for $\lambda = -200$ and $\varepsilon = 1.001$. In the former case the isola has almost completely shrunk and the turning point on the principal curve arises at $b = 132.1283$, while in the latter one the turning point arises at $b = 134.0460$.

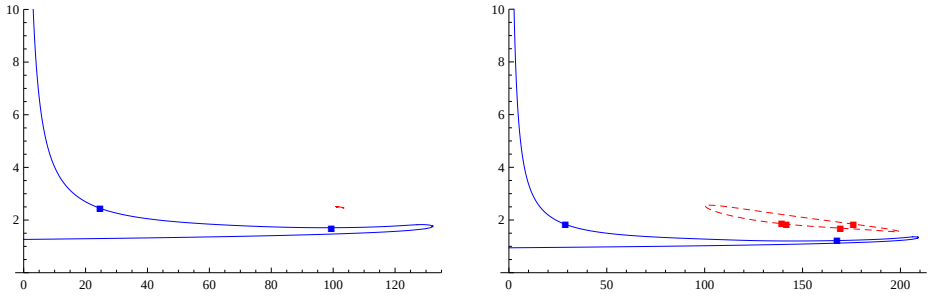

Figure 3.20: Bifurcation diagrams with weight $a_b^{3,11.0084}$ for $\lambda = -200$ (left) and $\lambda = -230$ (right).

The fact that these isolas shrink to a single point as ε separates away from 1 is far from being in conflict with the high multiplicity result of Chapter 1 , as we can recover the shrunk loops by choosing appropriate (smaller) values of λ. This becomes apparent by comparing the two diagrams of Figure 3.20. Both of them were computed for $\varepsilon = 11.0084$, but in the first one we used $\lambda = -200$ and in the second one $\lambda = -230$. In general, the smaller λ is, the larger is the isola.

3.6. Conclusions

Tough path-following coupled with pseudo-spectral collocation has provided very accurate solvers for ascertaining the structure of the bifurcation diagrams of the steady-state solutions in a wide variety of Reaction-Diffusion equations and systems, there has not been, up to the best of our knowledge, any attempt for stressing such continuation methods through the computation of highly intricate global bifurcation diagrams whose structure is known 'a priori', like those of this dissertation.

From the analytical results of Chapter 1, Problem (3.1), with the particular choice (3.2), exhibits very complex global bifurcation diagrams for sufficiently

large $-\lambda > 0$; the larger $-\lambda$ is, the more complex are these diagrams. However, from Chapter 1, their structure is completely understood. Namely, they consist of a primary curve establishing an homotopy between the unique positive solution of (3.3) and the metasolution (3.4) plus a finite number of closed loops emanating from it at a sequence of values of $\lambda \downarrow -\infty$. Essentially, as λ decreases, the primary curve spirals over itself generating a loop after every half counterclockwise rotation around u_0, as it has been illustrated analytically in Section 1.6 and numerically in Section 3.4.

As a consequence of our numerics, we were able to determine the dimensions of the unstable manifolds of all positive solutions of (3.1), which cannot be calculated by pure analytical methods with the existing analytical tools. They vary when a turning or a bifurcation point is crossed. Moreover, the unique linearly stable solution of (3.1) is the minimal one, as rigorously proved in Chapter 2.

Other phenomena which were not observed in Chapter 1 are the fact that the range of values of b for which (3.1) admits a positive solution approximates $[0, \infty)$ as $\lambda \downarrow -\infty$, and that, rather astonishingly, all the solutions of (3.1) approximate 0 in the sublinear part for all $b > 0$ if $\lambda \downarrow -\infty$, though the number of solutions of (3.1) grows arbitrarily. This strong squashing effect makes the numerical computation of the solutions of (3.1) an extremely challenging task for $\lambda < -2000$. The rigorous proof of these phenomena is going to be published in [55]

Actually, we were able to compute these intricate global bifurcation diagrams because we already knew their global structure. Otherwise, it would have been extremely difficult to reconstruct them numerically for $\lambda \leq -800$. Therefore, this work is a paradigm of how mathematical analysis aids the numerical study of a problem, and simultaneously the numerical studies confirm, illuminate and complete the analysis.

From the point of view of the applications in population dynamics, the results of Chapter 3 establish that, under facilitative effects in competitive media, the harsher are the environmental conditions, the richer is the dynamics of the species. Although this is a rather astonishing result, it should not be forgotten that if the habitat is extremely polluted, which is measured by the size of $-\lambda$, all the steady states of the parabolic problem associated to (3.1) should be small in the sublinear part; but not necessarily in the superlinear one, due to the facilitative effect among the individuals of the species. This facilitative effect provides the sufficient synergy in order to increase the complexity of the dynamics, even in the harshest conditions; this, in spite of being rather reasonable, is still very surprising from an ecological perspective.

The fact that the number of steady states grows arbitrarily as the degree of

inhabitability of the environment blows up, as an effect of interspecific facilitative effects, has been observed for the first time in this work in the context of spatial ecology and it might be a relevant feature in the theory of ecosystems.

Finally, the numerical experiments presented in Section 3.5 suggest that the general multiplicity patterns established in Chapter 1 for the special case of piecewise constant weight, still hold for more general weight functions, not necessarily piecewise constant. However, the topological structure of the underlying bifurcation diagrams can change as the weight loses the nice symmetries of (3.2) causing the emergence of a family of isolas perturbing from the original loops bifurcated from the primary curve of the symmetric problem. Moreover, rather naturally, the number of solutions of (3.1) might grow as a consequence of the wiggly behavior of the weight, even if it is symmetric, through the emergence of a higher number of turning points along the bifurcated loops from the primary curve. All these experiments encourage the research of analytical tools, which seem not to be available, to prove rigorously the new phenomenologies presented here numerically.

Resumen

Introducción y objetivos

Esta tesis "Análisis matemático y tratamiento numérico de una clase de problemas de valores de contorno de tipo elíptico superlineal indefinido"estudia varias propiedades de los estados estacionarios positivos del problema de evolución

$$\begin{cases} u_t - \Delta u = \lambda u + a(x)u^p, & t > 0, \quad x \in \Omega, \\ u(t,x) = M > 0, & t > 0, \quad x \in \partial\Omega, \\ u(0,x) = u_0(x) \geq 0, & x \in \Omega, \end{cases} \tag{R.1}$$

donde Ω es un dominio (conjunto abierto y conexo) acotado de $\mathbb{R}^N$, $N \geq 1$, con frontera regular $\partial\Omega$, $\lambda \in \mathbb{R}$, $p > 1$ y $M \in (0, \infty]$ son constantes y $u_0 : \Omega \to \mathbb{R}$ es una función no negativa. Los estados estacionarios de (R.1) son las soluciones positivas del siguiente problema elíptico asociado a (R.1)

$$\begin{cases} -\Delta u = \lambda u + a(x)u^p & \text{en } \Omega, \\ u(x) = M & \text{sobre } \partial\Omega. \end{cases} \tag{R.2}$$

En estos modelos, $a(x)$ es una función acotada y medible que puede cambiar de signo en Ω; se le suele llamar *peso*. Si $a < 0$ en Ω, entonces

$$\lambda u + a(x)u^p < \lambda u$$

para todo $u \geq 0$ y, por eso, el problema es *sublineal*, mientras que si $a > 0$, entonces

$$\lambda u + a(x)u^p > \lambda u$$

y el problema es de tipo *superlineal*. En el caso en que a cambia signo, que es el caso tratado en esta tesis, el problema se dice de tipo *superlineal indefinido*.

En dinámica de poblaciones, (R.1) modela la evolución de una especie en el hábitat Ω que está rodeado por regiones donde la densidad de población es M. En estos modelos, $u(t,x)$ representa la densidad de la especie en el punto

$x \in \Omega$ y al cabo del tiempo $t > 0$, mientras que $u_0 > 0$ es la densidad de población inicial. La magnitud λ mide la tasa intrínseca neta de natalidad ($\lambda > 0$) o mortalidad ($\lambda < 0$) de la especie en Ω. En la naturaleza esa tasa es negativa cuando se usan pesticidas en altas concentraciones o una cierta región es contaminada por la introducción de determinadas sustancias químicas, venenos o productos de desecho, mientras que es positiva en presencia de condiciones climáticas favorables o abundancia de sustancias nutritivas.

La no linealidad logística generalizada mide las relaciones interespecíficas entre los individuos de la especie u, que compiten por los recursos naturales en la región Ω_-, donde $a < 0$, mientras que cooperan en la región Ω_+, donde $a > 0$. Cuando $a = 0$ en algún subdominio Ω_0, la población experimenta en esa zona una ley de crecimiento exponencial que se conoce como ley de Malthus por la presencia de recursos ilimitados. Por lo tanto, en nuestro problema superlineal indefinido, estos tres comportamientos pueden manifestarse simultáneamente.

A pesar de que hay muchos análisis exhaustivos sobre pruebas experimentales de competición interespecífica (véase por ejemplo T. W. Shoener [69] y J. H. Connell [23]) y las interacciones positivas han sido ampliamente documentadas entre organismos de diferentes reinos, ya que pueden contribuir significativamente a las necesidades del uno con el otro sin compartir los mismos recursos (véase por ejemplo G. E. Hutchinson [39], J. L. Wulff [70], M. B. Saffo [67]), encontrar interacciones positivas entre organismos similares en la abundancia parece ser una tarea muy complicada desde el punto de vista empírico, ya que estas interacciones no aparecen asiladas, sino conjuntamente con las de carácter competitivo. De todas formas, de acuerdo con el principio de estrés abiótico de M. D. Bertness y R. M. Callaway [10], la importancia de las interacciones positivas en las comunidades de plantas aumenta bajo estrés abiótico o presión de los consumidores. Varios estudios empíricos apoyan la validez de la ipótesis de estrés abiótico y en realidad un número sustancial de interacciones positivas en comunidades de plantas ha sido identificado en duras condiciones ambientales (véase por ejemplo R. M. Callaway, L. R. Walker [15] y F. I. Pugnaire [65]). Consecuentemente, (R.1) parece ser un modelo matemático bastante razonable para estudiar los efectos combinados de facilitación y competición en hábitats contaminados, es decir cuando $\lambda < 0$.

En relación con las condiciones de frontera, en el caso singular $M = \infty$, se entiende que

$$\lim_{d(x,\partial\Omega)\downarrow 0} u(x) = \infty,$$

donde $d(x, \partial\Omega)$ es la distancia del punto x a la frontera de Ω. Estas soluciones son conocidas como *soluciones largas* o *soluciones de blow-up* del problema.

Aunque esta condición de frontera infinita pueda parecer carente de sentido desde el punto de vista de la interpretación biológica, el caso no es este,

dado que las soluciones largas juegan un papel fundamental en la dinámica del problema parabólico, como descrito en el caso sublineal en [46]. Por esta razón, su estudio es imperativo también en problemas superlineales indefinidos, como quedó de manifiesto en [46, 59].

Naturalmente, hay una enorme literatura sobre el caso sublineal, tanto para condiciones de frontera homogéneas como no homogéneas. Por la precisión, el rango exacto de λ, dependiendo del peso y del dominio Ω, para los que (R.2) admite solución ha sido determinado en este contexto a través de sub- y supersoluciones. Además, con métodos de comparación, que están basados fuertemente en la sublinealidad del peso, se ha probado la unicidad de solución (véase por ejemplo [30, 46]). Resultados análogos se cumplen para las soluciones largas, aunque, además de los métodos de monotonía, hay que tratar la delicada cuestión de determinar la tasa de explosión en $\partial\Omega$ de las soluciones para obtener la unicidad (véase por ejemplo [19, 20, 21, 22, 44, 46, 47]).

Los problemas superlineales indefinidos también han generado cierta literatura, pero principalmente para condiciones de frontera Dirichlet homogéneas (véase [3, 7, 8, 9, 36, 37, 42, 43, 45]). De todas formas los elegantes métodos de monotonía que dan la clave para obtener la mayoría de los resultados en los problemas sublineales no son válidos en el caso superlineal indefinido, lo cual hace que el análisis matemático sea mucho más sofisticado técnicamente. En realidad, se pierde la unicidad de solución, hecho en el que radica la importancia de la presente memoria. Además los diagramas de bifurcación relacionados cambian drásitcamente. Sin embargo, el problema superlineal indefinido (R.2), con condiciones de frontera no homogéneas, no ha sido estudiado aún. Este es el caso que desarrollamos en esta tesis.

Contenido

En el Capítulo 1 estudiamos un ejemplo paradigmático de (R.2) en el caso unidimensional. Por la precisión consideramos

$$\begin{cases} -u'' = \lambda u + a_b(x)u^p & \text{en } (0,1), \\ u(0) = u(1) = M, \end{cases} \tag{R.3}$$

con el peso constante a trozos

$$a_b(x) := \begin{cases} -c & \text{si } x \in (0,\alpha) \cup (1-\alpha, 1), \\ b & \text{si } x \in (\alpha, 1-\alpha), \end{cases} \tag{R.4}$$

donde $c > 0$, $b \geq 0$ y $\alpha \in (0, 0{,}5)$.

Cuando $b = 0$, (R.3) es una ecuación difusiva logística perturbación del caso en que $a(x) < 0$ para todo $x \in \Omega = (0,1)$. Dado que $a_0 = 0$ en $\Omega_0 = (\alpha, 1-\alpha)$,

en esa región la especie u crece según la ley de Malthus de la dinámica de poblaciones y, en particular, los recursos naturales son ilimitados allí, mientras que la evolución de u está gobernada por la ley logística, con exponente p, en $\Omega_- = (0,\alpha) \cup (1-\alpha, 1)$.

Más precisamente, como caso muy especial de J. M. Fraile et al. [30], si $b = M = 0$, entonces (R.3) posee una única solución (necesariamente simétrica con respecto de 0,5) si, y sólo si,

$$\pi^2 < \lambda < \lambda_\alpha := \left(\frac{\pi}{1-2\alpha}\right)^2.$$

Además, si la denotamos por u_λ, resulta que u_λ bifurca desde 0 en $\lambda = \pi^2$ y que bifurca desde infinito en λ_α. En realidad,

$$\lim_{\lambda \uparrow \lambda_\alpha} u_\lambda(x) = \begin{cases} \ell_\alpha(x) & x \in [0,\alpha), \\ \infty & x \in [\alpha, 0{,}5], \end{cases}$$

donde ℓ_α es la única solución del problema singular

$$\begin{cases} -u'' = \lambda_\alpha u - cu^p & \text{en } (0,\alpha) \\ u(0) = 0, \quad u(\alpha) = \infty \end{cases}$$

(véase J. García-Melián et al. [32], J. López-Gómez y J. C. Sabina [60] y J. López-Gómez [44, 46]). El mismo resultado es cierto para todo $M > 0$ si $b = 0$ pero, en este caso, u_λ está definida no solamente para $\lambda > \pi^2$, sino para todo $\lambda < \lambda_\alpha$ (véase [46]). En todos esos casos, cuando la (única) solución existe, de acuerdo con J. López-Gómez [46], es un atractor global para la contraparte unidimensional de (R.1)

$$\begin{cases} \partial_t u - \partial_{xx} u = \lambda u + a_b(x) u^p & x \in (0,1), \quad t > 0, \\ u(0,t) = u(1,t) = M, & t > 0, \\ u(x,0) = u_0(x), & x \in (0,1). \end{cases}$$

Si en (R.3) consideramos una vez más el caso $b = 0$ y suponemos además $\lambda < 0$, entonces necesariamente $u_\lambda < M$ en el hábitat, siendo $u'' > 0$. A la luz de nuestra interpretación biológica del modelo, esto significa que a través de los extremos del área contaminada $(0,1)$ hay un flujo continuo de individuos que mueren en el interior a una tasa $\lambda < 0$ por la acción del contaminante. Este flujo continuo de individuos a través de la frontera de la región contaminada hace que se pueda mantener la población al nivel u_λ cuando el tiempo crece. Básicamente, lo mismo ocurre si $\lambda > 0$ y la longitud del intervalo $(\alpha, 1-\alpha)$ es lo suficientemente pequeña como para que $\lambda < [\pi/(1-2\alpha)]^2$. Sorprendentemente, cuando la tasa de natalidad de la especie, medida por λ, cruza el umbral

$[\pi/(1-2\alpha)]^2$, la población está acotada en $(0,\alpha)\cup(1-\alpha,1)$, como pasa en modelo logístico clásico, mientras que crece hacia infinito en $(\alpha,1-\alpha)$, que es la región donde la evolución de u está gobernada por la ley de Malthus.

Todos estos aspectos cambian drásticamente cuando $b>0$, incluso en el caso más sencillo $M=0$. De hecho en ese caso en bien sabido que existe $b^*>0$ tal que para todo $0<b<b^*$ existe un único

$$\lambda_t=\lambda_t(b)\in(\pi^2,\lambda_\alpha)$$

tal que:

a) (R.3) no admite ninguna solución si $\lambda>\lambda_t(b)$;

b) (R.3) admite, al menos, una solución si $\lambda\leq\lambda_t(b)$;

c) (R.3) admite al menos dos soluciones para todo $\lambda\in(\pi^2,\lambda_t(b))$.

Además,

$$\lim_{b\downarrow 0}\lambda_t(b)=\lambda_\alpha \quad \text{y} \quad \lim_{b\uparrow b^*}\lambda_t(b)=\pi^2.$$

Por otro lado, si $b\geq b^*$, entonces (R.3) admite una solución positiva si y sólo si $\lambda\leq\pi^2$. Estos resultados son consecuencia directa de la teoría general desarrollada en J. López-Gómez [42], H. Amann y J. López-Gómez [7], y R. Gómez-Reñasco y J. López-Gómez [36, 37], donde algunos hallazgos pioneros de H. Berestycki et al. [8, 9], y S. Alama y G. Tarantello [3] fueron mejorados sustancialmente.

Bastante sorprendentemente, aunque (R.3) parezca tan sencillo, en el caso general $b>0$ y $0<M\leq\infty$ hay muy pocos resultados sobre la estructura global del conjunto de soluciones de (R.3). Entre ellos, J. Mawhin, D. Papini y F. Zanolin [63] establecieron algunos resultados de multiplicidad para soluciones que cambian de signo, J. López-Gómez [45] probó la existencia y el carácter globalmente atractivo de la solución minimal de (R.3) cuando $M=\infty$ para $b>0$ suficientemente pequeño y, recientemente, J. García-Melián determinó la forma general del diagrama de bifurcación para un prototipo general multidimensional de (R.3) para $M=\infty$ y $\lambda=0$, usando b como parámetro de bifurcación principal. El uso de b como parámetro en el contexto de problemas superlineales indefinidos es una estrategia que se remonta, por lo menos, a J. López-Gómez [43].

Como estamos suponiendo (R.4), nuestro problema es autónomo en cada uno de los intervalos donde a_b es constante y podemos aplicar técnicas de diagrama de fases en cada una de esas regiones.

Algunas técnicas similares, pero para problemas bastante diferentes, han sido usadas por Harris [38] y Dambrosio [28] en relación a problemas de valores de contorno no homogéneos de la forma

$$\begin{cases} -u'' = f(u) + h \quad \text{en} \ \ (0,1) \\ u(0) = A,\ u(1) = B. \end{cases} \tag{R.5}$$

En [38] al autor considera el caso de no linealidades de salto $f(u)/u \to C, D$ cuando $u \to \pm\infty$, mientras en [28] se trata el caso superlineal $f(u)/u \to +\infty$ cuando $u \to \pm\infty$. La principal diferencia de nuestro estudio con respecto de los anteriores como [28, 38] es que en nuestra situación trabajamos con un problema superlineal indefinido, debido al cambio de signo del peso $a_b(x)$ y además mostramos contextualmente el papel crucial que juega el parámetro λ cuando $\lambda < 0$. Estas características producen resultados de multiplicidad que no son comparables con los casos mencionados arriba. Por la precisión, para el problema (R.5) en el caso superlineal se obtiene un gran número de soluciones oscilatorias que cambian de signo (véase [28]) y, como se probó en [63], ese comportamiento fuertemente oscilatorio es exhibido también por las soluciones explosivas de $-u'' = a(x)f(u)$, cuando $a(x)$ (como en nuestro caso) es negativo en un entorno de $t = 0, 1$ y positivo en el la zona central del dominio, pero estas soluciones en general no eran positivas, como pasa en este trabajo, donde encontramos para el problema (R.3) una nueva y amplia clase de múltiples soluciones largas que son positivas y oscilan alrededor de un nivel positivo (véase la Sección 1.3). Este resultado de multiplicidad se basa en la rápida oscilación de las soluciones de (R.3) para λ suficientemente negativo. Determinamos además (véase la Sección 1.6) la estructura topológica de las curvas de bifurcación de estas soluciones oscilatorias positivas, en dependencia del parámetro b, la cual resulta ser extremadamente rica y sorprendente. Además, a diferencia de los trabajos [28, 38], pudimos tratar en el mismo marco tanto el caso $M \in \mathbb{R}$ como $M = +\infty$, lo que nos ha permitido encontrar también un resultado de multiplicidad para soluciones largas (Sección 1.7).

En el Capítulo 2 consideramos el problema general $N-$dimensional (R.1) con $M \in (0, +\infty)$ y el principal resultado es la unicidad del estado estacionario positivo linealmente estable (véase la Sección 2.5). El resultado es absolutamente no trivial, a la luz de los resultados del Capítulo 1, dado que el modelo puede tener un número arbitrariamente grande de estados estacionarios. Las técnicas usadas en este Capítulo difieren sustancialmente de las del Capítulo 1 ya que el problema no es más autónomo a trozos ni tampoco unidimensional. Las técnicas usadas se basan en unas continuaciones locales y globales, así como en unas estimaciones variacionales globales.

Como en el Capítulo 1, la unicidad del estado estacionario linealmente estable para el caso de condiciones de frontera homogéneas ya se conocía por

los trabajos de R. Gómez-Reñasco y J. López-Gómez in [36, 37], pero en este caso la situación es diferente ya que, debido a las condiciones de frontera no homogéneas, la solución $u = 0$ no es más solución, sino subsolución, y esto cambia la dinámica del problema.

Además obtenemos algunos resultados óptimos de existencia y multiplicidad gracias a unos argumentos topológicos y de monotonía adicionales (véanse las Secciones 2.4 y 2.6). Una vez más, resultados de la misma naturaleza ya se conocían para el caso de condiciones de frontera homogéneas (véase [7]) pero son nuevos en nuestro contexto.

Algunos resultados análogos han sido obtenidos recientemente para soluciones largas por J. García-Melián en [31], pero sólo en el caso $\lambda = 0$, en que sólo se espera que haya dos soluciones, como es explicado en el Capítulo 1. Como en esta tesis, la teoría de [31] adapta las ideas y los métodos de [36, 37].

Finalmente, en el Capítulo 3 presentamos un estudio detallado de varios diagramas de bifurcación surgidos en los capítulos anteriores, computados numéricamente, así como las técnicas que hemos utilizado para obtenerlos. Bastante sorprendentemente, de los experimentos numéricos se desprende que el rango de b positivos para los que (R.3) admite soluciones positivas crece sin límitaciones cuando λ decrece a $-\infty$, mientras que, simultáneamente, las soluciones del problema decaen a 0 en la parte sublineal. Eso es bastante razonable a la luz de la interpretación biológica del modelo. Efectivamente, si se usan grandes cantidades de pesticidas, aunque la especie no desaparezca, gracias al continuo flujo de individuos a través de la frontera, su densidad debe ser pequeña al menos en la región donde hay competición intraespecífica en el hábitat contaminado. Sin embargo, en la región donde los efectos facilitativos juegan su papel, es decir donde el modelo es superlineal, estos efectos superan, en el caso de las soluciones linealmente inestables, el aplastamiento de forma considerable. De cualquier manera, el hecho de que la complejidad de la dinámica crezca al ser las condiciones ambientales más crudas, dependiendo del tamaño de λ, es bastante sorprendente y tremendamente intrigante. Aunque debe estar provocado por los efectos facilitativos, es una fenómeno radicalmente nuevo nunca antes documentado.

El análisis matemático del Capítulo 1 ha facilitado enormemente el análisis numérico del Capítulo 3, donde esos diagramas de bifurcación han sido computados combinando unos algoritmos de continuación actualizados con metódos espectrales y colocación. De hecho el conocimiento de las propiedades cualitativas de los diagramas probadas en el Capítulo 1 ha sido crucial en el desarrollo de los métodos numéricos del Capítulo 3, ya que los puntos de retorno son muy cerrados debido al fenómeno de achatamiento descrito arriba y las direcciones de bifurcación muy próximas entre sí, lo cual ha causado graves problemas al

implementar los códigos númericos clásicos, que han tenido que ser adaptados para recuperar los diagramas establecidos teóricamente en el Capítulo 1.

Una vez superados estos problemas computacionales, hemos podido usar los códigos para obtener numéricamente los diagramas de bifurcación de (R.3) para una serie de pesos diferentes de (R.4). Los resultados de estos experimentos numéricos están presentados en la Sección 3.5 y esencialmente muestran que el teorema de multiplicidad del Capítulo 1 parece ser cierto para clases de pesos a_b muy generales, aunque la estrúctura topológica de los diagramas puede variar dramáticamente dependiendo de las propiedades de simetría del peso. A nuestro entender, no hay instrumentos analíticos para probar rigurosamente esos resultados. Desde esta perspectiva, esta tesis muestra cuan fructífera es la interacción entre el análisis matemático y numérico en la práctica. De hecho, parece imposible concebir cómo se hubieran podido calcular todos esos diagramas de bifurcación tan achatados sin conocer previamente su estructura topológica fina.

Queremos concluir este resumen remarcando que el contenido de esta tesis ha dado origen a los artículos de investigación [61] (Capítulo 1), [57] (Capítulo 2) y [55, 56] (Capítulo 3), que han sido enviados para ser publicados.

Conclusiones

Aunque los métodos de path-following combinados con colocación pseudo-espectral han proporcionado códigos numéricos muy precisos para establecer la estructura de diagramas de bifurcación de estados estacionarios en una gran variedad de ecuaciones y sistemas de Reacción-Difusión, no nos consta que haya existido intento alguno para llevarlos al límite computando diagramas globales de bifurcación tan intrincados como los de esta memoria, cuya estructura fuese conocida "a priori".

En efecto, a partir de los resultados analíticos del Capítulo 1, el problema (3.1), con la elección particular (3.2), presenta diagramas de bifurcación globales extraordinariamente complejos para $-\lambda > 0$ suficientemente grande; tanto más cuanto mayor sea $-\lambda$. Sin embargo, con el análisis del Capítulo 1, su estructura es completamente conocida. Precisamente están formados por una curva primaria que establece una homotopía entre la única solución positiva de (3.3) y la metasolución (3.4) más un número finito de lazos adicionales que emanan desde ella para una sucesión de valores de $\lambda \downarrow -\infty$. Esencialmente, cuando λ decrece, la curva primaria rota sobre sí misma, espiralándose y generando un lazo después de cada rotación en sentido antihorario alrededor de u_0, como ha quedado ilustrado analíticamente en la Sección 1.6 y numéricamente en la Sección 3.4.

Como consecuencia de nuestros experimentos numéricos, hemos conseguido determinar las dimensiones de las variedades inestables de todas las soluciones positivas de (3.1), que no pueden ser calculadas analíticamente con las herramientas puramente analíticas existentes. Tales dimensiones varían cada vez que se cruza un punto de retorno o un punto de bifurcación, creciendo o decreciendo según que nos acerquemos, o nos alejemos, a la solución trivial. Además, hemos demostrado rigurosamente en el Capítulo 2 que la única solución linealmente estable de (3.1) es la minimal.

Otros fenómenos que hemos detectado numéricamente y que no habían sido previamente observados en el Capítulo 1 son el hecho de que el rango de valores de b para los que (3.1) posee soluciones positivas debe aproximar $[0, \infty)$ cuando $\lambda \downarrow -\infty$ y que, curiosamente, todas las soluciones de (3.1) aproximan 0 en la parte sublineal, para cualquier $b > 0$, cuando $\lambda \downarrow -\infty$, aunque el número de soluciones de (3.1) crezca arbitrariamente. Este marcado efecto de "aplastamiento sublineal"hace que la computación numérica de las soluciones de (3.1) sea un auténtico desafío científico para $\lambda < -2000$. La demostración rigurosa de estos fenómenos va a aparecer publicada en [55].

Hay que reconocer que, en realidad, hemos sido capaces de computar esos intrincados diagramas globales de bifurcación porque conocíamos previamente su estructura. De no haber sido así, creemos que hubiera sido extraordinariamente difícil reconstruirlos numéricamente para $\lambda \leq -800$. Por lo tanto, este trabajo es un aunténtico paradigma de cómo el análisis matemático ayuda el estudio numérico de un problema y simultáneamente el análisis numérico confirma, ilumina y completa el análisis.

Desde el punto de vista de las aplicaciones a la dinámica de poblaciones, los resultados del Capítulo 3 establecen que, bajo efectos facilitativos en medios competitivos, cuanto más hostiles sean las condiciones ambientales, más rica es la dinámica de la especie. Aunque este resultado sea extraordinariamente sorprendente, no hay que olvidar que cuando el hábitat esté muy contaminado, lo que se mide con el tamaño de $-\lambda$, todos los estados estacionarios del problema parabólico asociado a (3.1) deberían de ser pequeños en la parte sublineal del modelo; pero no necesariamente en la superlineal, por el efecto facilitativo entre los individuos de la especie. Este efecto facilitativo genera la suficiente sinergia para incrementar la complejidad de la dinámica, incluso en las condiciones más adversas imaginables; lo que, siendo natural, no deja de ser extraordinariamente sorprendente desde el punto de vista de la Ecología.

El hecho de que el número de estados estacionarios crece arbitrariamente cuando el grado de inhabitabilidad del ambiente se dispara, como consecuencia de los efectos facilitativos intraespecíficos, ha sido observado por primera vez en este trabajo en el marco de la ecología espacial y podría llegar a constituir

una aportación muy relevante a la teoría de ecosistemas.

Finalmente, los experimentos numéricos presentados en la Sección 3.5 sugieren que los patrones generales de multiplicidad establecidos en el Capítulo 1 en el caso especial del peso constante a trozos siguen siendo ciertos para pesos más generales, no necesariamente constantes a trozos, aunque sabemos que la estructura topológica global de los correspondientes diagramas de bifurcación puede variar dramáticamente si el peso pierde las simetrías de (3.2), porque tal reducción de simetría en el peso se traduce en una pérdida de simetría en los diagramas que provoca la aparición de "isolas"que perturban desde los lazos originales bifurcados a lo largo de la rama primaria del problema simétrico. Además, de forma bastante natural, el número de soluciones de (3.1) puede aumentar como consecuencia del comportamiento ondulatorio nodal del propio peso, incluso si este es simétrico, a través del surgimiento de puntos de retorno adicionales a lo largo de los lazos bifurcados desde la curva primaria. Todos nuestros experimentos numéricos en esta dirección demandan imperativamente el desarrollo de nuevos instrumentos analíticos, que, por lo que sabemos, no están disponibles, para probar rigurosamente los nuevos fenómenos presentados aquí numéricamente.

Bibliography

[1] S. Agmon, A. Douglis and L. Niremberg, Estimates near the boundary for solutions of elliptic partial differential equations satisfying general boundary conditions I, *Comm. Pure Appl. Maths.* **12** (1959), 623–727.

[2] S. Agmon, A. Douglis and L. Niremberg, Estimates near the boundary for solutions of elliptic partial differential equations satisfying general boundary conditions II, *Comm. Pure Appl. Maths.* **17** (1964), 35–92.

[3] S. Alama and G. Tarantello, Elliptic problems with nonlinearities indefinite in sign, *J. Funct. Anal.* **141** (1996), 159–215.

[4] E. L. Allgower and K. Georg, *Introduction to Numerical Continuation Methods*, SIAM Classics in Applied Mathematics 45, SIAM, Philadelphia, 2003.

[5] H. Amann, Multiple positive fixed points of asymptotically linear maps, *J. Funct. Anal.* **17** (1974), 174–213.

[6] H. Amann, Fixed point equations and nonlinear eigenvalue problems in ordered Banach spaces, *SIAM Rev.* **18** (1976), 620–709.

[7] H. Amann and J. López-Gómez, A priori bounds and multiple solutions for superlinear indefinite elliptic problems, *J. Diff. Eqns.* **146** (1998), 336–374.

[8] H. Berestycki, I. Capuzzo-Dolcetta and L. Nirenberg, Superlinear indefinite elliptic problems and nonlinear Liouville theorems, *Top. meth. Nonl. Anal.* **4** (1994), 59–78.

[9] H. Berestycki, I. Capuzzo-Dolcetta and L. Nirenberg, Variational methods for indefinite superlinear homogeneous elliptic problems, *Nonl. Diff. Eqns. Appns.* **2** (1995), 553–572.

[10] M. D. Bertness and R. M. Callaway, Positive interactions in communities, *Trends in Ecology and Evolution* **9** (1994), 191–193.

[11] M. Bertsch and R. Rostamian, The principle of linearized stability for a class of degenerate diffusion equations, *J. Diff. Eqns.* **57** (1985), 373–405.

[12] F. Brezzi, J. Rappaz, P.A. Raviart, Finite dimensional approximation of nonlinear problems, Part I: Branches of Nonsingular Solutions, *Numer. Math.* **36** (1980), 1–25.

[13] F. Brezzi, J. Rappaz, P.A. Raviart, Finite dimensional approximation of nonlinear problems, Part II: Limit Points, *Numer. Math.* **37** (1981), 1–28.

[14] F. Brezzi, J. Rappaz, P.A. Raviart, Finite dimensional approximation of nonlinear problems, Part III: Simple bifurcation points, *Numer. Math.* **38** (1981), 1–30.

[15] R. M. Callaway and L. R. Walker, Competition and facilitation: A synthetic approach to interactions in plant communities, *Ecology* **78** (1997), 1958–1965.

[16] S. Cano-Casanova, Existence and structure of the set of positive solutions of a general class of sublinear elliptic non-classical mixed boundary value problems, *Nonlinear Anal. TMA* **49** (2002), 361–430.

[17] C. Canuto, M. Y. Hussaini, A. Quarteroni and T. A. Zang, *Spectral methods in Fluid Mechanics*, Springer, Berlin, 1988.

[18] A. Casal, J. C. Eilbeck and J. López-Gómez, Existence and uniqueness of coexistence states for a predator-prey model with diffusion, *Diff. Int. Eqns.* **7** (1994), 411–439.

[19] F.C. Cirstea and V.D. Radulescu, Existence and uniqueness of blow-up solutions for a class of logistic equations, *Commun. Contemp. Math.* **4** (2002), 559–586.

[20] F.C. Cirstea and V.D. Radulescu, Uniqueness of the blow-up boundary solution of logistic equation with absorption, *C. R. Acad. Sci. Paris Sér. I* **335** (2002), 447–452.

[21] F.C. Cirstea and V.D. Radulescu, Asymptotics for the blow-up boundary solution of the logistic equation with absorption,*C. R. Acad. Sci. Paris Sér. I* **336** (2003), 231–236.

[22] F.C. Cirstea and V.D. Radulescu, Solutions with boundary blow-up for a class of nonlinear elliptic problems, *Houston J. Math.* **29** (2003), 821–829.

[23] J. H. Connell, On the prevalence and relative importance of interspecific competition: evidence from field experiments, *Amer. Natur.* **122** (1983), 661–696.

[24] M. G. Crandall and P. H. Rabinowitz, Bifurcation from simple eigenvalues, *J. Funct. Anal.* **8** (1971), 321–340.

[25] M. G. Crandall and P. H. Rabinowitz, Bifurcation, perturbation from simple eigenvalues and linearized stability, *Arch. Rat. Mech. Anal.* **52** (1973), 161–180.

[26] M. Crouzeix and J. Rappaz, *On Numerical Approximation in Bifurcation Theory*, Recherches en Mathématiques Appliquées 13. Masson, Paris, 1990.

[27] Y. Du, S. Li, Nonlinear Liouville theorems and a priori estimates for indefinite superlinear elliptic equations, *Adv. Differential Equations* **10** (2005) 841–860.

[28] W. Dambrosio, Time-map techniques for some boundary value problems, *Rocky Mountain J. Math.* **28** (1998), 885–926.

[29] J. C. Eilbeck, The pseudo-spectral method and path-following in Reaction-Diffusion bifurcation studies, *SIAM J. of Sci. Stat. Comput.* **7** (1986), 599–610.

[30] J. Fraile, P. Koch-Medina, J. López-Gómez and S. Merino, Elliptic eigenvalue problems and unbounded continua of positive solutions of a semilinear elliptic equation, *J. Diff. Eqns.* **127** (1996), 295–319.

[31] J. García-Melián, Multiplicity of positive solutions to boundary blow up elliptic problems with sign-changing weights, *J. Funct. Anal.* **261** (2011), 1775–1798.

[32] J. García-Melián, R. Gómez-Reñasco, J. López-Gómez and J. C. Sabina de Lis, Point-wise growth and uniqueness of positive solutions for a class of sublinear elliptic problems where bifurcation from infinity occurs, *Arch. Rat. Mech. Anal.* **145** (1998), 261–289.

[33] B. Gidas and J. Spruck, Global and local behavior of positive solutions of nonlinear elliptic equations, *Comm. Pure Appl. Math.* **34** (1981), 525–598.

[34] B. Gidas and J. Spruck, A priori bounds for positive solutions of nonlinear elliptic equations, *Comm. Partial Differential Equations* **6** (1981), 883–901.

[35] D. Gilbarg and N. S. Trudinger, *Elliptic Partial Differential Equations of Second Order*, Springer, Classics in Mathematics, Berlin-Heilderberg, 2001.

[36] R. Gómez-Reñasco and J. López-Gómez, The effect of varying coefficients on the dynamics of a class of superlinear indefinite reaction diffusion equations, *J. Diff. Eqns.* **167** (2000), 36–72.

[37] R. Gómez-Reñasco and J. López-Gómez, The uniqueness of the stable positive solution for a class of superlinear indefinite reaction diffusion equations, *Diff. Int. Eqns.* **14** (2001), 751–768.

[38] G. A. Harris, The influence of boundary data on the number of solutions of boundary value problems with jumping nonlinearities, *Trans. Amer. Math. Soc.* **321** (1990), 417–464.

[39] G. E. Hutchinson, *The Ecological Theater and the Evolutionary Play*, Yale University Press, New Haven, Connecticut, 1965.

[40] H. B. Keller, *Lectures on Numerical Methods in Bifurcation Problems*, Tata Insitute of Fundamental Research, Springer, Berlin, 1986.

[41] J. López-Gómez, *Estabilidad y Bifurcación Estática. Aplicaciones y Métodos Numéricos*, Cuadernos de Matemática y Mecánica, Serie Cursos y Seminarios N° 4, Santa Fe, 1988.

[42] J. López-Gómez, On the existence of positive solutions for some indefinite superlinear elliptic problems, *Comm. Part. Diff. Eqns.* **22** (1997), 1787–1804.

[43] J. López-Gómez, Varying bifurcation diagrams of positive solutions for a class of indefinite superlinear boundary value problems, *Trans. Amer. Math. Soc.* **352** (1999), 1825–1858.

[44] J. López-Gómez, Large solutions, metasolutions, and asymptotic behavior of the regular positive solutions of a class of sublinear parabolic problems, *El. J. Diff. Eqns.* **Conf. 05** (2000), 135–171.

[45] J. López-Gómez, Global existence versus blow-up in superlinear indefinite parabolic problems, *Sci. Math. Jpn.* **61** (2005), no. 3, 493–516, e2004, 449–472.

[46] J. López-Gómez, Metasolutions: Malthus versus Verhulst in Population Dynamics. A dream of Volterra, in *Handbook of Differential Equations*

"Stationary Partial Differential Equations", edited by M. Chipot and P. Quittner, Elsevier Science B. V., North Holland, Chapter 4, pp. 211–309, Amsterdam 2005.

[47] J. López-Gómez, Optimal uniqueness theorems and exact blow-up rates of large solutions, *J. Diff. Eqns.* **224** (2006), 385–439.

[48] J. López-Gómez, *Linear Second Order Elliptic Operators*, World Scientific Publishing, Singapore, 2013.

[49] J. López-Gómez, J. C. Eilbeck, K. Duncan and M. Molina, Structure of solution manifolds in a strongly coupled elliptic system, IMA Conference on Dynamics of Numerics and Numerics of Dynamics (Bristol, 1990), *IMA J. Numer. Anal.* **12** (1992), 405–428.

[50] J. López-Gómez and M. Molina-Meyer, The maximum principle for cooperative weakly coupled elliptic systems and some applications, *Diff. Int. Eqns.* **7** (1994), 383–398.

[51] J. López-Gómez and M. Molina-Meyer, Superlinear indefinite systems: beyond Lotka-Volterra models, *Journal of Differential Equations* **221** (2006), 343–411.

[52] J. López-Gómez and M. Molina-Meyer, The competitive exclusion principle versus biodiversity through segregation and further adaptation to spatial heterogeneities, *Theoretical Population Biology* **69** (2006), 94–109.

[53] J. López-Gómez and M. Molina-Meyer, Biodiversity through co-opetition, *Discrete and Continuous Dynamical Systems B* **8** (2007), 187–205.

[54] J. López-Gómez and M. Molina-Meyer, Modeling coopetition, *Mathematics and Computers in Simulation* **76** (2007) 132–140.

[55] J. López-Gómez, M. Molina-Meyer and A. Tellini, Intricate dynamics caused by facilitation in competitive environments within polluted habitat patches, Submitted.

[56] J. López-Gómez, M. Molina-Meyer and A. Tellini, Intricate bifurcation diagrams for a class of one-dimensional superlinear indefinite problems of interest in population dynamics, To appear in Dynamical Systems and Differential Equations, DCDS Supplement 2013 Proceedings of the 9th AIMS International Conference (Orlando, Florida, USA).

[57] J. López-Gómez, M. Molina-Meyer and A. Tellini, The uniqueness of the linearly stable positive solution for a class of superlinear indefinite problems with nonhomogeneous boundary conditions, Submitted.

[58] J. López-Gómez, M. Molina-Meyer and M. Villareal, Numerical Computation of Coexistence States, *SIAM J. Numer. Anal.* **29** (1992), 1074–1092.

[59] J. López-Gómez and P. Quittner, Complete and energy blow-up in indefinite superlinear parabolic problems, *Discrete Continuous Dyn. Systems* **14** (2006), 169–186.

[60] J. López-Gómez and J. C. Sabina de Lis, First variations of principal eigenvalues with respect to the domain and poiunt-wise growth of positive solutions for problems where bifurcation from infinity occurs, *J. Diff. Eqns.* **148** (1998), 47–64.

[61] J. López-Gómez, A. Tellini and F. Zanolin, High multiplicity and complexity of the bifurcation diagrams of large solutions for a class of superlinear indefinite problems, Submitted.

[62] A. Lunardi, *Analytic Semigroups and Optimal Regularity in Parabolic Problems*, Progeress in Nonlinear Differential Equations and their Applications Vol. 16, Birkhäuser, Basel, 1995.

[63] J. Mawhin, D. Papini and F. Zanolin, Boundary blow-up for differential equations with indefinite weight, *J. Diff. Eqns.* **188** (2003), 33–51.

[64] S. I. Pohozaev, On the eigenfunctions of the equation $\Delta u + \lambda f(u) = 0$, *Soviet Math. Doklady* **6** (1965), 1408–1411.

[65] F. I. Pugnaire (Editor), *Positive Plant Interactions and Community Dynamics*, Fundación BBVA, CRC Press, Boca Raton, 2010.

[66] P. H. Rabinowitz, Some global results for nonlinear eigenvalue problems, *J. Funct. Anal.* **7** (1971), 487–513.

[67] M. B. Saffo, Invertebrates in endosymbiotic associations, *Amer. Zool.* **32** (1992), 557–565.

[68] D. Sattinger, *Topics in Stability and Bifurcation Theory*, Lectures Notes in Mathematics 309, Springer, Berlin, 1973.

[69] T. W. Shoener, Field experiments on interspecific competition, *Amer. Natur.* **122** (1983), 240–285.

[70] J. L. Wulff, Clonal organisms and the evolution of mutualism. In Jackson, J.B.C., Buss, L.W., Cook, R.E. (Eds.), *Population Biology and Evolution of Clonal Organisms*, pp. 437–466, Yale University Press, New Haven, Connecticut, 1985.